

JYU DISSERTATIONS 552

Kalle Kansanen

Open Hybrid Quantum Systems



UNIVERSITY OF JYVÄSKYLÄ
FACULTY OF MATHEMATICS
AND SCIENCE

JYU DISSERTATIONS 552

Kalle Kansanen

Open Hybrid Quantum Systems

Esitetään Jyväskylän yliopiston matemaattis-luonnontieteellisen tiedekunnan suostumuksella
julkisesti tarkastettavaksi yliopiston Ylistönrinteen salissa FYS1
syyskuun 2. päivänä 2022 kello 12.

Academic dissertation to be publicly discussed, by permission of
the Faculty of Mathematics and Science of the University of Jyväskylä,
in Ylistönrinne, auditorium FYS1, on September 2, 2022 at 12 o'clock noon.



JYVÄSKYLÄN YLIOPISTO
UNIVERSITY OF JYVÄSKYLÄ

JYVÄSKYLÄ 2022

Editors

Ilari Maasilta

Department of Physics, University of Jyväskylä

Ville Korhakangas

Open Science Centre, University of Jyväskylä

Copyright © 2022, by University of Jyväskylä

ISBN 978-951-39-9188-3 (PDF)

URN:ISBN:978-951-39-9188-3

ISSN 2489-9003

Permanent link to this publication: <http://urn.fi/URN:ISBN:978-951-39-9188-3>

Abstract

The recent technological and scientific advances has allowed for the fabrication and ever-progressing characterization of interacting quantum mechanical systems. I focus on the theoretical description of such hybrid quantum systems. Specifically, I discuss two prototypical classes of light-matter systems: polaritonic and optomechanical systems. They are characterized by linear and nonlinear quantum mechanical interactions, respectively. I introduce possible physical realizations, discuss light-matter interaction giving rise to polaritons, and derive optomechanical interaction for a ferromagnetic system. The experimental reality also requires an understanding of dissipation and decoherence. I therefore describe how input-output formalism can be employed to model the optical response of open hybrid quantum systems. In addition, I discuss the possibility of the electromagnetic vacuum modifying chemistry by the formation of hybridized light-matter states, polaritons. These theoretical approaches to open hybrid quantum systems have wider applicability than their physical realizations and further elucidates the possibilities of light-matter interaction.

This dissertation is composed of an introductory text and five publications — three of which have been published while two are under peer review at the time of writing.

Tiivistelmä (Abstract in Finnish)

Teknologinen ja tieteellinen kehitys on mahdollistanut vuorovaikuttavien kvanttimekaanisten systeemien valmistamisen sekä karakterisoinnin. Keskityn tällaisten kvanttimekaanisten hybridisysteemien teoreettiseen kuvaukseen. Erityisesti tarkastelen kahta hyvin yleistä valon ja aineen vuorovaikutuksesta seuraavaa luokkaa hybridisysteemeille: polaritonisia sekä optomekaanisia systeemejä. Ne kattavat sekä lineaariset että epälineaariset kvanttimekaaniset vuorovaikutukset. Esittelen lukuisia fysikaalisia toteutuksia, käyn läpi polaritoneihin johtavan valon ja aineen vuorovaikutuksen teoriaa sekä johdan optomekaanisen kytkennän ferromagneettiselle systeemille. Käytännössä vaaditaan kuitenkin myös dissipaation ja dekoherenssin ymmärtämistä. Esittelen sen tähden, miten näiden tosiasiallisesti avoimien kvanttimekaanisten hybridisysteemien optista vastetta voidaan kuvata. Näiden asioiden lisäksi käsittelen niin sanottua polaritonista kemiaa, eli mahdollisuutta muokata kemiallisia reaktioita elektromagneettisen tyhjiön ja aineen vuorovaikutuksella. Tämän väitöskirjan muodostamalla teoreettisella lähestymistavalla on hyötyä monenlaisille hybridisysteemeille, ja toisaalta se auttaa ymmärtämään entistä paremmin valon ja aineen vuorovaikutusta.

Tämä väitöskirja koostuu johdanto-osasta sekä viidestä julkaisusta, joista kaksi on väitöskirjan julkaisun aikaan vielä vertaisarvioitavana.

- Author** Kalle Kansanen
Department of Physics and Nanoscience Center
University of Jyväskylä
Finland
- Supervisor** Tero Heikkilä
Department of Physics and Nanoscience Center
University of Jyväskylä
Finland
- Pre-examiners** Jyrki Piilo
Department of Physics and Astronomy
University of Turku
Finland
- Claudiu Genes
Max Planck Institute for the Science of Light
Department of Physics
University of Erlangen
Germany
- Opponent** Göran Johansson
Department of Physics
Department of Microtechnology and Nanoscience
Chalmers University of Technology
Sweden

Preface

I have conducted the research reported in this dissertation at the University of Jyväskylä from June 2018 to June 2022. This work has been generously supported the Magnus Ehrnrooth foundation and the Academy of Finland (projects 317118 and 321982). The financial support has allowed me to truly focus on research and on the betterment of myself, of which I am very grateful.

I wish to thank my supervisor, professor Tero Heikkilä for taking me aboard and guiding me through the whole arduous process. The dissertation would not have been possible without my esteemed opponent, prof. Göran Johansson, and the pre-examiners of the thesis, prof. Claudiu Genes and prof. Jyrki Piilo. I extend my sincere thanks to them as well.

When I started my undergraduate studies in Jyväskylä a decade ago, I didn't really know what I was up for. I have enjoyed the journey enormously. I have met some really clever people, interesting personalities, and great friends. Specifically, I thank Henri Hänninen who has taken all the same steps as me, just slightly faster, for his lasting friendship.

The graduate studies in the Nanoscience Center has been extremely enlightening. It is genuinely a nice place to work. There are too many people to thank for simply having interesting discussions and generating an intellectually exciting environment. I shall single out, nevertheless, prof. Gerrit Groenhof and assoc. prof. Jussi Toppari for all the professional collaborations. I also thank all the other coauthors who are not anymore or who never were associated with NSC: Camillo Tassi, Aili Asikainen, Harshad Mishra, and assoc. prof. Mika Sillanpää. As surrogates of the whole NSC, I thank the members of our group I have had the pleasure to meet, like Faluke, Teemu, Risto, Kurt, Subrata, Andrii, and Pauli, as well as the people who have shared the same office space, like Jaakko, Mira, Heli, Elli, Johannes, and Henri L. For those remaining in the office, I certainly hope that the next guy or gal does not bother you as much as I did, but I hope you had as much fun as I did.

The support of my extended family has been overwhelming. It has been a key factor during my whole life. I am indebted. The love and the support of my wife, Tita, has been invaluable to me during this journey, as it will be in the future. I dedicate this thesis to her.

Kalle Kansanen, June 2022, Jyväskylä

List of publications

This thesis consists of an introductory part and of the following publications:

- [I] K. S. U. Kansanen, A. Asikainen, J. J. Toppari, G. Groenhof and T. T. Heikkilä, Theory for the stationary polariton response in the presence of vibrations, *Physical Review B* **100** 245426 (2019).
- [II] K. S. U. Kansanen, J. J. Toppari and T. T. Heikkilä, Polariton response in the presence of Brownian dissipation from molecular vibrations, *The Journal of Chemical Physics* **154** 044108 (2021).
- [III] K. S. U. Kansanen, C. Tassi, H. Mishra, M. A. Sillanpää and T. T. Heikkilä, Magnomechanics in suspended magnetic beams, *Physical Review B* **104** 214416 (2021).
- [IV] K. S. U. Kansanen and T. T. Heikkilä, Cavity-induced bifurcation in classical rate theory, (2022), arXiv:2202.12182 [cond-mat.stat-mech].
- [V] K. S. U. Kansanen, Theory for polaritonic quantum tunneling, (2022), arXiv:2204.13490 [quant-ph].

Author's contribution

I performed the majority of the theoretical derivations, provided all the figures with the exception of Fig. 6 in [III] and Fig. S5 in [IV] together with numerical simulations, and participated in the writing of the text in all publications.

Contents

1	Introduction	1
2	Polaritons: hybridization of light and matter	5
2.1	Quantum electrodynamics of light-matter coupling	5
2.2	Jaynes–Cummings model and its extensions	10
2.3	Role of dissipation	14
2.4	Electronic strong coupling and vibrations	17
3	Polaritonic chemistry: a physicist’s viewpoint	23
3.1	Idea of vacuum-modified chemistry	23
3.2	Understanding polaritonic chemistry	25
3.3	Quantum tunneling regime — a toy model	29
3.4	Collectivity from classical theory	31
4	Optomechanics: nonlinear interactions	37
4.1	Cavity optomechanics	37
4.2	Magnomechanics	39
4.3	Many facets of hybrid quantum systems	52
5	Conclusion	54
	References	56
	Included publications	65

Liika on liikaa ja tyhjä tyhjä.

Kaarlo Marjanen
Miten oppia puhujaksi, 2. painos
(WSOY, 1950)

Chapter 1

Introduction

Physics strives to explain nature as emerging from simple premises. However, we intuitively know that the world around us isn't particularly simple. This conundrum is explained by interactions: if we have a model of nature that consists only of, say, elementary particles with well-defined properties, it is the interactions between these particles that produce incredible complexity. Fundamentally, all you need is to understand these elements, particles and their interactions, and physics is finished. In practice, such a program is just exceedingly difficult.

Another viewpoint is offered by a few modern fields within physics, for instance, condensed matter theory. We accept that there are emergent features arising from elementary interactions that can be modelled as is. Perhaps, there is some inner structure we are neglecting and, thus, our approach is necessarily incomplete. If such a phenomenological theory is able to explain our observations, nevertheless, it gives an insight to our reality. Fundamental physics is also physics of emergence and collective behavior [1].

Recent technological advances have lead to the possibility of constructing physical systems, involving many elementary particles, that can be fully understood only in a quantum mechanical description. Furthermore, we are at a point where manufacturing a hybrid of distinct systems is possible. This gives rise to the field of *hybrid quantum systems* [2–7]. Their potential is inspiring. The platform provided by hybrid quantum systems can be used to devise more accurate sensing and measurement technology. In the far-distant future, it would be beneficial and, therefore, reasonable to use our knowledge of quantum mechanics in communication and information processing tasks [8–11]. Hybrid quantum systems play a key role in such quantum networks [12, 13] as they provide a way to transduce information between different physical realizations. For example, we could still carry information over long distances by light but perhaps hope to further process it in an electronic or mechanical system.

We do not construct hybrid quantum systems as to show our technological prowess. They allow for studying fundamental physics. All hybrid systems are based on light-matter interactions or electromagnetism — it is currently quite difficult to think of technologies based on gravitational or nuclear forces. On one hand, light provides a probe to new materials and physical effects. One can think of, for instance, metamaterials with designed optical properties [14, 15] or inferring

non-local electronic correlations of topological states using spectroscopy [16]. On the other hand, the possibility of connecting multiple separate systems allows for collective effects [17] as well as observing quantum mechanical features of our world like quantized energies and entanglement [18–21].

When I write about hybrid quantum systems, there is a level of abstraction involved. It represents an idealized and imagined version of reality. Rather, what we have is systems coupled to measurement devices and whatever environment they are in. Such interactions we have trouble controlling. In the study of quantum mechanics, we tend to call them *open quantum systems* [22]. We can only begin to approximate and cleverly work around such complexity. It brings about a new set of physics: How do we understand any experiment in practice? At the same time, it brings about a set of philosophical questions on the arrow of time and the physical meaning of information.

As interesting as the foundational questions are, the focus of this thesis far more practical and rooted in shorter-term goals. One of the main questions presented here is the issue of understanding optical, frequency-resolved, measurements of hybrid quantum systems. It is a question partially motivated by experiments. Thus, the hybrid systems come with certain physical realizations. I focus on the specifics: what is the underlying cause or interaction that results in a hybrid quantum system. Nevertheless, the ideas of this dissertation can likely be used for many realizations I do not discuss here.

This dissertation focuses on two separate physical systems highlighting different aspects of hybrid quantum systems. First, I discuss polaritons. It is a short-hand name for light-matter systems whose quantum mechanical interaction can be presented in a linear form. Strictly speaking, polaritons are the hybridized excitations of light and matter, much like photons are the excitations of light. They can be created by, for instance, inserting atoms or molecules in an optical cavity. The hybridization between the vacuum electromagnetic field and the matter produces a very distinct optical response (as discussed in Ch. 2). Much of the recent interest in polaritons is due to the idea, coming far outside physics, that the light-matter coupling may produce changes in chemical reactivity (as discussed in Ch. 3). Second, I discuss opto- and magnomechanics in Ch. 4. It provides another prototypical class of hybrid quantum systems which are characterized by nonlinear interactions. Optomechanics refers to the idea that light carries momentum and can induce radiation-pressure force on matter. Of subsequent interest is magnomechanics; magnetization of a ferromagnetic material may produce similar interaction.

I explicitly state the purpose of the introductory part of the dissertation. I describe the thoughts we had before any work was done, the many misguided steps I took, and what we ultimately learned. The structure of this dissertation is therefore not that of an article. I want to use this opportunity to recollect what was (or still is) difficult for me to understand. My aim is to interweave these difficulties with the basic physical principles and descriptions so that the included publications may be understood. I hope that these choices make this text worth something.

Some reading advice I should give: This thesis is somewhat technical and assumes that the reader is familiar with advanced quantum mechanics [23, 24]. The unit convention is that of $\hbar = 1$ almost everywhere. This means that whenever I write an angular frequency (often symbolized by ω) I tend to mean energy (as the two are related by $E = \hbar\omega$). I do not separate quantum mechanical operators from their classical counterparts by any typographical feature. I think that it is clear from the context which one I mean. In contrast, I try to carefully denote vectors by a bold typeface (for instance, \mathbf{x} refers to a vector living in three-dimensional space but x_k to its component k) in this introductory text, because there is no unifying convention in the included publications.

The theory of quantum electrodynamics describes Nature as absurd from the point of view of common sense. And it agrees fully with experiment. So I hope you accept Nature as She is — absurd.

Richard P. Feynman
QED: The Strange Theory of Light and Matter
(Princeton University Press, 1985)

Chapter 2

Polaritons: hybridization of light and matter

In this chapter, I discuss the low-energy, non-relativistic quantum description of light-matter interaction in detail. It gives rise to hybridized quantum states which are termed as polaritons. I here describe their optical response within the input-output formalism, which is also the focus of [I] and [II].

Hybridization of light and matter states elucidates foundational questions in quantum theory as well as leads to interesting applications. Historically, it started from coupling atoms to microwave and optical cavities to provide new measurement and quantum control techniques. The trapping of photons in cavities allowed for preparing quantum states of light, entanglement of atoms, non-destructive measurements, and seeing decoherence of quantum systems; the inevitable destruction of quantum information [25, 26]. In many ways, it has provided a foundation for the quantum technological revolution.

Replacing atoms by organic molecules provides many more possibilities for applications and investigations at the boundary of classical and quantum worlds. The matter degrees of freedom are greatly increased. Recently, the hybridization of photons with such large matter systems has been shown to be possible — first in semiconductors [27, 28] and then in other optical systems. It allows for modifying optical properties [29], creation of hybrid Bose–Einstein condensates [28] and a new type of laser [30], and it has been suggested to affect chemistry of the involved molecules, for example. The modification to chemistry is discussed in Ch. 3 while this chapter focuses on optical properties.

2.1 Quantum electrodynamics of light-matter coupling

The theory of quantum electrodynamics (QED) provides the most accurate description of interactions between light and matter. Its development formed the foundation for the standard model of physics with the techniques of quantum field theory and renormalization. In the classical limit, it corresponds to Maxwell's equations.

In the case of coupling molecular degrees of freedom to low-intensity light fields, much of the complicated and beautiful machinery of QED can be avoided [31]. There is no need for constructing a Lorentz invariant description of the matter, for instance. (Here, I also neglect spins.) The focus of this chapter is quite opposite from the physics tradition I have been entrenched in: to understand the light-matter coupling in large molecular systems involving many degrees of freedom. I briefly introduce the idea behind the quantization of light-matter interaction [32].

The classical electrodynamics is characterized by Maxwell's equations, and the effect of electric and magnetic fields to charged particles by Lorentz force [33, 34]. If point-like particles of charge e_i and mass m_i are subjected to an electromagnetic field, their positions \mathbf{q}_i obey the equation of motion

$$m_i \dot{\mathbf{q}}_i = e_i \mathbf{E}(\mathbf{q}_i, t) + e_i \dot{\mathbf{q}}_i \times \mathbf{B}(\mathbf{q}_i, t), \quad (2.1)$$

presuming that the electric field \mathbf{E} and the magnetic field strength \mathbf{B} are independent of the velocity of the particle (or, in other words, neglecting classical renormalization of fields).

Next, the electric and magnetic fields can be simplified and partially unified. Consider the Gauss law for magnetism and the Maxwell–Faraday equation,

$$\nabla \cdot \mathbf{B} = 0 \quad \text{and} \quad \nabla \times \mathbf{E} = -\frac{\partial \mathbf{B}}{\partial t}, \quad (2.2)$$

respectively. It immediately follows that $\mathbf{B} = \nabla \times \mathbf{A}$ satisfies the first equation. The electric field must then be $\mathbf{E} = -\partial \mathbf{A} / \partial t - \nabla \phi$ in order to satisfy the second equation. The quantity ϕ is often called scalar potential and \mathbf{A} vector potential. It is important to note that these potentials are not physical but rather a mathematical tool, called *gauge fields*. This is reflected in the fact that the potentials can be transformed according to $\mathbf{A} \rightarrow \mathbf{A} - \nabla f$ and $\phi \rightarrow \phi + \partial f / \partial t$ for an arbitrary scalar function f without changing the physical electric and magnetic fields.

With the renewed definitions of the electric and magnetic field in terms of the vector and scalar potential it is possible to derive the energy contained within the coupling. This means dwelling into Lagrangian and Hamiltonian formalism of classical mechanics [35]. First, the Lagrange function L can be deduced by matching the associated Euler–Lagrange equation to Eq. (2.1). This gives

$$L = \sum_i \left[\frac{1}{2} m_i \dot{\mathbf{q}}_i^2 + e_i \dot{\mathbf{q}}_i \cdot \mathbf{A}_i - e_i \phi_i \right] + L_{EM}, \quad (2.3)$$

where L_{EM} is an electromagnetic Lagrange function independent of the positions \mathbf{q}_i , while the potentials are evaluated at these positions, $\phi_i \equiv \phi(\mathbf{q}_i, t)$ and $\mathbf{A}_i \equiv \mathbf{A}(\mathbf{q}_i, t)$. Finding the Hamilton function is then a matter of using the Legendre transformation. The canonical momenta \mathbf{p}_i are modified by the coupling and, in this case, read as $\mathbf{p}_i = \partial L / \partial \dot{\mathbf{q}}_i = m_i \dot{\mathbf{q}}_i + e_i \mathbf{A}_i$. We arrive at the typical starting point of the discussions on light–matter coupling [32], the minimal coupling Hamiltonian H for a collection of point-like particles

$$H = \sum_i \left[\frac{(\mathbf{p}_i - e_i \mathbf{A}_i)^2}{2m_i} + e_i \phi_i \right] + H_{EM}. \quad (2.4)$$

This result is often highlighted as obeying the principle of minimal substitution, i.e., we only had to change $\mathbf{p}_i \rightarrow \mathbf{p}_i - e_i \mathbf{A}_i$. One should note that the particles feel the vector and scalar potentials only locally.

In the low-energy theory, the gauge freedom of the vector and scalar potentials can be used advantageously to choose a gauge which gives the easiest frame to work in. There are two common choices: the Coulomb gauge and the dipole gauge. Here, I first discuss the Coulomb gauge while the dipole gauge is derived in the quantum description.

In the Coulomb gauge, the vector potential is chosen so that $\nabla \cdot \mathbf{A} = 0$ holds. Thus, $\nabla \cdot \mathbf{E} = -\nabla^2 \phi$. The Gauss law in this gauge gives

$$\nabla \cdot \mathbf{E} = -\nabla^2 \phi = \rho / \epsilon_0, \quad (2.5)$$

where ρ is the charge density and ϵ_0 the vacuum permittivity. The solution to this Poisson equation for point-like charges $\rho = \sum_i e_i \delta(\mathbf{q} - \mathbf{q}_i)$ is the Coulomb potential $\phi(\mathbf{q}) = \sum_i e_i / (4\pi\epsilon_0 |\mathbf{q} - \mathbf{q}_i|)$, explaining the name of the gauge. Thus, it is physically reasonable to denote $\sum_i e_i \phi_i = V(\{\mathbf{q}_i\})$ and treat it as a molecular or atomic potential.

The remaining Maxwell's equation, Ampère–Maxwell equation,

$$\nabla \times \mathbf{B} = \mu_0 \mathbf{J} + \mu_0 \epsilon_0 \frac{\partial \mathbf{E}}{\partial t}, \quad (2.6)$$

allows for fixing the vector potential \mathbf{A} . Here, \mathbf{J} is the charge current and μ_0 is the vacuum permeability. It gives a wave equation that reads as

$$\nabla^2 \mathbf{A} - \frac{1}{\mu_0 \epsilon_0} \frac{\partial^2 \mathbf{A}}{\partial t^2} = -\mu_0 \mathbf{J} - \frac{1}{\mu_0 \epsilon_0} \nabla \frac{\partial \phi}{\partial t}. \quad (2.7)$$

Since the Coulomb gauge fixes $\nabla \cdot \mathbf{A} = 0$, it is possible to replace the right-hand side with the component J_0 of the current obeying $\nabla \cdot \mathbf{J}_0 = 0$. Without charges, we see the historically important result that light is an electromagnetic wave traveling in vacuum. Thus, $c = 1/\sqrt{\mu_0 \epsilon_0}$ is the speed of light. It is the foundation of quantization in the non-relativistic theory as well, since the effect of moving charges is often neglected. Here, it corresponds to a mental image of almost-stationary charges in molecules, for instance.

The energy of the electromagnetic field can be derived from the Euler–Lagrange equation which should match the Maxwell's equations. This gives for the Hamiltonian, in terms of the electric and magnetic field,

$$H_{EM} = \frac{1}{2} \epsilon_0 \int d^3 \mathbf{q} \left(\mathbf{E}^2 + c^2 \mathbf{B}^2 \right). \quad (2.8)$$

The integration is taken over the whole space of the fields.

The quantization of the molecular system is straightforward as it is enough to promote the canonical coordinates to operators with the commutation relation $[q_i, p_j] = i\delta_{ij}$. A much more complicated issue is the quantization of electromagnetic modes because of the wide range of possible systems. Here, postponing the discussion of realistic systems, I assume an empty cubic box of volume \mathcal{V} with ideally reflecting bounding surfaces. In the absence of any moving charges, the

electromagnetic modes inside the box obey the wave equation (2.7) and it can be solved in the Fourier space. The quantization process can be framed in the typical way of finding canonical coordinates and setting up the commutation relations. However, it is more conventional and often useful to use dimensionless bosonic operators instead. I omit these steps here. The vector potential can be written in terms of a wave vector \mathbf{k} and two orthogonal unit polarization vectors $\boldsymbol{\varepsilon}_\lambda$ ($\mathbf{k} \cdot \boldsymbol{\varepsilon}_\lambda = 0$ and $\boldsymbol{\varepsilon}_\lambda \cdot \boldsymbol{\varepsilon}_{\lambda'} = \delta_{\lambda\lambda'}$) as

$$\mathbf{A}(\mathbf{q}, t) = \sum_{\mathbf{k}} \sum_{\lambda} \boldsymbol{\varepsilon}_\lambda \sqrt{\frac{1}{2\varepsilon_0\omega_{\mathbf{k}}\mathcal{V}}} \left[a_{\mathbf{k}\lambda} e^{i(\mathbf{k}\cdot\mathbf{q}-\omega_{\mathbf{k}}t)} + a_{\mathbf{k}\lambda}^\dagger e^{-i(\mathbf{k}\cdot\mathbf{q}-\omega_{\mathbf{k}}t)} \right], \quad (2.9)$$

where $[a_{\mathbf{k}\lambda}, a_{\mathbf{k}'\lambda'}^\dagger] = \delta_{\mathbf{k}\mathbf{k}'}\delta_{\lambda\lambda'}$. In empty space, the dispersion relation between the frequency $\omega_{\mathbf{k}}$ and the wave vector \mathbf{k} is found to be simply $\omega_{\mathbf{k}} = c|\mathbf{k}|$. Inserting the quantized vector potential to the Hamiltonian leads to, after a relatively long calculation,

$$H_{EM} = \sum_{\lambda, \mathbf{k}} \omega_{\mathbf{k}} \left(a_{\mathbf{k}\lambda}^\dagger a_{\mathbf{k}\lambda} + \frac{1}{2} \right). \quad (2.10)$$

Here, the polarization plays no other role than providing two copies of the electromagnetic mode. More generally, the frequency $\omega_{\mathbf{k}}$ may depend on it.

In principle, it seems I am done. I have presented the quantized form of the vector potential and the electromagnetic Hamiltonian which can be inserted to the Hamiltonian in Eq. (2.4). However, the resulting expression is difficult to use. The vector potential in the light-matter coupling can be further simplified by physical reasoning. If the charge system is smaller than the wavelength of the light, an atom or a molecule for instance, the wave functions change appreciably on a size scale that is much smaller than the wavelength $2\pi/|\mathbf{k}|$. Thus, the evidently quantum mechanical factor $e^{i\mathbf{k}\cdot\mathbf{q}}$ can be replaced by a classical value $e^{i\mathbf{k}\cdot\mathbf{r}_i}$, where \mathbf{r}_i denotes the approximative position of the charge system. This is known as *the dipole approximation*.

A conventional form of the light-matter Hamiltonian is obtained when the many-charge system is represented by energy eigenstates without radiation. Let us assume that there are identical and distinguishable copies of the same system, mental image being atoms or molecules, which are labelled by the subscript n . I assume here that the Coulomb interaction between the different systems can be neglected. Furthermore, I do not include the term proportional to A^2 in Eq. (2.4) assuming that it is negligibly small. When the light-induced modification to energies is small, it appears as a reasonable assumption. If $c_{n\nu}^\dagger$ generates an excitation of energy $E_{n\nu}$ to the charge system n , then the Hamiltonian reads as

$$H = H_{EM} + \sum_{n,\nu} E_{n\nu} c_{n\nu}^\dagger c_{n\nu} + \sum_{\lambda, \mathbf{k}} \sum_{n,\nu,\mu} \left(g_{n,\mathbf{k}\lambda,\nu\mu} a_{\mathbf{k}\lambda} + g_{n,\mathbf{k}\lambda,\nu\mu}^* a_{\mathbf{k}\lambda}^\dagger \right) c_{n\nu}^\dagger c_{n\mu}, \quad (2.11)$$

where the light-matter coupling constant is

$$g_{n,\mathbf{k}\lambda,\nu\mu} = i(E_{n\mu} - E_{n\nu}) \sqrt{\frac{1}{2\varepsilon_0\omega_{\mathbf{k}}\mathcal{V}}} (\boldsymbol{\varepsilon}_\lambda \cdot \mathbf{d}_{n,\nu\mu}) e^{i\mathbf{k}\cdot\mathbf{r}_n}. \quad (2.12)$$

Here, $\mathbf{d}_{n,\nu\mu}$ is the dipole moment of the system n projected to the energy eigenstates $|\psi_{n\nu}\rangle$, defined as $\mathbf{d}_{n,\nu\mu} = \langle \psi_{n\nu} | \sum_{i \in n} e_i \mathbf{q}_i | \psi_{n\mu} \rangle$.

This is the intellectual foundation on which [I], [II], [IV], and [V] is based. The light-matter interaction is now quantized, and the interpretation is clear: it is possible for the matter, the charge system, to get excited by the absorption of a photon or to relax by emitting one. Evidently, this is a low-energy limit of QED as it is straightforward to imagine processes which employ several photons. If there is no energy transfer, the coupling vanishes. The coupling constant (2.12) itself depends both on the zero-point fluctuations of the electromagnetic field (through the square root term) as well as on the direction of the transition dipole moment $\mathbf{d}_{n,\nu\mu}$ with respect to the polarization vector $\boldsymbol{\varepsilon}_\lambda$ and the position of the system \mathbf{r}_n within the field. These latter findings hold only in the dipole approximation.

The dipole gauge presents another useful choice for calculations regarding light-matter interaction. It more directly shows that it is indeed the dipole moment that couples to the electromagnetic field, regardless of what the underlying degrees of freedom within the dipole moment are. The dipole gauge can be derived from the Coulomb gauge by the so-called Power–Zienau–Woolley gauge transformation [36, 37]. It requires the dipole approximation together with a long-wavelength assumption. That is, it is assumed that $\mathbf{k} \cdot \mathbf{r}_n$ is constant for all systems and the vector potential is fully independent of the positions $A(\mathbf{q}) \equiv A(0)$. In the quantum formulation, it is a unitary transformation, defined by $U = \exp[i\mathbf{d} \cdot A(0)]$ where $\mathbf{d} = \sum_i e_i \mathbf{q}_i$ is the total dipole moment operator [38, 39]. Since $A(0)$ commutes with \mathbf{q}_i and \mathbf{p}_i , the transformation on Eq. (2.4) gives

$$H_{PZW} = UHU^\dagger = H_{EM} + \sum_i \frac{\mathbf{p}_i^2}{2m_i} + V(\{\mathbf{q}_i\}) - \mathbf{d} \cdot \mathbf{E} + \sum_{k\lambda} \frac{1}{2\epsilon_0 \mathcal{V}} (\boldsymbol{\varepsilon}_\lambda \cdot \mathbf{d})^2. \quad (2.13)$$

Here, $\mathbf{E} = -\partial A(0)/\partial t$. This expression is particularly useful for semiclassical analysis because the dipole moment can be directly specified as $\mathbf{d} = \mathbf{d}(\{\mathbf{q}_i\})$. There is no reference to any energy states as in the Coulomb gauge. Moreover, one can associate the dipole moment \mathbf{d} to an electronic or vibrational mode of a molecule. Here, by vibrational I refer to nuclear motion within the molecule. The price to pay for this description is the dipole self-energy term proportional to $(\boldsymbol{\varepsilon}_\lambda \cdot \mathbf{d})^2$. It appears formally divergent, only renormalized by restricting the number of photon modes. Note that the dipole self-energy is second order in the zero-point fluctuations of the electromagnetic field and, in this sense, small compared to the dipole interaction $\mathbf{d} \cdot \mathbf{E}$.

The long-wavelength assumption is crucial to the derivation of the dipole-gauge Hamiltonian. If there is position dependence in the form of phase factors, the vector potentials at different positions do not commute. When one generalizes the transformation for multiple dipole moments at different positions as $U = \exp[i \sum_n \mathbf{d}_n \cdot A_n]$, the dipole interaction follows as $\sum_n \mathbf{d}_n \cdot \mathbf{E}_n$. However, there is a wide variety of terms that are second order in the zero-point fluctuations. One should be able to neglect them if the fluctuations are small enough. This line of thinking is present in [IV] and in [V].

The derivation of light-matter coupling I presented provides a nice physical picture of photon exchange but there are a few issues when applied to physical

systems. They are something to be aware of.

First, the choice of gauge should not matter as the vector potential A is not an observable. But it does when further assumptions are made. Gauge issues especially arise when the matter Hamiltonian is further approximated to only a handful of energy levels (i.e., the Hilbert space is truncated) in the context of very strong light-matter coupling. For instance, the energy spacing between levels in the hybrid system and the number of emitted photons may then depend on the gauge unless it is specifically accounted for [40–42]. Furthermore, the exclusion of the second-order term, A^2 in the Coulomb gauge and $(\epsilon_\lambda \cdot \mathbf{d})^2$ in the dipole gauge, has some unphysical theoretical consequences. It removes gauge invariance but also may break coordinate invariance even if the long-wavelength limit $\mathbf{k} \rightarrow 0$ is taken, lead to a radiating ground state, and destroy bound states [43, 44]. For this reason, the dipole gauge may appear more favourable as the calculation of the dipole self-energy term $(\epsilon_\lambda \cdot \mathbf{d})^2$ can be more straightforward than including A^2 . (If A contained only a single mode, then A^2 can be dealt with by redefining the bosonic operator $a_{\mathbf{k},\lambda}$ so that it corresponds to neglecting A^2 outright.)

Second, not all electromagnetic fields are well described within an empty box of volume \mathcal{V} with ideally reflecting surfaces. In fact, few are. The mental image in the derivation is that of optical cavities. However, the mirrors forming an optical cavity are never ideally reflecting but, rather, photons in the cavity escape to their electromagnetic environment. This poses a problem: how to make sure that the correspondence principle holds and that the quantization procedure works when the classical system should already be treated as an open system? In the case of electromagnetism, one of the solutions is the introduction of classical quasi-normal modes [45]. This is intimately connected with the definition and magnitude of the effective mode volume \mathcal{V}_{eff} of a confined light mode that should replace the quantization volume \mathcal{V} in the light-matter coupling constant (2.12). Smaller the mode volume \mathcal{V}_{eff} , larger the light-matter coupling. It has led to a considerable search for as small \mathcal{V}_{eff} as possible [46, 47].

Lastly, there is a wide range of metallic and dielectric systems that can support electromagnetic resonances. Common examples are plasmon and surface-plasmon-polariton (SPP) excitations. They are a consequence of oscillations of electrons in the metal. SPPs form specifically at a metal-dielectric interface. The focus of [I] is on the light-matter coupling between molecules and SPPs. The description in terms of classical electrodynamics is changed which then adds to quantization considerations. (The quantization of SPPs is discussed in [48], for instance.) Fundamentally, the light-matter coupling can still be described in the form of the Hamiltonian (2.11) but with different mode volume \mathcal{V}_{eff} , polarization ϵ_λ , and dispersion relation $\omega_{\mathbf{k}} = \omega(\mathbf{k})$.

2.2 Jaynes–Cummings model and its extensions

Let us then focus on relatively straightforward Hamiltonians that follow from the general expression (2.11). There is a rich history for such models [49–51].

First, consider a single degree of freedom described by a two-level system, e.g., an electronic excitation of a single atom. If the energy spacing of the electronic

ground and excited state matches, for instance, the fundamental frequency of an optical cavity, the higher order electromagnetic modes can be neglected to a good approximation. In this case, the Hamiltonian (2.11) may be simplified to

$$H = \omega_0 \sigma^\dagger \sigma + \omega_c a^\dagger a + (ga + g^* a^\dagger) (\sigma + \sigma^\dagger). \quad (2.14)$$

In this expression, σ (σ^\dagger) refers to the annihilation (creation) operator of the excitation in the two-level system. This is often called the Dicke model [49]. Here, it is more of a starting point than the point of interest.

It makes sense to modify the Dicke model because working with it is cumbersome. Physically, there is a clear motivation: if the two-level system and the cavity are on resonance and $\omega_c = \omega_0$ holds, then the terms σa and $\sigma^\dagger a^\dagger$ in the Hamiltonian change the energy by $2\omega_0$ whereas the other terms retain the value of energy. This can be seen also by moving to the interaction frame with the unitary transformation $U = \exp[i(\omega_0 \sigma^\dagger \sigma + \omega_c a^\dagger a)t]$. One can show that $U^\dagger a U = a e^{i\omega_c t}$ and $U^\dagger \sigma U = \sigma e^{i\omega_0 t}$. Consequently, on resonance, the interaction term $U^\dagger \sigma a U = \sigma a e^{i2\omega_0 t}$ rotates very fast compared to $U^\dagger \sigma^\dagger a U = \sigma^\dagger a$. The often-used argument is that the exponential averages out over time. Thus, *the rotating-wave approximation* neglects these oscillatory terms [32]. The approximation however breaks down at very strong couplings g [52].

A prototypical light-matter model obtained from the Dicke model by rotating-wave approximation is called the Jaynes–Cummings model [50]. Its Hamiltonian reads as

$$H_{JC} = \omega_0 \sigma^\dagger \sigma + \omega_c a^\dagger a + g \sigma^\dagger a + g^* a^\dagger \sigma. \quad (2.15)$$

Now, the total number of excitations is preserved as $[H_{JC}, \sigma^\dagger \sigma + a^\dagger a] = 0$. Thus, the two systems, the molecule and the cavity, simply interchange excitations at a rate g . It should be recalled that the eigenfrequencies ω_0 and ω_c are here assumed to be in close proximity of one another.

Finally, after all these steps, I can specify polaritons more concretely. They are the excited eigenstates or the excitations of the Jaynes–Cummings Hamiltonian. Since the number of excitations is a constant, one can deduce that there are an infinite amount of subspaces based on the number n of cavity photons. For each subspace, there are two relevant states: $|n+1, g\rangle$ and $|n, e\rangle$, where g (e) refers to the ground (excited) state of the molecule. An exception is the true ground state $|0, g\rangle$ which forms a subspace of its own. I write the operation of the Hamiltonian to the n -photon subspace states in a matrix form as

$$\begin{pmatrix} H_{JC} |n+1, g\rangle \\ H_{JC} |n, e\rangle \end{pmatrix} = \begin{pmatrix} (n+1)\omega_c & g\sqrt{n+1} \\ g^*\sqrt{n+1} & n\omega_c + \omega_0 \end{pmatrix} \begin{pmatrix} |n+1, g\rangle \\ |n, e\rangle \end{pmatrix} \equiv \mathcal{H}_n \begin{pmatrix} |n+1, g\rangle \\ |n, e\rangle \end{pmatrix}. \quad (2.16)$$

The diagonalization of the coefficient matrix \mathcal{H}_n gives the polaritonic states, which now hybridize the two states in play, and gives the two eigenenergies

$$E_\pm(n) = n\omega_c + \frac{\omega_c + \omega_0}{2} \pm \sqrt{(n+1)|g|^2 + (\omega_0 - \omega_c)^2/4}. \quad (2.17)$$

In this thesis, my focus is on the single-excitation subspace with $n = 0$ since it is the lowest energy subspace, relevant for many experiments. The cavity is in the electromagnetic vacuum state or it contains a single photon. On resonance, $\omega_c = \omega_0$, the energy level splitting between the polariton states is the smallest but the levels are still separated by

$$\Omega = 2|g|, \quad (2.18)$$

which is called the vacuum Rabi splitting [32]. (Sometimes, it is denoted by R and, often, “vacuum” is omitted.) Moreover, the higher (lower) energy polariton state is referred as the upper (lower) polariton in short.

Note that the coefficient matrix \mathcal{H}_0 [as defined in Eq. (2.16) with $n = 0$] serves also to define the original Jaynes–Cummings Hamiltonian. I write it in a quadratic form as

$$H_{JC} = \begin{pmatrix} a^\dagger & \sigma^\dagger \end{pmatrix} \mathcal{H}_0 \begin{pmatrix} a \\ \sigma \end{pmatrix}. \quad (2.19)$$

It is now evident that it does not matter for the lowest energy subspace whether σ is a ladder operator of a two-level system or a harmonic oscillator. It is expected.

A straightforward but important extension of the Jaynes–Cummings model is N identical systems coupled to a single cavity mode. It is often called the Tavis–Cummings model [51]. With the lessons learned, I directly write it in a matrix presentation as

$$H_{TC} = \begin{pmatrix} a^\dagger & \sigma_1^\dagger & \dots & \sigma_N^\dagger \end{pmatrix} \begin{pmatrix} \omega_c & g_1 & g_2 & \dots & g_N \\ g_1^* & \omega_0 & 0 & \dots & 0 \\ g_2^* & 0 & \omega_0 & \ddots & \vdots \\ \vdots & \vdots & \ddots & \ddots & 0 \\ g_N^* & 0 & \dots & 0 & \omega_0 \end{pmatrix} \begin{pmatrix} a \\ \sigma_1 \\ \vdots \\ \sigma_N \end{pmatrix}. \quad (2.20)$$

The solution of the eigenvectors is not straightforward anymore but the eigenvalues can be solved analytically from the $(N + 1)$ -dimensional coefficient matrix \mathcal{H}_0 .¹ The polariton eigenenergies are

$$E_{\pm} = \frac{\omega_c + \omega_0}{2} \pm \sqrt{\sum_{i=1}^N |g_i|^2 + (\omega_0 - \omega_c)^2/4}, \quad (2.21)$$

while there are $N - 1$ states of energy ω_0 . This is visualized in Fig. 1(a). Comparing to the Jaynes–Cummings eigenenergies (2.17), $|g|^2$ has been replaced by $N \langle |g|^2 \rangle$ where $\langle \cdot \rangle$ represents the arithmetic average over N couplings (i.e., $\langle |g|^2 \rangle = \sum_{i=1}^N |g_i|^2 / N$). Consequently, the vacuum Rabi splitting is $\Omega = 2\sqrt{N} \sqrt{\langle |g|^2 \rangle}$.

The Tavis–Cummings model provides important insight to many experiments in the field of polaritons. The fact that the Rabi splitting $\Omega \propto \sqrt{N}$ can be enhanced

¹If $D(N) = \det(\mathcal{H}_0)$ for N systems so that $D(1) = \omega_0\omega_c - |g_1|^2$, then one can derive and use the recursion relation $D(N) = \omega_0 D(N-1) - |g_N|^2 \omega_0^{N-1}$ for $N \geq 2$ to find the eigenvalues.

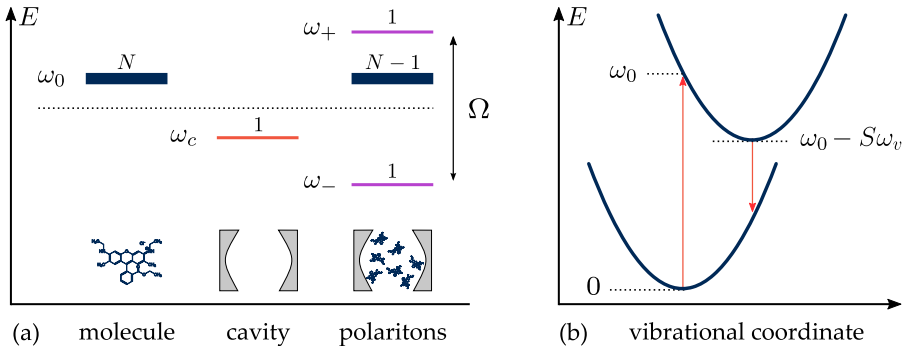


FIGURE 1: (a) Eigenenergies and associated degeneracies of the Tavis–Cummings model. (b) Potential energy diagram associated with molecules in the Holstein–Tavis–Cummings model.

by adding more and more molecules makes the experimental observation of polaritons feasible. Since in many cases the individual couplings are very weak, it is enough increase the concentration of the molecules within the cavity to enhance the total coupling. However, as becomes relevant in the next chapter, it also means that there are many more states at the unperturbed molecular energy ω_0 (when $N - 1 \gg 2$). These states do not have any photonic component but rather they are superpositions over molecular states [53, 54]. They also turn out to be optically invisible as shown in the next section. Thus, these states are often called dark states or exciton reservoir in polaritonics literature.

Finally, to end this section, I shortly discuss the model in [I] and [II]. Its motivation is to describe a cavity and organic molecules with an electronic excitation but also vibrational states. These two molecular degrees of freedom may be coupled. It causes *Stokes shift*: the absorption and fluorescence frequency of molecules need not be the same. The energy that excites the molecule goes partially to the vibrational modes, to the generation of phonons. The simplest model Hamiltonian that captures this effect adds to the Tavis–Cummings Hamiltonian a vibrational mode of frequency ω_v for each two-level system [55]. Hence, one more name needs to be added to the model. It is now called the Holstein–Tavis–Cummings model and it reads as

$$H_{HTC} = H_{TC} + \sum_{i=1}^N \left[\omega_v b_i^\dagger b_i + \sqrt{S} \omega_v \sigma_i^\dagger \sigma_i (b_i + b_i^\dagger) \right]. \quad (2.22)$$

The coupling between vibrations and electronic states is characterized, for historical reasons, by the dimensionless Huang–Rhys factor S [56]. More generally, one can add multiple vibration modes, each with different Huang–Rhys factors.

The molecular part in the Holstein–Tavis–Cummings model corresponds to the picture originally thought of by Franck and Condon [57, 58]. Writing vibrational part in terms of quadrature operators $q = (b + b^\dagger) / \sqrt{2}$ shows that the vibrational ground state in the electronic excited state is shifted by \sqrt{S} compared to the electronic ground state. The picture in the eigenspace of the vibrational coordinate q is thus that of two displaced harmonic oscillators, as in Fig. 1(b). Stokes shift follows

when the electronic excitation is fast compared to vibrational motion, $\omega_0 \gg \omega_v$, and its lifetime long compared to the time scale of vibrational relaxation. That is, the decay rate of the electronic excitation κ_m is much smaller than the decay rate of phonons γ , or $\kappa_m \ll \gamma$. The most likely electronic transitions are then those that do not involve changes in the vibrational state represented by up- and downward arrows in Fig. 1(b).

2.3 Role of dissipation

In polaritonics, one talks about weak, strong and ultrastrong coupling to categorize the effects of light-matter coupling. In the previous section, there is however only a single dimensionless parameter, Ω/ω_0 , determining the strength of the coupling. Realistically, the light and the matter interact with their environment leading to dissipation, which is intimately related to finite linewidths in the optical spectrum. This gives rise to another parameter relating the polaritonic linewidth Γ to the total coupling Ω as Ω/Γ . Now, one can identify a regime as weak coupling if Ω/ω_0 and Ω/Γ are small whereas ultrastrong-coupling regime is characterized by a large fraction Ω/ω_0 at which point the assumptions of the low-energy light-matter interaction start to break down [52]. Strong-coupling regime lies between the two. One can then ask: What is the polaritonic linewidth Γ in terms of the dissipation rates of the individual systems? Does dissipation affect the optically observed Rabi splitting?

The exact answers to these questions depend on the models used. They are answered, in my opinion, in a physically reasonable and pleasing way with the input-output formalism. I introduce the important ideas by an example calculation by starting from the literature results and then modifying them based on the physical setup.

Input-output theory of quantum optics refers to a form of scattering theory. It can be derived in the typical open quantum system scheme of defining the quantum system of interest, the environment, and the interaction between the two [22]. Specifically, it is assumed that, for a system operator a and bosonic environment operators b_k , the interaction resembles the rotating wave approximated form $\sum_k \lambda_k (b_k^\dagger a + a^\dagger b_k)$ with some coupling constants λ_k . I omit the derivation here — see e.g. [59]. Importantly, the derivation is done within the Heisenberg picture of time-dependent operators. The input and output fields are defined in terms of the environment operators and connected by the system. In terms of the system's dynamics, the input field may be seen as external noise on the system while there is also an associated dissipative term. The dynamical equation of the system could be called quantum Langevin equation in this point of view. When the input field is specified with certain correlations, the input-output formalism is equivalent with the quantum master equation for the density matrix in the Lindblad form (or Gorini–Kossakowski–Sudarshan–Lindblad equation) providing a Markovian description of the open quantum system dynamics [59].

Let us then consider an optical cavity which encloses N molecules. Suppose this system is well described by the Tavis–Cummings model in the single-excitation subspace. That is, I treat the operators σ_j in Eq. (2.20) as obeying the bosonic

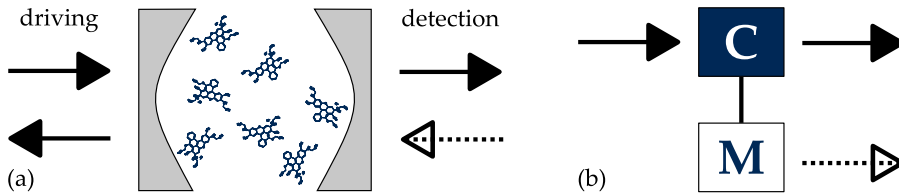


FIGURE 2: Schematic input-output pictures. (a) Cavity containing molecules probed by incoming light (driving) and reflected back; part of the light is emitted to the other side (detection). The fluctuations from the detection side, depicted by the dashed arrow, are neglected. (b) The important fields in the example calculation: Specifically, cavity (C) is driven and it mediates the emission as well. It is coupled to molecules (M) whose direct fluorescence is neglected.

commutation relations $[\sigma_i, \sigma_j^\dagger] \approx \delta_{ij}$. The polaritonic system is probed through the cavity by driving it with laser light. One can then measure either the reflected or the transmitted light. For simplicity, I assume that the transmitted light does not interfere with the driving laser but is really due to cavity leakage. There are two sets of environmental modes for the cavity: one set allows for the driving and reflection and the other set allows for the transmission. These are physically separated by the cavity as in Fig. 2.

The equations of the motion in the input-output formalism are

$$\dot{a} = -i\omega_c a - i \sum_j g_j^* \sigma_j - \frac{\kappa}{2} a - \sqrt{\kappa} a_{\text{in}}, \quad (2.23a)$$

$$\dot{\sigma}_j = -i\omega_m \sigma_j - i g_j a - \frac{\kappa_m}{2} \sigma_j - \sqrt{\kappa_m} \sigma_{\text{in},j}. \quad (2.23b)$$

Here, κ and κ_m are the dissipation rates for the cavity and the molecules, respectively. I assume here that every mode has an associated and separate bath — the possibility of transferring energy or information through a common bath is neglected — but all molecules are similarly coupled to their own baths.

Next, one can divide the input operators based on the environmental modes. The cavity input operator a_{in} separates into contributions from the driving and thermal fluctuations. Thus, I denote $\sqrt{\kappa} a_{\text{in}} = \sqrt{\kappa_{\text{ext}}} a_{\text{in}}^d + \sqrt{\kappa_{\text{int}}} a_{\text{in}}^{\text{th}}$. The drive couples to the system with the rate κ_{ext} whereas the thermal fluctuations couple with κ_{int} . In total, $\kappa_{\text{ext}} + \kappa_{\text{int}} = \kappa$.

A typical quantum optical description of fluctuations (so-called white noise approximation) is achieved by setting $\langle a_{\text{in}}^{\text{th}}(t) \rangle = 0$ and $\langle a_{\text{in}}^{\text{th}\dagger}(t) a_{\text{in}}^{\text{th}}(t') \rangle = n_{\text{th}} \delta(t - t')$, where n_{th} is the number of thermal photons at the cavity frequency ω_c . Since in the optical regime ω_c is much larger than the typical temperature scales, I approximate $n_{\text{th}} \approx 0$ here. Since the input-output equations (2.23) are linear, one can effectively forget about the thermal input operator $a_{\text{in}}^{\text{th}}$. The same holds for the molecule operators $\sigma_{\text{in},j}$ as I assume that the molecules and the cavity are nearly resonant, $\omega_0 \approx \omega_c$. I omit the thermal input operators from the notation.

Formally, input operators depend on the environmental states in the past. In the same vein, output operators describe the present in terms of the future. These operators are then connected by the system in the present through input-output

relations

$$a_{\text{out}}(t) - a_{\text{in}}(t) = \sqrt{\kappa}a(t) \quad \text{and} \quad \sigma_{j,\text{out}}(t) - \sigma_{j,\text{in}}(t) = \sqrt{\kappa_m}\sigma_j(t). \quad (2.24)$$

Here, I want to emphasize that these relations provide a “scattering” picture that is independent of any detectors or such — they really tell only about causality. We then assign to the cavity output operator a_{out}^d the meaning that it describes really those fields that connect to the detectors. Further taking into account that there are two sides to the cavity, I write for the cavity instead

$$a_{\text{out}}^R - a_{\text{in}}^d = \sqrt{\kappa_{\text{ext}}^R}a \quad \text{and} \quad a_{\text{out}}^T = \sqrt{\kappa_{\text{ext}}^T}a, \quad (2.25)$$

where now $\kappa_{\text{ext}}^{R/T}$ describe the coupling rate to the detectors of the reflected and transmitted signal. The assumption about the drive and the transmitted radiation not interfering is encoded by disregarding the input term in the latter equation.

In this dissertation, I focus on measurements which probe the stationary response of the system. (As a theoretical tool, input-output formalism works also for investigating time-dependent response.) A natural observable in this case is the transmitted power spectral density [60] which is given by

$$S^T(\omega) = \frac{1}{2\pi} \int d\tau e^{i\omega\tau} \langle a_{\text{out}}^{T\dagger}(t)a_{\text{out}}^T(t+\tau) \rangle, \quad (2.26)$$

where t can be set to zero due to stationarity. In short, I call this quantity the (optical) spectrum. A similar quantity can be devised for the reflected power as well as the driving power.

We have all the tools to calculate the spectrum of the Tavis–Cummings polariton system. First, note how useful working in Fourier space is for this problem: the spectrum is a Fourier transform of the autocorrelation function and the linearity of the equations of motion (2.23) allow for a straightforward calculation. In Fourier space²,

$$a(\omega) = \frac{1}{i(\omega - \omega_c) - \kappa/2} \left[i \sum_j g_j^* \sigma_j(\omega) + \sqrt{\kappa_{\text{ext}}} a_{\text{in}}^d(\omega) \right], \quad (2.27a)$$

$$\sigma_j(\omega) = \frac{ig_j}{i(\omega - \omega_0) - \kappa_m/2} a(\omega). \quad (2.27b)$$

These expressions gather all the definitions and approximations made so far. They allow solving the cavity operator $a(\omega)$ in terms of the driving field $a_{\text{in}}^d(\omega)$. They are linearly related in Fourier space as $a(\omega) = r(\omega)a_{\text{in}}^d(\omega)$. If we assume a classical monochromatic drive of frequency ω_d so that $a_{\text{in}}^d(\omega) = \alpha\delta(\omega - \omega_d)$, the spectrum can be resolved to be

$$S^T(\omega) = \int d\omega' \langle a_{\text{out}}^{T\dagger}(\omega')a_{\text{out}}^T(\omega) \rangle \quad (2.28)$$

$$= |\alpha|^2 \kappa_{\text{ext}}^T |r(\omega)|^2 \delta(\omega - \omega_d), \quad (2.29)$$

²Here, I choose the convention that the Fourier transform of a function $f(t)$ is given by $f(\omega) = \frac{1}{2\pi} \int dt e^{i\omega t} f(t)$. It implies that the inverse transformation $f(t) = \int d\omega e^{-i\omega t} f(\omega)$. Furthermore, the Fourier transformation of df/dt becomes $-i\omega f(\omega)$. I denote $f^\dagger(\omega)$ as the Fourier transform of $f^\dagger(t)$.

where the essence of the polaritonic spectrum is contained in the function

$$r(\omega) = \frac{\sqrt{\kappa_{\text{ext}}}}{i(\omega - \omega_c) - \kappa/2 + \frac{\sum_j |g_j|^2}{i(\omega - \omega_0) - \kappa_m/2}}. \quad (2.30)$$

It is also important to note that the response under monochromatic drive is equally monochromatic. There are no inelastic processes included in this model of a cavity that could modify the frequency.

Let us quickly analyze the polaritonic spectrum, i.e., focus on the function $r(\omega)$. There are four important parameters: the detuning $\omega_c - \omega_0$, the dissipation rates κ and κ_m and the total coupling $\sum_j |g_j|^2 = N \langle |g|^2 \rangle$. If $\kappa = \kappa_m = 0$ is taken, the response $r(\omega)$ diverges at the Tavis–Cummings polariton frequencies (2.21). The response vanishes at ω_0 which explicitly shows that the other $N - 1$ eigenstates are indeed dark. For so small dissipation rates that the polariton frequencies ω_{\pm} are hardly modified, the response function on resonance $\omega_0 = \omega_c$ simplifies near these polariton frequencies to

$$|r(\omega)|^2 \approx \frac{\kappa_{\text{ext}}/4}{(\omega - \omega_{\pm})^2 + \frac{1}{4} \left(\frac{\kappa}{2} + \frac{\kappa_m}{2} \right)^2}, \quad (2.31)$$

which shows that the polaritonic linewidth Γ is in fact just an average $(\kappa + \kappa_m)/2$. (I obtain this by calculating the first-order Taylor polynomial around ω_{\pm} of the denominator and then assuming κ, κ_m are small compared to $N \langle |g|^2 \rangle$.) In the same limit, one can also find the polariton frequencies ω_{\pm} by finding the extremal points of $|r(\omega)|^2$. On resonance $\omega_0 = \omega_c$, the result is

$$\omega_{\pm} \approx \omega_0 \pm \sqrt{N \langle |g|^2 \rangle + \kappa \kappa_m / 4}. \quad (2.32)$$

Thus, it seems that dissipation can increase the observed Rabi splitting. This of course holds only for small linewidths because, at some point, the polariton peaks should coalesce if $N \langle |g|^2 \rangle \ll \Gamma = (\kappa + \kappa_m)/2$. A few examples of polaritonic spectra are plotted in Fig. 3.

2.4 Electronic strong coupling and vibrations

As mentioned in Sec. 2.2, the Tavis–Cummings model is not necessarily a good description of all molecules. Molecular vibrations and their coupling to an electronic excitation changes the optical properties of molecules. The effect of Stokes shift on the polaritonic spectrum at first quite unclear. What is the role of the fluorescence or absorption frequency? Furthermore, vibrations have their own intricate dynamics and provide another dissipation channel.

These points are motivated by experiments. One experiment was more motivating than others for us: it was observed that the amount of Stokes shift strongly affected the light emitted from a polaritonic system [61]. There are a few different observations. First, the experiment was conducted using surface-plasmon-polaritons (SPPs) which are strongly coupled to nearby molecules. The radiative

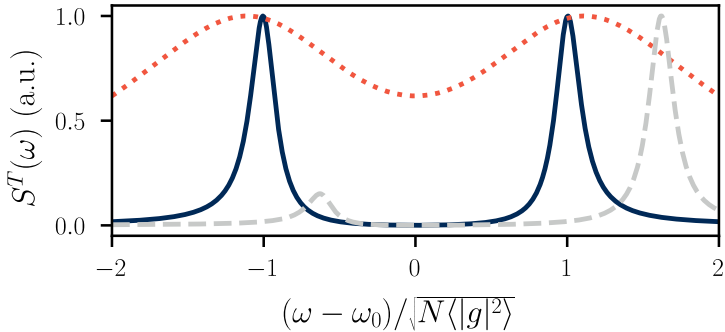


FIGURE 3: Normalized cavity emission S^T for the Tavis–Cummings model. Here, $\kappa = \kappa_m$ for simplicity. The blue solid curve and orange dotted curve have no detuning, $\omega_0 = \omega_c$, but in the former $\kappa/\sqrt{N \langle |g|^2 \rangle} = 0.2$ and in the latter $\kappa/\sqrt{N \langle |g|^2 \rangle} = 2$. The gray dashed line corresponds to the blue one except it is detuned so that $\omega_c - \omega_0 = \sqrt{N \langle |g|^2 \rangle}$.

decay of SPPs is often due to surface imperfections but, nevertheless, the emission is polarized according to a specific polarization direction set by the bare SPP. So much so that in the orthogonal polarization almost no emission is observed. This polarization dependence was changed by coupling the SPP to molecules — the emission to the orthogonal polarization became possible. Furthermore, the smaller the Stokes shift of the molecules, the more orthogonally polarized emission there was. Second, the “symmetry” of the polariton peaks on resonance was changed: the upper polariton peak intensity decreased as the Stokes shift increased.

Input-output formalism is particularly suited to model this kind of an experiment. It is natural to extend the definition of output fields to include different polarizations. The role of the polarization is also evident in the light-matter coupling as discussed in Sec. 2.1. In the case of a SPP–molecule system, the molecules can also directly emit through a thin dielectric layer they are embedded in. This is the solution we present in [I] to the question why emission is observed in both polarizations. Even though the surface-plasmon-polariton is driven, the light-matter interaction transfers energy to the molecules which can radiate it. The SPP couples only to a certain polarization but the molecules can couple to any polarization if their dipole moments are not ordered but rather point to random directions. Furthermore, we expect that the emission from the SPP and molecules is incoherent.

Let me denote the polarization in which the bare SPP emits by p and the orthogonal direction by s . The generalization of the output fields that are “transmitted”, taking into account all the above points, is

$$\Sigma_{\text{out},p}^T = \sqrt{\kappa_o^T} c + \sqrt{\kappa_m^T} \sum_j (\hat{\mathbf{d}}_j \cdot \hat{\mathbf{u}}_p) \sigma_j, \quad (2.33a)$$

$$\Sigma_{\text{out},s}^T = \sqrt{\kappa_m^T} \sum_j (\hat{\mathbf{d}}_j \cdot \hat{\mathbf{u}}_s) \sigma_j. \quad (2.33b)$$

Here, the unit vectors $\hat{\mathbf{d}}_j$ and $\hat{\mathbf{u}}$ denote the direction of the dipole moment of the

molecule j and the polarization, respectively. The inclusion of the dot product between them is in line with what we know about light-matter coupling, Sec. 2.1.

Figuring out the input-output description for such an involved system is one of the main points of [I]. The other important point is the solution of the input-output equations involving the Holstein–Tavis–Cummings model. I omit the technical details here but I shortly discuss the underlying assumptions. I also note that similar techniques are used in Ref. [62] that worked out the solution independently of us at the same time.

The vibrational mode brings forth a nonlinear interaction. It is discussed at length in Ch. 4. For instance, the dynamics of the bosonic operator b of the vibrations depends on $\sigma^\dagger\sigma$. This term can be neglected in the single-excitation subspace, assuming that the molecules are in their electronic ground state for the most part. Then, vibrations provide another bath for the electronic excitation mode, *exciton* in short, σ . We further assume that there are no induced correlations between the SPP or cavity mode and vibrations — it represents a mean-field approximation. In such a case, the input-output equations can be approached using so-called polaron transformation that diagonalizes the molecular system (i.e., exciton and vibrations) alone. Considering first molecular spectroscopy, or the input-output equations without the SPP, allows us to identify absorption and fluorescence functions of the molecules, $A(\omega)$ and $F(\omega; \omega_d)$ respectively [see Eqs. (2.37) and (2.38) below]. I discuss their mathematical definitions later on but, using Fig. 1(b) as an intuition-building tool, the absorption should be maximized at $\omega = \omega_0$ and the fluorescence at $\omega = \omega_0 - 2S\omega_v$ if $\omega_d \approx \omega_0$. In contrast to the cavity case, the molecular vibrations now provide inelastic scattering so that fluorescence at frequency ω depends on the probe frequency ω_d .

The response function $r(\omega)$ presented in the previous section is changed to

$$\frac{r(\omega)}{\sqrt{\kappa_{\text{ext}}}} = \left[i(\omega - \omega_c) - \frac{\kappa}{2} + N \langle |g|^2 \rangle A(\omega) \right]^{-1}. \quad (2.34)$$

That is, we changed the Lorentzian function $[i(\omega - \omega_0) - \kappa_m/2]^{-1}$ to $A(\omega)$. The SPP response under strong coupling is thus solely defined by the absorption properties of the molecules.

In the calculation of the polarized emission spectrum, one has to take into account or model incoherence. That is, we do not wish to accidentally include coherence between the molecules, e.g., all the molecules are in the same phase. The light-matter coupling constants g_j are important to this end. Note that, in the dipole approximation, $g_j \propto e^{ik \cdot r_j}$ where r_j is the position of the molecule. In the experiment [61], the molecules are distributed over much larger distance than the wavelength of the SPP mode. The phase factor is then randomized uniformly. If one neglects this dependence (which does not change the polariton eigenenergies), the fluorescence contains spurious coherence effects, sub- or superradiance. I found this the hard way as, at first, it didn't cross my mind that the phases of g_j would matter.

The polarized emission spectrum in this incoherent limit is

$$S_s^T(\omega; \omega_d) = |\alpha r(\omega_d)|^2 C_s F(\omega; \omega_d), \quad (2.35a)$$

$$S_p^T(\omega; \omega_d) = |\alpha r(\omega_d)|^2 \left[\kappa_o^T \delta(\omega - \omega_d) + C_p F(\omega; \omega_d) \right], \quad (2.35b)$$

where $C_{p/s}$ are constants determining the rate at which the decay of electronic excitations is observed. [See Eq. (32) in [I] for the definitions.]

These equations, I think, are the main result of [I]. The emission to s -polarization becomes possible because of the light-matter coupling and random orientations of the dipole moments. The absorption modifies the polariton response function $r(\omega)$ which in turn modifies the fluorescence F of the molecules. The p -polarized emission is partly due to the radiative decay of SPPs and partly due to the molecular fluorescence. The relative magnitude of these emissions is determined by the transmission rates κ_o^T and C_p — their ratio is essentially a fitting constant in experiments.

The functions A and F have, of course, definitions that are related to vibrations. We find that there are two important vibrational correlators. They are expressed using an operator $Q_j = \exp\left[\sqrt{S}(b_j^\dagger - b_j)\right]$ that resembles the displacement operator of vibrations [63]. The two- and four-point correlators

$$\left\langle Q_j^\dagger(\omega_1) Q_j(\omega_2) \right\rangle = P(\omega_1) \delta(\omega_1 + \omega_2), \quad (2.36a)$$

$$\left\langle Q_j^\dagger(\omega_1) Q_j(\omega_2) Q_j^\dagger(\omega_3) Q_j(\omega_4) \right\rangle = L(\omega_1, \omega_2, \omega_4) \delta(\omega_1 + \omega_2 + \omega_3 + \omega_4), \quad (2.36b)$$

define the absorption and the fluorescence functions as

$$A(\omega) = \int dE \frac{P(E + S\omega_v)}{i(\omega - \omega_0 - E) - \frac{\kappa_m}{2}}, \quad (2.37)$$

$$F(\omega; \omega_d) = \int d\omega_1 d\omega_2 \frac{L(\omega_1, \omega_d - \omega - \omega_1, \omega_2)}{[i(\omega_1 - \omega_0 + S\omega_v) - \frac{\kappa_m}{2}][i(\omega_2 + \omega_0 - S\omega_v) - \frac{\kappa_m}{2}]}. \quad (2.38)$$

The fluorescence function F is difficult to interpret but the absorption function A gives rise to a very clear interpretation. The expression of $A(\omega)$ is simply the convolution of the Lorentzian function we have without vibrations, and then a function $P(E)$ that describes the vibrations. In fact, it has a probability interpretation due to our choice of the Fourier transformation conventions: $P(E)$ gives the probability to transform E amount of energy to or from vibrations in the excitation process. So it simply tells the amount of phonons generated when $E > 0$. The negative energies ($E < 0$) are related to so-called anti-Stokes processes where the electronic excitations happens from an excited vibrational state. The maximum of $P(E)$ is roughly at $E = S\omega_v$ which matches the intuitive picture in Fig. 1(b). Furthermore, thermodynamics dictates that $P(E)/P(-E) = \exp(-E/k_B T)$ where T is the temperature of the vibrations. This relation is termed as the detailed balance. That is, at low temperature, no phonons can be absorbed from the environment and $P(E < 0) = 0$. Such functions $P(E)$ have been studied in other contexts, for instance, in charge tunneling where it would describe the energy absorbed or emitted to the environment during tunneling [24, 64, 65].

The presence of vibrations breaks the symmetry between the higher and lower energy polaritons. Theoretically, it is a direct consequence of $P(E)$, the probability to generate phonons. When a molecule is excited, a part of the energy can go to vibrations. This energy has of course a lower limit; that no energy went to

phonons. It means that the weight of the absorption spectrum moves towards higher energies. This interferes with the upper polariton peak — a part of the energy in the polariton state goes to vibrations — and its optical response is thus weakened.

The essence of [III] is the evaluation of the function $P(E)$ in the case of vibrational dissipation. One can view this work as an open quantum system generalization of the absorption function defined by Huang and Rhys in the 1950s [56]. The function $P(E)$ can be evaluated for an input-output model but our focus is on a slightly different model. The issue with the input-output formalism is that it assumes the rotating-wave approximation. It is well suited for optical systems. The question is about the characteristic frequency scales of the system at hand and the scale produced by the interaction with their environment — the relaxation rate. For an optical cavity, $\omega_c \gg \kappa$ typically holds. However, the vibrational time scales are much longer than those in the cavity. It can thus be that the dissipation rate γ of the vibrations is of the same order with the frequency ω_v , and that the relevant environmental modes are higher frequency than the vibrations. This is the case for (quantum) Brownian motion. The vibrational dynamics is then described by the equations of motion for the position and momentum quadratures, $x_j = (b_j + b_j^\dagger)/\sqrt{2}$ and $p_j = i(b_j^\dagger - b_j)/\sqrt{2}$, as

$$\dot{x}_j = \omega_v p_j, \quad (2.39a)$$

$$\dot{p}_j = -\omega_v x_j - \gamma p_j + \xi, \quad (2.39b)$$

where the noise ξ is not white but rather has the autocorrelation

$$\langle \xi(t)\xi(t') \rangle = \int d\omega \exp[-i\omega(t-t')] \frac{\gamma\omega}{2\pi\omega_v} \left[\coth\left(\frac{\omega}{2k_B T}\right) + 1 \right]. \quad (2.40)$$

The noise ξ is specified so that it obeys the detailed balance relation and, so, should accurately describe thermal fluctuations [66].

The description of the vibrations and their thermal fluctuations allows for the calculation of the function $P(E)$ and, consequently, the absorption function $A(\omega)$. This alone allows solving the cavity spectrum. The main observation of [III] is that the observed Rabi splitting is affected by the vibrational dissipation in many ways. For instance, it becomes dependent on temperature. The larger the temperature, the larger the molecular linewidth and the observed Rabi splitting.

What I however could not figure out was how to approach the solution of the fluorescence F . The four-point correlator is rather difficult to solve for. I was only able to solve it in the limit of no vibrational dissipation $\gamma \rightarrow 0$ in [I]. I find it rather unfortunate: it would have been nice to confirm that the Stokes shift follows from vibrational dissipation. That is, if a molecule is excited, it mostly emits at the fluorescence frequency. On the other hand, it seems obvious that the typical argument should fail without vibrational dissipation. It would be interesting to understand how the transition to the Franck–Condon picture in Fig. 1(b) happens as it must somehow be related to vibrational decoherence on the electronic excited state.

Such a regime is less pure from a fundamental point of view

P. Lalanne, W. Yan, K. Vynck,
C. Sauvan and J-P. Hugonin
*Light interaction with photonic
and plasmonic resonances*
Laser & Photonics Reviews **12**, 170013 (2018)

Chapter 3

Polaritonic chemistry: a physicist's viewpoint

In this chapter, I discuss the possibility of changes in chemistry by the formation of polaritons. I first give an overview of some important results in polaritonic chemistry, both experimental and theoretical. Then, I focus on our own work in [IV] and in [V] which provides some insight into this complex field from statistical physics. These publications consider vibrational strong coupling and ground-state reactions so that electronic excitations do not play a role at all.

3.1 Idea of vacuum-modified chemistry

It is evident that light can alter chemical reactions, for there would be no intelligent life on Earth without photosynthesis. It is equally evident that there are physical consequences of the electromagnetic vacuum such as the polaritons discussed in the previous chapter, the Casimir effect [67], and the Lamb shift [68, 69]. Could the electromagnetic vacuum affect chemical reactions as well?

Over the past two decades, this has been an inspiring question right on the border of (quantum) physics and chemistry. The intuition is that the formation of polaritons changes the energetics of molecules, dictating the likelihood of reactions. The molecules get to borrow some qualities from the light. This requires strong enough light-matter coupling which means that microcavities or similar fabricated electromagnetic vacua are needed. At the same time, the hybrid states including many systems behave collectively, and thus, it would seem natural that the more molecules participate, the stronger the effect. It seems reasonable if one associates the vacuum Rabi splitting as the measure of the “total” coupling.

Controlling chemistry by vacuum would clearly have a great technological benefit, if the effect is strong enough. In practice, the fabrication of microcavities is relatively straightforward and, so, polaritonic systems should be readily available. It though seems mysterious to physical intuition. What even is the polaritonic effect? Does the vacuum somehow enhance or slow down the rate of reactions? Both have been claimed to happen [70–74], which is in some ways troubling if one hopes for a generic polaritonic effect. It could be, of course, intimately connected to specific reactants or molecules or the types of reactions. For a physicist not well-versed in chemistry it is also slightly troubling. Nevertheless, I was so intrigued by

the ideas of collectivity and coherence between light and matter that I hoped to understand at least a part of it.

The field of polaritonic chemistry is young and there is not yet fully-formed consensus on what is going on. Theoretically, it really is an unsolved problem. Its difficulty arises from combining quantum electrodynamics and chemistry, and the fact that computational methods are not readily usable. Furthermore, it is impossible to simulate the typical experimental realizations of polaritonic systems which contain a very large number of molecules. We are thus at a point where we try to build intuition on what is important. I first introduce what other people have considered and focus then on the main points of [IV] and [V].

3.1.1 Overview of experimental works

I give a quick summary on the present status of claimed effects in polaritonic chemistry. I roughly outline a few experimental works, but much more detailed descriptions can be found in several other outstanding reviews [75–77].

Polaritonic chemistry has been investigated both for electronic and vibrational strong coupling. The important difference between the two is the energy scale: vibrational energies are typically of the order 10 meV whereas electronic excitations are several orders of magnitude higher, 1 eV. This restricts the possible optical systems if they are to provide a resonant effect. Therefore, electronic strong coupling is commonly studied in plasmonic or sub-micrometer-sized cavity systems with molecules embedded in a solid environment, while vibrational strong coupling can be studied in optical cavities supporting microfluidistics (the separation between the mirrors being of order 10 μm). The size of optical cavities is often further increased by matching higher-order modes of the cavity to the vibrational resonance. Microfluidistic approach is evidently more useful for applications than embedding reactants in solids. It also provides, in principle, the possibility to track chemical reactions by other than optical means.

Let me next highlight some experimental results.

In the case of electronic strong coupling, isomerization of molecules¹ has been claimed to be affected by strong coupling. In this experiment that has marked a starting point to the field of polaritonic chemistry, tuning the optical cavity into resonance with one of the excitation energies of a molecule modifies the rate of isomerization [78]. Another experiment shows that a chemical reaction with oxygen that destroys optical properties of a dye molecule is greatly slowed down in a plasmonic system as the vacuum Rabi splitting is increased [79]. The effect is reportedly not resonant, as in the other example, but rather depends almost linearly on the detuning between the plasmon frequency ω_c and the molecular excitation energy ω_0 . The rate is slowed down more when $\omega_c < \omega_0$ than on resonance $\omega_c = \omega_0$; although, the detuning range is at most roughly ten percent (i.e., $|\omega_c - \omega_0|/\omega_0 \lesssim 0.1$).

Due to the aforementioned experimental reasons, the focus has recently been mostly on vibrational strong coupling. The general idea is to couple a cavity

¹Isomer refers to a specific configuration of a molecule; isomerization is essentially a process of changing the shape of a molecule. Different isomers can have different properties.

to a vibrational mode that is relevant for the chemical process — and since we don't really know what is going on, this seems to be an arduous trial and error approach. Nevertheless, it has been reported that the formation of polaritons can both slow down [70, 71] and speed up reactions [73, 74]. A common theme in these reports is that the polaritonic effect is resonant and, often, the magnitude of the effect is proportional to the Rabi splitting. Furthermore, the cavity vacuum mode can reportedly induce a change in the ratio of two different reaction rates, effectively allowing for the selection of the predominant reaction product from a single reactant [72]. It has also been claimed that underlying molecular symmetries of vibrational modes play a role in determining the modification due to the vacuum field [80].

As interesting and seemingly many-faceted the reported effects are, some scientifically necessary asterisks must be added. There are only a few groups in the world providing these inspiring experimental results — in fact, I have referenced only works from three groups. Furthermore, these are not straightforward experiments as one has to have great control over both optics and chemistry. A few failed replication attempts have been reported [81, 82]. Especially, Ref. [82], which tries to replicate the experiment in Ref. [73], fails to see any polaritonic effect.

3.2 Understanding polaritonic chemistry

There are many theoretical approaches to polaritonic chemistry — so many in fact that there are even reviews on them [83–87]. Here, I give a very biased overview, focusing on the analytical results within a subsection of polaritonic chemistry concerning ground-state reactions. This means that there is no discussion on the modern computational techniques like density-functional theory (DFT) and quantum mechanics/molecular mechanics (QM/MM) simulations in the context of polaritonics. I genuinely believe that there must be a way to understand the issue from some simple physical principles and illustrations. To limit the scope, my focus is on reaction rates and how they are affected by the formation of polaritons.

Before going on with the discussion on polaritonics, there is a need to go through some nomenclature and theoretical framework of physical chemistry.

3.2.1 Physical picture of chemical reactivity

Chemical reactions are categorized into adiabatic and diabatic reactions [88, 89]. The notion comes from the fact that chemistry involves molecules, and the interactions between the electronic and nuclear degrees of freedom depend on the specific molecular system. In the adiabatic regime, the electrons are assumed to equilibrate much faster than the nuclear motion. This is formalized in the Born–Oppenheimer approximation which separates the wavefunction of the molecule into nuclear and electronic degrees of freedom. Effectively, it allows one to think of reactions happening on a potential energy surface depending only on nuclear coordinates while the electronic system is integrated over. One may extend this line of thought to excited states as well. This is particularly useful in photochemistry [89] but, otherwise, it is often enough to focus on the ground state. The diabatic, or nonadiabatic,

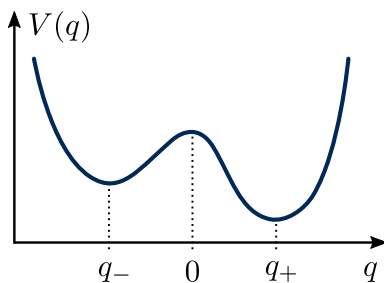


FIGURE 4: One-dimensional potential energy surface $V(q)$ entailing two states, denoted by coordinates q_{\pm} , separated by an energy barrier.

reactions are those where the time-separation argument fails. The electronic system becomes partially excited during the nuclear motion. This can be represented by an effective interaction between the different electronic states, and, if this interaction is small, the Fermi golden rule should hold to a good approximation.

I should note that both [IV] and [V] consider toy models of adiabatic ground-state reactions. They are the focus here. I review their basic description here for reference.

The adiabatic reactions may be classically characterized with a potential $V(q)$ where q represents the nuclear coordinates [90]. The different molecular states are identified as the minima of the potential. In this regime, the crown jewel of reaction rate theories is the transition state theory. The mental model it provides seems to be popular and well-utilized, and it supports naturally some quantum modifications.

The principal idea of the classical transition state theory can be elucidated for an one-dimensional potential $V(q)$ describing a molecular system. For simplicity, let us assume there are two minima separated by a potential barrier as in Fig. 4. When the molecule is in contact with a heat bath, it is expected that there are transitions between the two minima due to thermal activation. The nature of the argument is then statistical: if the molecule is prepared so that it is initially in one of the states, there is over time a finite probability to find the molecule in the other state as well. However, it is often prohibitive to calculate the full probability distribution in terms of the position q and time t . The transition state theory solves this problem by instead considering only the flux of probability or population over the barrier. That is, the transition rate is assumed to be proportional to the probability to find the molecule in a state that corresponds to the coordinate q at the maximum of the potential and with a momentum p that leads the molecule into the other state. Concretely, let us fix that $q = 0$ corresponds to the maximum point of the potential (i.e., the transition state) and the molecule is initially prepared in a state that corresponds to negative $q = q_-$. The transition rate to the state with positive $q = q_+$ is given by

$$\Gamma = \langle \delta(q)\theta(p)p/m \rangle. \quad (3.1)$$

Here, $\theta(p)$ is the Heaviside function, $\delta(q)$ is the Dirac delta function, and m is the effective mass of the mode. The probability distribution of coordinates and

momenta is then argued from statistical physics. Since the molecule is prepared in the state around $q = q_-$, the initial distribution would be well approximated even if the other state at $q = q_+$ was neglected. It however requires that the rate of transitions is much slower than the internal dynamics within the well. Effectively, this argument amounts to a harmonic approximation of the potential $V(q)$ around q_- . Then, the likelihood $P(q, p)$ for the coordinate and its associated momentum to have values q and p , respectively, follows the Boltzmann form $P(q, p) \propto \exp[-H(q, p)/(k_B T)]$ when the heat bath enclosing the molecule is at temperature T and $H(q, p)$ is the classical Hamiltonian, or the energy, of the molecule. Now, $H(q, p) \approx \frac{p^2}{2m} + \frac{1}{2}m\omega_0^2(q - q_-)^2$. This avoids the potentially difficult calculation of the full partition function, let alone the full dynamical problem. Thus, evaluating the expectation value gives

$$\Gamma_{TST} \approx \frac{\omega_0}{2\pi} \exp\left[-\frac{V(0)}{k_B T}\right], \quad (3.2)$$

which can be identified with the Arrhenius rate expression.

This idea is readily extended to describe more involved systems. The main problem becomes the identification of the transition states and relevant reaction pathways. Somehow, the multidimensional information residing in the nuclear coordinates \mathbf{q} must be projected to a one-dimensional space. Without dwelling in the issues of uniqueness of the transition state and other issues, the same argument can be generalized to multidimensional system [90, 91]. The resulting equation is known as the Eyring equation [92] and it reads as

$$\Gamma = \kappa \frac{k_B T}{h} \frac{\mathcal{Z}^\ddagger}{\mathcal{Z}_i} \exp\left(-\frac{E_b}{k_B T}\right). \quad (3.3)$$

Here, E_b refers to the potential energy barrier [instead of $V(0)$]. The partition function \mathcal{Z}_i is evaluated in the well from which the transition happens, typically in the harmonic approximation. The quantity \mathcal{Z}^\ddagger is formally identified as a partition function at the transition state: For a multidimensional system, this state should be at a saddle point of the full potential $V(\mathbf{q})$ with only a single unstable mode. The harmonic approximation at the transition state is utilized again in the calculation of \mathcal{Z}^\ddagger which contains all other modes except the unstable one. Furthermore, both \mathcal{Z}_i and \mathcal{Z}^\ddagger can be calculated in the quantum regime, resulting in quantum transition state theory. The modification due to multiple degrees of freedom is sometimes called the Grote–Hynes factor $\kappa_{GH} = \Gamma/\Gamma_{TST}$. Lastly, κ is an ad hoc transmission coefficient characterizing the recrossings back to the initial well which could have been included in the one-dimensional rate expression as well. Here, $\kappa = 1$ everywhere.

3.2.2 Overview of theory efforts in polaritonic chemistry

The analytical efforts to describe polaritonic chemistry of adiabatic ground-state reactions are best summed as modifications of the transition state theory result (3.3).

Due to the complexity of the full N -body polaritonic problem, there has been considerable focus on single-molecule polaritonic chemistry. In these cases, it

has been noted that the Grote–Hynes factor κ_{GH} can provide cavity frequency-dependent changes to reaction rates [39, 93]. This assumes that the transition state has an associated dipole moment. In the simplest case of a one-dimensional molecular potential, it reads as $\kappa_{GH} = \lambda/\omega_b$, where ω_b is the barrier frequency — $\omega_b^2 \propto -\partial_q^2 V(q)|_{q=0}$ in Fig. 4 — and λ is the barrier frequency modified by the light-matter coupling. The latter frequency λ is obtained by substituting to the lower polaritonic eigenenergy E_- in Eq. (2.17) that $\omega_0 \rightarrow -\omega_b$ under the rotating-wave approximation. In this model, the cavity decreases the reaction rate if the barrier frequency ω_b , not the well frequency ω_0 , is in resonance with the cavity.

A particularly transparent calculation for an N -body system is provided by Zhdanov [94], who also uses one-dimensional potential surfaces for molecules. The main assumption is that the reactant well is at resonance with the cavity while the product well and the barrier frequency are either so far detuned that the light-matter coupling to them can be neglected or that they are simply optically inactive. The quantum mechanical model describing the reactant molecules and the cavity is the Tavis–Cummings model with equal coupling constants $g_i = g$ (although, it is called Dicke model in the article). The calculation then proceeds with using the eigenenergies (2.21) to calculate the energy barrier and the quantum mechanical partition functions when, in the transition state, one of the N molecules resides on top of the potential barrier. The transmission coefficient κ is assumed to be unchanged by the coupling. In the leading order of the Rabi splitting Ω , this results in the reaction rate Γ_g that reads as

$$\frac{\Gamma_g}{\Gamma_0} \approx 1 + \frac{\Omega^2}{4N(k_B T)^2} \left(\frac{k_B T}{\omega_0} - \frac{e^{-\omega_0/k_B T}}{[1 - e^{-\omega_0/k_B T}]^2} \right), \quad (3.4)$$

where Γ_0 is the reaction rate without the cavity. The term in brackets is negative when $k_B T \gtrsim \omega_0$ and positive otherwise — if temperature is high, the rate is decreased. More importantly, this result clearly shows the scaling with respect to N : Even though the Rabi splitting Ω is compared to the temperature, only one of the N molecules can be in the transition state resulting in an extra factor of N in the denominator. Since at resonance $\Omega = 2\sqrt{N}g$, the factors of N exactly cancel and $\frac{\Omega^2}{4N(k_B T)^2} = \frac{g^2}{(k_B T)^2}$. Truly, one compares the single-molecule light-matter coupling strength to the temperature which is assumed to be small in experiments. Thus, there appears to be almost no change in the reaction rate, $\Gamma_g \approx \Gamma_0$. Similar considerations and conclusions are present in a few other works [38, 95]. It has been further noted that if one treats the nuclear and photonic coordinates classically, the energy barrier E_b is changed only by the N -independent dipole self-energy term [38].

There is also a contrasting viewpoint. Yang and Cao have argued that the collective effect of polaritonics is similar to the difference between the Jaynes–Cummings and Tavis–Cummings models [93]. That is, it is implied that one could use the single-molecule ($N = 1$) reaction rate modification and then further modify the rate by replacing $g \rightarrow \sqrt{N}g$. This is mechanistically in line with what is presented in Sec. 2.2 but seems to be at odds with the saddle point formulation of the multidimensional transition state theory.

3.3 Quantum tunneling regime — a toy model

My initial idea was this:

By definition, the existence of polaritons is due to coherence or, to be more exact, coherent exchange of energy between light and matter. At the same time, quantum tunneling is a coherence phenomenon as it follows from the wave-like qualities of matter. They could be intimately linked and the polaritonic effect would be explained as a genuine quantum effect.

The coupling of a tunneling system to a cavity does change its tunneling rate. However, this does not depend on the number of systems which means that the effect is not collective. For this reason, as the result closely mirrors that in the thermal activation regime [Eq. (3.4)], I pondered a lot whether or not to write it down. I concluded that I should; the result is [V].

Polaritonic quantum tunneling is nevertheless interesting as it can be compared to the reported high-temperature results. For instance, Eq. (3.4) implies that the reaction rate increases very slightly when $k_B T < \omega_0$. Polaritonic tunneling gives another type of insight and, furthermore, it is a difficult problem whose solution might have some relevance for other hybrid quantum systems as well. This is because the tunneling of a polaritonic system concerns very many systems. It greatly differs from the typical setting where a single system, perhaps coupled to a dissipative environment, escapes a potential barrier.

Finding a suitable approach to polaritonic quantum tunneling took a while. I became somewhat familiar with the approaches and viewpoints of both physics and chemistry. Within physics the literature is already vast [90, 96–100]. Tunneling is relevant to fields like cosmology, particle and nuclear physics, and condensed matter theory [97, 101]. In chemistry, the focus is more on quantum corrections and theoretical generalizations for thermally activated processes [102–104].

The method I eventually ended up using to describe polaritonic quantum tunneling is called the $\text{Im } F$ method, $\text{Im } F$ referring to the imaginary part of the free energy [96]. It was developed in the 1960s by Langer in the context of bubble nucleation [105]. The approach differs quite a lot from, e.g., the transition state theory and can be devised fully in the quantum formalism.

Consider again a two-well system as in Fig. 4 with a large energy difference between the wells. When the temperature of the environment is very low compared to other energies, there is no thermal activation. Thus, the only way the system can relax is by tunneling through the barrier. This relaxation means that all the states in the metastable well have a finite lifetime. In the Hamiltonian formalism this is a problem because these states are not proper energy eigenstates. If we were to disregard this, however, we could proceed with writing the partition function for the metastable well alone,

$$\mathcal{Z} = \sum_n e^{-\beta E_n} \rightarrow e^{-\beta E_0} \quad \text{when } \beta E_n = E_n/k_B T \gg 1. \quad (3.5)$$

Here, E_0 represents the lowest energy in the system. Now, still suspending the disbelief on Hamiltonian formalism not holding here, we can deduce that E_0 must also contain the information about the finite lifetime. If the system was somehow initialized in the lowest energy state, its probability to remain in the state *should*

decay in time. Since this probability is given by $|\exp(itE_0)|^2$, the only resolution is that E_0 contains an imaginary part, that is,

$$|\exp(itE_0)|^2 = |\exp(it \operatorname{Re} E_0 - t \operatorname{Im} E_0)|^2 = \exp(-2t \operatorname{Im} E_0) \neq 1. \quad (3.6)$$

A finite and constant decay rate $\Gamma = 2 \operatorname{Im} E_0$ can now be related back to the partition function \mathcal{Z} and the free energy F as

$$\Gamma = -\frac{2}{\beta} \operatorname{Im} \ln \mathcal{Z} = 2 \operatorname{Im} F, \quad (3.7)$$

where the free energy is defined as in statistical physics by $F = -\ln \mathcal{Z} / \beta$. Even though my argumentation here seems rather sketchy, it can be shown, through rather complex analytical continuation tricks, that the classical transition state theory can be derived in the same way from an imaginary part of a classical partition function — only the prefactor changes [98, 106].

There is a wealth of literature on how to calculate the imaginary part of the free energy, especially in the limit of low temperature [96–98, 101]. The central idea is to use path integral formalism in semiclassical approximation to evaluate the partition function $\mathcal{Z} = \operatorname{tr}(e^{\beta H})$. It amounts to finding classical periodic solutions in an inverted potential and the quadratic fluctuations around them. In the low-temperature limit, these solutions are called instantons.

The $\operatorname{Im} F$ method is suitable for polaritonics because it naturally extends to many degrees of freedom. For instance, without doing any difficult calculations, it is straightforward to infer the tunneling rate of N independent and distinguishable systems. That is, if a single system has a tunneling rate $\Gamma_0 = -2 \operatorname{Im} \ln \mathcal{Z}_0 / \beta$, then the factorization of partition functions for the N -body system, $\mathcal{Z} = \mathcal{Z}_0^N$ results in the total tunneling rate $\Gamma = N\Gamma_0$. The $\operatorname{Im} F$ method has been utilized in open quantum systems extensively because one can naturally introduce an environment for the tunneling system and integrate it out. One of the landmark results is by Caldeira and Leggett who showed that friction or dissipation leads to exponential suppression of the tunneling rate [107]. In [V], I however neglected the coupling to the environment and the dissipation it produces, as the main focus was on the collective polaritonic effect: How does the polaritonic quantum tunneling rate depend on the number N of systems?

The model I used in [V] for the molecular potential is as simple as possible in order to have a solvable problem. In the spirit of the transition state theory, I assume that there is a metastable potential where the system, a molecular degree of freedom, is trapped. The presence of the true potential minimum is neglected. The potential $V(q)$ of a single system is assumed to depend only on a single coordinate q . Furthermore, the coupling to the vacuum of the cavity is through this coordinate. This is in line with the dipole approximation presented in Sec. 2.1. The Hamiltonian of the tunneling system is

$$H = \frac{1}{2} \sum_{i=1}^N p_{q_i}^2 + \frac{1}{2} p_x^2 + \sum_{i=1}^N V(q_i) + \frac{1}{2} \omega_c^2 x^2 + \sqrt{\omega_0 \omega_c} \sum_{i=1}^N g_i x q_i, \quad (3.8)$$

$$V(q) = \begin{cases} \frac{1}{2} \omega_0^2 q^2, & q \leq a, \\ -\infty, & q > a, \end{cases} \quad (3.9)$$

where x is the single-mode cavity quadrature of eigenfrequency ω_c . Here, p_{q_i} and p_x are the momentum associated with q_i and x , respectively, and they have been rescaled so that they contain the effective masses of the modes. The reasoning for this kind of model is that, in the potential well, the energy levels with finite lifetime are reasonably well approximated by a harmonic oscillator. (Formally, this is true at least in the $a \rightarrow \infty$ limit.) Thus, this is nothing but a metastable version of the Tavis–Cummings model discussed in Sec. 2.2 without the rotating-wave approximation.

I quote here a simplified version of the low-temperature tunneling rate modification caused by the cavity, as it serves as a starting point for the next section as well, leaving all the details in [V]. In the strong-coupling regime, the presence of the cavity modifies the total tunneling rate (which is proportional to the number N of systems) by a factor

$$r = \frac{\Gamma(N)}{N\Gamma_0} \approx \left\langle \frac{\omega_H}{\omega_0} \exp \left[-S_0 \left(\frac{\omega_H}{\omega_0} - 1 \right) \right] \right\rangle. \quad (3.10)$$

Here, Γ_0 refers to the single-system tunneling rate without the light-matter coupling and $S_0 = 2E_b/\omega_0$ is the bare action determining Γ_0 as $\Gamma_0 \propto e^{-S_0}$. In the high-temperature limit, $S_0 = E_b/(k_bT)$ as in the Arrhenius rate expression. The angular brackets remind that if the light-matter couplings g_i have some distribution, we should average over it. The polaritonic effect is tidily contained within the harmonic mean frequency defined as

$$\frac{\omega_H}{\omega_0} = \frac{N \langle g^2 \rangle}{\frac{N \langle g^2 \rangle - g^2}{\omega_0} + g^2 \left(\frac{1+\delta}{2} \frac{1}{\omega_+} + \frac{1-\delta}{2} \frac{1}{\omega_-} \right)}, \quad (3.11)$$

where ω_{\pm} are the polariton eigenfrequencies and $\delta = (\omega_0^2 - \omega_c^2)/(\omega_+^2 - \omega_-^2)$ describes detuning. The light-matter couplings are as if weighing factors of the harmonic mean. Importantly, however, the bare frequency ω_0 obtains a weighing factor proportional to the number N of systems whereas the polariton frequencies ω_{\pm} have a weight of unity. This corresponds to the picture of the eigenstates discussed in the context of the Tavis–Cummings model. Thus, when the number N of systems is large and the individual couplings small, no modification is to be found and $r \approx 1$. Moreover, the polaritonic effect appears not to be resonant as the tunneling rate is not maximized at $\omega_0 = \omega_c$.

3.4 Collectivity from classical theory

There are many ways to approach a difficult physical problem. More often than not, however, the first approach is quite similar independently of the problem. To use the case of polaritonic chemistry as an example, this first approach is to take well-known theories concerning reaction rates and try to modify them to accommodate polaritons. If it works out then it is done. If it does not, well, then there is truly a problem or even a crisis. The resolution in physics is often that one had to think about the underlying principles of the theory carefully. However,

without taking the first approach and seeing it fail, it is very difficult to come to understand the cause of the problem.

After a lot of thought, we at least see one failure of the reaction rate theories when naively applied to polaritonics. This applies to the whole quantum tunneling calculation as well.

Consider the expression in Eq. (3.10). It seems to imply that the rate of escape from a metastable potential per system is $\Gamma(N) = r(N)\Gamma_0$, where I have explicitly denoted the dependence on the number N of trapped systems forming the polariton states. Presumably, this relation should describe how the number N of trapped systems evolves. Since Γ describes the instantaneous rate of escape, I would write

$$\frac{d}{dt}N = -\Gamma(N)N \quad (3.12)$$

as the equation that determines the population $N(t)$ at time t . It definitely makes sense without the polaritonic interaction in which case $\Gamma(N) = \Gamma_0$ leads to an exponential decay of the population.

Is this accurate for an interacting system in general? No, it is not. Rather, it seems that we have inadvertently assumed something about the system. I will argue this from another perspective.

Let us consider an alternative, probabilistic description for the N trapped systems. When $p_j(t)$ is the probability to find the j th system still trapped at time t , the expected value of systems is $\langle N \rangle = \sum_j p_j(t)$. Intuitively, the probability $p_j(t)$ must decay in time. I shall conjecture, as many have done, that this probability decays according to an equation similar to the number of systems, that is,

$$\frac{d}{dt}p_j(t) = -\Gamma_j p_j(t), \quad (3.13)$$

where the rate Γ_j could depend on the system. Here, the different systems can couple differently to the cavity, and they may not behave identically anymore. The question is whether or not Eq. (3.12) corresponds to summing over Eq. (3.13) which gives

$$\frac{d}{dt} \langle N \rangle = \sum_j \Gamma_j p_j = \langle \Gamma \rangle \langle N \rangle + \sum_j \delta\Gamma_j p_j, \quad (3.14)$$

where I have divided the rate into a mean and a deviation as $\Gamma_j = \langle \Gamma \rangle + \delta\Gamma_j$. If we identify N in Eq. (3.12) with the expectation value $\langle N \rangle$, it appears that some kind of mean-field approximation has been made. I have neglected the fluctuation of the rates. Furthermore, it is not clear if $\langle \Gamma \rangle$ corresponds to $\Gamma(N)$ when the number of systems is not fixed from the start.

The beginning of this story is mostly rationalization after writing [IV] to be perfectly honest. At first, our focus was including all the molecular states and not just the one from which the system escapes. These other states were fully neglected in the quantum tunneling calculation — including them is fairly difficult. The intuition was and is that all the molecules forming the polariton must know each other. They can discuss through the vacuum of the cavity, after all, even if they are in different states. Somehow this should be represented by the transition

rates Γ_j . This line of thought became clearer to us after a presentation by Mark Dykman on atoms in magneto-optical traps in the context of time crystals [108]. A fully distinct physical system leads to similar modeling considerations but with an entirely different interpretation.

Often, Eq. (3.13) is called a master equation [109, 110]. It is straightforwardly generalized to multiple states. Dropping the system index j for now and denoting the possible states by Greek letters, its general form reads as

$$\frac{d}{dt}p_\mu(t) = \sum_\nu \Gamma_{\nu\mu}p_\nu(t) - \left(\sum_\nu \Gamma_{\mu\nu}\right)p_\mu(t). \quad (3.15)$$

Here, $\Gamma_{\mu\nu}$ describes the transition rate from the state μ to the state ν . The change of probability is related to the difference between the inflow (first term) and the outflow (second term) of probability. This equation encodes the fact that the total probability $\sum_\mu p_\mu$ does not change and so it can be set to unity.

The master equation provides an evidently Markovian description of a system. The likelihood of transitions between different states depends only on the state of the system at that time. Here, it is justified by the separation of time scales: rate of transitions is assumed to be small compared to other internal frequency scales [90, 109, 110].

An important realization is that $\Gamma_{\mu\nu}$'s must be related to thermodynamics. Considering a classical system of fixed number N of constituents in a thermal bath of temperature T and some energies E_μ associated to the state μ , the thermal equilibrium should correspond to the Boltzmann distribution

$$p_\mu(t \rightarrow \infty) \propto \exp\left(-\frac{E_\mu}{k_B T}\right), \quad (3.16)$$

where k_B is the Boltzmann constant. If the system thermalizes and the stationary state of the system corresponds to the Boltzmann distribution — as we may assume for a polaritonic system which is not driven — the issue is resolved by assuming that

$$\frac{\Gamma_{\mu\nu}}{\Gamma_{\nu\mu}} = \exp\left[\frac{E_\mu - E_\nu}{k_B T}\right]. \quad (3.17)$$

This assumption is called the detailed balance, since it fixes the in- and outflow of probabilities to be the same in the stationary state ($\frac{d}{dt}p_\mu = 0$) [109].

In [IV], the principal idea is that the detailed balance may be used in conjunction with a simple model for polaritonic energies to describe the collective stochastic behavior of a polaritonic system. The states and their energies are associated with the minima of a potential function that mimics Eq. (3.8). The molecules themselves are described by a potential with two minima as in Fig. 4. The minima are associated with molecular states (in chemistry, for instance, the reactant and product state of a unimolecular reaction).

In the polaritonic system, different molecules effectively interact through the cavity. Modifying the state of one molecule will affect the cavity state which in turn will affect another molecule. The strength and the type of the interaction depends on the light-matter terms $g_j x q_j$. Compare this term to the classical example of

spring connecting two masses at x and q_j . It is otherwise the same but, now, we can have either repulsive or attractive interactions described by the sign of g_j . Though, the only thing that can matter is the sign difference due to the $U(1)$ symmetry of the vacuum field. (There cannot be an observable change in physics if we transformed $x \rightarrow -x$.) The effective interactions between molecules are of the second order in the light-matter coupling — the effective coupling between molecules j and k is then proportional to $g_j g_k$. The total potential energy of the polaritonic system depends on the state of every molecule through these effective couplings. More technically, the potential energy minima which we associate to molecular states change. *The cavity induces a potential energy term that depends on the collective state* — whether the molecules are in one minimum or in the other.

This results in collective behavior that drastically differs from the “mean-field picture” of using transition rates calculated by e.g. transition state theory within the master equation. We even predict spontaneous symmetry breaking: Even if the two molecular states had the same energy, all the molecules would go to the same state because of the cavity-induced interaction. This requires only two conditions. First, the Rabi splitting must be large enough. This is easy as we can simply increase the number N of molecules. Second, the effective interactions between the molecules should be of roughly equal strengths. That is, the light-matter constants g_j should be similar or, more technically, the standard deviation of g 's should be small compared to their average. If this latter condition is not fulfilled and there is a large range of couplings, the polaritonic system does something peculiar: it minimizes the energy by separating the molecules based on their coupling constants g_j . Those with a larger coupling will go to another state than those with smaller coupling. For example, one can imagine a case where half of the molecules have a coupling constant g_0 and the other half has exactly the opposite phase coupling $-g_0$. The molecules with the same coupling attract one another while those with different sign repel — and so, the two halves predominantly have different states. This describes phase separation based on the light-matter coupling which does not change the macroscopic number of reactants and products in the steady state.

I note that these changes to the stationary state of the polaritonic system are reflected in the transition rates. The attractive interaction between molecules slows down the reaction rates.

In polaritonic chemistry experiments, I expect that the variance of g 's is large. This means that phase separation is more likely but it would be difficult to confirm and the fluctuations in the light-matter couplings may destroy it. Again, the effect is not resonant because the cavity frequency ω_c describes only how difficult it is for the molecules to change the cavity state. The dimensionless parameter describing the light-matter interaction turns out to be $\Omega / \sqrt{\omega_0 \omega_c}$, i.e., the Rabi splitting is compared to the eigenfrequencies in the system. This kind of a thermodynamic argument does therefore not produce an effect that is directly relatable to existing experiments. However, if the disorder leading to different light-matter couplings can be or is experimentally removed, we predict that the formation of polaritons has a strong effect on chemistry and can even cause a phase transition.

Our work in [IV] shows an approach to collective reactivity that is far removed from the perspective of the transition state theory. Furthermore, it highlights that

the distribution of light-matter coupling constants g has an observable effect. It is surprising in the sense that this distribution does not change the polaritonic eigenenergies which depend only on $\langle g^2 \rangle$. But it really does change the effective (repulsive *or* attractive) interactions between molecules which affect the underlying collective chemistry.

What is curious about this classical argumentation and consequent results is that it seems fully incommensurate with the quantum tunneling calculation presented in the previous section. Even if one takes into account the fact that the tunneling rates are dependent on the individual light-matter couplings g_i , the results remain different. The only resolution I see is that the presence of the true minimum energy state, not just the metastable one, plays an important role. It seems impossible to “factorize” the polaritonic system in a way assumed by the transition state theory and the quantum tunneling calculation. For collective systems, these approaches give only a part of the picture.

Inexhaustible
The strength of fire is running through me
Spine like beam of light
What mortal could ever break this force?

Joseph Duplantier
Gojira – Backbone
From Mars to Sirius
(Prosthetic Records, 2005)

Chapter 4

Optomechanics: nonlinear interactions

There is a world of hybrid quantum systems beyond polaritons that are characterized by bilinear Hamiltonians. These nonlinear systems are the focus of the present chapter. I use so-called cavity optomechanics as a prototypical example. Our work in [III] considers magnomechanics that is closely connected to this field. Here, the main role is reserved for a detailed understanding of opto- or magnomechanical interactions while the openness of such systems plays more of a supporting role.

4.1 Cavity optomechanics

Whereas polaritons are formed by a coherent exchange of energy between two systems, optomechanics follows if one system can alter the resonant frequency of another system. In cavity optomechanics, this idea becomes reality: mechanical motion of the cavity itself causes a change in its resonant frequency [111, 112]. This nonlinear interaction between light and matter is mediated by a radiation-pressure force.

Optomechanics has profoundly elucidated the boundary between quantum and classical worlds. The optomechanical interaction has been used to cool macroscopic mechanical resonators close to their quantum mechanical ground state [113, 114]. Two such resonators have been entangled with its help [20, 21, 115, 116]; a famous point of contention in the early days of quantum mechanics [117]. The control of these systems has allowed for establishing relationship between the entropy cost and accuracy of clocks [118] as well as sensitive and even quantum-limited measurements [119–121]. Of applied interest is the signal processing made possible by optomechanical nonlinearities [122, 123] and the fact that optomechanics could work as a mediator or an interface of quantum information between different physical systems [4, 124, 125].

Optomechanics can be understood from elementary physical arguments. Consider a standing wave between two parallel plates. If one plate is fixed but the other one is allowed to move while remaining parallel, the standing wave has to change. Let us assume some initial distance L between the plates and a small displacement x in the moving plate. From the physics of waves we know that a standing wave is possible only if there is exactly an integer amount of half wave-

lengths $\lambda/2$ between the plates. This relation reads as $L + x = m\lambda/2$ with m being an integer. Let us assume it is independent of the speed v of the wave. Then, the frequency f of the standing wave is

$$f(x) = \frac{v}{\lambda} = \frac{mv}{2} \cdot \frac{1}{L+x} = \frac{mv}{2L} \left[1 - \frac{x}{L} + \left(\frac{x}{L}\right)^2 + \dots \right]. \quad (4.1)$$

When the displacement x is small compared to L , that is, $|x| \ll L$, we may neglect all terms beyond the first order term x/L to a good approximation.

I inadvertently define the displacement x so that $x > 0$ corresponds to moving the plates away from one another. This is reflected in the sign of x in the frequency $f(x)$. Farther the plates, lower the frequency. If such directionality did not exist, the standing wave would not be affected by the motion at all and there would be no optomechanics to speak of.

For a wide range of media the standing waves within them are well described by harmonic oscillators. This is the case for the electromagnetic vacuum within a cavity, for instance. The energy stored in the standing waves in the quantum description is thus

$$H = hf(x)a^\dagger a \simeq \hbar\omega_0(1 - x/L)a^\dagger a, \quad (4.2)$$

where $\omega_0 = 2\pi f(0) = m\pi v/L$ is the bare eigenfrequency of the standing wave while x is still treated classically. Curiously enough, the radiation-pressure force is now encoded into this elementary model: the classical force on the moving plate is given by $F = -\partial_x \langle H \rangle = \frac{\hbar\omega_0}{L} n$ where $n = \langle a^\dagger a \rangle$ is the expected number of photons in the system. Again, the signs matter as a positive force means that the plates are pushed apart by the standing waves. It seems reasonable, considering that the wave is reflected at the plates.

Finally, optomechanical interaction is obtained by claiming that the motion of the moving plate can be described by a harmonic oscillator as well. Then, the total energy of the optomechanical system is

$$H = \hbar\omega_0 a^\dagger a + \hbar\omega_m b^\dagger b + \hbar g a^\dagger a (b + b^\dagger). \quad (4.3)$$

This conventional form of the Hamiltonian follows from denoting the mechanical eigenfrequency by ω_m and the optomechanical coupling by $g = x^{\text{ZPM}} \partial f / \partial x |_{x=0}$, where x^{ZPM} is the quantum mechanical zero-point amplitude defined by $x = x^{\text{ZPM}}(b + b^\dagger)$.

In this simple example, we found only a nonlinear interaction between light and matter. What if there is a linear interaction present, for instance $a^\dagger b + b^\dagger a$? In cavity optomechanics, they are often neglected because the typical optical frequency is many orders of magnitude larger than the mechanical one, $\omega_0 \gg \omega_m$. Similar to the idea of rotating wave approximation, the operators in the interaction are in the interaction frame $a \rightarrow ae^{-i\omega_0 t}$ and $b \rightarrow be^{-i\omega_m t}$ so that $a^\dagger b$ rotates at a frequency $\omega_0 - \omega_m$ which is fast compared to ω_m . Neglecting the linear terms is another form of the rotating wave approximation.

In practice, one successful type of an optomechanical system has been an electric microwave circuit with a mechanical element. The cavity is then essentially an

LC-oscillator. In these approaches, mechanical motion modulates the capacitance of the circuit which in turn modifies the resonant frequency. Alternative optomechanical systems that more clearly correspond to the above model include patterned photonic crystals [113] and flexible optical cavities [126, 127]. The derivation of the Hamiltonian in each case matches that of Eq. (4.3) with a different frequency $f(x)$ and a different mechanical mode x .

4.2 Magnomechanics

Magnomechanics is a magnetic variation of cavity optomechanics. Simply put, the idea is to replace the often-used microwave cavity by a ferromagnetic resonance (FMR). The opto- or magnomechanical coupling is caused by magnetic shape anisotropies that change the FMR frequency.

This is a relatively new idea. The first experimental evidence of the magnomechanical coupling in the sense of Eq. (4.3) was published in 2016 [128] and, as far as I know, there is only one other experimental work at the time of writing [129]. Both of these experiments employ a ferromagnetic sphere embedded in a microwave cavity. The idea, more or less, is to drive the microwave cavity which interacts with the magnetic degree of freedom, FMR, which in turn excites vibrational modes of the sphere due to the magnetoelastic interaction. The cavity works as a lens to the magnomechanical system.

Besides the physical interest of replacing an optical system by a magnetic one, there is a technological benefit. Optomechanics in the microwave regime has had prolonged success and, the name notwithstanding, the typical wavelengths of light are then of the order of millimeters. This constrains how small the elements in the resonator can be — of the order of millimeters. It might not seem like much. However, it makes quantum information applications with many such systems impractical. A quantum computer capable of full-fledged error correction based on microwave technology and trapped ions requires a chip larger than a football field if it is to factorize a 1024-bit number [130]. Without the microwave cavities, the optomechanical systems could be much smaller, and magnetic systems offer an interesting alternative in that regard. Furthermore, magnetic systems have more parameters, more knobs, to tune such as an external magnetic field. These allow for a tunable magnomechanical coupling.

4.2.1 Ferromagnetic resonance

The magnetization of a ferromagnetic sample can be made to precess at a rate that depends on external factors. This precession is the FMR. As in the case of nuclear magnetic resonance or other spin resonances, it can be seen by applying a strong static magnetic field to the sample and probing it with an alternating magnetic field oriented in the perpendicular direction relative to the static field. Fundamentally, ferromagnetism is caused by the angular momentum carried by the electrons of the material, but FMR is a phenomenon well understood from classical electromagnetism [131].

If a ferromagnet consists only of a single domain, its magnetic state is described by a single magnetization vector \mathbf{M} , independent of the position within the magnet. Subjecting the magnet to an external magnetic field \mathbf{H} results in an effective magnetic field \mathbf{H}_{eff} within it. This effective field includes the response of the magnet to the external field — this is to be discussed at length. In any case, the magnetization \mathbf{M} and the effective field \mathbf{H}_{eff} interact. They would prefer aligning with one another and, thus, the magnetization experiences a torque. Dynamically, this is described by the equation of motion

$$\frac{d\mathbf{M}}{dt} = -\gamma\mathbf{M} \times \mathbf{H}_{\text{eff}} - \lambda\mathbf{M} \times (\mathbf{M} \times \mathbf{H}_{\text{eff}}), \quad (4.4)$$

which is also called the Landau–Lifshitz–Gilbert equation [132]. The proportionality constant γ in the torque is the gyromagnetic ratio which can vary from the free electron value in different materials. The damping, or dissipation, is represented by the latter term proportional to λ which is a phenomenological parameter. Physically, this equation is constructed so that it describes a rotating magnetization; for all times, the magnitude of the magnetization remains constant. Its value is called the saturation magnetization $M_S = |\mathbf{M}|$.

The ferromagnetic resonance mode is the time-dependent solution of Eq. (4.4). (The time-independent solution is that \mathbf{M} is parallel to \mathbf{H}_{eff} .) For a constant effective field \mathbf{H}_{eff} in the z direction and in the absence of dissipation, $\lambda = 0$, the magnetization in the x and y directions is given by Eq. (4.4) as

$$\begin{pmatrix} M_x(t) \\ M_y(t) \end{pmatrix} = \exp\left[\gamma|\mathbf{H}_{\text{eff}}|t \begin{pmatrix} 0 & -1 \\ 1 & 0 \end{pmatrix}\right] \begin{pmatrix} M_x(0) \\ M_y(0) \end{pmatrix} \quad (4.5)$$

$$\equiv \begin{pmatrix} \cos(\omega_K t) & -\sin(\omega_K t) \\ \sin(\omega_K t) & \cos(\omega_K t) \end{pmatrix} \begin{pmatrix} M_x(0) \\ M_y(0) \end{pmatrix} \quad (4.6)$$

with any initial condition. The solution describes magnetization that rotates around the z axis at the angular frequency $\omega_K = \gamma|\mathbf{H}_{\text{eff}}|$. This is the FMR frequency. The z component follows from the normalization condition $M_z^2 = M_S^2 - M_x^2 - M_y^2$ and is a constant in the present case. Often, however, the effective field \mathbf{H}_{eff} depends on the magnetization \mathbf{M} . This may change the circular precession to an elliptic one.

The effective field \mathbf{H}_{eff} describes FMR fully. It can include

- 1) the external field \mathbf{H} ,
- 2) the demagnetizing field \mathbf{H}_{dm} that describes the shape-dependent response to the external field as to satisfy the boundary conditions of the Maxwell's equations,
- 3) the magnetoelastic field \mathbf{H}_{me} to model the material-dependent interplay between elastic deformations and magnetism,
- 4) the crystal anisotropy field \mathbf{H}_{an} to take into account the possible magnetic contribution from the lattice structure of the material.

Similar to the concept of force in classical mechanics, the effective field is a superposition of all such fields. Its main value is differentiating magnetic effects while retaining one cohesive framework of the magnetic system.

In some cases, the idea of fields is helpful. In others, it can be more useful to work with the free-energy density \mathcal{F} associated with the field. It plays an important role, as it determines the magnomechanical Hamiltonian. The two frameworks are connected by the functional derivative relation

$$\mu_0 \mathbf{H}_i = -\frac{\delta}{\delta \mathbf{M}} \mathcal{F}_i, \quad (4.7)$$

where μ_0 is the vacuum permeability. For instance, in this definition, the external field \mathbf{H} corresponds to $\mathcal{F}_{\text{ext}} = -\mu_0 \mathbf{M} \cdot \mathbf{H}$.

Magnetoelastic interaction is conventionally written in terms of the free energy. For cubic crystals¹ specifically, the magnetoelastic free-energy density is estimated by [133, 134]

$$\mathcal{F}_{\text{me}} = \frac{B_1}{M_S^2} (M_x^2 \epsilon_{xx} + M_y^2 \epsilon_{yy} + M_z^2 \epsilon_{zz}) + \frac{2B_2}{M_S^2} (M_x M_y \epsilon_{xy} + M_x M_z \epsilon_{xz} + M_y M_z \epsilon_{yz}), \quad (4.8)$$

where $B_{1/2}$ are material- and sample-dependent magnetoelastic constants [134], and the elastic deformation is encoded in the strain tensor defined as

$$\epsilon_{ij} = \frac{1}{2} \left(\frac{\partial u_i}{\partial x_j} + \frac{\partial u_j}{\partial x_i} + \sum_k \frac{\partial u_k}{\partial x_i} \frac{\partial u_k}{\partial x_j} \right). \quad (4.9)$$

The vector field \mathbf{u} describes displacement from an assumed neutral position of the magnet and, here, the notation x_i should be understood as referring to the coordinate system $(x, y, z) = (x_1, x_2, x_3)$. Focusing on the terms in the strain that are linear in u , it can be seen that B_1 describes deformations that change the size of the magnet whereas B_2 describes the effect of shear to the magnetization. I was surprised to learn that B_1 can be of either sign: some materials wish to shrink and some to expand when magnetized in order to minimize the free energy. In contrast, the conventional (cubic crystal) ferromagnetic materials dislike shear in which case B_2 is a positive constant [134].

Crystal anisotropy field describes the effect of crystal structure on magnetization. It can lead to preferred direction of magnetization with respect to the underlying lattice axes of the material. In a similar spirit to the magnetoelastic energy, this magnetocrystalline free-energy density for cubic crystals is estimated by

$$\mathcal{F}_{\text{an}} = \frac{K_1}{M_S^4} \left(M_x^2 M_y^2 + M_y^2 M_z^2 + M_z^2 M_x^2 \right) + \frac{K_2}{M_S^6} M_x^2 M_y^2 M_z^2 \quad (4.10)$$

with some constants K_1 and K_2 [133]. This expression, as well as the magnetoelastic free energy, follows from symmetry arguments — such as invariance under

¹I mistakenly implied in [III] that this is a general quality of magnetoelasticity independent of the crystal structure. It is not. In the context of [III], there is only a single relevant strain component and, thus, the change can only be in the relevant magnetization component and the magnitude of the effective magnetoelastic constant. It is also consistent with CoFeB as the possible magnetic material for the experiments.

axis permutation — and only including the lowest order terms in the magnetization [135]. In [III] the crystal anisotropies are neglected as we assume the magnetoelastic effects to be stronger. In any case, it does not change the physics of magnomechanics.

Magnomechanics is realized in a ferromagnetic system alone since the magnet can have vibrational modes. Magnomechanical coupling is evidently in the demagnetizing and magnetoelastic fields. In principle, the crystal anisotropies may also be connected to the shape and motion of the magnet. Such effects are assumed to be small in comparison to other shape effects.

4.2.2 Suspended magnetic beam

The program to finding the magnomechanical coupling of a vibrating single-domain magnetic beam follows: First, all the free energies related to the effective magnetic field must be specified. From the free-energy description, the stationary state of the magnetization within the beam may be obtained. This lays the foundations of quantization. The FMR mode around the stationary state can be solved and then quantized. All the while the magnetization and the FMR mode depends on the shape of the beam. Allowing the beam to vibrate and quantizing those vibrations, the magnomechanical coupling can be found.

The remaining premise is how the beam geometry should be defined. There are two clear candidates: a bridge and a cantilever. Their only difference is that, in a bridge, the two ends of the beam are fixed (and thus it is also called doubly-clamped beam) whereas a cantilever has only one fixed end and the other one is free to move about. In practice and in theory, they work differently. Herein, as in [III], my focus is on a bridge setup.

There are three directions to be defined: the beam axis, the external static field to generate the FMR mode, and the external alternating field to drive the FMR. Our choice is partially experimentally motivated. We set the beam axis and the external static field in the same plane, while the alternating field is perpendicular to this plane. It allows for varying the direction of the static field while retaining the perpendicularity to the driving field. Furthermore, as discussed later on, the static field can be used in devising measurement and driving schemes.

The beam itself should be as low mass m as possible to benefit the vibrational qualities of the magnet. Especially, the zero-point motion amplitude x^{ZPM} is proportional to $1/\sqrt{m}$. Practically, this is achieved by making very thin beams. The relevant beams for magnomechanics are thus of height h , width w , and length L so that $L > w \gg h$. The smaller the width, the more sense it makes to describe the beam as an one-dimensional object. This greatly simplifies the description of deformations: the displacement \mathbf{u} has a single non-vanishing component with a functional relationship $u_x = u_x(z)$ when the beam axis is in the z direction. It is a reasonable approximation for beams of finite width, as well.

The setup is depicted in Fig. 5. At this point, one might observe a problem without proceeding with the calculations. There is no difference if the beam would have been displaced downwards instead of upwards as in Fig. 5. There is no directionality, there is no magnomechanics.

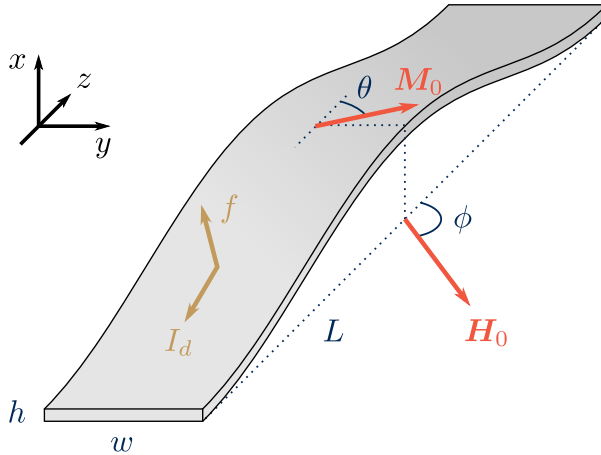


FIGURE 5: Sketch of a beam with a displacement. Here, I_d represents a current which causes a Lorentz force f on the beam in the presence of a static magnetic field H_0 . For other symbols, see the main text. Reprinted with permission from [III], Copyright American Physical Society.

This problem can be solved by introducing directionality in two different ways. The setup can be modified so that the static field points out of the plane of the beam. Alternatively, we can assume that there is a static deformation — similar to Fig. 5 — and the beam vibrates around the already-deformed configuration. I am unsure which realization came first, but such deformation is also observed experimentally. It is a consequence of fabricating multi-layer beams. The practical idea is to have an insulating magnetic layer and a separate conducting layer for using currents in measurements.

Theoretically, we proceed by dividing the deformation $u_x \equiv u$ into a static and a dynamical component by

$$u(z, t) = u_0(z) + u_1(z, t) \quad (4.11)$$

together with an assumption that the static deformation is large in the sense of $u_0 \gg u_1$. I drop the subscript x for simplicity. This approach requires the calculation to be second order in u in order to calculate the effect of the vibrations to first order which are proportional to u_1 . In accordance, the dynamics of the beam are described by a nonlinear Euler–Bernoulli beam equation

$$\rho A \frac{\partial^2 u}{\partial t^2} + EI_x \frac{\partial^4 u}{\partial z^4} - \left[-P + \frac{EA}{2L} \int_0^L dz \left(\frac{\partial u}{\partial z} \right)^2 \right] \frac{\partial^2 u}{\partial z^2} = f, \quad (4.12)$$

where $A = wh$ is the beam cross-section area and $I_x = wh^3/12$ the bending modulus, ρ the density, E the Young's modulus, P the axial load or compression, and f a possible external force on the beam.

Our idea was initially to describe the deformed beam by setting $P = 0$ and by specifying a finite derivative for $u_0(z)$ at the ends of the beam. However, this does not result in beams that look physical. The point is that P describes compression

or tension in the system. This differs greatly from simple boundary conditions. We then understood that the compression may follow from the internal tension between different layers of beam. Here, it is P that causes the static deformation. More conventionally, it describes an axial force which is easy to test: Put a piece of paper on a table and softly push two sides towards one another. At first, the paper resists but with enough force it will deform upwards. This is called the buckling transition. The deformed configuration follows if $P > 4\pi^2 EI_x / L^2$. In contrast, take a piece of paper and bend it from two opposite edges to the same direction while trying to keep your hands as far apart as possible. The result is quite different: the center remains very flat and there is a great tension. This is what setting $P = 0$ and fixing the boundary conditions would describe.

Finally, the demagnetizing field \mathbf{H}_{dm} can be specified. It follows from the magnetostatic part of the Maxwell's equations, that is, $\nabla \cdot \mathbf{B} = 0$ and $\nabla \times \mathbf{H} = 0$. The difference between \mathbf{B} and \mathbf{H} is the magnetization \mathbf{M} . The role of demagnetizing field is to modify the \mathbf{H} -field so that the magnetostatic equations are satisfied. We have that

$$\mathbf{B} = \begin{cases} \mu_0 \mathbf{H}^{\text{out}} = \mu_0 (\mathbf{H}_0 + \mathbf{H}_{\text{dm}}), & \text{outside the beam,} \\ \mu_0 (\mathbf{H}^{\text{in}} + \mathbf{M}) = \mu_0 (\mathbf{H}_0 + \mathbf{H}_{\text{dm}} + \mathbf{M}), & \text{inside the beam.} \end{cases} \quad (4.13)$$

More often than not, the demagnetizing field outside the magnet is called a stray field. The analytical solution of these equations is admissible only in special cases. If we approximate the beam as infinitely thin and as having infinite width and length, the demagnetizing field of a deformed magnet can be obtained by a boundary condition argument: the magnetostatic equations require that the \mathbf{B} -field is continuous in the normal direction of the beam and the \mathbf{H} -fields continuous in the tangential directions. Without deformation the stray field is zero, and using this as an ansatz gives the conditions for the normal (subscript n) and tangential (t) components of the demagnetizing field

$$H_{\text{dm},n} = -M_n, \quad H_{\text{dm},t} = 0, \quad H_{\text{dm},y} = 0. \quad (4.14)$$

This expression shows that the magnetization wishes to follow the shape of the deformed beam. Here, we assume that the ferromagnet however remains as a single domain and that the deformation does not induce position dependence in the magnetization. In the end, it is useful to transform the local coordinate system (n, t) that depends on the deformation $u(z)$ to the original coordinate system (x, z) . This gives, finally,

$$\begin{pmatrix} H_{\text{dm},x} \\ H_{\text{dm},z} \end{pmatrix} = \frac{1}{1 + [\partial_z u]^2} \begin{pmatrix} -1 & \partial_z u \\ \partial_z u & -[\partial_z u]^2 \end{pmatrix} \begin{pmatrix} M_x \\ M_z \end{pmatrix}. \quad (4.15)$$

and the corresponding free-energy density

$$\frac{\mathcal{F}_{\text{dm}}}{\mu_0} = \frac{1}{2} \frac{1}{1 + [\partial_z u]^2} M_x^2 - \frac{\partial_z u}{1 + [\partial_z u]^2} M_x M_z + \frac{1}{2} \frac{[\partial_z u]^2}{1 + [\partial_z u]^2} M_z^2. \quad (4.16)$$

Without the deformation only $\mathcal{F}_{\text{dm}} = \mu_0 M_x^2 / 2$ remains. Turning the magnetization towards x , out of plane, costs energy. Consequently, in magnetism literature, x would be called a hard axis.

We assume that the strain producing the static deformation produces such a large effect that it overpowers any crystal anisotropies in the material. In other cases, such anisotropies might be necessary to include.

The classical Hamiltonian, the total free energy, is obtained by integrating over the beam. At this point, many of the terms disappear due to the boundary conditions of doubly-clamped beam $u(z = 0) = u(z = L) = 0$. In the end, there are only four terms

$$\mathcal{H}/(whL) = -\mu_0 \mathbf{H} \cdot \mathbf{M} + \frac{B_1}{M_S^2} M_z^2 \bar{\epsilon}_{zz} + \mu_0 M_x^2 / 2 + \mu_0 (M_z^2 - M_x^2) \bar{\epsilon}_{zz} \quad (4.17)$$

with the strain now averaged over the beam as

$$\bar{\epsilon}_{zz} = \frac{1}{L} \int_0^L dz \frac{1}{2} \left(\frac{\partial u}{\partial z} \right)^2. \quad (4.18)$$

To reaffirm the point about the necessity of the static deformation, observe that the strain depends only on the square of u . Thus, the energy changes as much to upward as to downward displacements, and there is no magnomechanics without the buckling of the beam in an in-plane magnetic field.

The steps to the magnomechanical coupling follow the program set about in the beginning of this section. The static magnetization is obtained by minimizing the total free energy while considering a static field $\mathbf{H} = \mathbf{H}_0$ and a strain $\bar{\epsilon}_{zz}$. Due to the demagnetizing field, it prefers to stay in the yz plane (refer to the coordinate system in Fig. 5). The magnetic system can be quantized and the FMR frequency can be solved for a fixed strain, then expanded around the static and dynamic deformations, u_0 and u_1 respectively. The explicit form of u_0 and the eigenmode decomposition of u_1 is obtained from the Euler–Bernoulli equation. Finally, the vibrations can be quantized as well. (In [III] the order is slightly different; we first expand the strain and then quantize the magnetization but the result is the same.)

One important difference between opto- and magnomechanics is the quantization. In contrast to the cavity mode, the magnetization \mathbf{M} is not quantized as a bosonic mode but rather obeys the commutation relations $[M_i, M_j] = i \sum_k \epsilon_{ijk} M_k$ with the fully antisymmetric Levi–Civita tensor ϵ_{ijk} [23]. These are of course the commutation relations of spin or angular momentum as well, arising from the same considerations. Especially, one can relate the magnetization M to a spin M_S system. This is the macrospin model. The magnetization in a coordinate system $(x'y'z')$ — which is chosen so that z' points into the direction of the static magnetization — can be mapped to a bosonic mode m by the Holstein–Primakoff transformation

$$\frac{M_{z'}}{M_S} = 1 - \zeta m^\dagger m, \quad \frac{M_{+'}}{M_S} = \sqrt{2\zeta} \sqrt{1 - \frac{\zeta}{2} m^\dagger m}, \quad \frac{M_{-'}}{M_S} = \sqrt{2\zeta} m^\dagger \sqrt{1 - \frac{\zeta}{2} m^\dagger m}, \quad (4.19)$$

where $\zeta = \hbar\gamma/(whLM_S)$ is a dimensionless parameter and $M_{\pm'} = M_{x'} \pm iM_{y'}$ are the ladder operators. Here, ζ characterizes the ratio between the classical

energy $\mu_0 \omega h L M_S^2$ stored within the magnet and a single quantum of energy at the frequency $\gamma \mu_0 M_S$. For magnets whose volume is larger than a few cubic nanometers, typically $\zeta \ll 1$. Moreover, we retain the bosonic description similar to optomechanics, if we can assume that the number n of excitations of the mode m , which are called now *magnons*, is such that $n\zeta \ll 1$ as well. In such a case, one can only consider the lowest-order expansion in ζ so that $M_{\pm'} \propto m$. It however limits how much the magnon mode can be driven before there are saturation effects.

The magnomechanical coupling of the n th vibrational mode in the deformed beam setup obeys

$$g_{m,n} = 2(g_n^{\text{me}} - g_n^{\text{dm}}) \left(c \cos^2 \theta + \frac{1}{c} \cos 2\theta \right) - 2c g_n^{\text{dm}}, \quad (4.20)$$

where θ is the angle of the magnetization vector \mathbf{M} with respect to the z direction, c is a squeezing factor related to the ellipticity of the FMR mode, and two separate coupling constants are given by

$$g_n^{\text{me}} = -\bar{\beta}_n \frac{h x_n^{\text{ZPM}}}{L^2} \frac{\gamma B_1}{M_S}, \quad (4.21a)$$

$$g_n^{\text{dm}} = +\bar{\beta}_n \frac{h x_n^{\text{ZPM}}}{L^2} \gamma \mu_0 M_S, \quad (4.21b)$$

$$\bar{\beta}_n = \frac{L}{h} \int_0^L dz (\partial_z u_0) (\partial_z \chi_n). \quad (4.21c)$$

The dimensionless parameter $\bar{\beta}_n$ contains the information about static deformation and vibration modes as χ_n is the n th vibrational eigenmode corresponding to the eigenfrequency ω_n .

The squeezing factor c is also related to a truly magnetic property resulting from the free energy: hysteresis. In the process of minimizing the free energy with respect to the magnetization, there can be a local minimum in addition to the global one. Since the minima depend on the external field as well, the magnetization may remain in the energetically unfavored state as the external field is varied. Here, it is due to the magnetoelastic and demagnetizing fields in the presence of a static deformation. The resulting model for hysteresis closely imitates a seminal description in the field, the Stoner–Wohlfarth model. Hysteresis is characterized by a coercive field H_c . When the strength of the magnetic field is below H_c , there are multiple minima. The coercive field when the external magnetic field is in the y direction, perpendicular to the beam axis, can be solved and it reads

$$H_c = 2 \left| \frac{B_1}{\mu_0 M_S^2} + 1 \right| \epsilon_{zz}^{(0)} M_S. \quad (4.22)$$

The superscript (0) is to emphasize that the strain here is due to the static deformation.

The squeezing factor c describes, on a more technical level, how much the momentum quadrature of the magnon mode m must be squeezed in order to diagonalize the FMR Hamiltonian. It is given by

$$c = \sqrt{\frac{H_0 \cos(\theta - \phi) + H_c \zeta \cos(2\theta)}{H_0 \cos(\theta - \phi) + (1 - 2\bar{\epsilon}_{zz}^{(0)}) M_S + H_c \zeta \cos^2(\theta)}}, \quad (4.23)$$

where $\zeta = \text{sign}(-B_1 - \mu_0 M_S^2) = \pm 1$, $|\mathbf{H}_0| = H_0$ is the magnitude of the static external field and ϕ its direction as in Fig. 5. Without the strain, the value of the squeezing factor is simply $c = \sqrt{H_0/(H_0 + M_S)}$. The fact that squeezing is always present in magnon systems has given rise to discussion how it can be utilized in, for instance, entanglement [136, 137] and generation of quantum states [138].

In every expression there is a competition between the demagnetizing and magnetoelastic fields. This is characterized by the ratio $B_1/(\mu_0 M_S^2) = -g_n^{\text{me}}/g_n^{\text{dm}}$. There are two distinct regimes, that of $B_1 < -\mu_0 M_S^2$ and that of $B_1 > -\mu_0 M_S^2$. In the former case, the fields have an opposite tendency and the magnetoelasticity wins. Magnetization in the z direction is strongly preferred and, thus, z is an easy axis. In the latter case, either the fields have the same tendency or demagnetizing field wins making z a hard axis. These regimes have different hysteresis curves and thus can be experimentally separated.

The magnomechanical coupling in the end depends only the magnetic parameters $B_1/(\mu_0 M_S^2)$ and H_0/M_S , and the mechanical parameters like the static strain $\bar{\epsilon}_{zz}^{(0)}$ and the “mode overlap” $\bar{\beta}_n$. From the Euler–Bernoulli equation (4.12) it follows that these mechanical parameters are mapped one-to-one to maximum of the static deformation $u_m = \max |u_0(z)|$. For instance, the dimensionless parameter $\bar{\beta}_n$ is plotted in Fig. 6 in terms of u_m .

The magnomechanical constant in the case of dominating demagnetizing field and a negative magnomechanical constant, $0 > B_1 > -\mu_0 M_S^2$, is graphed in Fig. 7 as a function of the direction of the external magnetic field. The inset represents the hysteresis curve, focusing on the relation between the magnetization and the external field in the y direction. What appears interesting and unexpected at first is that the coupling is larger for the hysteretic part and may diverge. In these points, the local minimum is also very unstable in the sense that the energy barrier to escape from the state goes to zero. A closer look also reveals that a larger magnetic field does not necessarily result in a larger coupling. Rather, the coupling changes sign and is even zero at some configurations.

After all that work, it would seem that finding that the magnomechanical coupling can simply vanish due to an unfortunate choice magnetic field is discouraging. It is not so. Having a system with tunable interaction is exactly what we are after. Moreover, even if the optomechanical interaction in the sense of the Hamiltonian (4.3) is not present, there are higher-order terms that were neglected. One of them is the so-called cross-Kerr term of type $a^\dagger ab^\dagger b$. Such terms can be finite even without the static deformation since they do not have an immediate issue with symmetry.

4.2.3 Brief comment on other geometries

The magnomechanical coupling follows in a similar fashion for a cantilever — a thin beam fixed only on one end. In contrast to the bridge, it is enough to take into account only the first order displacement u in the magnetoelastic and demagnetizing fields. Then, the total magnetic free energy of the cantilever depends on the position of the free end $u(L)$. The shape-dependent free-energy terms are proportional to $M_x M_z u(L)$ and the relevant magnetoelastic constant is the shear

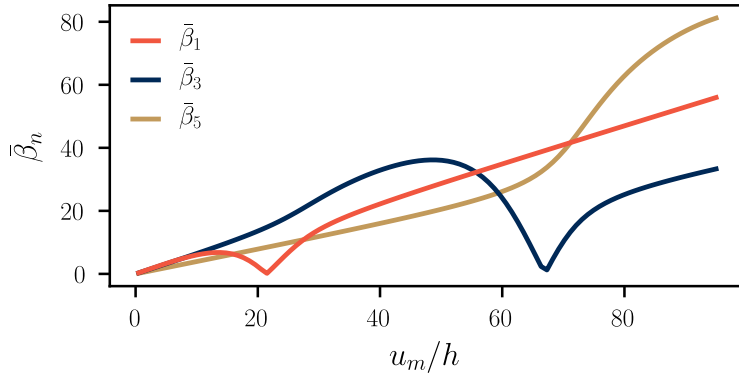


FIGURE 6: The dimensionless parameter $\bar{\beta}_n$ for five first modes as a function of the maximum deformation u_m . Here, $n = 1$ is the lowest order mode, and $\bar{\beta}_n = 0$ for $n = \text{even}$ modes. For small deformations $\bar{\beta}_n \propto u_m/h$, but the nonlinearity of the Euler–Bernoulli equation results in a nonlinear behaviour for large deformations. Reprinted with permission from [III], Copyright American Physical Society.

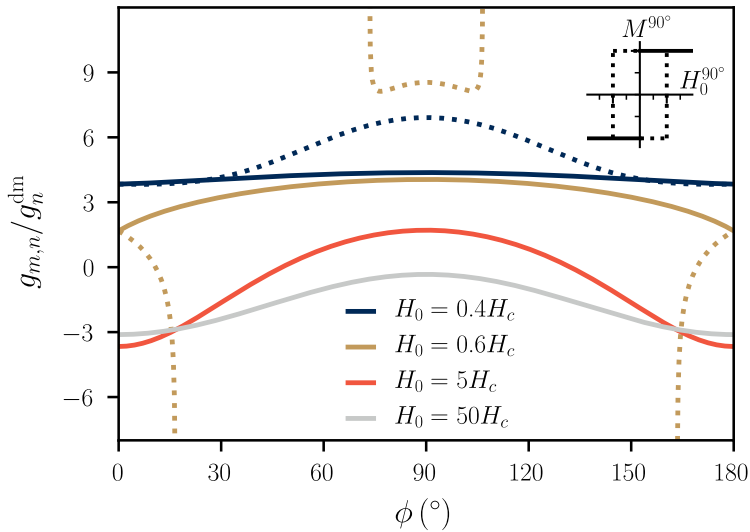


FIGURE 7: Magnomechanical coupling constant $g_{m,n}$ as a function of the external field direction ϕ . The different curves represent different magnetic field strengths H_0 ; the dotted lines correspond to the metastable magnetization configuration. The parameters are $u_m/L = 0.1$ and $B_1 = -0.6\mu_0 M_S^2$ so that $50H_c \approx M_S$. The inset shows the corresponding hysteresis curve for components perpendicular to the beam. Reprinted with permission from [III], Copyright American Physical Society.

constant B_2 . The symmetry argument remains: if the external magnetic field is in the plane of the neutral position of the cantilever, there is no magnomechanical interaction.

Somewhat more interesting is the question of “bulky” systems. For instance, the ferromagnetic materials in [128, 129] are in the shape of spheres. The theoretical analysis in [128] argues that the magnomechanical coupling can be found by quantizing the magnetization in the magnetoelastic energy and then gathering the terms which give an optomechanical interaction. This leads to magnomechanical coupling proportional to

$$g \propto \frac{B_1}{V} \int d^3x (\epsilon_{xx} + \epsilon_{yy} - 2\epsilon_{zz}), \quad (4.24)$$

when the FMR mode is precessing around the z axis and V is the spherical magnet volume. At this point, again, symmetry seems to play a somewhat confusing role: the coupling vanishes for mechanical modes that retain the spherical shape without shear. For the strains, I mean that only $\epsilon_{xx} = \epsilon_{yy} = \epsilon_{zz}$ are non-vanishing. This happens even though the magnetoelastic energy cares whether the sphere shrinks or expands. There is a clear directionality. However, it does not affect the FMR mode. This is a simple consequence of the magnetoelastic energy; for such a shrinking or expanding sphere the relevant term is

$$\mathcal{F}_{\text{me}} = \frac{B_1}{M_S^2} (M_x^2 \epsilon_{xx} + M_y^2 \epsilon_{yy} + M_z^2 \epsilon_{zz}) \rightarrow B_1 \frac{M_x^2 + M_y^2 + M_z^2}{M_S^2} \epsilon_{zz} = B_1 \epsilon_{zz}. \quad (4.25)$$

That is, there is no coupling between the strain and the magnetization if the magnitude of the magnetization remains constant.² Ultimately, this is not much of a problem since there are many other mechanical modes that have a finite magnetoelastic coupling. As a final remark on spheres, I note that the magnomechanical coupling g scales as $g \propto 1/D^2$ with D being the diameter of the sphere, so the magnetic systems are in fact small, of the order of few hundred micrometers [128]. This is similar to the deformed beam geometry wherein $g \propto 1/L^2$ if all other parameters are fixed.

4.2.4 Input–output scheme

The advance of the beam setup of Fig. 5 is that both the FMR and the mechanical mode can be driven individually. The signs of magnomechanical interaction may be observed as changes in reflection or transmission of the driving signals.

If the magnetic beam is conducting, which can be achieved either by using a ferromagnetic metal or by constructing bilayer beam with separate conducting and insulating ferromagnetic layers, a current I_d can be driven through it. This produces a Lorentz force per unit length as $f = I_d \mu_0 (H_0 \sin \phi + M_S \sin \theta)$ pointing always to the normal direction of the beam (the contribution proportional to M_S assumes that the current is flowing through the magnet). At the same time, the vibrations of the beam produce an electromotive force due to induction. This seems reasonable if one considers the beam to be a part of circuit enclosing some area

²For a sphere, the demagnetizing field is $H_{\text{dm}} = -M/3$ [131]. That is, it is independent of the size.

and, thus, some magnetic flux. The vibrations of the beam change the flux. These ideas are called the magnetomotive scheme.

The FMR mode is driven by an alternating magnetic field h , produced by an alternating current in a microwave line. This requires “a good contact” as the spatial extent of the FMR mode and the driving field must have an overlap. The FMR mode can be seen as an absorption of power in the driving process, or alternatively with an external antenna measuring the transmitted microwaves.

An interesting feature (or a possible nuisance) is that the drives can interact. The current I_d that drives the mechanical vibrations produces a Lorentz force together with the alternating field h . This force is to the y direction and may drive transverse vibrations. However, the frequency scales of the mechanical and FMR mode are often of different orders, and thus, this cross-driving can be neglected.

The picture of the input and output fields is readily applicable. Phenomenologically, I write for the diagonalized (and bosonized) FMR mode l and the vibrational mode b

$$\dot{l} = \frac{i}{\hbar} [H_S, l] - \frac{\kappa}{2} l - \sqrt{\kappa_e} l_{\text{in}}, \quad (4.26)$$

$$\dot{b} = \frac{i}{\hbar} [H_S, b] - \frac{\gamma}{2} b - \sqrt{\gamma_e} b_{\text{in}}, \quad (4.27)$$

where H_S is the full magnomechanical Hamiltonian similar to Eq. (4.3)

$$H_S/\hbar = \omega_K l^\dagger l + \omega_m b^\dagger b + g_m l^\dagger l (b^\dagger + b). \quad (4.28)$$

The dynamical equations are supplemented with the relations $l_{\text{out}} = l_{\text{in}} + \sqrt{\kappa_e} l$ and $b_{\text{out}} = b_{\text{in}} + \sqrt{\gamma_e} b$. These equations allow for, eventually, the solution of the reflection coefficient; how much of a probe signal gets reflected. This provides the way to observe magnomechanics.

The dissipation rates κ and γ for the FMR and the vibrations, respectively, play an important role in optomechanics [111]. In general, for any quantum application, it is required the modes are of high quality, that is, $\omega_m \gg \gamma$ and $\omega_K \gg \kappa$. In cavity optomechanics and thus in magnomechanics, the relation of ω_m to κ is also important. In [III] we assume that the FMR dissipation rate or linewidth is much larger than the mechanical eigenfrequency, $\kappa \gg \omega_m$. The opposite limit of $\omega_m \gg \kappa$ is called the resolved-sideband limit. Many of the experiments mentioned in the beginning of the section rely on this regime but, for instance, the signal processing effects do not.

To enhance the magnomechanical coupling, the FMR mode should be driven. The drive also linearizes the coupling Hamiltonian. One can redefine the FMR mode in such a case by $l = \sqrt{n} + \delta l$, where n is the number of excitations, magnons, uphold by the drive in the presence of dissipation, and δl represents deviation from this equilibrium. If the deviations are assumed small, the second-order term $\delta l^\dagger \delta l$ may be neglected in the interaction, and the Hamiltonian simplifies to

$$H_S/\hbar = \omega_K \delta l^\dagger \delta l + \omega_m b^\dagger b + \sqrt{n} g_m (\delta l + \delta l^\dagger) (b^\dagger + b). \quad (4.29)$$

Here, the terms proportional only to $b + b^\dagger$ and $\delta l + \delta l^\dagger$ have been displaced away to the definitions of b and δl .

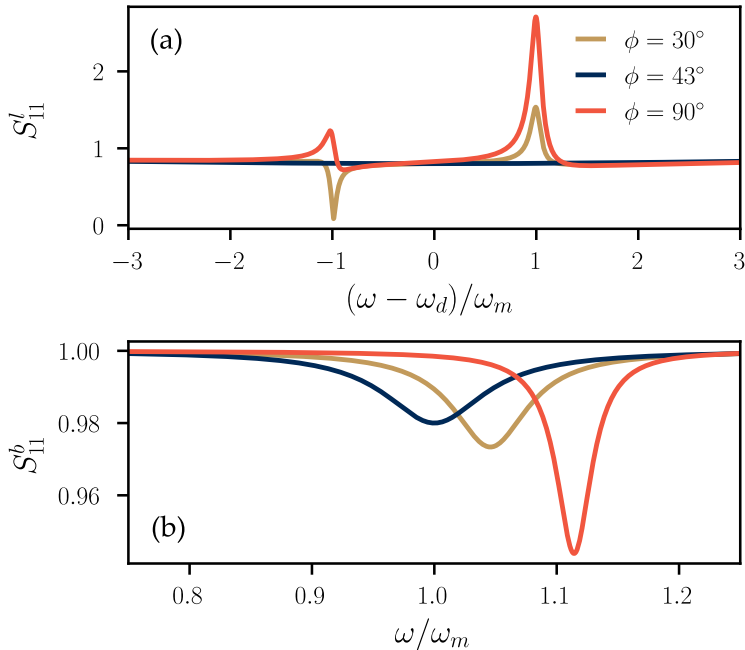


FIGURE 8: Reflection coefficients for the (a) FMR and (b) mechanical mode. The external field strength is fixed by $H_0 = 5H_c$ while the other parameters are as in Fig. 7. In (b), $\omega_d = \omega_K - \omega_m$ whereas in (a) $\omega_d = \omega_K$. The relevant parameters are fixed by $2\sqrt{n}g^{\text{dm}} = 0.8\omega_m$ and $\kappa = 15\omega_m$, $\gamma = 0.1\omega_m$ and $\kappa_e/\kappa = 0.1$, $\gamma_e/\gamma = 0.01$. Reprinted with permission from [III], Copyright American Physical Society.

In the description $l = \sqrt{n} + \delta l$, it is implicitly assumed that the number n of magnons obeys some classical equation, depending on the driving power. The deviation δl then obeys, in fact, the same input-output equation as l itself. Thus, it is somewhat common and convenient, although slightly confusing, to rename $\delta l \rightarrow l$.

Due to the linearity of the Hamiltonian the outputs and the inputs are linearly related. Such a relation holds in frequency space as well. This in turn gives the transmission, reflection, and transduction coefficients. For instance, the reflection coefficient S_{11}^l of the FMR mode is $l_{\text{out}} = S_{11}l_{\text{in}} + \dots$ whereas the transduction coefficient S_{1b} from mechanics to FMR follows from $l_{\text{out}} = S_{1b}b_{\text{in}} + \dots$

Focusing on the reflection coefficients, magnomechanics in the non-resolved sideband regime gives rise to the amplification of microwave signals and a “magnetic” spring effect. Fig. 8(a) shows the amplification, given a drive frequency ω_d that is resonant with the FMR mode, $\omega_d = \omega_K$. The reflection coefficient becomes greater than unity at the sideband frequencies $\omega_K \pm \omega_m$ at the strongest couplings. The latter means that the FMR mode shifts the resonance frequency of the vibrations. Thus, the mechanical system absorbs the most power at a frequency that depends on the magnomechanical coupling. This results in magnetic field-dependent dips in the reflection coefficient as shown in Fig. 8(b).

4.3 Many facets of hybrid quantum systems

An interesting aspect of hybrid quantum systems is that we can easily imagine a single system that exhibits both linear and nonlinear interactions. Likewise, it is easy to imagine systems with more than two physically important modes. The latter I already mentioned in passing: the successful experiments on magnomechanics [128, 129] employ magnons, photons, and phonons at the same time. The purpose of this penultimate section is to take a broader look on such systems, going beyond [I]–[V].

Magnon-photon-phonon systems have recently seen also theoretical attention. There are two relevant classes: systems with both opto- and magnomechanical interactions and systems with one nonlinear and one linear interaction. For instance, one can add to the magnomechanical interaction a linear resonant interaction between a FMR mode and a light mode as in [128, 129]. It has been suggested that these partly linear, partly nonlinear systems can be used to investigate tripartite entanglement [139] and that magnons could enhance ground-state cooling of a mechanical resonator [140]. On the other hand, the combined opto- and magnomechanical interaction can be used to effectively probe the magnons optically [141]. That is, there is ground to cover in understanding how opto- or magnomechanical effects are modified by the presence of a coupling to another degree of freedom.

Next, I must point out a direct connection between the discussion of polaritons in Ch. 2 and optomechanics: the field of molecular optomechanics [142, 143]. Physically, the point is to couple a molecular vibration mode to a cavity instead of an electronic excitation. Optomechanical interaction follows from the dipole interaction and the classical argument of the depolarizing field (that is the electric field equivalent of the demagnetizing field). If the dipole moment \mathbf{d} of a molecule depends on the classical electric field \mathbf{E} as $\mathbf{d} = \mathbf{d}_0 + \alpha\mathbf{E}$ where α is polarizability tensor [33], then the dipole interaction $\mathbf{d} \cdot \mathbf{E}$ results in an interaction proportional to $\mathbf{E} \cdot (\alpha\mathbf{E})$. This term modifies the eigenfrequencies of the cavity. Optomechanical interaction is then achieved if α depends on a vibrational coordinate of the molecule. This interaction has been suggested as the mechanism behind surface- and tip-enhanced Raman scattering [143] which are widely-used spectroscopic tools for studying vibrational resonances of molecules.

Organic molecules provide innately different frequency scales through their vibrational and electronic excitations. In Ch. 2, the mental picture is of light-matter coupling to the higher-energy electronic excitation while the much lower-energy vibrations perturb the coupling. In molecular optomechanics, it can be inversely asked how does the higher energy electronic state perturb the optomechanical interaction.

The presence of different energy scales begs the general question of “emergent” resonances: What can be achieved by tuning, for example, some interaction energy between two systems on resonance with a third one? This is relevant for schemes utilizing dressed (i.e. driven) spin states as qubits [144] which can be seen as a form of Floquet engineering [145–148]. In the same vein, the possibility of tuning system resonances with respect to dissipation rates as to realize reservoir engineering has been suggested as another tool for future devices [149–151].

“Beware of the man who works hard to learn something, learns it, and finds himself no wiser than before,” Bokonon tells us. “He is full of murderous resentment of people who are ignorant without having come by their ignorance the hard way.”

Kurt Vonnegut

Cat's cradle

(Holt, Rinehart and Winston, 1963)

Chapter 5

Conclusion

I hope that you have learned as much by reading this introductory part as I have writing it, and feel ready to tackle the actual scientific publications right after the list of references. Before embarking on such an arduous journey, let me conclude by summarizing what is important in this introduction and how it connects to the five included publications.

I show through detailed examples a few physical phenomena and principles underlying hybrid quantum systems. The generality of quantum mechanical framework means that the types of hybrid systems described here are representative. We could have chosen some other starting points and arrived at a similar description. However, knowing the system is only a part of the relevant physics. I therefore focus on describing measurements and dissipation channels. For the physical realizations of hybrid quantum systems considered in this dissertation, the main tool is the input-output formalism. It is particularly suited for stationary, frequency-resolved, optical measurements. Its usage in the context of molecular systems strongly coupled to confined electromagnetic modes is the heart of publication [I] where it is extensively described. An extended discussion in the same framework about dissipation and its effect on polaritonic spectroscopy can be found in [II].

I show that hybrid quantum systems are not only interesting because of, say, their quantum informational possibilities, like utilizing non-classical correlations in quantum computing and communication, but they pose new challenges to our physical understanding. Particularly curious is the case of polaritonic or vacuum-modified chemistry. Understanding the transitions or reactions within a hybrid system still remains difficult. In this introduction, I give an outlook to the field and how our work in [IV] and [V] fits in. Here, my focus is more on the physical ideas so that their concrete manifestations are left to the publications. It remains to be seen whether or not polaritonic chemistry will have such a foundational impact as understanding the role of the electromagnetic vacuum had in the theory of quantum electrodynamics and in physics at large. Whatever the case, it is exciting.

Finally, I discuss nonlinear interactions in the context of hybrid quantum systems. I specifically focus on a new field, magnomechanics, to highlight the process of figuring out the quantum mechanical interaction. In the context of magnetism, it is quite involved. I outline the relevant physical ingredients and the important results. A more detailed understanding can be obtained from [III]. I hope that this

introduction and the publication together can give new ideas on how to approach magnomechanical systems and help realizing their technological potential.

Hybrid quantum systems will certainly thrive and see much more attention given to them in the future. The prospect of quantum technological revolution fuels the efforts. We will see continued interest in the field of quantum information and sensing and, in short term, a great devotion to utilizing magnetic systems in its applications on top of the state-of-the-art research lines like superconducting circuits. I will not try to predict the future any further — it is futile since one's imagination has limits — as we have only scratched the surface of the possibilities of hybrid quantum systems. I will, however, conclude that they will not only pose engineering challenges but questions of fundamental physics.

References

- [1] P. W. Anderson, More is different, *Science* **177** 393–396 (1972).
- [2] Z.-L. Xiang, S. Ashhab, J. Q. You and F. Nori, Hybrid quantum circuits: superconducting circuits interacting with other quantum systems, *Rev. Mod. Phys.* **85** 623–653 (2013).
- [3] M. Wallquist, K. Hammerer, P. Rabl, M. Lukin and P. Zoller, Hybrid quantum devices and quantum engineering, *Phys. Scr.* **T137** 014001 (2009).
- [4] A. Laucht, F. Hohls, N. Ubbelohde, M. F. Gonzalez-Zalba, D. J. Reilly, S. Stobbe, T. Schröder, P. Scarlino, J. V. Koski, A. Dzurak, C.-H. Yang, J. Yoneda, F. Kuemmeth, H. Bluhm, J. Pla, C. Hill, J. Salfi, A. Oiwa, J. T. Muhonen, E. Verhagen, M. D. LaHaye, H. H. Kim, A. W. Tsen, D. Culcer, A. Geresdi, J. A. Mol, V. Mohan, P. K. Jain and J. Baugh, Roadmap on quantum nanotechnologies, *Nanotechnology* **32** 162003 (2021).
- [5] G. Kurizki, P. Bertet, Y. Kubo, K. Mølmer, D. Petrosyan, P. Rabl and J. Schmiedmayer, Quantum technologies with hybrid systems, *PNAS* **112** 3866–3873 (2015).
- [6] D. Lachance-Quirion, Y. Tabuchi, A. Gloppe, K. Usami and Y. Nakamura, Hybrid quantum systems based on magnonics, *Appl. Phys. Express* **12** 070101 (2019).
- [7] A. A. Clerk, K. W. Lehnert, P. Bertet, J. R. Petta and Y. Nakamura, Hybrid quantum systems with circuit quantum electrodynamics, *Nat. Phys.* **16** 257–267 (2020).
- [8] G. Alber, T. Beth, M. Horodecki, P. Horodecki, R. Horodecki, M. Rötteler, H. Weinfurter, R. Werner and A. Zeilinger, *Quantum information: an introduction to basic theoretical concepts and experiments*, Springer Series in Modern Physics (Springer, 2001).
- [9] N. D. Mermin, *Quantum computer science: an introduction* (Cambridge University Press, 2007).
- [10] S. Aaronson, *Quantum computing since Democritus* (Cambridge University Press, 2013).
- [11] J. Preskill, Quantum Computing in the NISQ era and beyond, *Quantum* **2** 79 (2018).
- [12] H. J. Kimble, The quantum internet, *Nature* **453** 1023–1030 (2008).
- [13] W. Kozłowski and S. Wehner, Towards large-scale quantum networks, *Proceedings of the Sixth Annual ACM International Conference on Nanoscale Computing and Communication* **3** 1–7 (2019).
- [14] V. M. Shalaev, Optical negative-index metamaterials, *Nat. Photonics* **1** 41–48 (2007).
- [15] Z. Wang, F. Cheng, T. Winsor and Y. Liu, Optical chiral metamaterials: a review of the fundamentals, fabrication methods and applications, *Nanotechnology* **27** 412001 (2016).

- [16] J. Bloch, A. Cavalleri, V. Galitski, M. Hafezi and A. Rubio, Strongly correlated electron–photon systems, *Nature* **606** 41–48 (2022).
- [17] M. Reitz, C. Sommer and C. Genes, Cooperative quantum phenomena in light–matter platforms, *PRX Quantum* **3** 010201 (2022).
- [18] Y. Chu, P. Kharel, T. Yoon, L. Frunzio, P. T. Rakich and R. J. Schoelkopf, Creation and control of multi-phonon Fock states in a bulk acoustic-wave resonator, *Nature* **563** 666–670 (2018).
- [19] E. A. Wollack, A. Y. Cleland, R. G. Gruenke, Z. Wang, P. Arrangoiz-Arriola and A. H. Safavi-Naeini, Quantum state preparation and tomography of entangled mechanical resonators, *Nature* **604** 463–467 (2022).
- [20] C. F. Ockeloen-Korppi, E. Damskäg, J. M. Pirkkalainen, M. Asjad, A. A. Clerk, F. Massel, M. J. Woolley and M. A. Sillanpää, Stabilized entanglement of massive mechanical oscillators, *Nature* **556** 478–482 (2018).
- [21] R. Riedinger, A. Wallucks, I. Marinković, C. Lösschnauer, M. Aspelmeyer, S. Hong and S. Gröblacher, Remote quantum entanglement between two micromechanical oscillators, *Nature* **556** 473–477 (2018).
- [22] H.-P. Breuer and F. Petruccione, *The theory of open quantum systems* (Oxford University Press, 2002).
- [23] J. J. Sakurai and J. Napolitano, *Modern quantum mechanics*, 2nd ed. (Cambridge University Press, 2017).
- [24] Y. V. Nazarov and J. Danon, *Advanced quantum mechanics: a practical guide* (Cambridge University Press, 2013).
- [25] S. Haroche, Nobel lecture: Controlling photons in a box and exploring the quantum to classical boundary, *Rev. Mod. Phys.* **85** 1083–1102 (2013).
- [26] D. J. Wineland, Nobel lecture: Superposition, entanglement, and raising Schrödinger’s cat, *Rev. Mod. Phys.* **85** 1103–1114 (2013).
- [27] D. G. Lidzey, D. D. C. Bradley, M. S. Skolnick, T. Virgili, S. Walker and D. M. Whittaker, Strong exciton–photon coupling in an organic semiconductor microcavity, *Nature* **395** 53–55 (1998).
- [28] H. Deng, H. Haug and Y. Yamamoto, Exciton-polariton Bose-Einstein condensation, *Rev. Mod. Phys.* **82** 1489–1537 (2010).
- [29] K. Stranius, M. Hertzog and K. Börjesson, Selective manipulation of electronically excited states through strong light–matter interactions, *Nat. Commun.* **9** 2273 (2018).
- [30] S. Christopoulos, G. B. H. von Högersthal, A. J. D. Grundy, P. G. Lagoudakis, A. V. Kavokin, J. J. Baumberg, G. Christmann, R. Butté, E. Feltin, J.-F. Carlin and N. Grandjean, Room-temperature polariton lasing in semiconductor microcavities, *Phys. Rev. Lett.* **98** 126405 (2007).
- [31] M. E. Peskin and D. V. Schröder, *An introduction to quantum field theory* (Westview Press, 1995).
- [32] D. F. Walls and G. J. Milburn, *Quantum optics*, 2nd ed. (Springer, 2008).
- [33] J. D. Jackson, *Classical electrodynamics*, 3rd ed. (John Wiley & Sons, 1998).
- [34] I. S. Grant and W. R. Phillips, *Electromagnetism*, 2nd ed. (John Wiley & Sons, 1994).
- [35] S. T. Thornton and J. B. Marion, *Classical dynamics of particles and systems*, 5th ed. (Brooks/Cole, 2003).

- [36] E. A. Power and S. Zienau, Coulomb gauge in non-relativistic quantum electrodynamics and the shape of spectral lines, *Phil. Trans. R. Soc. A* **251** 427–454 (1959).
- [37] P. W. Atkins and R. G. Woolley, The interaction of molecular multipoles with the electromagnetic field in the canonical formulation of non-covariant quantum electrodynamics, *Proc. R. Soc. A* **319** 549–563 (1970).
- [38] T. E. Li, A. Nitzan and J. E. Subotnik, On the origin of ground-state vacuum-field catalysis: equilibrium consideration, *J. Chem. Phys.* **152** 234107 (2020).
- [39] X. Li, A. Mandal and P. Huo, Cavity frequency-dependent theory for vibrational polariton chemistry, *Nat. Commun.* **12** 1–9 (2021).
- [40] O. Di Stefano, A. Settineri, V. Macri, L. Garziano, R. Stassi, S. Savasta and F. Nori, Resolution of gauge ambiguities in ultrastrong-coupling cavity quantum electrodynamics, *Nat. Phys.* **15** 803–808 (2019).
- [41] M. A. D. Taylor, A. Mandal, W. Zhou and P. Huo, Resolution of gauge ambiguities in molecular cavity quantum electrodynamics, *Phys. Rev. Lett.* **125** 123602 (2020).
- [42] D. M. Rouse, B. W. Lovett, E. M. Gauger and N. Westerberg, Avoiding gauge ambiguities in cavity quantum electrodynamics, *Sci. Rep.* **11** 1–10 (2021).
- [43] V. Rokaj, D. M. Welakuh, M. Ruggenthaler and A. Rubio, Light–matter interaction in the long-wavelength limit: no ground-state without dipole self-energy, *J. Phys. B* **51** 034005 (2018).
- [44] C. Schäfer, M. Ruggenthaler, V. Rokaj and A. Rubio, Relevance of the quadratic diamagnetic and self-polarization terms in cavity quantum electrodynamics, *ACS Photonics* **7** 975–990 (2020).
- [45] P. Lalanne, W. Yan, K. Vynck, C. Sauvan and J.-P. Hugonin, Light interaction with photonic and plasmonic resonances, *Laser Photonics Rev.* **12** 1700113 (2018).
- [46] P. R. Dolan, G. M. Hughes, F. Grazioso, B. R. Patton and J. M. Smith, Femtoliter tunable optical cavity arrays, *Opt. Lett.* **35** 3556–3558 (2010).
- [47] C. Carnegie, J. Griffiths, B. de Nijs, C. Readman, R. Chikkaraddy, W. M. Deacon, Y. Zhang, I. Szabó, E. Rosta, J. Aizpurua and J. J. Baumberg, Room-temperature optical picocavities below 1 nm³ accessing single-atom geometries, *J. Phys. Chem. Lett.* **9** 7146–7151 (2018).
- [48] A. Archambault, F. Marquier, J.-J. Greffet and C. Arnold, Quantum theory of spontaneous and stimulated emission of surface plasmons, *Phys. Rev. B* **82** 035411 (2010).
- [49] R. H. Dicke, Coherence in spontaneous radiation processes, *Phys. Rev.* **93** 99–110 (1954).
- [50] E. T. Jaynes and F. W. Cummings, Comparison of quantum and semiclassical radiation theories with application to the beam maser, *Proc. IEEE* **51** 89–109 (1963).
- [51] M. Tavis and F. W. Cummings, Exact solution for an N -molecule–radiation-field Hamiltonian, *Phys. Rev.* **170** 379–384 (1968).
- [52] P. Forn-Díaz, L. Lamata, E. Rico, J. Kono and E. Solano, Ultrastrong coupling regimes of light-matter interaction, *Rev. Mod. Phys.* **91** 025005 (2019).
- [53] C. Gonzalez-Ballester, J. Feist, E. Gonzalo Badía, E. Moreno and F. J. Garcia-Vidal, Uncoupled dark states can inherit polaritonic properties, *Phys. Rev. Lett.* **117** 156402 (2016).
- [54] M. Du and J. Yuen-Zhou, Catalysis by dark states in vibropolaritonic chemistry, *Phys. Rev. Lett.* **128** 096001 (2022).

- [55] F. Herrera and F. C. Spano, Cavity-controlled chemistry in molecular ensembles, *Phys. Rev. Lett.* **116** 238301 (2016).
- [56] K. Huang and A. Rhys, Theory of light absorption and non-radiative transitions in f-centres, *Proc. Royal Soc. A* **204** 406–423 (1950).
- [57] J. Franck, Elementary processes of photochemical reactions, *Trans. Faraday Soc.* **21** 536–542 (1926).
- [58] E. Condon, A theory of intensity distribution in band systems, *Phys. Rev.* **28** 1182–1201 (1926).
- [59] C. W. Gardiner and M. J. Collett, Input and output in damped quantum systems: quantum stochastic differential equations and the master equation, *Phys. Rev. A* **31** 3761–3774 (1985).
- [60] C. Gardiner and P. Zoller, *Quantum noise: a handbook of Markovian and non-Markovian quantum stochastic methods with applications to quantum optics*, 3rd ed., Springer Series in Synergetics (Springer, 2004).
- [61] S. Baieva, O. Hakamaa, G. Groenhof, T. T. Heikkilä and J. J. Toppari, Dynamics of strongly coupled modes between surface plasmon polaritons and photoactive molecules: the effect of the stokes shift, *ACS Photonics* **4** 28–37 (2017).
- [62] M. Reitz, C. Sommer and C. Genes, Langevin approach to quantum optics with molecules, *Phys. Rev. Lett.* **122** 203602 (2019).
- [63] R. J. Glauber, Coherent and incoherent states of the radiation field, *Phys. Rev.* **131** 2766 (1963).
- [64] T. T. Heikkilä, *The physics of nanoelectronics: transport and fluctuation phenomena at low temperatures* (Oxford University Press, 2013).
- [65] G.-L. Ingold and Y. V. Nazarov, Charge tunneling rates in ultrasmall junctions, *Single charge tunneling* (Springer, 1992) 21–107.
- [66] V. Giovannetti and D. Vitali, Phase-noise measurement in a cavity with a movable mirror undergoing quantum brownian motion, *Phys. Rev. A* **63** 023812 (2001).
- [67] H. B. G. Casimir and D. Polder, The influence of retardation on the London-van der Waals forces, *Phys. Rev.* **73** 360–372 (1948).
- [68] W. E. Lamb and R. C. Retherford, Fine structure of the hydrogen atom by a microwave method, *Phys. Rev.* **72** 241–243 (1947).
- [69] H. A. Bethe, The electromagnetic shift of energy levels, *Phys. Rev.* **72** 339–341 (1947).
- [70] A. Thomas, J. George, A. Shalabney, M. Dryzhakov, S. J. Varma, J. Moran, T. Chervy, X. Zhong, E. Devaux, C. Genet, J. A. Hutchison and T. W. Ebbesen, Ground-state chemical reactivity under vibrational coupling to the vacuum electromagnetic field, *Angew. Chem. Int. Ed.* **55** 11462–11466 (2016).
- [71] R. M. A. Vergauwe, A. Thomas, K. Nagarajan, A. Shalabney, J. George, T. Chervy, M. Seidel, E. Devaux, V. Torbeev and T. W. Ebbesen, Modification of enzyme activity by vibrational strong coupling of water, *Angew. Chem. Int. Ed.* **58** 15324–15328 (2019).
- [72] A. Thomas, L. Lethuillier-Karl, K. Nagarajan, R. M. A. Vergauwe, J. George, T. Chervy, A. Shalabney, E. Devaux, C. Genet, J. Moran and T. W. Ebbesen, Tilting a ground-state reactivity landscape by vibrational strong coupling, *Science* **363** 615–619 (2019).

- [73] J. Lather, P. Bhatt, A. Thomas, T. W. Ebbesen and J. George, Cavity catalysis by cooperative vibrational strong coupling of reactant and solvent molecules, *Angew. Chem. Int. Ed.* **58** 10635–10638 (2019).
- [74] J. Lather and J. George, Improving enzyme catalytic efficiency by co-operative vibrational strong coupling of water, *J. Phys. Chem. Lett.* **12** 379–384 (2020).
- [75] F. J. Garcia-Vidal, C. Ciuti and T. W. Ebbesen, Manipulating matter by strong coupling to vacuum fields, *Science* **373** eabd0336 (2021).
- [76] A. D. Dunkelberger, B. S. Simpkins, I. Vurgaftman and J. C. Owrutsky, Vibration-cavity polariton chemistry and dynamics, *Annu. Rev. Phys. Chem.* **73** 429–451 (2022).
- [77] M. Hertzog, M. Wang, J. Mony and K. Börjesson, Strong light–matter interactions: a new direction within chemistry, *Chem. Soc. Rev.* **48** 937–961 (2019).
- [78] J. A. Hutchison, T. Schwartz, C. Genet, E. Devaux and T. W. Ebbesen, Modifying chemical landscapes by coupling to vacuum fields, *Angew. Chem. Int. Ed.* **51** 1592–1596 (2012).
- [79] B. Munkhbat, M. Wersäll, D. G. Baranov, T. J. Antosiewicz and T. Shegai, Suppression of photo-oxidation of organic chromophores by strong coupling to plasmonic nanoantennas, *Sci. Adv.* **4** eaas9552 (2018).
- [80] Y. Pang, A. Thomas, K. Nagarajan, R. M. A. Vergauwe, K. Joseph, B. Patrahaui, K. Wang, C. Genet and T. W. Ebbesen, On the role of symmetry in vibrational strong coupling: the case of charge-transfer complexation, *Angew. Chem. Int. Ed.* **59** 10436–10440 (2020).
- [81] M. V. Imperatore, J. B. Asbury and N. C. Giebink, Reproducibility of cavity-enhanced chemical reaction rates in the vibrational strong coupling regime, *J. Chem. Phys.* **154** 191103 (2021).
- [82] G. D. Wiesehan and W. Xiong, Negligible rate enhancement from reported cooperative vibrational strong coupling catalysis, *J. Chem. Phys.* **155** 241103 (2021).
- [83] R. F. Ribeiro, L. A. Martínez-Martínez, M. Du, J. Campos-Gonzalez-Angulo and J. Yuen-Zhou, Polariton chemistry: controlling molecular dynamics with optical cavities, *Chem. Sci.* **9** 6325–6339 (2018).
- [84] F. Herrera and J. Owrutsky, Molecular polaritons for controlling chemistry with quantum optics, *J. Chem. Phys.* **152** 100902 (2020).
- [85] D. S. Wang and S. F. Yelin, A roadmap toward the theory of vibrational polariton chemistry, *ACS Photonics* **8** 2818–2826 (2021).
- [86] T. E. Li, B. Cui, J. E. Subotnik and A. Nitzan, Molecular polaritonics: chemical dynamics under strong light–matter coupling, *Annu. Rev. Phys. Chem.* **73** 43–71 (2022).
- [87] J. Fregoni, F. J. Garcia-Vidal and J. Feist, Theoretical challenges in polaritonic chemistry, *ACS Photonics* **9** 1096–1107 (2022).
- [88] P. Atkins, J. de Paula and J. Keeler, *Physical chemistry*, 11th ed. (Oxford University Press, 2017).
- [89] T. Förster, Diabatic and adiabatic processes in photochemistry, *Pure Appl. Chem.* **24** 443–450 (1970).
- [90] P. Hänggi, P. Talkner and M. Borkovec, Reaction-rate theory: fifty years after Kramers, *Rev. Mod. Phys.* **62** 251–341 (1990).

- [91] B. Peters, Reaction coordinates and mechanistic hypothesis tests, *Annu. Rev. Phys. Chem.* **67** 669–690 (2016).
- [92] H. Eyring, The activated complex in chemical reactions, *J. Chem. Phys.* **3** 107–115 (1935).
- [93] P.-Y. Yang and J. Cao, Quantum effects in chemical reactions under polaritonic vibrational strong coupling, *J. Phys. Chem. Lett.* **12** 9531–9538 (2021).
- [94] V. P. Zhdanov, Vacuum field in a cavity, light-mediated vibrational coupling, and chemical reactivity, *Chem. Phys.* **535** 110767 (2020).
- [95] J. A. Campos-Gonzalez-Angulo and J. Yuen-Zhou, Polaritonic normal modes in transition state theory, *J. Chem. Phys.* **152** 161101 (2020).
- [96] J. Ankerhold, *Quantum tunneling in complex systems*, 1st ed., Springer Tracts in Modern Physics (Springer, 2007).
- [97] A. Altland and B. D. Simons, *Condensed matter field theory*, 2nd ed. (Cambridge University Press, 2010).
- [98] H. Kleinert, *Path integrals in quantum mechanics, statistics, polymer physics, and financial markets*, 5th ed. (World Scientific, 2009).
- [99] U. Weiss, *Quantum dissipative systems*, 4th ed. (World Scientific, 2012).
- [100] J. Zinn-Justin, *Path integrals in quantum mechanics* (Oxford University Press, 2005).
- [101] R. F. Dashen, B. Hasslacher and A. Neveu, Nonperturbative methods and extended-hadron models in field theory. I. Semiclassical functional methods, *Phys. Rev. D* **10** 4114–4129 (1974).
- [102] W. H. Miller, Semiclassical limit of quantum mechanical transition state theory for nonseparable systems, *J. Chem. Phys.* **62** 1899–1906 (1975).
- [103] W. H. Miller, S. D. Schwartz and J. W. Tromp, Quantum mechanical rate constants for bimolecular reactions, *J. Chem. Phys.* **79** 4889–4898 (1983).
- [104] J. Cao and G. A. Voth, A unified framework for quantum activated rate processes. I. General theory, *J. Chem. Phys.* **105** 6856–6870 (1996).
- [105] J. S. Langer, Theory of the condensation point, *Ann. Phys.* **41** 108–157 (1967).
- [106] I. Affleck, Quantum-statistical metastability, *Phys. Rev. Lett.* **46** 388–391 (1981).
- [107] A. O. Caldeira and A. J. Leggett, Influence of dissipation on quantum tunneling in macroscopic systems, *Phys. Rev. Lett.* **46** 211–214 (1981).
- [108] M.-S. Heo, Y. Kim, K. Kim, G. Moon, J. Lee, H.-R. Noh, M. I. Dykman and W. Jhe, Ideal mean-field transition in a modulated cold atom system, *Phys. Rev. E* **82** 031134 (2010).
- [109] N. G. Van Kampen, *Stochastic processes in physics and chemistry*, 3rd ed. (Elsevier, 2007).
- [110] C. Gardiner, *Stochastic methods: a handbook for the natural and social sciences*, 4th ed., Springer Series in Synergetics (Springer, 2009).
- [111] M. Aspelmeyer, T. J. Kippenberg and F. Marquardt, Cavity optomechanics, *Rev. Mod. Phys.* **86** 1391 (2014).
- [112] Y. Chen, Macroscopic quantum mechanics: theory and experimental concepts of optomechanics, *J. Phys. B* **46** 104001 (2013).

- [113] J. Chan, T. P. M. Alegre, A. H. Safavi-Naeini, J. T. Hill, A. Krause, S. Gröblacher, M. Aspelmeyer and O. Painter, Laser cooling of a nanomechanical oscillator into its quantum ground state, *Nature* **478** 89–92 (2011).
- [114] J. D. Teufel, T. Donner, D. Li, J. W. Harlow, M. S. Allman, K. Cicak, A. J. Sirois, J. D. Whittaker, K. W. Lehnert and R. W. Simmonds, Sideband cooling of micromechanical motion to the quantum ground state, *Nature* **475** 359–363 (2011).
- [115] L. Mercier de Lépinay, C. F. Ockeloen-Korppi, M. J. Woolley and M. A. Sillanpää, Quantum mechanics-free subsystem with mechanical oscillators, *Science* **372** 625–629 (2021).
- [116] S. Kotler, G. A. Peterson, E. Shojaee, F. Lecocq, K. Cicak, A. Kwiatkowski, S. Geller, S. Glancy, E. Knill, R. W. Simmonds, J. Aumentado and J. D. Teufel, Direct observation of deterministic macroscopic entanglement, *Science* **372** 622–625 (2021).
- [117] A. Einstein, B. Podolsky and N. Rosen, Can quantum-mechanical description of physical reality be considered complete?, *Phys. Rev.* **47** 777–780 (1935).
- [118] A. N. Pearson, Y. Guryanova, P. Erker, E. A. Laird, G. A. D. Briggs, M. Huber and N. Ares, Measuring the thermodynamic cost of timekeeping, *Phys. Rev. X* **11** 021029 (2021).
- [119] F. Lecocq, J. B. Clark, R. W. Simmonds, J. Aumentado and J. D. Teufel, Quantum nondemolition measurement of a nonclassical state of a massive object, *Phys. Rev. X* **5** 041037 (2015).
- [120] C. F. Ockeloen-Korppi, E. Damskäg, J.-M. Pirkkalainen, T. T. Heikkilä, F. Massel and M. A. Sillanpää, Noiseless quantum measurement and squeezing of microwave fields utilizing mechanical vibrations, *Phys. Rev. Lett.* **118** 103601 (2017).
- [121] S. Hong, R. Riedinger, I. Marinković, A. Wallucks, S. G. Hofer, R. A. Norte, M. Aspelmeyer and S. Gröblacher, Hanbury Brown and Twiss interferometry of single phonons from an optomechanical resonator, *Science* **358** 203–206 (2017).
- [122] C. F. Ockeloen-Korppi, E. Damskäg, J.-M. Pirkkalainen, T. T. Heikkilä, F. Massel and M. A. Sillanpää, Low-noise amplification and frequency conversion with a multiport microwave optomechanical device, *Phys. Rev. X* **6** 041024 (2016).
- [123] F. Ruesink, M.-A. Miri, A. Alù and E. Verhagen, Nonreciprocity and magnetic-free isolation based on optomechanical interactions, *Nat. Commun.* **7** 13662 (2016).
- [124] A. P. Reed, K. H. Mayer, J. D. Teufel, L. D. Burkhardt, W. Pfaff, M. Reagor, L. Sletten, X. Ma, R. J. Schoelkopf, E. Knill and K. W. Lehnert, Faithful conversion of propagating quantum information to mechanical motion, *Nat. Phys.* **13** 1163–1167 (2017).
- [125] M. Mirhosseini, A. Sipahigil, M. Kalaei and O. Painter, Superconducting qubit to optical photon transduction, *Nature* **588** 599–603 (2020).
- [126] C. H. Metzger and K. Karrai, Cavity cooling of a microlever, *Nature* **432** 1002–1005 (2004).
- [127] J. D. Thompson, B. M. Zwickl, A. M. Jayich, F. Marquardt, S. M. Girvin and J. G. E. Harris, Strong dispersive coupling of a high-finesse cavity to a micromechanical membrane, *Nature* **452** 72–75 (2008).
- [128] X. Zhang, C.-L. Zou, L. Jiang and H. X. Tang, Cavity magnomechanics, *Sci. Adv.* **2** e1501286 (2016).
- [129] C. A. Potts, E. Varga, V. A. S. V. Bittencourt, S. Viola Kusminskiy and J. P. Davis, Dynamical backaction magnomechanics, *Phys. Rev. X* **11** 031053 (2021).

- [130] B. Lekitsch, S. Weidt, A. G. Fowler, K. Mølmer, S. J. Devitt, C. Wunderlich and W. K. Hensinger, Blueprint for a microwave trapped ion quantum computer, *Sci. Adv.* **3** e1601540 (2017).
- [131] C. Kittel, On the theory of ferromagnetic resonance absorption, *Phys. Rev.* **73** 155–161 (1948).
- [132] T. L. Gilbert, A phenomenological theory of damping in ferromagnetic materials, *IEEE Trans. Magn.* **40** 3443–3449 (2004).
- [133] C. Kittel, Physical theory of ferromagnetic domains, *Rev. Mod. Phys.* **21** 541–583 (1949).
- [134] D. Sander, The correlation between mechanical stress and magnetic anisotropy in ultrathin films, *Rep. Prog. Phys.* **62** 809 (1999).
- [135] T. Miyazaki and H. Jin, *The physics of ferromagnetism*, Springer Series in Materials Science (Springer, 2012).
- [136] A. Kamra, W. Belzig and A. Brataas, Magnon-squeezing as a niche of quantum magnonics, *Appl. Phys. Lett.* **117** 090501 (2020).
- [137] H. Y. Yuan, S. Zheng, Z. Ficek, Q. Y. He and M.-H. Yung, Enhancement of magnon-magnon entanglement inside a cavity, *Phys. Rev. B* **101** 014419 (2020).
- [138] S. Sharma, V. A. S. V. Bittencourt, A. D. Karenowska and S. Viola Kusminskiy, Spin cat states in ferromagnetic insulators, *Phys. Rev. B* **103** L100403 (2021).
- [139] J. Li, S.-Y. Zhu and G. S. Agarwal, Magnon-photon-phonon entanglement in cavity magnomechanics, *Phys. Rev. Lett.* **121** 203601 (2018).
- [140] M. Asjad, J. Li, S.-Y. Zhu and J. Q. You, Magnon squeezing enhanced ground-state cooling in cavity magnomechanics, (2022), arXiv:2203.10767 [quant-ph].
- [141] Z.-Y. Fan, R.-C. Shen, Y.-P. Wang, J. Li and J. Q. You, Optical sensing of magnons via the magnetoelastic displacement, *Phys. Rev. A* **105** 033507 (2022).
- [142] F. Benz, M. K. Schmidt, A. Dreismann, R. Chikkaraddy, Y. Zhang, A. Demetriadou, C. Carnegie, H. Ohadi, B. De Nijs, R. Esteban, J. Aizpurua and J. J. Baumberg, Single-molecule optomechanics in “picocavities”, *Science* **354** 726–729 (2016).
- [143] P. Roelli, C. Galland, N. Piro and T. J. Kippenberg, Molecular cavity optomechanics as a theory of plasmon-enhanced Raman scattering, *Nat. Nanotechnol.* **11** 164–169 (2016).
- [144] A. Laucht, R. Kalra, S. Simmons, J. P. Dehollain, J. T. Muhonen, F. A. Mohiyaddin, S. Freer, F. E. Hudson, K. M. Itoh, D. N. Jamieson, J. C. McCallum., A. S. Dzurak and A. Morelle, A dressed spin qubit in silicon, *Nat. Nanotechnol.* **12** 61–66 (2017).
- [145] T. Oka and S. Kitamura, Floquet engineering of quantum materials, *Annu. Rev. Condens. Matter Phys.* **10** 387–408 (2019).
- [146] M. Rodriguez-Vega, M. Vogl and G. A. Fiete, Low-frequency and Moiré–Floquet engineering: a review, *Ann. Phys.* **435** 168434 (2021).
- [147] C. Weitenberg and J. Simonet, Tailoring quantum gases by Floquet engineering, *Nat. Phys.* **17** 1342–1348 (2021).
- [148] M. Reitz and C. Genes, Floquet engineering of molecular dynamics via infrared coupling, *J. Chem. Phys.* **153** 234305 (2020).
- [149] J. F. Poyatos, J. I. Cirac and P. Zoller, Quantum reservoir engineering with laser cooled trapped ions, *Phys. Rev. Lett.* **77** 4728–4731 (1996).

- [150] A. Metelmann and A. A. Clerk, Nonreciprocal photon transmission and amplification via reservoir engineering, *Phys. Rev. X* **5** 021025 (2015).
- [151] T. M. Mendonça, A. M. Souza, R. J. de Assis, N. G. de Almeida, R. S. Sarthour, I. S. Oliveira and C. J. Villas-Boas, Reservoir engineering for maximally efficient quantum engines, *Phys. Rev. Research* **2** 043419 (2020).

I

**THEORY FOR THE STATIONARY POLARITON RESPONSE
IN THE PRESENCE OF VIBRATIONS**

by

K. S. U. Kansanen, A. Asikainen, J. J. Toppari, G. Groenhof, T. T. Heikkilä

Physical Review B **100**, 245426 (2019)

Reproduced with permission. Copyright 2019 American Physical Society.

Theory for the stationary polariton response in the presence of vibrations

Kalle S. U. Kansanen ¹, Aili Asikainen ^{1,2}, J. Jussi Toppari ¹, Gerrit Groenhof ³, and Tero T. Heikkilä ¹

¹*Department of Physics and Nanoscience Center, P.O. Box 35, FI-40014 University of Jyväskylä, Finland*

²*Department of Computer Science, School of Science, Aalto University, FI-00076 Aalto, Finland*

³*Department of Chemistry and Nanoscience Center, P.O. Box 35, FI-40014 University of Jyväskylä, Finland*



(Received 3 May 2019; revised manuscript received 27 September 2019; published 23 December 2019)

We construct a model describing the response of a hybrid system where the electromagnetic field—in particular, surface plasmon polaritons—couples strongly with electronic excitations of atoms or molecules. Our approach is based on the input-output theory of quantum optics, and in particular it takes into account the thermal and quantum vibrations of the molecules. The latter is described within the $P(E)$ theory analogous to that used in the theory of dynamical Coulomb blockade. As a result, we are able to include the effect of the molecular Stokes shift on the strongly coupled response of the system. Our model then accounts for the asymmetric emission from upper and lower polariton modes. It also allows for an accurate description of the partial decoherence of the light emission from the strongly coupled system. Our results can be readily used to connect the response of the hybrid modes to the emission and fluorescence properties of the individual molecules, and thus are relevant in understanding any utilization of such systems, such as coherent light harvesting.

DOI: [10.1103/PhysRevB.100.245426](https://doi.org/10.1103/PhysRevB.100.245426)

I. INTRODUCTION

Photonic structures, such as optical cavities or surface plasmon polaritons, can modify an electromagnetic vacuum field by confining the light to smaller volumes and restricting the number of available photonic modes. Any electronic excitation inside such modified vacuum can interact much more strongly with the confined light mode. This interaction can become strong enough for the coupling energy to show up in the absorption and emission spectra of such systems, suggesting the formation of hybrid light-matter states, called polaritons. Common examples studied in this strong-coupling limit are single atoms [1], excitons in semiconductors [2], and photoactive molecules [3,4].

More recently, strong coupling of molecules with confined light modes has been the focus of interest because the hybridization between light and matter into polaritons not only delocalizes the excitation over many molecules, but also changes their potential-energy surface, and thus provides a new way to control chemistry [5]. Experiments on strongly coupled molecules have already shown (i) suppression of photo-oxidation of TBDC J-aggregates coupled to plasmonic nanoprisms [6], and of photoisomerization of Spiropyran inside an optical cavity [7]; (ii) enhanced electronic conductivity in organic semiconductors [8]; (iii) intermolecular excitation energy transfer over large distances inside optical cavities [9,10]; and (iv) enhanced decay of triplet states in erythrosine B molecules [11]. Since polaritons are like interacting dressed photons with mass, they can undergo Bose-Einstein condensation even at room temperature [12], which further enables very efficient and thresholdless polariton lasing [13,14].

Strong coupling between a single molecule and electromagnetic field is very hard to achieve [15,16]. The common way to circumvent this problem is to couple multiple molecules to the same photonic mode. Often these systems are

still described within effective two-state models accounting only for the two polaritonic states [17]. However, such a description disregards the fact that the visible polariton modes are now superpositions of several molecular excitations and the photonic mode, and they are not the only eigenmodes of the system. The response of the whole system also depends on the presence of “dark modes,” i.e., superpositions having no photonic component. These dark modes become relevant especially when dissipation processes within the molecules, such as those linked to vibrations, are included. In this case, they can dramatically affect the predicted guiding of the chemistry, and even the validity of the whole concept. They have been taken into account in some multiscale simulations coupling the investigated molecules to thermal environments [18]. However, those simulations often consider the transient response, whereas the majority of experiments on light-matter coupling concern stationarily driven setups.

Here we construct a detailed description of the stationarily driven response of the strongly coupled system, taking into account the effect of inhomogeneous broadening of the molecular response due to quantum and thermal vibrations of the molecules. We take the vibrations into account via the $P(E)$ theory analogous to that used in Coulomb blockade [19,20]. This theory describes the probability of absorbing (for $E > 0$) or emitting ($E < 0$) the energy E to/from the vibrations. For the specific models of harmonic vibrations, such a $P(E)$ function can be calculated exactly. In general, we find how this $P(E)$ is related to the absorption and emission spectra of individual molecules. Therefore, an alternative approach is to deduce an effective $P(E)$ for the measured spectra of individual molecules. The resulting fluorescence spectrum is similar to that found via quantum many-body theory [21]. However, in these approaches, only the transient response is considered which requires assumptions on the initial state of the system. In our work, the focus is on the stationary

response, in which case different conservation laws and their explicit breaking come into focus. What is more, we connect this fluorescence spectrum directly to the absorption/emission spectrum of the strongly coupled system. In a certain limit of parameters, the resulting inhomogeneous broadening of the molecular absorption/emission then determines the linewidth of the polariton modes. In particular, our model explains the asymmetric emission spectra of upper and lower polaritons seen in many experiments [22–27], as well as the varying polarization of that emission depending on the quantum coherence of the system, as shown recently [22].

Besides the detailed description of the vibrations, we include polarization of the confined light field and the positions of the molecules. The position of a molecule with respect to the light field only amounts to a phase factor to the light-matter coupling, but collectively it leads to experimentally observable effects. Perhaps the most striking effect is the superradiance due to coherent emission described by Dicke in the 1950s [28], but conversely it is seen in the usual experiments where many molecules are distributed over a region larger than the light wavelength. On the other hand, the polarization of the light and the transition dipole moment of a molecule determine whether there is coupling at all: if these directions are perpendicular, the coupling vanishes. This provides another way to control light-matter interaction which could be used in applications [29]. In this paper, we describe both the incoherent and coherent limits of polaritonics.

Although many aspects of our theory can be generalized to any confined light mode, such as resonances of Fabry-Pérot cavities, here we focus in particular on surface plasmon polaritons (below, plasmons) driven by an external light field. Plasmons are evanescent like electromagnetic modes propagating along a metal-dielectric surface with a two-dimensional momentum \vec{k} along the surface. In general, they have a nonlinear dispersion $\omega(\vec{k})$, and due to the evanescent nature their electromagnetic field is highly confined to the surface. Because of this confinement, the dipolar coupling to molecular excitations residing at the surface can be made strong [3,23], leading to the observed avoided crossing between the two systems and thus offering the possibility to control photochemical reactions. A typical way to launch plasmons is via the Kretschmann configuration, i.e., coupling an external electromagnetic field to the surface modes via a prism [30]. In this setup, the angle with which the light enters the prism determines a specific plasmon \vec{k} vector. Hence, in this work, we concentrate on a single plasmon mode with defined \vec{k} and a generic frequency ω_c .

To be specific, we consider the plasmon-molecule system in the strong-coupling regime. We describe the plasmon by a single bosonic mode c of frequency ω_c and a given polarization \hat{u}_{pl} with respect to its wave vector \vec{k} . A concrete example of such a plasmon is the surface plasmon polariton traveling along an interface in the xy plane in the y direction with $\hat{u}_{pl} = (0, \sin \beta, \cos \beta)$ as in Fig. 1(a). The plasmon interacts with N identical molecules [31,32], which we approximate as two-level systems with transition frequency ω_m . We denote the rising (lowering) operator of a molecule with σ_j^\dagger (σ_j). As in typical experiments, we assume that the electric dipole moments of the molecules point in uniformly random

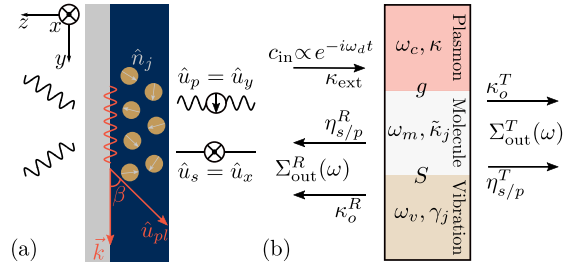


FIG. 1. (a) The measurement setup in which a surface plasmon polariton is excited on an interface where it can strongly couple to molecules. (b) Schematic with relevant parameters to the input-output formalism.

directions \hat{n}_j . Following the standard approach of quantum optics [33,34], the Hamiltonian of the strong-coupled system is in the rotating wave approximation ($\hbar = 1$),

$$H_{s-c} = \omega_c c^\dagger c + \sum_{j=1}^N (\omega_m \sigma_j^\dagger \sigma_j + g_j \sigma_j^\dagger c + g_j^* c^\dagger \sigma_j). \quad (1)$$

The position \vec{r}_j of a molecule affects the coupling g_j in two ways: it contains a complex phase factor due to the phase of the plasmon, and the coupling strength depends on the distance to the interface. If this distance is independent of the polarization, the latter effect may be disregarded and the average value used. Also, the coupling strength depends on the angle between the plasmon polarization and dipole moment of a molecule. Thus, we write $g_j = g e^{i\vec{k} \cdot \vec{r}_j} (\hat{n}_j \cdot \hat{u}_{pl})$.

In addition to the strong-coupled system, we include the vibrational modes of the molecules. We assume a single vibration mode b_j per molecule with eigenfrequency ω_v , but the generalization to multiple modes is straightforward (Appendix A). These vibrations and their interactions are described by

$$H_v = \sum_{j=1}^N \omega_v b_j^\dagger b_j + \sum_{j=1}^N \omega_v \sqrt{S} \sigma_j^\dagger \sigma_j (b_j^\dagger + b_j). \quad (2)$$

The coupling between electronic and vibrational modes is quantified with a dimensionless parameter \sqrt{S} , the Huang-Rhys factor [35], which is related to the Stokes shift measured in fluorescent emission.

We seek an approach to find the response of the strongly coupled plasmon-molecule system in the presence of vibrations. To this end, we employ the input-output formalism of quantum optics [36,37]. We assume that there are separate bosonic baths for each molecule, vibration, and plasmon to which the coupling is linear in σ_j , b_j , and c , respectively. In the Markov approximation, these couplings are described by the dissipation rates $\tilde{\kappa}_j$, γ_j , and κ of the molecules, vibrations, and plasmon. In the following, we suppose identical molecules and vibrations so that $\gamma_j = \gamma$ and $\tilde{\kappa}_j = \tilde{\kappa}$. We neglect the thermal fluctuations of plasmons and molecules here as $\hbar\omega_m, \hbar\omega_c \gg k_B T$ even at room temperature. We simplify the molecule-vibration Hamiltonian by introducing a new polaron operator $\sigma_j^S = e^{\sqrt{S}(b_j^\dagger - b_j)} \sigma_j \equiv Q_j \sigma_j$. Lastly,

we assume a low driving power which corresponds to the single-excitation limit $\sigma^\dagger \sigma \approx 0$. We find that when $\frac{\hbar\omega_v}{k_B T} > \frac{\gamma S}{2\kappa_m}$, where $\kappa_m = \bar{\kappa} + \gamma S$ is the total effective damping rate of the individual molecules, the dynamics of the vibrational modes b_j are approximately uncoupled from the plasmon-molecule system, as shown in Appendix B. This allows us to use the Caldeira-Leggett model [38] for the vibrational dynamics. The plasmon and molecular equation are, in this case,

$$\dot{c} = -i\omega_c c - i \sum_j g_j^* \sigma_j^S Q_j^\dagger - \frac{\kappa}{2} c - \sqrt{\kappa_{\text{ext}}} c_{\text{in}}, \quad (3a)$$

$$\dot{\sigma}_j^S = -i\tilde{\omega}_m \sigma_j^S - i g_j Q_j c - \frac{\kappa_m}{2} \sigma_j^S - \sqrt{\kappa_m^{\text{ext}}} Q_j \sigma_{\text{in},j}, \quad (3b)$$

where $\tilde{\omega}_m = \omega_m - S\omega_v$ is the renormalized molecular frequency, while κ_{ext} and κ_m^{ext} are the couplings to external driving fields. For the plasmon-molecule system, we assume that only the plasmon is driven so that $c_{\text{in}} = \alpha e^{-i\omega_d t}$ and $\sigma_{\text{in},j} = 0$.

We model a measurement on the plasmon-molecule system so that the incoming light c_{in} produces a reflected Σ_{out}^R and transmitted Σ_{out}^T field. These fields contain both the plasmon and the molecular emission, but not the emission of phonons from the vibrations because they are usually not measured. Phonon emission hence allows for a loss of energy in the process, so that the power in the output fields can be lower than the one in the input. We also separately include coupling to s - and p -polarized light represented by $\hat{u}_p = \hat{u}_y$ and $\hat{u}_s = \hat{u}_x$ [Fig. 1(a)]. Since the propagating plasmon cannot emit s -polarized light to the direction perpendicular to the interface but the molecules have no directional preference, we consider s - and p -polarized output fields separately. The output fields obey a general expression,

$$\Sigma_{\text{out},s/p}^{T/R} = (\delta_R^{T/R} c_{\text{in}} + \sqrt{\kappa_o^{T/R}} c) \delta_p^{s/p} + \sum_j \eta_{j,s/p}^{T/R} \sigma_j. \quad (4)$$

In this equation, $\delta_R^T = 0$ and $\delta_R^R = 1$, meaning that only the reflected field interferes with the input field. The $\delta_p^{s/p}$ is defined similarly because the plasmon couples only to p -polarized modes. The constants $\eta_{j,s/p}^{T/R}$ describe the coupling of the molecule electronic states to the environmental s - and p -polarized free-space modes, and thus $\eta_{j,s/p}^{T/R} = \sqrt{\kappa_m^{T/R}} (\hat{n}_j \cdot \hat{u}_{s/p})$. These fields and couplings to the system are represented schematically in Fig. 1(b). The output spectral density is obtained from

$$S_{s/p}^{T/R}(\omega; \omega_d) = \frac{1}{2\pi} \int dt e^{i\omega t} \langle \Sigma_{\text{out},s/p}^{T/R\dagger}(0) \Sigma_{\text{out},s/p}^{T/R}(t) \rangle, \quad (5)$$

where ω is the frequency of the output field and ω_d is the driving frequency.

We note that the Markov approximation leading to Eqs. (3) disregards the heating of the various baths of the plasmons, molecules, and vibrations. These heating effects can be disregarded when the heat conductance from those baths to other degrees of freedom exceeds that due to the losses described by κ , κ_m , and γ .

II. $P(E)$ THEORY

The presence of the vibrations makes the input-output equations (3) nonlinear as they contain products of different dynamical fields. This nonlinearity leads to an inelastic (fluorescent) response of the molecules to the light field, where the emitted light from the molecules takes place at lower frequencies than the absorption. This is often referred as the Stokes shift. In order to take this nonlinearity into account in the output spectra, we introduce $P(E)$ theory similar to the one in a dynamical Coulomb blockade [19]. Recently, the same problem has been discussed in Ref. [39] using similar methods, but only in a specific limit of vibrations (see below). The identification of $P(E)$ allows for a more general approach, also enabling the resolution of polariton emission, which is lacking from Ref. [39]. Let us first define $P(t) = \langle Q_j^\dagger(t) Q_j(0) \rangle$ and its Fourier transform,

$$P(E) = \frac{1}{2\pi} \int dt e^{iEt} P(t). \quad (6)$$

When the molecules are identical, $P(E)$ does not depend on the molecule index j ; this assumption is easily lifted if needed. The $P(E)$ function normalizes to unity and is real for stationary vibrations, i.e., $\langle Q_j^\dagger(t + \tau) Q_j(\tau) \rangle = \langle Q_j^\dagger(t) Q_j(0) \rangle$ for any time τ . We can thus interpret the $P(E)$ function as a probability distribution of transforming energy E to the vibrations ($E > 0$), or vice versa ($E < 0$). This $P(E)$ function is characterized by four parameters: vibration eigenfrequency ω_v , their linewidth γ , Huang-Rhys factor S , and temperature T of their bath. It constitutes a full description of the response of the vibrations.

We present a general derivation of the $P(E)$ function and a related L function assuming Gaussian thermal fluctuations. Then, we derive $P(E)$ analytically in the limit in which γ vanishes. In this regime, $P(E)$ is related to the absorption function defined by Huang and Rhys [35]. However, our analytic results for the response also apply in the case of general γ and can be used for different models of vibrations.

A. Derivation of $P(E)$

We now derive the $P(E)$ function analytically in a similar manner as in the context of dynamical Coulomb blockade [19]. To establish notation, we omit the molecular index j here and denote $x = b^\dagger + b$ and $p = i(b^\dagger - b)$, the dimensionless position and momentum operator, respectively. Then, we may write $Q^\dagger(t) = e^{i\sqrt{S}p(t)}$ in the correlator $P(t)$, which is the inverse Fourier transform of $P(E)$. This correlator can be evaluated for thermal vibrations. If the vibrations are described by a harmonic-oscillator Hamiltonian, the fluctuations are Gaussian and the weak version of the Wick's theorem (see, e.g., Ref. [19] and an example of a non-Gaussian $P(E)$ in Ref. [40]) applies. We identify $P(t)$ as the characteristic function of fluctuations of the stochastic quantity $p(t) - p(0)$, where everywhere in the calculations $p(t)$ should be ordered to the left of $p(0)$. We assume the thermal vibrations to be stationary, and therefore the expectation value of $p(t) - p(0)$ vanishes [as $\langle p(t) \rangle = \langle p(0) \rangle$ for stationary vibrations]. Consequently, for Gaussian fluctuations, we can write the characteristic function in terms of the variance alone. In that

case [20],

$$P(t) = e^{\mathcal{T}((i\sqrt{S}[p(t)-p(0)])^2)/2} = e^{S((p(t)-p(0))p(0))}, \quad (7)$$

where the latter equality uses the fact that $\langle p(t)^2 \rangle = \langle p(0)^2 \rangle$. The operator \mathcal{T} takes care of ordering $p(t)$ before $p(0)$, but that operator is no longer needed in the second equality because, there, $p(t)$ always precedes $p(0)$ in operator products.

Now, $p(t)$ can be obtained by solving the quantum Langevin equations without the rotating wave approximation (also known as the Caldeira-Leggett model [38]),

$$\dot{x}(t) = \omega_v p(t), \quad \dot{p}(t) = -\omega_v x(t) - \gamma p(t) + \xi(t), \quad (8)$$

where γ is the linewidth of vibrations, and ξ is a Langevin force describing the thermal fluctuations. It has the correlator

$$\langle \xi(t)\xi(t') \rangle = \int d\omega \exp[-i\omega(t-t')] S_\xi(\omega), \quad (9)$$

where the noise correlator is given by

$$S_\xi(\omega) = \frac{\gamma\omega}{\pi\omega_v} \left[\coth\left(\frac{\omega}{2k_B T}\right) + 1 \right] \quad (10)$$

for thermal noise [41].

The Langevin equations (8) can be solved via Fourier transform. The result is

$$\begin{pmatrix} x(\omega) \\ p(\omega) \end{pmatrix} = \frac{1}{\omega^2 - \omega_v^2 + i\omega\gamma} \begin{pmatrix} -\omega_v \\ i\omega \end{pmatrix} \xi(\omega). \quad (11)$$

After some Fourier analysis with the help of Eqs. (9)–(11), we find $P(t) = e^{J(t)-J(0)}$ according to Eq. (7), with

$$\begin{aligned} J(t) &= S\langle p(t)p(0) \rangle \\ &= \frac{S\gamma}{\pi\omega_v} \int d\omega e^{-i\omega t} \frac{\omega^3}{(\omega^2 - \omega_v^2)^2 + \omega^2\gamma^2} \\ &\quad \times \left[\coth\left(\frac{\omega}{2k_B T}\right) + 1 \right]. \end{aligned} \quad (12)$$

The resulting $P(E)$ is thus governed by three dimensionless parameters: the Huang-Rhys factor S , the quality factor of vibrations ω_v/γ , and the relative temperature $k_B T/\omega_v$. Note that in the Caldeira-Leggett model, $J(t)$ is related to the vibrational spectral density $J_v(t) = S\omega_v^2 \langle x(t)x(0) \rangle$ via their respective Fourier transforms by $J_v(\omega) = J(\omega)/\omega^2$.

A simpler expression for $J(t)$ is obtained if, instead of the Caldeira-Leggett model, one uses the usual quantum optical equation $\dot{b} = -(i\omega_v + \frac{\gamma}{2})b + \sqrt{\gamma}b_{\text{in}}$, as in [39] for example. Then, for white noise $\langle b_{\text{in}}(t)b_{\text{in}}^\dagger(t') \rangle = (n_{\text{th}} + 1)\delta(t-t')$, we find

$$J(t) = S(n_{\text{th}} + 1)e^{-i\omega_v t - \frac{\gamma}{2}|t|} + S n_{\text{th}} e^{i\omega_v t - \frac{\gamma}{2}|t|}. \quad (13)$$

Here, $n_{\text{th}} = (e^{\omega_v/(k_B T)} - 1)^{-1}$ is the Bose factor, i.e., the mean number of thermal phonons at the vibrational frequency ω_v . We arrive at the same solution from the Caldeira-Leggett model by using the method of residues to calculate the integral (12) and then approximating $\gamma \ll \omega_v$. This is hence the limit where Ref. [39] is valid. However, typical multiscale quantum chemistry calculations assume the opposite limit of a large $\gamma \gtrsim \bar{\kappa}$, where molecular vibrations decay before the photon excitation.

Lastly, there are two general properties of the $P(E)$ function worth noting. First, since $P(t)$ may be regarded as a characteristic function of the probability distribution $P(E)$, the raw moments of the energy can be expressed as

$$\mathbb{E}(E^n) = i^n \frac{d^n P(t)}{dt^n} \Big|_{t=0} = i^n \frac{d^n e^{J(t)}}{dt^n} \Big|_{t=0}. \quad (14)$$

With the help of this formula, the mean and variance of $P(E)$ can be found. Second, the Kubo-Martin-Schwinger (KMS) relation for thermal fluctuations at temperature T leads to the detailed balance condition (or emission-absorption asymmetry) for $P(E)$,

$$P(-E) = \exp\left(-\frac{E}{k_B T}\right) P(E). \quad (15)$$

This asymmetry in $P(E)$ is relevant for the anti-Stokes part of the spectrum. Some approximations, such as the white-noise approximation, break this balance condition.

B. L function

Another quantity we encounter that is relevant for the emission spectrum of a molecule is the Fourier transform of the four-point correlator,

$$L(t_1, t_2, t_3) = \langle Q^\dagger(t_1)Q(t_2)Q^\dagger(0)Q(t_3) \rangle. \quad (16)$$

This function is clearly related to $P(t)$ as for certain time arguments it coincides with the definition of $P(t)$, e.g., $L(t, 0, 0) = P(t)$. Using the same assumptions as in the derivation of $P(E)$, we may write

$$L(t_1, t_2, t_3) = e^{-S\mathcal{T}((p(t_1)-p(t_2)+p(0)-p(t_3))^2)/2}, \quad (17)$$

where \mathcal{T} orders operator products so that they are in the same order as in Eq. (16). Now, since the vibrations are stationary, we may write L in terms of $P(t)$'s,

$$L(t_1, t_2, t_3) = \frac{P(t_1 - t_2)P(t_1 - t_3)P(t_2)P(-t_3)}{P(t_1)P(t_2 - t_3)}. \quad (18)$$

Even if we can fully calculate $J(t)$, the Fourier transform of L is not straightforward to evaluate numerically in the general case.

C. $\gamma = 0$ limit

Next, we consider the limit in which the dissipation rate of vibrations vanishes and derive expressions for both $P(E)$ and L . We note that the definition of $J(t)$, given by Eq. (12), contains a nascent δ function,

$$\tilde{P}(\omega) = \frac{1}{\pi} \frac{\gamma\omega^2}{(\omega_v^2 - \omega^2)^2 + \omega^2\gamma^2}, \quad (19)$$

which in the limit $\gamma \rightarrow 0$ reduces to $\tilde{P}(\omega) = \frac{1}{2}[\delta(\omega - \omega_v) + \delta(\omega + \omega_v)]$. Therefore,

$$J(t) = S(n_{\text{th}} + 1)e^{-i\omega_v t} + S n_{\text{th}} e^{i\omega_v t}. \quad (20)$$

Note that this coincides with the limit $\gamma \rightarrow 0$ in the white-noise model given by Eq. (13). The corresponding characteristic function $P(t)$ is known in probability theory to be that of the *Skellam distribution* [42]. It is a distribution that describes the difference of two independent Poisson processes. In our

case, these processes are the emission and absorption of phonons. $P(E)$ then describes the total number of phonons transferred from/to vibrations to/from their environment. The resulting $P(E)$ function is

$$P(E) = \sum_{k=-\infty}^{\infty} p_k(S)\delta(E - k\omega_v), \quad (21a)$$

$$p_k(S) = e^{-S(2n_{\text{th}}+1)} \left(1 + \frac{1}{n_{\text{th}}}\right)^{\frac{k}{2}} I_k[2S\sqrt{n_{\text{th}}(n_{\text{th}}+1)}], \quad (21b)$$

where $I_k(x)$ is the modified Bessel function of the first kind. In the zero-temperature limit, $p_k(S) = e^{-S\frac{S_k}{kT}}$ for $k \geq 0$ and $p_k(S) = 0$ for $k < 0$, i.e., the probability to emit phonons becomes Poissonian and the absorption probability vanishes.

We find the average and variance of the $\gamma = 0$ distribution by using Eqs. (14) and (20),

$$\mathbb{E}(E) = S\omega_v \quad \text{and} \quad \text{var}(E) = (2n_{\text{th}} + 1)S\omega_v^2. \quad (22)$$

The variance depends on the temperature so that for high temperatures $k_B T \gg \omega_v$, the variance is directly proportional to the temperature: $\text{var}(E) \approx 2S\omega_v k_B T$. It should be noted that both the variance and the average are proportional to S , which

also holds for a Poissonian quantity. The physical picture is that the mean of E describes the Stokes shift in the molecules, whereas the variance (or standard deviation) is connected with the inhomogeneous broadening of the molecular linewidth due to vibrations.

Finally, we derive L in the $\gamma \rightarrow 0$ limit using Eq. (18). It is necessary to simplify $1/P(t)$ in order to find the Fourier transform of L . Since $P(t) = e^{J(t)-J(0)}$ and $J(t) \propto S$, we may find $1/P(t)$ by changing $S \rightarrow -S$ in Eq. (21). Using the parity of the modified Bessel function of the first kind $I_k(-x) = (-1)^k I_k(x)$, we can express the inverse as

$$\begin{aligned} 1/P(t) &= \sum_{k=-\infty}^{\infty} p_k(-S)e^{-ik\omega_v t} \\ &= \sum_{k=-\infty}^{\infty} (-1)^k \exp[2S(2n_{\text{th}} + 1)] p_k(S) e^{-ik\omega_v t}. \end{aligned} \quad (23)$$

Below, we omit the S dependence and denote $p_k(S) = p_k$.

The Fourier transform of L is straightforward with the help of Eq. (23). We obtain

$$\begin{aligned} L(\omega_1, \omega_2, \omega_3) &= \frac{1}{(2\pi)^3} \int dt_1 dt_2 dt_3 L(t_1, t_2, t_3) e^{i\omega_1 t_1 + i\omega_2 t_2 + i\omega_3 t_3} \\ &= \sum_{k_1, k_2, k_3, k_4, k_5, k_6} (-1)^{k_1 + k_2} p_{k_1} p_{k_2} p_{k_3} p_{k_4} p_{k_5} p_{k_6} e^{4S(2n_{\text{th}}+1)} \delta(\omega_1 - [k_1 + k_3 + k_4]\omega_v) \\ &\quad \times \delta(\omega_2 - [k_2 - k_3 + k_5]\omega_v) \delta(\omega_3 + [k_2 + k_4 + k_6]\omega_v). \end{aligned} \quad (24)$$

This result can be used to obtain the fluorescence spectrum of a molecule. The expression is slightly cumbersome to use because the six sums obtain values from $-\infty$ (or from 0 when $T = 0$) to ∞ . This problem is alleviated by the rapid decrease of p_k as a function of k . Consequently, Eq. (24) is straightforward to compute numerically.

III. STOKES SHIFT

Before solving the full plasmon-molecule problem, we illustrate how the $P(E)$ theory is used to model a measurement of the Stokes shift in a molecule-vibration system. This is achieved by removing the plasmon term from Eq. (3b) and driving the molecules, i.e., adding the term $\sigma_{\text{in},j} = \frac{\alpha e^{i\theta_j}}{\sqrt{N}} \delta(\omega - \omega_d)$ where θ_j represents the phase of the driving field for molecule j . The driving is scaled so that the total input power spectral density is given by $I_{\text{in}} = |\alpha|^2 \delta(\omega - \omega_d)$. Then, we solve Eq. (3b) with Fourier transform and convolution theorem. The spectra $S^{T/R}$ are found from Eq. (5) when the output fields are changed to $\Sigma_{\text{out}}^{T/R} = \sum_j (\sqrt{\kappa_m^{T/R}} \sigma_j + \delta_R^{T/R} \sigma_{\text{in},j})$. Here, the ‘‘reflected’’ field should not be understood literally, but rather as the field that contains the driving field. The ‘‘transmitted’’ field is fully from the molecular fluorescence. Since $\sigma_j = Q_j^\dagger \sigma_j^S$ and the solution σ_j^S of Eq. (3b) depends on Q_j , we encounter a four-point correlator $\langle Q_j^\dagger(\omega_1) Q_j(\omega_2) Q_k^\dagger(\omega_3) Q_k(\omega_4) \rangle$ in the calculation of

$S^{T/R}$. Here, $Q_j^\dagger(\omega)$ refers to the Fourier transform of $Q_j^\dagger(t)$. Assuming that the vibration modes are independent and identical in different molecules, the correlator factorizes into two-point correlators when $j \neq k$. These resulting two- and four-point correlators are related to $P(E)$ by

$$\langle Q_j^\dagger(\omega_1) Q_j(\omega_2) \rangle = P(\omega_1) \delta(\omega_1 + \omega_2), \quad (25a)$$

$$\begin{aligned} \langle Q_j^\dagger(\omega_1) Q_j(\omega_2) Q_j^\dagger(\omega_3) Q_j(\omega_4) \rangle \\ = L(\omega_1, \omega_2, \omega_4) \delta(\omega_1 + \omega_2 + \omega_3 + \omega_4), \end{aligned} \quad (25b)$$

where $L(\omega_1, \omega_2, \omega_4)$ is the Fourier transform of Eq. (18) in the general case.

When discussing the response of molecules to driving, it is useful to introduce a frequency $\Delta = \omega_d - \tilde{\omega}_m$, which is the detuning between the driving and renormalized molecular frequency. Without vibrations, the molecular response is characterized by $\chi(\Delta) = (i\Delta - \frac{\kappa_m}{2})^{-1}$, which describes Lorentzian absorption and emission spectra. However, in the presence of vibrations, the information about the spectral properties is contained in

$$A(\Delta) = \int dE P(E) \chi(\Delta - E) \quad (26)$$

and

$$\begin{aligned} F = \int d\omega_1 d\omega_2 L(\omega_1, \omega_d - \omega - \omega_1, \omega_2) \\ \times \chi(\omega_1 - \Delta) \chi(\omega_2 + \Delta). \end{aligned} \quad (27)$$

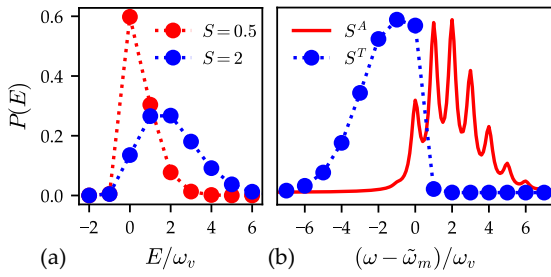


FIG. 2. (a) $P(E)$ functions for $\gamma = 0$ showing the weights of δ -function peaks when $\frac{\kappa_m}{\omega_v} = 0.5$ and $\frac{\hbar\omega_T}{\omega_v} = 0.5$. (b) The normalized emission and absorption with $S = 2$. Emission is evaluated with the driving frequency $\omega_d = \tilde{\omega}_m$. Here, we choose $\kappa_m^{T/R} = \kappa_m^{\text{ext}} = \frac{\kappa_m}{10}$.

These functions are associated with absorption and fluorescence of molecules, respectively, and play an important role in the plasmon-molecule problem.

A. Incoherent limit

Let us assume that molecules are randomly arranged, so that the phase θ_j is random. Averaging over them, the resulting spectra are

$$\frac{S^{T/R}(\omega; \omega_d)}{|\alpha|^2} = \kappa_m^{T/R} \kappa_m^{\text{ext}} F(\Delta; \omega - \omega_d) + \delta_R^{T/R} \left[1 + 2\sqrt{\kappa_m^{T/R} \kappa_m^{\text{ext}}} \text{Re}[A(\Delta)] \right] \delta(\omega - \omega_d). \quad (28)$$

The emission spectrum S^T is determined by F , which describes inelastic scattering (output field frequency ω different from driving frequency ω_d). In the “reflected” field S^R , we also find the input power spectral density I_{in} and a term proportional to A representing absorption.

Both F and A are straightforward to determine from Eqs. (21) and (24), i.e., when the vibrational linewidth $\gamma \rightarrow 0$. Then, F is also δ peaked at frequencies $\omega - \omega_d = m\omega_v$ with an integer m . The absorption spectrum is obtained from power conservation $S^A(\omega_d) = I_{\text{in}} - S^T - S^R$ evaluated at the driving frequency $\omega = \omega_d$ and it is mostly determined by A . In Fig. 2(b), we have plotted the emission spectrum S^T along with the absorption spectrum S^A . The absorption maximum is at the bare molecular frequency ω_m , while the emission maximum is at approximately $\omega_m - 2S\omega_v$. The difference is the Stokes shift. The spectra correspond to the results describing the transient response obtained with Green functions [21]. However, in our stationary model, the absorption is not a mirror image of the emission because the emission may also happen from the excited vibrational states.

B. Coherent limit

Besides the experimentally more typical incoherent situation, we look at the coherent limit. Then the phase $e^{i\theta_j}$ is fixed. This happens, for instance, when the distance between the molecules is much smaller than the wavelength of the driving field or the molecules are in a suitably chosen lattice.

We renormalize the input in this case to be $\sigma_{\text{in},j} = \frac{\alpha}{N} e^{-i\omega_d t}$ so that again the total input power is distributed evenly and is independent of the number of molecules N . Then, the calculation can be repeated to give

$$\begin{aligned} \frac{S^{T/R}(\omega; \omega_d)}{|\alpha|^2} &= \delta_R^{T/R} \left| 1 + \sqrt{\kappa_m^{T/R} \kappa_m^{\text{ext}}} A(\Delta) \right|^2 \delta(\omega - \omega_d) \\ &+ \kappa_m^{T/R} \kappa_m^{\text{ext}} \left[\frac{F}{N} + \left(\delta_T^{T/R} - \frac{1}{N} \right) |A(\Delta)|^2 \delta(\omega - \omega_d) \right]. \end{aligned} \quad (29)$$

Interestingly, we obtain an explicit dependence on the number N of molecules for two terms. One of those terms is the inelastic emission term F , which means that for large N , the spectra are mostly elastic. However, if the vibrations are absent, i.e., $S = 0$ which leads to $P(E) = \delta(E)$, $F = |A(\Delta)|^2 \delta(\omega - \omega_d)$ and the $1/N$ -dependent terms cancel. Therefore, this coherent effect is not related to the sub- or superradiance of molecules described by Dicke [28]. Rather, it is related to vibrations and their enhanced nonradiative emission, which shows up as a diminishing fluorescence as the number of molecules increases.

IV. PLASMON-MOLECULE SYSTEM

With the tools developed in Secs. II and III, we can return to the problem of a strongly coupled plasmon-molecule system and find the polarized spectra of the system using Eqs. (3) (with only the plasmon being driven, i.e., $\sigma_{\text{in},j} = 0$ in this case). We integrate Eq. (3b) from an initial time $t_i \rightarrow -\infty$ to $t_f = t$ and neglect the initial condition $\sigma_j^S(t_i)$ which has no role in a stationary situation. We substitute this into Eq. (3a), which leads to

$$\begin{aligned} \dot{c} &= - \left(i\omega_c + \frac{\kappa}{2} \right) c - \sqrt{\kappa_{\text{ext}}} c_{\text{in}} \\ &- \sum_j |g_j|^2 \int_{-\infty}^t dt' e^{i(\tilde{\omega}_m + \frac{\kappa}{2})(t-t')} Q_j^\dagger(t) Q_j(t') c(t'). \end{aligned} \quad (30)$$

At this point, we average the equation over the fluctuating vibrations and use a mean-field approximation. This leads to the $P(E)$ function since $\langle Q_j^\dagger(t) Q_j(t') \rangle c(t') = P(t-t') c(t')$. Consequently, the elastic response of the plasmon is given by $c(t) = \alpha r(\omega_d) e^{-i\omega_d t}$, where

$$\frac{r(\omega_d)}{\sqrt{\kappa_{\text{ext}}}} = \left[i(\omega_d - \omega_c) - \frac{\kappa}{2} + \sum_j |g_j|^2 A(\Delta) \right]^{-1}. \quad (31)$$

Vibrations provide a channel of relaxation, broadening the response which is associated with the real part of A . The imaginary part contains information about the frequencies of the polariton modes. When the vibrations are absent, i.e., $S = 0$ and $P(E) = \delta(E)$, the usual strong-coupling response is obtained as $A \rightarrow \chi$ with Rabi splitting proportional to $\sqrt{\sum_j |g_j|^2}$ at $\omega_c = \omega_m$. When the vibrations are present, especially the upper polariton branch is perturbed, as Fig. 3 shows.

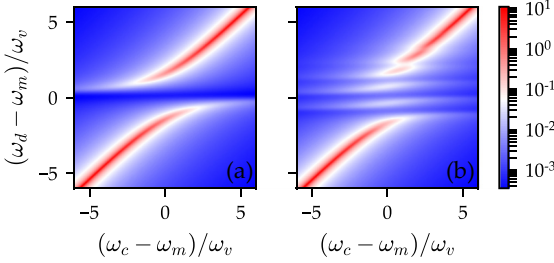


FIG. 3. Response function $|r(\omega_d)|^2/\omega_v$ of Eq. (31) for a single molecule for (a) $S = 0$ and (b) $S = 1$. The other parameters are $g/\omega_v = 1.5$, $\frac{k_B T}{\omega_v} = 0.5$, $\kappa/\omega_v = 0.1$, $\kappa_{\text{ext}} = \kappa/2$, and $\kappa_m/\omega_v = 0.5$. The response function also determines the direct plasmon emission spectrum.

Finally, σ_j^S can be solved from Eq. (3b) in terms of Q_j by Fourier transformation using the convolution theorem and $c(\omega) = \alpha r(\omega_d)\delta(\omega - \omega_d)$. Then we have all we need to evaluate the output spectra with Eqs. (4) and (5).

A. Incoherent polaritonic response

Let us consider a large number N of identical molecules with random dipole moment directions \hat{n}_j . In this case, we can replace the sums over the molecule index with an integral over a surface of a sphere, $\sum_j \rightarrow \frac{N}{4\pi} \int d\Omega$. Then, because $g_j = g e^{i\vec{k}\cdot\vec{r}_j}(\hat{n}_j \cdot \hat{u}_{pl})$ where $\hat{u}_{pl} = (0, \sin\beta, \cos\beta)$ is the plasmon polarization vector, the square of the Rabi splitting in Eq. (31) is $\sum_j |g_j|^2 = N g^2/3 \equiv g_N^2$. We assume that the positions of the N molecules are random over a region that is large compared to the wavelength of the plasmon so that we may replace $e^{i\vec{k}\cdot(\vec{r}_j - \vec{r}_k)} \rightarrow \delta_{jk}$ for an ensemble average. Using these assumptions, the polarization dependence shows up in the spectra as the coefficients

$$C_{s/p} = \sum_{j,k} g_j \eta_{j,s/p}^{T/R} (g_k \eta_{k,s/p}^{T/R})^* = \begin{cases} \frac{\kappa_m^{T/R} g_N^2}{5} \\ \frac{\kappa_m^{T/R} g_N^2}{5} [2 - \cos 2\beta], \end{cases} \quad (32)$$

where the upper/lower line is for s/p . Above, only the terms where $j = k$ contribute in the sum, which results in four-point correlators as in Eq. (25b).

The s - and p -polarized emission spectra are

$$S_s^T(\omega; \omega_d) = |\alpha r(\omega_d)|^2 C_s F, \quad (33a)$$

$$S_p^T(\omega; \omega_d) = |\alpha r(\omega_d)|^2 [\kappa_o^T \delta(\omega - \omega_d) + C_p F]. \quad (33b)$$

The main difference between the s - and p -polarized spectra is because the plasmon emits only p -polarized light. The molecular fluorescence is also slightly enhanced in this polarization for $\beta \neq 0$.

Both the s - and p -polarized emission spectra are now represented with F and A found in molecular fluorescence given by Eq. (28). Therefore, the emission of a strongly coupled plasmon-molecule system is related to the properties of the plasmon and the molecules separately with a few parameters describing the plasmon-molecule coupling strength and their

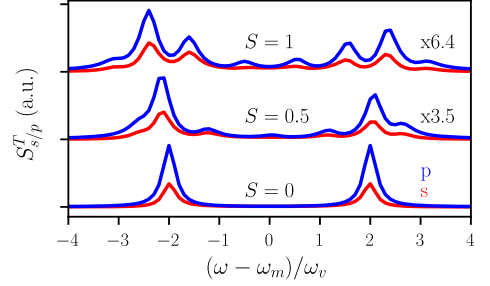


FIG. 4. Elastic emission spectra for s and p polarization (red and blue curves, respectively) from a plasmon-molecule system with $\omega_c = \omega_m$. The different curves are offset and scaled for clarity. The parameters are the same as in Fig. 3, except for $\frac{g_N}{\omega_v} = 2$, $\beta = \frac{\pi}{12}$, $\kappa_o^T = \kappa/2$, $\kappa_m^T = \kappa_m/3$, and $\frac{k_B T}{\omega_v} = 1$.

intrinsic decay rates. Note also that these results hold for any $P(E)$, i.e., these results are independent of the vibrational model.

Since only the terms with F contribute to the inelastic emission, for a given driving frequency ω_d , the ratio of p - and s -polarized emission at $\omega \neq \omega_d$ is $S_p^T/S_s^T = 2 - \cos(2\beta)$. For example, for an interface of vacuum and silver in the Drude model [34,43], $\beta \approx \frac{\pi}{12}$ and $S_p^T/S_s^T \approx 1.13$ at $\omega_c = 2\text{ eV}$. This ratio is otherwise independent of the system.

In Fig. 4, we have plotted the elastic emission spectra from Eqs. (33) using the $P(E)$ function (21). The s - and p -polarized emission are similar for small S , but for larger values the competition between the plasmon and molecule emission becomes more noticeable. The ratio between elastically emitted p - and s -polarized power is controlled by the ratio between κ_o^T and $C_{s/p}$ and the detuning $\omega_c - \omega_m$.

We find that the upper and lower polariton modes emit asymmetrically as in other approaches [39,44–50] and experiments [22–25,51]. This is caused by the asymmetry of the effective dissipation rate $\Gamma = \kappa/2 - g_N^2 \text{Re}[A(\Delta)]$, which is related to the molecule's absorption spectrum. The number of molecules affects the dissipation rate only via the size of the Rabi splitting. Analytical insight can be obtained when $k_B T \ll \hbar\omega_v$ and $S \ll 1$. Then, we may consider only single-phonon processes. When $g_N > \omega_v$, we find the polariton frequencies from the response function (31) for zero detuning $\omega_c = \omega_m$ to be approximately

$$\omega_{\pm} = \omega_m \pm g_N + \frac{S\omega_v}{2} \frac{1}{\pm g_N/\omega_v - 1}. \quad (34)$$

Thus, the vibrations affect both the position of the polariton peaks as well as the size of the Rabi splitting. At these frequencies, the dissipation rate in the first order of κ_m is given by

$$\Gamma_{\pm} = \frac{\kappa}{2} + \frac{\kappa_m}{2} \left[1 + \frac{S\omega_v^2}{(g_N \mp \omega_v)^2} + \frac{S\omega_v^2}{g_N(g_N \mp \omega_v)} \right]. \quad (35)$$

Due to vibrations, the dissipation rate of the upper polariton (Γ_+) is larger than the dissipation rate of the lower polariton (Γ_-), which suppresses the upper polariton emission compared to the lower polariton.

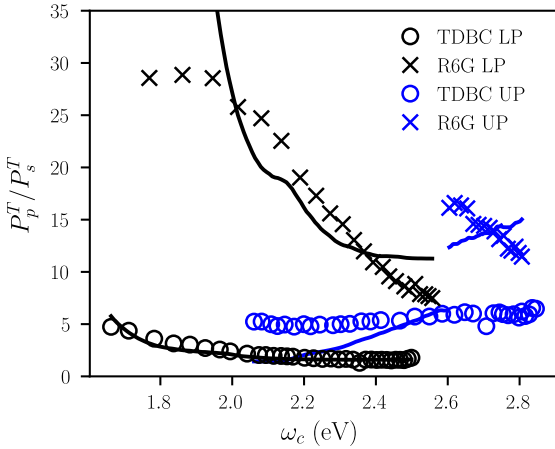


FIG. 5. Comparison of experimental polarization ratio data and corresponding theoretical fits for two different molecules. For TDBC, $\omega_m \approx 2.10$ eV and $2S\omega_v \approx 5$ meV, and for R6G, $\omega_m \approx 2.27$ eV and $2S\omega_v \approx 97$ meV. We estimate the plasmon linewidth to be $\kappa = 250$ meV. The Rabi splitting for TDBC is 167 meV and, for R6G, it is 337 meV. Our data on fluorescence of TDBC are limited below 2.6 eV so we cannot produce an estimate for the polarization ratio above 2.6 eV. In the legend, LP (UP) refers to lower (upper) polariton.

An alternative method of using the equations for polarized emission spectra (33) is to use experimental molecular absorption and fluorescence data. Then, to a good accuracy, the line shape of absorption is related to $\text{Re}(A)$ and fluorescence to F , as seen in Eq. (28). From the real part of A , the imaginary part may be found numerically by Hilbert transform (due to Kramers-Kronig relations). The response function is then determined from the plasmon eigenfrequency ω_c and its linewidth κ together with the strong-coupling constant g_N . Although g_N (and the magnitude of A) is unknown, it can be fixed so that it corresponds to a given Rabi splitting. Lastly, the coupling coefficients $C_{s/p}$ and κ_o^T/C_s are needed to evaluate the spectra. However, if we are only interested in the relative magnitudes, it is enough to fix the ratios κ_o^T/C_s and C_p/C_s . The latter ratio is given by the polarization angle β , which can be evaluated with the dielectric functions of the materials at the interface where the plasmon is excited. The former ratio κ_o^T/C_s is difficult to determine directly from the experiments, but it can be found by fitting to experimental data.

In Fig. 5, we employ the above method to compare the experimental results for the polarization ratio of the TDBC and R6G molecules from Ref. [22] to our model. Here, the polarization ratio P_p^T/P_s^T of the lower (upper) polariton is defined as the ratio of the p - and s -polarized emission peak intensity of the lower (upper) polariton. In our numerical analysis, we approximate the fluorescence data by a mirror image of the absorption data over the zero-phonon frequency $\bar{\omega}_m$. We assume that the fluorescence is effectively independent of the driving so that we can calculate and consider only the elastic emission (see, also, Appendix C). Adding the inelastic emission can only diminish the polarization ratio. Then we

calculate the polarization ratio using Eq. (33) and fit the coupling rate ratio κ_o^T/C_s to the experimental data for each branch separately.

For lower polariton peaks, we find reasonable agreement with the fitted theoretical curves and the experimental data. For upper polariton peaks, the correspondence is very limited. Theoretically, we would assume that the polarization ratio increases for the upper polariton for positive detunings, while for the lower polariton the ratio increases for negative detunings. This is caused by the polaritonic state becoming more plasmonic, which is seen from the response function being peaked at $\omega_d \approx \omega_c$ in Fig. 3. While these trends can be seen in Fig. 5, except for the R6G upper polariton branch, some features differ from the theoretical description. From an experimental point of view, the polarization ratio might be affected by any external noise, especially in regions of small s -polarized emission. In our modeling, we neglect the possible dependence of the plasmon linewidth and coupling rate on the plasmon eigenfrequency. Also, since we use the experimental absorption data to determine the spectra, the line shape far from the absorption maximum is also important.

The fitted ratio κ_o^T/C_s controls, generally speaking, the magnitude of the polarization ratio. The effect of Stokes shift seems to be important only at plasmon eigenfrequencies below the fluorescence frequency of the molecules, while the external coupling rates control the polarization ratio at higher frequencies. From the fit to the experimental data, we find that the ratio κ_o^T/C_s is larger for R6G than for TDBC. This implies that if the plasmonic emission rate remains the same for the TDBC and R6G samples, there is more molecular emission for TDBC than for R6G.

B. Coherent polaritonic response

If we assume that the plasmon couples strongly to the molecules and drives them coherently, the phase factor $e^{i\vec{k}\cdot\vec{r}_j}$ is fixed to a constant. This leads to the introduction of two different sums over the molecular indices,

$$\tilde{C}_{s/p} = \sum_j g_j \eta_{j,s/p}^{T/R} = \begin{cases} 0 \\ g_N \sqrt{\frac{N}{3}} \kappa_m^{T/R} \sin \beta, \end{cases} \quad (36)$$

where again the upper/lower line is for s/p . The sum in \tilde{C}_s vanishes because the plasmon polarization vector \hat{u}_{pl} is orthogonal to the s -polarization vector \hat{u}_s , making the product antisymmetric under reflection through the plane orthogonal to \hat{u}_s . This is what breaks the symmetry between the polarization directions emitted from the strongly coupled mode.

Then, we find the polarized emission spectra to be

$$S_s^T(\omega; \omega_d) = |\alpha r(\omega_d)|^2 C_s [F - |A(\Delta)|^2 \delta(\omega - \omega_d)], \quad (37a)$$

$$S_p^T(\omega; \omega_d) = |\alpha r(\omega_d)|^2 \kappa_o^T \left| 1 + i \frac{\tilde{C}_p}{\sqrt{\kappa_o^T}} A(\Delta) \right|^2 \delta(\omega - \omega_d) + |\alpha r(\omega_d)|^2 C_p [F - |A(\Delta)|^2 \delta(\omega - \omega_d)]. \quad (37b)$$

The s -polarized emission now vanishes fully when the vibrations are absent. This result shows that coherence is crucial

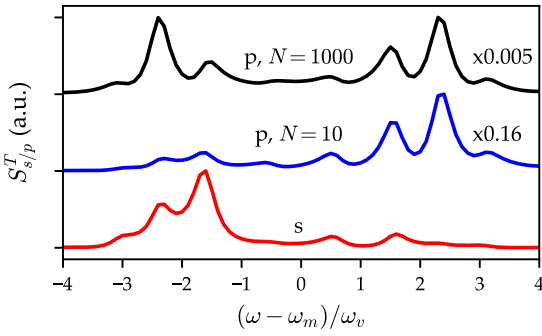


FIG. 6. Elastic emission spectra in the coherent case for two different numbers N of molecules. The curves for p -polarized emission (only ones depending on N) are offset and scaled. Here, $S = 1$ and the other parameters are the same as in Fig. 4.

to the destructive interference of emitted light [22], while the vibrations still provide a mechanism for a partial loss of coherence. On the other hand, the p -polarized spectrum contains the interference terms between the plasmon and molecular output fields. Similar to the Stokes shift case, there are terms with different powers of the number N of molecules. Considering the Rabi splitting (or g_N) to be fixed, there is one term with an extra N factor from \tilde{C}_p^2 and \sqrt{N} from \tilde{C}_p . Increasing N leads to mostly elastic p -polarized emission, as the inelastic terms and s -polarized emission are independent of N . In contrast to the Stokes shift case, the absence of vibrations does not remove the N dependence. Therefore, the result corresponds to superradiance [28].

Figure 6 shows that the coherence and the resulting interference between plasmonic and molecular emission have a qualitative effect on the elastic spectra. The difference between s - and p -polarized spectra becomes more evident. While the s -polarized emission is likely to occur on the lower polariton frequency, for the p -polarized emission, the upper polariton frequency may be favored depending on the relative magnitudes of κ_o^T , \tilde{C}_p , and C_p .

V. CONCLUSIONS

To summarize, we have constructed a model that allows one to describe the effect of vibrations on the strongly coupled stationary response of driven coupled light-matter modes. Depending on the case, one can either find the $P(E)$ function describing the absorption and emission of vibrations in a given model system, or relate the measured absorption and fluorescence of uncoupled molecules to $P(E)$. With small modifications, this approach can also be extended to the case of molecule-cavity systems [4,17,51–53], plasmonic lattices [54], and/or higher-order correlation functions of the emitted light [16]. Our quantum Langevin equation approach allows one to describe the stationary driven system, and hence it complements the often-used computational methods usually concentrating on transient response [18,45].

ACKNOWLEDGMENTS

We acknowledge the support from the Academy of Finland Center of Excellence program (Project No. 284594) and Projects No. 289947, No. 290677, and No. 317118.

APPENDIX A: GENERALIZATION TO MANY NONIDENTICAL AND INTERACTING VIBRATIONAL MODES

The $P(E)$ theory is straightforward to generalize to multiple vibrational modes when the modes couple linearly to the molecule. A general interaction term in the Hamiltonian is then $\lambda_{ijkl} b_{ij}^\dagger b_{kl} + \text{H.c.}$, where b_{ij} corresponds to the j th vibrational mode of the i th molecule. The molecule-vibrational Hamiltonian is then diagonalized by first diagonalizing the vibrational Hamiltonian and then using the polaron transformation. For simplicity, let us now discuss the case of a single molecule. After the diagonalization of the vibrational part, we may write the interaction Hamiltonian in terms of the new diagonal vibrational modes b_j as

$$H_{m+v} = \sum_{j=1}^M \omega_{v,j} \sqrt{S_j} \sigma^\dagger \sigma (x_j + u_j p_j), \quad (\text{A1})$$

where x_j and p_j are the position and momentum operator of vibrations. The term $u_j p_j$ follows from the fact that the molecule couples to the bare vibrational modes. Because in the Caldeira-Leggett model the position operator x_j couples to the position operator of an environmental (harmonic) mode, the diagonalization is incommensurate with this model unless $u_j = 0$. In the single-excitation limit, we may then introduce the operator $\sigma^S = Q\sigma \equiv \prod_j Q_j \sigma$, where $Q_j = e^{\sqrt{S_j}(b_j^\dagger - b_j)}$. Introducing many molecules into the situation only adds one external index to each operator. When there is no coupling to the plasmon, by following the same approximations as in the main text, we find that the dynamics is given by the input-output equation

$$\dot{\sigma}^S = -\left(i\tilde{\omega}_m + \frac{\kappa_m}{2}\right)\sigma^S - \sqrt{\kappa_m^{\text{ext}}} Q\sigma_{\text{in}}, \quad (\text{A2})$$

with $\tilde{\omega}_m = \omega_m - \sum_j S_j \omega_{v,j}$. The equation for b_j again decouples from the dynamics of σ^S in the single-excitation limit. Similarly to the case of a single vibrational mode, we find the two- and four-point correlators of Q in the calculation of the spectra. However, since $Q(t) = \prod_j Q_j(t)$, the Fourier transform of Q is always a convolution. After diagonalization, we may treat the modes as independent so this structure shows up as convolutions of $P(E)$'s and L 's defined in the earlier sections. Thus, we have

$$\langle Q^\dagger(\omega_1) Q(\omega_2) \rangle = P_{\text{tot}}(\omega_1) \delta(\omega_1 + \omega_2), \quad (\text{A3a})$$

$$\begin{aligned} \langle Q^\dagger(\omega_1) Q(\omega_2) Q^\dagger(\omega_3) Q(\omega_4) \rangle &= L_{\text{tot}}(\omega_1, \omega_2, \omega_4) \\ &\quad \times \delta(\omega_1 + \omega_2 + \omega_3 + \omega_4), \end{aligned} \quad (\text{A3b})$$

where $P_{\text{tot}}(E) = [P_1 * P_2 * \dots * P_M](E)$ is a convolution over M different modes, and similarly for L_{tot} . For example,

$$\begin{aligned} & [L_1 * L_2](\omega_1, \omega_2, \omega_3) \\ &= \int d\omega'_1 d\omega'_2 d\omega'_3 L_1(\omega_1 - \omega'_1, \omega_2 - \omega'_2, \omega_3 - \omega'_3) L_2(\omega'_1, \omega'_2, \omega'_3), \end{aligned} \quad (\text{A4})$$

where L_1 and L_2 are defined for a single mode as the Fourier transform of Eq. (16).

APPENDIX B: APPROXIMATION TO THE POLARON EQUATION

We discuss the consistency of the approximation that allows us to simplify the input-output equation of σ_j^S . The full dynamical equation of σ_j^S for the strongly coupled plasmon-molecule system, using the approach of [36], is given by

$$\begin{aligned} \dot{\sigma}_j^S = & -i\tilde{\omega}_m \sigma_j^S + ig_j Q_j \sigma_{z,j} c - \frac{\kappa_j}{2} \sigma_j^S + \sqrt{\tilde{\kappa}_j} Q_j \sigma_{z,j} \sigma_{\text{in},j} \\ & + \frac{\gamma_j \sqrt{S}}{2} \sigma_j^S (b_j - b_j^\dagger) + \sqrt{\gamma_j S} \sigma_j^S (b_{\text{in},j} - b_{\text{in},j}^\dagger). \end{aligned} \quad (\text{B1})$$

In the main text, we assumed the single-excitation limit in which $\sigma_{z,j} \approx -1$. In addition, we neglect the thermal fluctuations and set $\sigma_{\text{in},j} = 0$. Next we discuss when we can neglect the two last terms that are generated by the coupling of σ_j^S to the vibrational baths. This approximation effectively uncouples the vibrational dynamics from the dynamics of the polaron operator σ_j^S . As this approximation is related to the molecule-vibration system, the coupling to the plasmon may also be neglected, i.e. $g_j = 0$. For notational brevity, we omit the molecular index j . Let us consider an expansion $\sigma^S = \sigma_0^S + \tilde{\sigma}_1^S$, where σ_0^S is the solution of

$$\dot{\sigma}_0^S = -\left(i\tilde{\omega}_m + \frac{\kappa_m}{2}\right) \sigma_0^S - \sqrt{\kappa_m^{\text{ext}}} Q \sigma_{\text{in}}, \quad (\text{B2})$$

on Eq. (B1) with the above simplifications. Consequently, the dynamics of $\tilde{\sigma}_1^S$ is given by

$$\begin{aligned} \dot{\tilde{\sigma}}_1^S = & -\left(i\tilde{\omega}_m + \frac{\kappa_m}{2}\right) \tilde{\sigma}_1^S + \frac{\gamma \sqrt{S}}{2} (\sigma_0^S + \tilde{\sigma}_1^S) (b - b^\dagger) \\ & + \sqrt{\gamma S} (\sigma_0^S + \tilde{\sigma}_1^S) (b_{\text{in}} - b_{\text{in}}^\dagger). \end{aligned} \quad (\text{B3})$$

We may now construct the next order of the expansion by setting $\tilde{\sigma}_1^S = \sigma_1^S + \tilde{\sigma}_2^S$ and fixing σ_1^S to be the solution of

$$\begin{aligned} \dot{\sigma}_1^S = & -\left(i\tilde{\omega}_m + \frac{\kappa_m}{2}\right) \sigma_1^S + \frac{\gamma \sqrt{S}}{2} \sigma_0^S (b - b^\dagger) \\ & + \sqrt{\gamma S} \sigma_0^S (b_{\text{in}} - b_{\text{in}}^\dagger). \end{aligned} \quad (\text{B4})$$

This equation can be solved with the solution of σ_0^S . The dynamics of $\tilde{\sigma}_2^S$ is then determined by an equation similar to Eq. (B3), where $\tilde{\sigma}_1^S$ is replaced by $\tilde{\sigma}_2^S$ and σ_0^S by σ_1^S . Continuing this process gives then the expansion of $\sigma^S = \sum_{j=0}^{\infty} \sigma_j^S$. However, we focus only on the first order of the expansion.

Consider now that the molecule is driven coherently, $\sigma_{\text{in}} = \alpha e^{-i\omega_d t}$, so that the solution of Eq. (B2) is

$$\sigma_0^S(\omega) = \alpha \sqrt{\kappa_m^{\text{ext}}} \chi(\omega - \tilde{\omega}_m) Q(\omega - \omega_d). \quad (\text{B5})$$

Consequently, we obtain, from Eq. (B4),

$$\begin{aligned} \sigma_1^S(\omega) = & \sqrt{S} \chi(\omega - \tilde{\omega}_m) \\ & \times \left\{ i \frac{\gamma}{2} [\sigma_0^S * p](\omega) + \sqrt{\gamma} [\sigma_0^S * (b_{\text{in}} - b_{\text{in}}^\dagger)](\omega) \right\}, \end{aligned} \quad (\text{B6})$$

where $*$ denotes a convolution in the Fourier space.

We are now interested in the consistency of the expansion, but it is not straightforward to see the effect of the convolution and the underlying dynamics of the vibrations. For this reason, we compare the mean values of σ_0^S and σ_1^S . When the input operators of the vibrations represent thermal noise, the b_{in} terms do not contribute to the average. The expectation value of σ_0^S can be expressed as

$$\langle \sigma_0^S(\omega) \rangle = \alpha \sqrt{\kappa_m^{\text{ext}}} \chi(\omega - \tilde{\omega}_m) \langle Q(0) \rangle \delta(\omega - \omega_d). \quad (\text{B7})$$

For a thermal ensemble, $\langle Q(0) \rangle = \exp[-S(n_{\text{th}} + \frac{1}{2})]$. In the calculation of the average of σ_1^S , we need the generalized Wick theorem to write

$$S \langle p^n(t) p(0) \rangle = n J(t) \langle p^{n-1}(t) \rangle, \quad (\text{B8})$$

where $J(t)$ is the function defined in Eq. (12) and we define its Fourier transform by $J(t) = \int d\omega e^{-i\omega t} J(\omega)$. We obtain

$$\begin{aligned} \langle \sigma_1^S(\omega) \rangle &= \frac{\gamma}{2} \alpha \sqrt{\kappa_m^{\text{ext}}} \chi(\omega - \tilde{\omega}_m) \\ &\times \left[\int d\omega' \chi(\omega' + \omega_d - \tilde{\omega}_m) J(\omega') \right] \langle Q(0) \rangle \delta(\omega - \omega_d) \\ &= \frac{\gamma}{2} \left[\int d\omega' \chi(\omega' + \omega_d - \tilde{\omega}_m) J(\omega') \right] \langle \sigma_0^S(\omega) \rangle \\ &\equiv \mathcal{C} \langle \sigma_0^S(\omega) \rangle. \end{aligned} \quad (\text{B9})$$

Now we have a necessary condition for the consistency of the simplification: The parameter \mathcal{C} should be small compared to unity for the expansion to be sensible. It can be estimated by using the same approximation in Eq. (19) as in the $\gamma = 0$ calculation. Then (denoting $\Delta = \omega_d - \tilde{\omega}_m$),

$$\begin{aligned} \mathcal{C} &= \frac{\gamma S}{2} [(n_{\text{th}} + 1) \chi(\omega_v + \Delta) + n_{\text{th}} \chi(-\omega_v + \Delta)] \\ &\stackrel{\Delta = -\omega_v}{\approx} \frac{\gamma S}{\tilde{\kappa} + \gamma S} \frac{n_{\text{th}} + 1}{2}. \end{aligned} \quad (\text{B10})$$

In the last approximation, we have written the renormalized linewidth κ_m in terms of the bare linewidth of the molecule $\tilde{\kappa}$ and neglected the smaller term $\chi(-2\omega_v)$ for clarity. Now, it is clear that the consistency of the approximation is related to the temperature and the linewidths. This condition is always fulfilled when $n_{\text{th}} < 1$ or, alternatively, $\frac{\omega_v}{k_B T} > \ln(2) \approx 0.69$. It should be remembered that this is only a crude estimate and larger values of γ can diminish the value of \mathcal{C} .

APPENDIX C: CORRESPONDENCE TO EXPERIMENTS

In the experimental Kretschmann setup, a prism is used together with white light to excite the plasmons. The angle θ of incoming light with respect to the normal of the interface then determines the plasmon eigenfrequency ω_c . In our model,

which is based on a coherent single-frequency driving at ω_d , we can introduce a distribution $\rho(\omega_d)$ for light intensity. Then we can relate our theoretical model to the observed spectra by an integral relation

$$S_{s/p,\text{obs}}^{T/R}(\omega) = \int d\omega_d \rho(\omega_d) S_{s/p}^{T/R}(\omega; \omega_d). \quad (\text{C1})$$

The distribution $\rho(\omega_d)$ can include features of the driving light as well as the prism that couples the light to the interface. We can generally divide the theoretical spectrum into elastic and inelastic parts by $S_{s/p}^{T/R}(\omega; \omega_d) = S_{\text{el}}\delta(\omega - \omega_d) + S_{\text{inel}}(\omega; \omega_d)$.

Now, if we assume that the distribution of light is uniform and its bandwidth large compared to the plasmonic linewidth κ , we have

$$S_{s/p,\text{obs}}^{T/R}(\omega) = S_{\text{el}}(\omega) + \int d\omega_d S_{\text{inel}}(\omega; \omega_d). \quad (\text{C2})$$

The inelastic contribution is due to vibrations and molecular fluorescence [i.e., the function $F(\omega \neq \omega_d)$]. In the fit for Fig. 5, we disregard the contribution from S_{inel} because its main body is clearly separated from the elastic emission coming around the polariton frequencies.

-
- [1] G. Rempe, H. Walther, and N. Klein, *Phys. Rev. Lett.* **58**, 353 (1987).
- [2] C. Weisbuch, M. Nishioka, A. Ishikawa, and Y. Arakawa, *Phys. Rev. Lett.* **69**, 3314 (1992).
- [3] P. Törmä and W. L. Barnes, *Rep. Prog. Phys.* **78**, 013901 (2015).
- [4] X. Yu, Y. Yuan, J. Xu, K.-T. Yong, J. Qu, and J. Song, *Laser Photon. Rev.* **13**, 1800219 (2019).
- [5] M. Hertzog, M. Wang, J. Mony, and K. Börjesson, *Chem. Soc. Rev.* **48**, 937 (2019).
- [6] B. Munkhbat, M. Wersäll, D. G. Baranov, T. J. Antosiewicz, and T. Shegai, *Sci. Adv.* **4**, eaas9552 (2018).
- [7] J. A. Hutchison, T. Schwartz, C. Genet, E. Devaux, and T. W. Ebbesen, *Angew. Chem. Int. Ed.* **51**, 1592 (2012).
- [8] E. Orgiu, J. George, J. Hutchison, E. Devaux, J. Dayen, B. Doudin, F. Stellacci, C. Genet, J. Schachenmayer, C. Genes, G. Pupillo, P. Samorì, and T. Ebbesen, *Nat. Mater.* **14**, 1123 (2015).
- [9] X. Zhong, T. Chervy, S. Wang, J. George, A. Thomas, J. A. Hutchison, E. Devaux, C. Genet, and T. W. Ebbesen, *Angew. Chem. Int. Ed.* **55**, 6202 (2016).
- [10] X. Zhong, T. Chervy, L. Zhang, A. Thomas, J. George, C. Genet, J. A. Hutchison, and T. W. Ebbesen, *Angew. Chem. Int. Ed.* **56**, 9034 (2017).
- [11] K. Stranius, M. Hertzog, and K. Börjesson, *Nat. Commun.* **9**, 2273 (2018).
- [12] H. Deng, H. Haug, and Y. Yamamoto, *Rev. Mod. Phys.* **82**, 1489 (2010).
- [13] H. Deng, G. Weihs, D. Snoke, J. Bloch, and Y. Yamamoto, *Proc. Natl. Acad. Sci. USA* **100**, 15318 (2003).
- [14] S. Christopoulos, G. Baldassarri Hoger von Hogersthal, A. Grundy, P. G. Lagoudakis, A. V. Kavokin, J. J. Baumberg, G. Christmann, R. Butté, E. Feltn, J.-F. Carlin, and N. Grandjean, *Phys. Rev. Lett.* **98**, 126405 (2007).
- [15] R. Chikkaraddy, B. De Nijs, F. Benz, S. J. Barrow, O. A. Scherman, E. Rosta, A. Demetriadou, P. Fox, O. Hess, and J. J. Baumberg, *Nature (London)* **535**, 127 (2016).
- [16] D. Wang, H. Kelkar, D. Martin-Cano, D. Rattenbacher, A. Shkarin, T. Utikal, S. Göttinger, and V. Sandoghdar, *Nat. Phys.* **15**, 483 (2019).
- [17] T. Schwartz, J. A. Hutchison, J. Léonard, C. Genet, S. Haacke, and T. W. Ebbesen, *Chem. Phys. Chem.* **14**, 125 (2013).
- [18] G. Groenhof, C. Climent, J. Feist, D. Morozov, and J. J. Toppari, *J. Phys. Chem. Lett.* **10**, 5476 (2019).
- [19] G.-L. Ingold and Y. V. Nazarov, in *Single Charge Tunneling*, edited by H. Grabert and M. H. Devoret (Springer, New York, 1992), pp. 21–107.
- [20] T. T. Heikkilä, *The Physics of Nanoelectronics: Transport and Fluctuation Phenomena at Low Temperatures* (Oxford University Press, Oxford, 2013).
- [21] G. D. Mahan, *Many-Particle Physics* (Springer Science & Business Media, New York, 2013).
- [22] S. Baieva, O. Hakamaa, G. Groenhof, T. T. Heikkilä, and J. J. Toppari, *ACS Photon.* **4**, 28 (2017).
- [23] J. Bellessa, C. Bonnand, J. C. Plenet, and J. Mugnier, *Phys. Rev. Lett.* **93**, 036404 (2004).
- [24] T. K. Hakala, J. J. Toppari, A. Kuzyk, M. Pettersson, H. Tikkanen, H. Kunttu, and P. Törmä, *Phys. Rev. Lett.* **103**, 053602 (2009).
- [25] S. V. Baieva, T. K. Hakala, and J. J. Toppari, *Nanoscale Res. Lett.* **7**, 191 (2012).
- [26] M. A. Koponen, U. Hohenester, T. K. Hakala, and J. J. Toppari, *Phys. Rev. B* **88**, 085425 (2013).
- [27] S. Aberra Guebrou, C. Symonds, E. Homeyer, J. C. Plenet, Y. N. Gartstein, V. M. Agranovich, and J. Bellessa, *Phys. Rev. Lett.* **108**, 066401 (2012).
- [28] R. H. Dicke, *Phys. Rev.* **93**, 99 (1954).
- [29] P. Lodahl, S. Mahmoodian, S. Stobbe, A. Rauschenbeutel, P. Schneeweiss, J. Volz, H. Pichler, and P. Zoller, *Nature (London)* **541**, 473 (2017).
- [30] E. Kretschmann and H. Raether, *Z. Naturforsch. A* **23**, 2135 (1968).
- [31] In a usual experiment, the macroscopic number of molecules is embedded in a polymer layer forming an interface with a metallic layer. Then, the number N is the product of the molecular concentration and the effective mode volume of the plasmon. This volume should be proportional to the plasmon coherence length in the interface and the effective mode length defined in Ref. [32] if not limited by the system size.
- [32] A. Archambault, F. Marquier, J.-J. Greffet, and C. Arnold, *Phys. Rev. B* **82**, 035411 (2010).
- [33] D. F. Walls and G. J. Milburn, *Quantum Optics* (Springer, Berlin, 2008).
- [34] A. González-Tudela, P. A. Huidobro, L. Martín-Moreno, C. Tejedor, and F. J. García-Vidal, *Phys. Rev. Lett.* **110**, 126801 (2013).
- [35] K. Huang and A. Rhys, *Proc. R. Soc. A* **204**, 406 (1950).
- [36] C. W. Gardiner and M. J. Collett, *Phys. Rev. A* **31**, 3761 (1985).
- [37] Possible alternative approaches include the Lindblad master equation approach for the density matrix or the stochastic quantum jump approach. The previous approach would have to be written in the polaron basis to allow for a proper treatment of the

- effect of vibrations. The latter is most suitable for computational approaches.
- [38] A. O. Caldeira and A. J. Leggett, *Phys. Rev. Lett.* **46**, 211 (1981).
- [39] M. Reitz, C. Sommer, and C. Genes, *Phys. Rev. Lett.* **122**, 203602 (2019).
- [40] T. T. Heikkilä, P. Virtanen, G. Johansson, and F. K. Wilhelm, *Phys. Rev. Lett.* **93**, 247005 (2004).
- [41] V. Giovannetti and D. Vitali, *Phys. Rev. A* **63**, 023812 (2001).
- [42] J. G. Skellam, *J. R. Stat. Soc. A* **109**, 296 (1946).
- [43] H. U. Yang, J. D'Archangel, M. L. Sundheimer, E. Tucker, G. D. Boreman, and M. B. Raschke, *Phys. Rev. B* **91**, 235137 (2015).
- [44] T. Neuman and J. Aizpurua, *Optica* **5**, 1247 (2018).
- [45] J. del Pino, F. A. Y. N. Schröder, A. W. Chin, J. Feist, and F. J. Garcia-Vidal, *Phys. Rev. Lett.* **121**, 227401 (2018).
- [46] F. Herrera and F. C. Spano, *ACS Photon.* **5**, 65 (2018).
- [47] F. Herrera and F. C. Spano, *Phys. Rev. Lett.* **118**, 223601 (2017).
- [48] F. Herrera and F. C. Spano, *Phys. Rev. A* **95**, 053867 (2017).
- [49] M. A. Zeb, P. G. Kirton, and J. Keeling, *ACS Photon.* **5**, 249 (2017).
- [50] P. Michetti and G. C. La Rocca, *Phys. Rev. B* **77**, 195301 (2008).
- [51] J. Chovan, I. E. Perakis, S. Ceccarelli, and D. G. Lidzey, *Phys. Rev. B* **78**, 045320 (2008).
- [52] A. Canaguier-Durand, E. Devaux, J. George, Y. Pang, J. A. Hutchison, T. Schwartz, C. Genet, N. Wilhelms, J.-M. Lehn, and T. W. Ebbesen, *Angew. Chem. Int. Ed.* **52**, 10533 (2013).
- [53] T. Virgili, D. Coles, A. M. Adawi, C. Clark, P. Michetti, S. K. Rajendran, D. Brida, D. Polli, G. Cerullo, and D. G. Lidzey, *Phys. Rev. B* **83**, 245309 (2011).
- [54] T. K. Hakala, A. J. Moilanen, A. I. Väkeväinen, R. Guo, J.-P. Martikainen, K. S. Daskalakis, H. T. Rekola, A. Julku, and P. Törmä, *Nat. Phys.* **14**, 739 (2018).

II

POLARITON RESPONSE IN THE PRESENCE OF BROWNIAN DISSIPATION FROM MOLECULAR VIBRATIONS

by

K. S. U. Kansanen, J. J. Toppari, T. T. Heikkilä

The Journal of Chemical Physics **154**, 044108 (2021)

Reproduced from J. Chem. Phys. **154**, 044108 (2021), with the permission of
AIP Publishing. Copyright 2021 the Authors.

Polariton response in the presence of Brownian dissipation from molecular vibrations

Cite as: J. Chem. Phys. 154, 044108 (2021); doi: 10.1063/5.0036905

Submitted: 9 November 2020 • Accepted: 5 January 2021 •

Published Online: 27 January 2021



Kalle S. U. Kansanen,^{a)} J. Jussi Toppari, and Tero T. Heikkilä

AFFILIATIONS

Department of Physics and Nanoscience Center, University of Jyväskylä, P.O. Box 35, FI-40014 University of Jyväskylä, Finland

Note: This paper is part of the JCP Special Topic on Polariton Chemistry: Molecules in Cavities and Plasmonic Media.

^{a)}Author to whom correspondence should be addressed: kalle.s.u.kansanen@jyu.fi

ABSTRACT

We study the elastic response of a stationarily driven system of a cavity field strongly coupled with molecular excitons, taking into account the main dissipation channels due to the finite cavity linewidth and molecular vibrations. We show that the frequently used coupled oscillator model fails in describing this response especially due to the non-Lorentzian dissipation of the molecules to their vibrations. Signatures of this failure are the temperature dependent minimum point of the polariton peak splitting, the uneven polariton peak height at the minimum splitting, and the asymmetric shape of the polariton peaks even at the experimentally accessed “zero-detuning” point. Using a rather generic yet representative model of molecular vibrations, we predict the polariton response in various conditions, depending on the temperature, molecular Stokes shift and vibration frequencies, and the size of the Rabi splitting. Our results can be used as a sanity check of the experiments trying to “prove” results originating from strong coupling, such as vacuum-enhanced chemical reaction rate.

Published under license by AIP Publishing. <https://doi.org/10.1063/5.0036905>

I. INTRODUCTION

Strong coupling between electromagnetic modes and electronic excitations has emerged as a tool to modify internal material properties and dynamics in various systems from light harvesting¹ and energy transport^{2–5} to controlling photochemical reactions.^{6–9} The strong coupling regime is typically reached when the interaction-driven splitting of the dressed state, or polariton, eigenenergies becomes larger than their linewidth. Only then, the avoided crossing in the energy spectrum can be identified. This is rather clear in systems with a Lorentzian response that can be described by adding imaginary parts to the photon/exciton eigenenergies. However, in the case of molecules, the main cause of linewidth broadening often originates from vibrational dissipation, which does not typically produce a Lorentzian response. Here, we consider in detail a rather generic model system (two-level system and harmonic vibrations) to explore the effects of Brownian vibrational dissipation to the polaritonic spectrum. Comparing the results of such a model to the experimentally obtained polariton fingerprints then provides a sanity check of those experiments, helping to rule out spurious effects.

Our approach is based on the open quantum system model that we introduced in Ref. 10 to study the polariton response in the case where surface plasmon polaritons couple strongly with molecular excitations. Here, we modify this approach to concentrate on the case of a cavity containing a large number of molecules interacting with the cavity mode. The qualitative difference between these systems is that in the cavity case the molecular excitations are coupled with the free field only via the cavity field. We also focus on studying the role of vibrational dissipation on renormalizing the effective strong coupling parameters, especially in the case approaching the overdamped vibrations.

We consider the setup shown in Fig. 1. It consists of a cavity with eigenfrequency ω_c and linewidth κ_c , probed externally via a field coupling through one of the cavity mirrors. Inside the cavity, there are a (large) number N of molecules with excitation frequency ω_m . We denote the coupling energy between the cavity fundamental mode and a single exciton by g_j . At the same time, the molecular excitation couples to its vibration mode with eigenfrequency ω_v via a coupling strength $\sqrt{S}\omega_v$, where S is the Huang–Rhys factor.¹¹ We assume the vibrations to reside in a bath with temperature T , providing them with a linewidth γ . This vibrational coupling

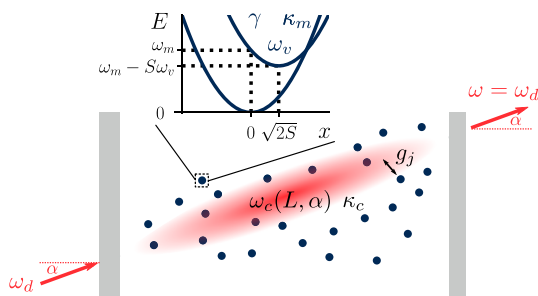


FIG. 1. Schematic picture of a measurement setup in which the cavity eigenfrequency ω_c is controlled by both the length L between the mirrors and the angle α of incident light of frequency ω_d . This confined light mode couples to molecules with harmonic vibrations. In this article, we focus on the elastic cavity emission or transmission, that is, the observed light power at frequency $\omega = \omega_d$. For explanation of other parameters, see the main text.

gives the individual molecules their Stokes shift and provides their inhomogeneous broadening.¹²

We illustrate the effects of this inhomogeneous broadening on the polariton eigenmodes via the system response in Fig. 2. Compared to the model in which the molecule response is taken as Lorentzian—known as the coupled oscillator model—the polaritonic spectrum has a few distinct features. First, the vibrations cause an asymmetry between the upper and lower polariton peaks, which is similar to that obtained by changing the detuning between the cavity and molecular frequency. However, this effect cannot be imitated by using a Lorentzian molecular response because this asymmetry is caused by the asymmetry of the molecular response. Second, we find

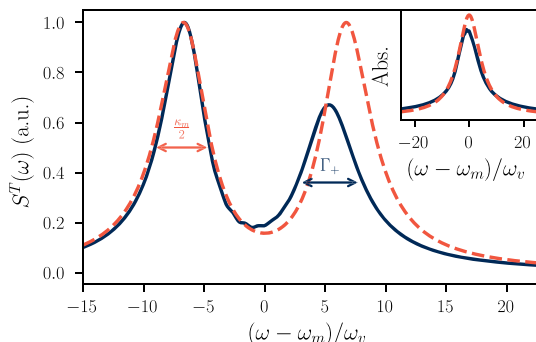


FIG. 2. Example of the polariton spectra under the coupled oscillator model (orange dashed line) and our $P(E)$ model (blue solid line), assuming a very high finesse cavity tuned so that the spacing between the polariton peaks is at its smallest. The inset shows the respective absorption profiles. Since the cavity dissipation κ_c is negligible, in the Lorentzian model, we find the Lorentzian polariton peaks whose linewidth is half of the “molecular” linewidth κ_m . When the vibrations and their dissipation are taken into account, one can find the non-Lorentzian behavior, renormalization of Rabi splitting, and changes in the linewidths.

that the polaritonic frequencies are renormalized, which affects the observed Rabi splitting.

A. Coupled oscillators

We briefly motivate the upcoming discussion with the often-used “coupled oscillators” model of polaritonics. It describes the cavity and excitonic modes as effectively harmonic oscillators; the cavity mode has the eigenfrequency ω_c , while for the exciton, it is ω_m . The rotating wave approximation is often made to simplify the coupling between these modes.¹³ Then, in the single-excitation subspace, the Hamiltonian for a single molecule in a cavity is given by ($\hbar = 1$ throughout the text)

$$H = \begin{pmatrix} \omega_c & g \\ g^* & \omega_m \end{pmatrix}. \quad (1)$$

This is the Jaynes–Cummings Hamiltonian.¹⁴ The polariton eigenfrequencies are then obtained by diagonalizing this matrix, which gives

$$\omega_{\pm} = \frac{\omega_c + \omega_m}{2} \pm \sqrt{|g|^2 + (\omega_c - \omega_m)^2/4}. \quad (2)$$

Perhaps, the most straightforward and often-used way to model dissipation is to introduce an imaginary shift in the eigenfrequencies. That is, we set $\omega_c \rightarrow \omega_c - i\kappa_c$ for the cavity and similarly $\omega_m \rightarrow \omega_m - i\kappa_m$ for the exciton. This method leads to Lorentzian line shapes for the cavity and the exciton alone. Consequently, if the dissipation is inserted to the polaritonic frequencies at resonance $\omega_c = \omega_m$, one finds

$$\omega_{\pm} = \omega_m - i\frac{\kappa_c + \kappa_m}{2} \pm \sqrt{|g|^2 - (\kappa_c - \kappa_m)^2/4}, \quad (3)$$

from which one infers $(\kappa_c + \kappa_m)/2$ to be the polariton linewidth.¹⁵

However, the molecular vibrations cannot often be neglected in molecular polaritonics. It is quite obvious that the vibrational modes have their own complex dynamics as well as coupling to their environment, which shape the absorption and fluorescence spectra of molecules. We show that even in the simplest vibrational models, the dissipative properties of the molecular vibrations, which in fact are the main source of line broadening, have quite intricate physics and thus effects on the polariton spectrum.

II. INPUT-OUTPUT THEORY OF MOLECULE-CAVITY SPECTROSCOPY

In this article, we consider a simplified model of a molecule as a two-level system with harmonic vibrations. In the language of operators, we associate a lowering operator σ to the electronic two-level system, while the phonons of vibrations are destroyed by b . The Hamiltonian is then characterized by the eigenenergies, ω_m and ω_v , of the two-level system and vibrations, respectively, and the dimensionless Huang–Rhys factor S quantifying their coupling

$$H_{\text{mol}} = \omega_m \sigma^\dagger \sigma + \omega_v b^\dagger b + \omega_v \sqrt{S} \sigma^\dagger \sigma (b + b^\dagger). \quad (4)$$

We assume that there are N identical particles that are described by this Hamiltonian.

Here, we consider that these molecules are embedded in a Fabry–Pérot cavity of eigenfrequency ω_c . For instance, the cavity eigenfrequency may be tuned by controlling the length of the cavity L and the incident light angle α by the relation $\omega_c = \frac{\pi c}{L} / \sqrt{1 - \sin^2(\alpha) / n_{\text{eff}}^2}$ where c is the speed of light and n_{eff} is the effective refractive index inside the cavity.¹⁶ The electronic coupling strength is described by a constant g_j . When we denote the cavity photon annihilation operator by c , the full Hamiltonian under the rotating wave approximation is

$$H = \omega_c c^\dagger c + \sum_{j=1}^N (H_{\text{mol},j} + g_j c^\dagger \sigma_j + g_j^* \sigma_j^\dagger c), \quad (5)$$

which is often referred to as the Holstein–Tavis–Cummings Hamiltonian.¹⁷ Under the assumption of identical particles, the relevant strong coupling constant is $\sum_{j=1}^N |g_j|^2 \equiv g_N^2$.

In order to observe anything spectroscopically, the cavity must be driven by an external light source, which we assume to have a low power so that we can concentrate on the lowest order response. We assume a laser drive at a driving frequency ω_d . Then, some light will leak out of the other side of the cavity. We are interested in this transmission spectrum $S^T(\omega; \omega_d)$, where, in general, ω is the frequency of the transmitted light. Any observed polaritonic emission is mediated by the cavity—there is no direct emission from the molecules. This simplifies the description of the spectrum as there cannot be interference between the cavity and molecular emission. In addition, the light emission should mostly be observed at the driving frequency. In this article, we neglect all processes that could cause inelastic behavior. This may be experimentally guaranteed by fixing the outgoing angle to be the same as the incident angle and measuring light power only at the frequency equal to the driving frequency $\omega = \omega_d$.

We assume that there exists an environment for each of the vibrational, excitonic, and cavity modes; coupling to these environments leads to dissipation. Both the driving and dissipation may be taken into account in the input–output formalism of quantum optics.¹⁸ It describes the quantum dynamics in the Heisenberg picture and can be considered an open quantum system modification to the Heisenberg equation. Without vibrations, this method gives similar results to those alluded in Eq. (3). However, the vibrations complicate finding the cavity reflection and transmission spectra notably as the equations of motion are nonlinear. The solution is obtained by moving into a polaron frame, i.e., finding the dynamics of $\sigma^S = \sigma e^{\sqrt{S}(b^\dagger - b)}$, which allows for simplifying approximations that in the end decouple the vibrational dynamics from those of the cavity-exciton system.^{10,19} The cavity transmission or emission spectrum is in this model $S^T(\omega; \omega_d) \propto |r(\omega_d)|^2 \delta(\omega - \omega_d)$ where the physics is contained in the cavity response function¹⁰

$$r(\omega_d) = \left[i(\omega_d - \omega_c) - \frac{\kappa_c}{2} + g_N^2 A(\omega_d - \omega_m + S\omega_v) \right]^{-1}. \quad (6)$$

The molecular contribution to the polaritonic spectrum is the absorption function

$$A(\omega) = \int dE \frac{P(E)}{i(\omega - E) - \kappa_m/2}. \quad (7)$$

The absorption profile of the molecule without the cavity is given by $\text{Re}[-A(\omega)]$. Here, $P(E)$ describes the probability to emit ($E > 0$) or absorb ($E < 0$) energy E to/from the vibrations. It can be expressed as

$$P(E) = \int \frac{dt}{2\pi} e^{iEt} \langle e^{\varphi(t)} e^{-\varphi(0)} \rangle = \int \frac{dt}{2\pi} e^{iEt} e^{J(t) - J(0)}, \quad (8)$$

where $\varphi(t) = \sqrt{S}[b^\dagger(t) - b(t)]$ is proportional to the momentum operator of the vibrations in the Heisenberg picture, while $J(t) = \langle \varphi(t)\varphi(0) \rangle$ is proportional to the momentum correlator. The Fourier convention has been chosen this way to allow for a probability interpretation: The energy integral over $P(E)$ amounts to unity. Furthermore, the same formalism extends to many vibrational modes: The total $P(E)$ in Eq. (7) is then a convolution of all the single-mode $P(E)$ functions.¹⁰

The expression of A is the convolution of the vibrational $P(E)$ and the electronic susceptibility. The latter alone would produce a Lorentzian line shape with linewidth κ_m . This linewidth follows from the assumption of excitonic dissipative environment, which does not couple to the observed far-field mode. It is renormalized by the coupling to vibrations as $\kappa_m = \tilde{\kappa} + S\gamma$, where $\tilde{\kappa}$ represents the dissipation rate of the electronic transition and γ is the dissipation rate of the vibrations.¹⁰ However, $P(E)$ ultimately determines the line shape in the presence of vibrations.

If there are no vibrations, $S = 0$ and $P(E) = \delta(E)$, the solution of $1/r(\omega) = 0$ gives exactly the polariton frequencies in Eq. (3). However, in this context, the frequencies are real. When $\omega_c, \omega_m, |g| \gg \kappa_c, \kappa_m$, one can first neglect the dissipation rates and minimize the imaginary part to find the polariton frequencies in Eq. (2). It is then straightforward to show that the behavior around these eigenfrequencies is Lorentzian and the real part gives the dissipation rate $(\kappa_c + \kappa_m)/2$. The proper way to find the polariton peaks would be to find the extremal points of $|r(\omega)|^2$, which gives the dissipative correction. A closed form solution is possible to obtain only at resonance $\omega_c = \omega_m$. It reads

$$\omega_{\pm} = \omega_m \pm \sqrt{|g|^2 \sqrt{1 + \frac{\kappa_m(\kappa_m + \kappa_c)}{2|g|^2}} - \kappa_m^2/4}. \quad (9)$$

The square root term may be approximated by $\sqrt{|g|^2 + \kappa_c \kappa_m/4}$ when $|g| \gg \kappa_m, \kappa_c$. This result differs from the coupled oscillator model in two ways: First, the dissipation strictly increases the spacing between polariton frequencies, or the Rabi splitting, when the coupling is large compared to the dissipation rates. This changes at the opposite limit when the dissipation rates dominate the coupling $|g|^2$, leading eventually to the disappearance of the polariton peaks. Second, the dissipation in the cavity and the molecule are, in general, not interchangeable as in the coupled oscillator model. This is a direct consequence of our assumptions: We only couple the external light source to the cavity and observe only its emission.

III. $P(E)$ THEORY UNDER BROWNIAN DISSIPATION

We now derive the $P(E)$ function assuming that the molecular vibrations are coupled to a bath of harmonic oscillators. This means solving the correlator $\langle e^{\varphi(t)} e^{-\varphi(0)} \rangle$ and then evaluating its Fourier transform. We note the recent similar approaches of Refs. 20 and 21 that model molecules embedded in a crystal taking into account coupling between the lattice vibrations and molecular vibrations.

The correlator $\langle e^{\varphi(t)} e^{-\varphi(0)} \rangle$ can be evaluated for different models,^{10,19,20} so let us make a general argument: Since the vibrations are harmonic, their fluctuations follow Gaussian statistics. Furthermore, we assume that these fluctuations are stationary, i.e., all correlators depend only on time differences and not on any specific time. By introducing a time ordering operator \mathcal{T} that always orders $\varphi(t)$ before $\varphi(0)$, we can write the correlator as $\mathcal{T}\langle e^{\varphi(t)-\varphi(0)} \rangle$. This may be identified as the characteristic function of the stochastic quantity $\varphi(t) - \varphi(0)$, which has a vanishing mean.^{22,23} In the case of Gaussian fluctuations, the correlator is fully determined by the variance $\mathcal{T}\langle [\varphi(t) - \varphi(0)]^2 \rangle / 2$, which equals to $J(t) - J(0)$.

Because vibrational modes are often low frequency compared to optical frequency, the quantum optical models of dissipation are not justified. This is because in the quantum optical case, the time scales of the system are generally assumed to be much smaller than its relaxation time. However, this is not a typical limit for molecular vibrations. This leads to a failure of the rotating wave approximation that is made to the system–environment coupling in the quantum optical formulation.²⁴ In the Brownian case (also called the Caldeira–Leggett model²⁵), the equations of motion for the position x and momentum p are

$$\dot{x} = \omega_v p, \quad \dot{p} = -\omega_v(x + \sqrt{2S}\sigma^\dagger\sigma) - \gamma p + \xi, \quad (10)$$

where ξ is the Langevin force of thermal fluctuations obeying a noise correlator,²⁶

$$\langle \xi(\omega)\xi(\omega') \rangle = \frac{\gamma\omega}{2\pi\omega_v} \left[\coth\left(\frac{\omega}{2k_B T}\right) + 1 \right] \delta(\omega + \omega'). \quad (11)$$

On average, the molecules are in their ground state since $\omega_m \gg k_B T$, so we neglect the $\sigma^\dagger\sigma$ -term in Eq. (10). This assumption decouples vibrational dynamics from those of the exciton. The solution of x and p can then be obtained in the Fourier space in terms of the force ξ .

By using $\varphi(t) = \sqrt{2S}p(t)$ and taking a few algebraic steps, we find an integral expression

$$J(t) = \frac{S\gamma}{\pi\omega_v} \int d\omega e^{-i\omega t} \frac{\omega^3}{(\omega^2 - \omega_v^2)^2 + \omega^2\gamma^2} \left[\coth\left(\frac{\omega}{2k_B T}\right) + 1 \right]. \quad (12)$$

It should be noted that this integral does not converge when $t = 0$, that is, the variance of momentum diverges. This is akin to the free Brownian particle for which the variance of the position diverges. We may solve the integral for $t \neq 0$ and deal with this divergence at a later point.

Whereas Ref. 10 computes $P(E)$ in the limit $\gamma \ll \omega_v$, here we solve the problem with an arbitrary γ/ω_v . We employ the method of residues to solve the integral for $t > 0$ by choosing an infinite radius semi-circle in the lower complex half-plane as the integration contour. Formally, we then set $J(t) - J(0) \equiv \tilde{J}(t)$ to vanish at time $t = 0$ and cut off the divergence. Finally, we can use the stationarity of vibrations to expand to negative times by the relation $J(-t) = J(t)^*$. These steps are taken to ensure the consistency of $P(E)$.

The integral in Eq. (12) may be separated into two contributions by the singularities of the integrand that lie inside the integration contour (see Fig. 3). On the one hand, there is the contribution of the singularities of the rational function $g(\omega) \equiv \omega^3 / [(\omega^2 - \omega_v^2)^2 + \omega^2\gamma^2]$, which is determined by the quality factor $Q = \omega_v/\gamma$ of vibrations. Especially, when $Q > 1/2$, there are two singularities with non-zero real frequencies, which are associated with underdamped motion. The value $Q = 1/2$ represents the critical damping of harmonic motion, while $Q < 1/2$ corresponds to the overdamped motion with two singularities on the imaginary axis. On the other hand, the hyperbolic cotangent has an infinite series of singularities at complex frequencies, which are related to the temperature. We term this *the Matsubara contribution*.

Since we want to calculate the Fourier transform of $P(t) = \exp[\tilde{J}(t)]$, it is useful to use the convolution theorem. It allows us to Fourier transform the individual components (each corresponding to one singularity/residue) and convolve the Fourier transforms together only in the end.

The calculation is tractable due to a group property of Lorentzian distributions under convolutions. We find that the Fourier transforms may be written in terms of two functions,

$$f_L(\omega; \omega_0, \Gamma) = \frac{1}{\pi} \frac{\Gamma}{(\omega - \omega_0)^2 + \Gamma^2}, \quad (13a)$$

$$g_L(\omega; \omega_0, \Gamma) = \frac{1}{\pi} \frac{\omega - \omega_0}{(\omega - \omega_0)^2 + \Gamma^2}. \quad (13b)$$

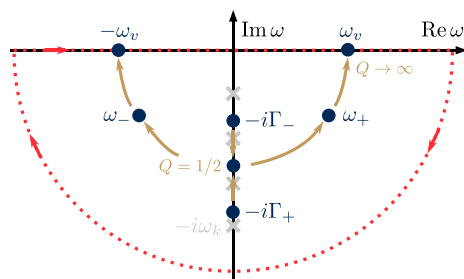


FIG. 3. Sketch of the singularities of $g(\omega)$ (blue circles) in the lower complex half-plane as a function of the quality factor Q . The singularities of $\coth(\omega/2k_B T)$ that lie on the imaginary axis are depicted by gray crosses. The red dotted line represents the integration contour for $t > 0$. This residue structure is mirrored in the upper complex half-plane.

We recognize f_L to be the Cauchy–Lorentz probability distribution function and g_L to be its Hilbert transform. We use these normalized functions as they integrate to unity (f_L) or to zero (g_L) for all parameters. In addition, these functions follow the convolution table,

$$[f_L(\omega_1, \Gamma_1) * f_L(\omega_2, \Gamma_2)](\omega) = f_L(\omega; \omega_1 + \omega_2, \Gamma_1 + \Gamma_2), \quad (14a)$$

$$[g_L(\omega_1, \Gamma_1) * f_L(\omega_2, \Gamma_2)](\omega) = g_L(\omega; \omega_1 + \omega_2, \Gamma_1 + \Gamma_2), \quad (14b)$$

$$[g_L(\omega_1, \Gamma_1) * g_L(\omega_2, \Gamma_2)](\omega) = -f_L(\omega; \omega_1 + \omega_2, \Gamma_1 + \Gamma_2). \quad (14c)$$

Often, only the Lorentzian component is taken into account. However, the role of g_L is to provide the emission–absorption asymmetry to $P(E)$. This general physical rule simply states that the temperature (of the environment) dictates the ratio of probabilities between the absorption and emission of energy E between the environment and the vibrations. To be more exact, this ratio is given by $P(E)/P(-E) = e^{-\beta E}$. This relation follows from the definition of $P(E)$ as a Fourier transform of $\langle e^{\varphi(t)} e^{-\varphi(0)} \rangle$ by using the definition of Heisenberg operators and the cyclic property of the trace when the vibration mode is in thermal equilibrium.²⁵

Next, we find the contributions of individual singularities to $J(t)$ and then calculate their Fourier transforms. The algebraic details of the Fourier transform are given in the [Appendix](#).

A. Residues of the rational function $g(\omega)$

Let us consider underdamped motion with $Q > 1/2$. We then find singular points at $\omega = \pm\tilde{\omega}_v \pm i\frac{\gamma}{2}$. The frequency $\tilde{\omega}_v = \omega_v \sqrt{1 - \frac{1}{4Q^2}}$ is the renormalized vibrational frequency. By the method described above, we find, for all times t ,

$$\tilde{J}_{\pm}(t) = [\text{Re}(D_{\pm}) + i\text{Im}(D_{\pm}) \text{sgn } t] \left(e^{\mp i\tilde{\omega}_v t - \frac{\gamma}{2}|t|} - 1 \right), \quad (15)$$

where $\text{sgn } t$ is the sign function ($\text{sgn } t = t/|t|$ for $t \neq 0$ and $\text{sgn } t = 0$ if $t = 0$) and

$$D_{-} = S \frac{\frac{i}{Q} - \frac{\omega_v}{\tilde{\omega}_v} \left(\frac{1}{2Q^2} - 1 \right)}{e^{\beta(\tilde{\omega}_v + i\frac{\gamma}{2})} - 1} \equiv \text{SN} \left[\frac{i}{Q} - \frac{\omega_v}{\tilde{\omega}_v} \left(\frac{1}{2Q^2} - 1 \right) \right], \quad (16a)$$

$$D_{+} = S(N^* + 1) \left[-\frac{i}{Q} - \frac{\omega_v}{\tilde{\omega}_v} \left(\frac{1}{2Q^2} - 1 \right) \right]. \quad (16b)$$

The constant N defined in D_{-} seems to be a complexification of the Bose function. If we set $\gamma = 0$, N would be the number n_{th} of thermal excitations. One can then readily associate D_{+} to emission and D_{-} to absorption.

The Fourier transform of $\exp[\tilde{J}_{\pm}(t)]$ is given by the following series representation:

$$P_{\pm}(E) = \mathcal{F}[\exp[\tilde{J}_{\pm}(t)]](E) = e^{-\text{Re}(D_{\pm})} \sum_{n=0}^{\infty} \frac{1}{n!} |D_{\pm}|^n \times \left[\cos(\phi_n^{\pm}) f_L \left(E; \pm n\tilde{\omega}_v, n\frac{\gamma}{2} \right) + \sin(\phi_n^{\pm}) g_L \left(E; \pm n\tilde{\omega}_v, n\frac{\gamma}{2} \right) \right], \quad (17)$$

where $\phi_n^{\pm} = \text{Im}(D_{\pm}) - n \arg(D_{\pm})$ is the angle that depends directly on the complex phase of the coefficient D_{\pm} . This series represents all the possible vibronic peaks: P_{+} describes all the processes where a certain number of vibronic excitations are created when the molecule is excited, while P_{-} describes the anti-Stokes processes of exciting the molecule from an excited vibrational state. Since we assume harmonic vibrations, there is no limit to the number of vibrational states, but accessing higher vibrational states is unlikely because of the dissipation. Note that without the angle dependence, $\phi_n^{\pm} = 0$, which happens when $\gamma = 0$ or $Q \rightarrow \infty$, the prefactors would follow the Poisson distribution with $D_{+} = S(n_{\text{th}} + 1)$ and $D_{-} = Sn_{\text{th}}$. Thus, the non-zero ϕ_n^{\pm} can be regarded as a sign of correlation between processes that involve multiple quanta of vibration.

In the overdamped limit, $Q < 1/2$, only a few changes are required in Eq. (17). First, there is no harmonic motion and, thus, $\mp\tilde{\omega}_v \rightarrow 0$. We rather have two dissipation rates so that

$$\frac{\gamma}{2} \rightarrow \Gamma_{\pm} = \omega_v \sqrt{\frac{1}{2Q^2} - 1 \pm \frac{1}{Q} \sqrt{\frac{1}{4Q^2} - 1}}. \quad (18)$$

In addition, the coefficients change to

$$D_{\pm} \rightarrow \frac{S}{2Q} \left[-i + \cot \left(\frac{\Gamma_{\pm}}{2k_B T} \right) \right] \left(1 \pm Q \sqrt{\frac{1 - 2Q^2}{1 + 2Q^2}} \right), \quad (19)$$

assuming that the singularities of $g(\omega)$ do not occur at the same point as those of the hyperbolic cotangent. Such coincidences would take place only at numerable points of continuous variables. We hence expect such double poles to have no observable consequences.

B. Matsubara contribution

The function $\coth(\omega/(2k_B T))$ has singularities at $\omega = i2\pi k_B T k$ for $k \in \{1, 2, \dots\}$. For any k , the contribution to $\tilde{J}(t)$ is given by

$$\tilde{J}_k(t) = C_k (e^{-\omega_k |t|} - 1), \quad C_k = \frac{4S}{\beta Q} \frac{\omega_k^3}{(\omega_k^2 + \omega_v^2)^2 - \gamma^2 \omega_k^2}. \quad (20)$$

Since there is no imaginary part in $\tilde{J}_k(t)$, its Fourier transform is simply a Lorentzian. The resulting P_k is then a series of $E = 0$ centered Lorentzians with a width that is multiples of the Matsubara frequency ω_k . Furthermore, it admits to a representation in terms of the incomplete Gamma function²⁷ as

$$P_k(E) = \mathcal{F}[\exp[\tilde{J}_k(t)]](E) = e^{-C_k} \left(\delta(E) - \text{Re} \left[\frac{(-C_k)^{i\frac{E}{\omega_k}}}{\pi \omega_k} \Gamma \left(-i\frac{E}{\omega_k}; -C_k, 0 \right) \right] \right). \quad (21)$$

The Matsubara contribution only widens $P(E)$.

When we consider the sum $\sum_k \tilde{J}_k(t)$, we encounter a logarithmic divergence as the sum behaves asymptotically as the harmonic series $\sum_k 1/k$. This is a well known feature of Ohmic dissipation,²⁸ which is characterized by the asymptotically linear ω dependence of the noise correlator in Eq. (11). Thus, we must

introduce a cutoff to the integral (12), which we may consider at the level of residues. Since the divergence is logarithmic, the results depend only weakly on the chosen cutoff. In this context, the Matsubara frequency ω_k is also the width parameter of P_k so that the corresponding distribution becomes wider and wider as higher and higher Matsubara frequencies are considered. Here, we choose the number of Matsubara modes by first choosing some cutoff frequency ω_L and then calculating $k_{\max} = \lfloor \omega_L / (2\pi k_B T) \rfloor$. For very low temperatures corresponding to $\omega_v / k_B T \gg 2\pi$, one may also choose to approximate the k -sum as an integral. However, this is not the limit we consider below. We set $\omega_v / k_B T \in [0.5; 4]$ and choose the cutoff frequency to be $\omega_L = 25\omega_v$ in our numerical analysis.

C. Absorption function

Using the results of Secs. III A and III B, we may now express the absorption function as a convolution

$$A(\omega) = [P_+ * P_- * P_1 * \dots * P_{k_{\max}} * \chi](\omega) \quad (22)$$

with the electronic susceptibility $\chi(\omega) = [i\omega - \kappa_m/2]^{-1}$ defined in Eq. (7). With the value of A , it is then straightforward to calculate the elastic spectrum $S^T(\omega)$ using the response function $r(\omega)$ of Eq. (6).

Due to the associativity of convolution, we may change the order of convolutions in A . This is numerically useful; as $\chi(\omega) = -\pi[f_L(\omega; 0, \kappa_m/2) + ig_L(\omega; 0, \kappa_m/2)]$, the susceptibility χ provides a constant to all the width parameters. By dividing the susceptibility into parts using the convolution rules, especially all the delta functions in Eq. (17) acquire a finite width proportional to κ_m . This facilitates a numerical method for the calculation of the convolutions, although it is possible also analytically. There are only a few numerical issues to be aware of: One must have a dense enough discretization of frequencies so that the peaks are well represented and a large range of values must be included so that there are no spurious edge effects in the calculation of convolutions.^{29–31}

Without numerical analysis, one can already have some insight to $P(E)$ and the resulting absorption function A . The effect of the Huang–Rhys factor S is twofold: Because the prefactors in P_{\pm} are similar to those of Poisson distribution, increasing S increases the support of the $P(E)$ function, i.e., there are more terms in the sum, which differ appreciably from zero. In addition, increasing S increases the effective dissipation rate κ_m in the molecular susceptibility χ , which further widens the absorption function A and increases the linewidth of individual vibronic peaks. The role of temperature T is similar to this because it allows for thermal excitations. Then, the molecular linewidth increases as the temperature is increased since there are more processes available, which result in the same amount of energy absorbed. The role of the Matsubara contribution is essentially to be a correction to this thermal broadening. In conjunction with S and T , the quality factor of Q then determines whether individual vibronic peaks may be observed and what the molecular linewidth is.

The derivation of $P(E)$ and A is here done for a single vibrational mode. As mentioned below Eq. (8), the definition of $P(E)$ extends to many vibrational modes through convolution. One can then identify each element of $P(E)$ (P_{\pm}, P_k) as in the single mode case

and convolve these elements together. For instance, if we have M identical but independent vibrational modes, the convolution over all P_{\pm} 's is straightforward to do and it only multiplies the Huang–Rhys factor S by M , i.e., $S \rightarrow MS$. Here, we assume this kind of case: The Huang–Rhys factors can be large, but we want to retain the tractability of the problem, so we use only the minimal number of free parameters.

IV. POLARITONIC SPECTRUM

Next, we discuss different features of the polaritonic spectrum, which change due to vibrational dissipation. The interest especially lies in the quantities that are inferred from experimental data: Rabi splittings, linewidths, and peak amplitudes.

Vibrations provide an asymmetry to the absorption due to the emission–absorption asymmetry, which manifests itself as a renormalization of the resonance condition. In the coupled oscillator model, there are three distinct features at resonance $\omega_c = \omega_m$: (1) The difference between the upper and lower polariton frequencies is at minimum, (2) the linewidths are the same and equal to the mean of cavity and exciton linewidths, and (3) the intensities of the peaks are equal. In the presence of vibrations, these conditions bifurcate to different values of detuning. The role of Brownian vibrational dissipation to this “bifurcation” has not been investigated to our knowledge. This phenomenon is often framed conversely as the asymmetry of the upper and lower polariton peaks, which has garnered both theoretical^{10,19,32–38} and experimental^{39–43} interest. The notion of asymmetry often follows in theory even after fixing the detuning to zero by setting $\omega_c = \omega_m$. However, this might not give the minimum polariton peak separation, i.e., the Rabi splitting. This is demonstrated in Fig. 4(a) where the polariton spectrum is plotted as a function of the detuning and the driving frequency.

A. Rabi splitting

Let us first discuss in detail the renormalization of the observed polariton frequencies ω_{\pm} and especially the Rabi splitting R . Here, we define the Rabi splitting as $R = \min_{\omega_c - \omega_m}(\omega_+ - \omega_-)$, and we denote the value $\omega_c - \omega_m$ at which this minimum is obtained

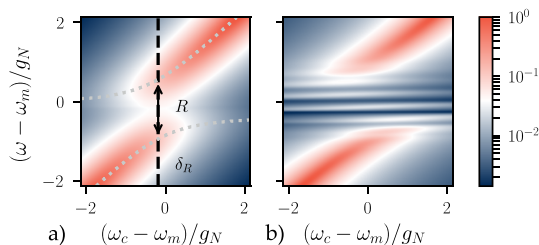


FIG. 4. Polaritonic spectrum $S^T(\omega)$ for (a) $Q = 0.9$ and $g_N = 7\omega_v$, and (b) $Q = 5$ and $g_N = 3.5\omega_v$. In (a), the gray dotted lines denote the position of the polariton peaks, while the black dashed line represents the detuning δ_R on which the Rabi splitting R is determined. We set $S = 1$, $g_N/\kappa_c = g_N/k_B T = 3.5$, and the dissipation rate of the electronic transition $\bar{\kappa}/g_N = 0.01$ in both the panels.

by δ_R . To avoid ambiguities, we only look at parameter regimes where the vibrational sub-peaks are suppressed. For instance, in Fig. 4(b), it is unclear how the Rabi splitting should be evaluated. This is rarely a problem in experiments with organic molecules.

We show in Fig. 5(a) how such an “experimentally inferred” Rabi splitting depends on the temperature T , vibration quality factor Q , and Huang–Rhys factor S . As in the case of the coupled oscillator model, the Rabi splitting depends on the molecular linewidth. For example, R increases with an increasing temperature, which may be attributed to the increase in the overall linewidth. However, the molecular line shape plays an important role. In Fig. 5, we have chosen two pairs of values for S and Q so that there are two different effective linewidths indicated by the solid and dashed lines. These linewidths are determined as the full width at half maximum (FWHM) of the absorption profile $\text{Re}(-A)$. We find that the Rabi splitting is closer to the value expected from the coupled oscillator model ($2g_N$ without any dissipation) with larger quality factors Q .

Contrary to the coupled oscillator model, the vibrational dissipation affects the relative position of the polariton frequencies to the uncoupled eigenfrequencies ω_m and ω_c . It is especially evident when the vibrations are of low quality. This follows from our definition of $P(E)$: If the vibrations are very dissipative, $P(E)$ becomes centered around $E = 0$ because a vibronic peak at $E = \pm n\hbar\omega_v$ has the width of $n\gamma/2$. Consequently, the absorption function $A(\omega - \omega_m + S\omega_v)$ in the response function and thus the absorption profile is peaked at $\omega = \omega_m - S\omega_v$. This results to a shift of $S\omega_v$ of the polariton peaks, which is most clearly seen as a shift in the local minimum of the polaritonic spectrum (see Fig. 2). If the vibrational quality

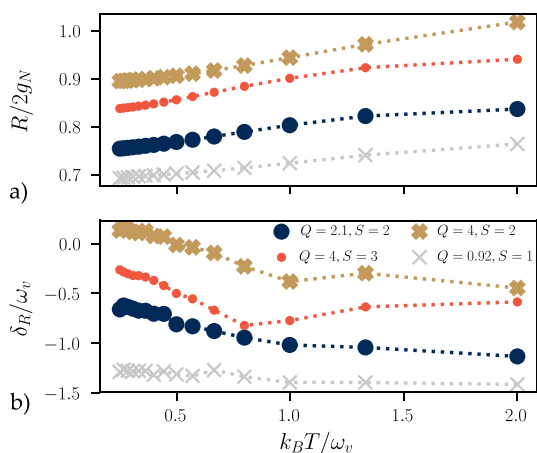


FIG. 5. (a) Rabi splitting R and (b) the corresponding detuning δ_R as a function of the temperature. The values of Q and S are chosen so that the absorption profile's linewidth at $k_B T = \omega_v$ is approximately equal for the circles and the crosses ($9.7\omega_v$ and $6.2\omega_v$, respectively). The temperatures are chosen so that the spacing between inverse temperatures is constant and each point corresponds to a different number of Matsubara modes. Here, $g_N = 7\omega_v$, $\kappa_c = 2\omega_v$, $\bar{\kappa} = 0.01\omega_v$.

factor is very high, $Q \gg 1$, then $\omega = \omega_m$ becomes again the absorption maximum.

An interesting consequence of the renormalization of polariton frequencies is that the detuning δ_R between the bare cavity mode and the molecular exciton at which the Rabi splitting is determined changes. This change is plotted in Fig. 5(b) as a function of temperature. A part of the shift in the detuning by the vibrations is caused by the renormalization of the absorption frequency described in the previous paragraph. However, even if this renormalization is taken into account, the effect still remains due to the change in the molecular line shape. The frequency range of the change in detuning is of the order of one vibrational frequency.

B. Linewidths

Next, we consider the issue of polaritonic linewidth. A natural point of comparison is the coupled oscillator model from which one infers the rule that the polariton linewidth is the mean of cavity and molecular linewidth, although only at resonance $\omega_c = \omega_m$. However, when vibrations are present, it is unclear what should be chosen as the molecular linewidth. One option is the full width at half maximum (FWHM) of the molecular absorption spectrum. Another option would be to deduce the value using a Lorentzian fit. We choose the former method because of its simplicity. Likewise, we use FWHMs as polariton linewidths. To this end, we choose larger Rabi splittings so that the polariton peaks are clearly separated.

In Fig. 6(a), we compare the polariton linewidths in the cases where the molecular broadening is Lorentzian (orange) or mostly caused by vibrations (blue). We observe that the vibrations change the detuning δ_T at which the upper and lower polaritons are of equal width $\Gamma_+ = \Gamma_-$. Since at $\omega_c = \omega_m$ we have $\Gamma_+ > \Gamma_-$, as is well established, it is not surprising that $\delta_T > 0$. The same effect may be seen in the ratio of upper/lower polariton peak intensities in Fig. 6(b), although to a much lesser extent. Together with the change in the

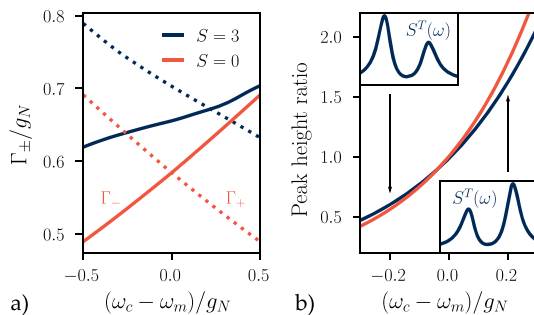


FIG. 6. (a) Estimated polariton linewidths Γ_{\pm} [the solid (dashed) line represents the lower (upper) polariton] and (b) the ratio of peak intensities of the upper and lower polariton as a function of detuning. The insets show the polaritonic spectrum $S^T(\omega)$ corresponding to negative and positive detuning. Here, we have chosen the effective molecular linewidth (FWHM of absorption) as the dissipation rate κ_m in the coupled oscillator model $S = 0$ (in orange). The parameters are $Q = 4$, $g_N = 10\omega_v$, $\kappa_c = 0.2g_N$, $\omega_v/k_B T = 1$, $\bar{\kappa} = 0.06\omega_v$.

detuning δ_R , it appears that the ratio is below unity, i.e., the lower polariton peak is of higher intensity than the upper polariton at the detuning at which the Rabi splitting is determined. This is in line with the previous experimental and theoretical analysis.^{10,19,32–43}

We also find that the polariton linewidths Γ_{\pm} under vibrational dissipation are in general larger than those of the coupled oscillator model. In our model, this is a consequence of the absorption function A whose real part is even more tail-heavy than Lorentzian distributions.

C. Limits of vibrational dissipation: Overdamping and high quality vibrations

So far, we have only considered the case in which the vibrations are underdamped and there exists a well defined vibrational frequency. For completeness, we briefly comment the changes of the polaritonic spectrum induced by the overdamped vibrations.

The effect of overdamping is that the absorption function becomes extremely tail-heavy as all the possible vibrational transitions are fully smeared by the dissipation. Consequently, the emission-absorption asymmetry causes a very notable asymmetry to the absorption, which is visible in the orange dashed line of Fig. 7. Compared to the blue curve that is closer to a Lorentzian profile, the renormalization of the Rabi splitting becomes very large. This is similar to what is observed in Fig. 5 for low Q values. The change in the polariton line shape is also notable but difficult to quantify.

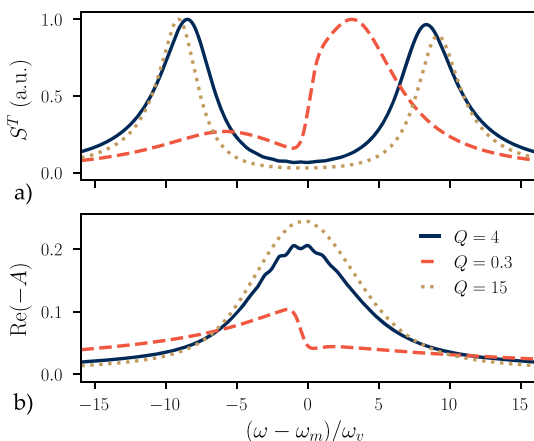


FIG. 7. Three examples of different line shapes that follow from the $P(E)$ theory to (a) the polariton spectrum and (b) absorption profile with the change of parameters. The blue line represents a Lorentzian-like case in which the vibrational dissipation dominates. The orange dashed line is in the overdamped limit, while the brown dotted line is in the opposite limit of high quality vibrations. The parameters are chosen so that FWHMs are the same for each case, approximately $9.1\omega_v$. The vibrational parameters are $S = \{4, 1, 0.51\}$, $\tilde{\kappa}_i/\omega_v = \{0.01, 0.01, 1.6\}$, $\omega_v/k_B T = \{1, 0.56, 1\}$ for $Q = \{4, 0.3, 15\}$, respectively. The polariton spectrum is calculated with $g_N = 9\omega_v$ and $\kappa_c/g_N \approx 0.11$ and the detuning $\omega_c = \omega_m$.

We have considered here mainly the cases in which the vibrational dissipation is in fact the main source of dissipation. However, it is possible that the vibrations are of very high quality, but there is a large dissipation rate of the electronic transition. In our model with only a single vibrational mode, this appears to be the only way, which leads to a Gaussian-like absorption profile. It is the opposite limit to the overdamped vibrations as the tails of absorption profile become less pronounced than in Lorentzian profiles. The effect on the results presented in Figs. 5 and 6 is that the values change, while the trends remain the same. These changes may be inferred by comparing the brown dotted line in Fig. 7 to the blue line that represents a Lorentzian-like case: The Rabi splitting is larger, while the polariton linewidths are smaller than those in the corresponding Lorentzian case.

V. CONCLUSIONS

In summary, we have presented an analytical model on the effect of Brownian vibrational dissipation to the polariton spectrum in a cavity measurement. Even though our approach is mathematically involved, it can provide richer physics than the coupled oscillator model. For most organic molecules, it should work as a much better approximation. The associated cost is that there are a few parameters more regarding vibrations whose determination from experimental data requires more work. However, our work provides some general checks to which the experimental data may be compared, such as the different detunings, which give the Rabi splitting, equal polariton linewidths, and equal peak intensities.

ACKNOWLEDGMENTS

K.S.U.K. acknowledges the financial support of the Magnus Ehrnrooth foundation. This work was supported by the Academy of Finland projects HYNEQ (Grant No. 317118) and Manipu-Light (Grant No. 323995). We thank Gerrit Groenhof for useful discussions.

APPENDIX: FOURIER TRANSFORM OF $\exp[\tilde{J}(t)]$

Formally, all the Fourier transforms in this work are of the form

$$\frac{1}{2\pi} \int dt e^{iEt} \exp[(a + ib \operatorname{sgn} t)(e^{i\omega_0 t - \Gamma|t|} - 1)], \quad (\text{A1})$$

where $a, b, \omega_0, \Gamma \in \mathbb{R}$ and $\Gamma > 0$. We use the convolution theorem to separate the Fourier transform into two parts before expanding the exponential into a Taylor series. Thus, we have

$$\begin{aligned} \frac{1}{2\pi} \int dt e^{iEt} e^{-a - ib \operatorname{sgn} t} &= e^{-a} \sum_{n=0}^{\infty} \frac{(-ib)^n}{n!} \frac{1}{2\pi} \int dt (\operatorname{sgn} t)^n e^{iEt} \\ &= e^{-a} \left[\delta(E) \cos b + \frac{\sin b}{\pi E} \right], \end{aligned} \quad (\text{A2})$$

which holds true when treated as the Cauchy principal value integral. At this point, we can recognize that formally $\delta(E) = f_L(E; 0, 0)$ and $1/(\pi E) = g_L(E; 0, 0)$. The second part of the transform is

$$\begin{aligned} & \frac{1}{2\pi} \int dt e^{iEt} \exp[(a + ib \operatorname{sgn} t) e^{i\omega_0 t - \Gamma|t|}] \\ &= \sum_{n=0}^{\infty} \frac{1}{n!} \sum_{k=0}^n \binom{n}{k} I_k^n, \end{aligned} \quad (\text{A3})$$

where, with the help of the binomial theorem,

$$I_k^n = \frac{a^{n-k}}{2\pi} \int dt (ib \operatorname{sgn} t)^k \exp[i(E + n\omega_0)t - n\Gamma|t|]. \quad (\text{A4})$$

Again, the expressions with even k differ from those of odd k . By direct evaluation, one can confirm that

$$\begin{aligned} & \frac{1}{2\pi} \int dt (\operatorname{sgn} t)^k \exp[i(E + n\omega_0)t - n\Gamma|t|] \\ &= \begin{cases} f_L(E; -n\omega_0, n\Gamma), & k \text{ even} \\ ig_L(E; -n\omega_0, n\Gamma), & k \text{ odd.} \end{cases} \end{aligned} \quad (\text{A5})$$

This result in conjunction with the convolution theorem leads directly to the convolution rules of f_L and g_L in Eq. (14). Furthermore, it can be used in I_k^n , which allows us to write expression (A3) as

$$\sum_{n=0}^{\infty} \frac{1}{n!} \left(f_L \sum_{k \text{ even}}^n + g_L \sum_{k \text{ odd}}^n \right) \binom{n}{k} a^{n-k} (ib)^k. \quad (\text{A6})$$

We omit the arguments of f_L and g_L for brevity. The even and odd binomial sums may be simplified by the relation

$$\frac{1}{2} [(a + ib)^n \pm (a - ib)^n] = \sum_{\substack{k \text{ even} \\ k \text{ odd}}}^n \binom{n}{k} a^{n-k} (ib)^k, \quad (\text{A7})$$

which follows from the binomial theorem. We denote now $z = a + ib = |z|e^{i\theta}$, which simplifies expression (A6) to

$$\sum_{n=0}^{\infty} \frac{|z|^n}{n!} [\cos(n\theta)f_L + \sin(n\theta)g_L]. \quad (\text{A8})$$

The last step of convolving the results together is then straightforward with the convolution rules and by using the sum rules of trigonometric functions. Thus, the Fourier transform (A1) is

$$\begin{aligned} e^{-a} \sum_{n=0}^{\infty} \frac{|z|^n}{n!} [\cos(b - n\theta)f_L(E; -n\omega_0, n\Gamma) \\ + \sin(b - n\theta)g_L(E; -n\omega_0, n\Gamma)]. \end{aligned} \quad (\text{A9})$$

We find Eqs. (17) and (21) of the main text by applying this result to \tilde{J}_{\pm} and \tilde{J}_k .

DATA AVAILABILITY

The data that support the findings of this study are available from the corresponding author upon reasonable request.

REFERENCES

- G. Groenhof and J. J. Toppari, "Coherent light harvesting through strong coupling to confined light," *J. Phys. Chem. Lett.* **9**, 4848–4851 (2018).
- D. M. Coles, N. Somaschi, P. Michetti, C. Clark, P. G. Lagoudakis, P. G. Savvidis, and D. G. Lidzey, "Polariton-mediated energy transfer between organic dyes in a strongly coupled optical microcavity," *Nat. Mater.* **13**, 712–719 (2014).
- X. Zhong, T. Chervy, S. Wang, J. George, A. Thomas, J. A. Hutchison, E. Devaux, C. Genet, and T. W. Ebbesen, "Non-radiative energy transfer mediated by hybrid light-matter states," *Angew. Chem., Int. Ed.* **55**, 6202–6206 (2016).
- X. Zhong, T. Chervy, L. Zhang, A. Thomas, J. George, C. Genet, J. A. Hutchison, and T. W. Ebbesen, "Energy transfer between spatially separated entangled molecules," *Angew. Chem., Int. Ed.* **56**, 9034–9038 (2017).
- K. Akulov, D. Bochman, A. Golombek, and T. Schwartz, "Long-distance resonant energy transfer mediated by hybrid plasmonic–photonic modes," *J. Phys. Chem. C* **122**, 15853–15860 (2018).
- J. A. Hutchison, T. Schwartz, C. Genet, E. Devaux, and T. W. Ebbesen, "Modifying chemical landscapes by coupling to vacuum fields," *Angew. Chem., Int. Ed.* **51**, 1592–1596 (2012).
- B. Munkhbat, M. Wersäll, D. G. Baranov, T. J. Antosiewicz, and T. Shegai, "Suppression of photo-oxidation of organic chromophores by strong coupling to plasmonic nanoantennas," *Sci. Adv.* **4**, eaas9552 (2018).
- R. F. Ribeiro, L. A. Martínez-Martínez, M. Du, J. Campos-Gonzalez-Angulo, and J. Yuen-Zhou, "Polariton chemistry: Controlling molecular dynamics with optical cavities," *Chem. Sci.* **9**, 6325–6339 (2018).
- J. Feist, J. Galego, and F. J. Garcia-Vidal, "Polaritonic chemistry with organic molecules," *ACS Photonics* **5**, 205–216 (2017).
- K. S. U. Kansanen, A. Asikainen, J. J. Toppari, G. Groenhof, and T. T. Heikkilä, "Theory for the stationary polariton response in the presence of vibrations," *Phys. Rev. B* **100**, 245426 (2019).
- K. Huang and A. Rhyss, "Theory of light absorption and non-radiative transitions in F-centres," *Proc. R. Soc. London, Ser. A* **204**, 406–423 (1950).
- G. D. Mahan, *Many-Particle Physics* (Springer Science & Business Media, 2013).
- D. F. Walls and G. J. Milburn, *Quantum Optics* (Springer Science & Business Media, 2007).
- E. T. Jaynes and F. W. Cummings, "Comparison of quantum and semiclassical radiation theories with application to the beam maser," *Proc. IEEE* **51**, 89–109 (1963).
- P. Törmä and W. L. Barnes, "Strong coupling between surface plasmon polaritons and emitters: A review," *Rep. Prog. Phys.* **78**, 013901 (2014).
- M. S. Skolnick, T. A. Fisher, and D. M. Whittaker, "Strong coupling phenomena in quantum microcavity structures," *Semicond. Sci. Technol.* **13**, 645 (1998).
- F. Herrera and F. C. Spano, "Cavity-controlled chemistry in molecular ensembles," *Phys. Rev. Lett.* **116**, 238301 (2016).
- C. W. Gardiner and M. J. Collett, "Input and output in damped quantum systems: Quantum stochastic differential equations and the master equation," *Phys. Rev. A* **31**, 3761 (1985).
- M. Reitz, C. Sommer, and C. Genes, "Langevin approach to quantum optics with molecules," *Phys. Rev. Lett.* **122**, 203602 (2019).
- M. Reitz, C. Sommer, B. Gurlek, V. Sandoghdar, D. Martin-Cano, and C. Genes, "Molecule-photon interactions in phononic environments," *Phys. Rev. Res.* **2**, 033270 (2020).
- C. Clear, R. C. Schofield, K. D. Major, J. Iles-Smith, A. S. Clark, and D. P. S. McCutcheon, "Phonon-induced optical dephasing in single organic molecules," *Phys. Rev. Lett.* **124**, 153602 (2020).
- T. T. Heikkilä, *The Physics of Nanoelectronics: Transport and Fluctuation Phenomena at Low Temperatures* (Oxford University Press, 2013).
- G.-L. Ingold and Y. V. Nazarov, "Charge tunneling rates in ultrasmall junctions," in *Single Charge Tunneling* (Springer, 1992), pp. 21–107.
- H.-P. Breuer and F. Petruccione, *The Theory of Open Quantum Systems* (Oxford University Press, 2002).

- ²⁵ A. O. Caldeira and A. J. Leggett, "Influence of dissipation on quantum tunneling in macroscopic systems," *Phys. Rev. Lett.* **46**, 211–214 (1981).
- ²⁶ V. Giovannetti and D. Vitali, "Phase-noise measurement in a cavity with a movable mirror undergoing quantum Brownian motion," *Phys. Rev. A* **63**, 023812 (2001).
- ²⁷ Defined as $\Gamma(z; a, b) = \int_a^b du u^{z-1} e^{-u}$.
- ²⁸ A. J. Leggett, S. Chakravarty, A. T. Dorsey, M. P. A. Fisher, A. Garg, and W. Zwerger, "Dynamics of the dissipative two-state system," *Rev. Mod. Phys.* **59**, 1 (1987).
- ²⁹ Our numerical approach is based on Python and especially its packages NumPy³⁰ (for linear algebra) and SciPy³¹ (for peak finding and evaluation of the linewidths). The scripts to produce the figures are available at <https://gitlab.jyu.fi/jyucmt/polariton-response-jcp2020>.
- ³⁰ C. R. Harris, K. J. Millman, S. J. van der Walt, R. Gommers, P. Virtanen, D. Cournapeau, E. Wieser, J. Taylor, S. Berg, N. J. Smith *et al.*, "Array programming with NumPy," *Nature* **585**, 357–362 (2020).
- ³¹ P. Virtanen, R. Gommers, T. E. Oliphant, M. Haberland, T. Reddy, D. Cournapeau, E. Burovski, P. Peterson, W. Weckesser, J. Bright *et al.*, "SciPy 1.0: Fundamental algorithms for scientific computing in python," *Nat. Methods* **17**, 261–272 (2020).
- ³² T. Neuman and J. Aizpurua, "Origin of the asymmetric light emission from molecular exciton–polaritons," *Optica* **5**, 1247–1255 (2018).
- ³³ J. del Pino, F. A. Y. N. Schröder, A. W. Chin, J. Feist, and F. J. Garcia-Vidal, "Tensor network simulation of non-Markovian dynamics in organic polaritons," *Phys. Rev. Lett.* **121**, 227401 (2018).
- ³⁴ F. Herrera and F. C. Spano, "Theory of nanoscale organic cavities: The essential role of vibration–photon dressed states," *ACS Photonics* **5**, 65–79 (2018).
- ³⁵ F. Herrera and F. C. Spano, "Absorption and photoluminescence in organic cavity QED," *Phys. Rev. A* **95**, 053867 (2017).
- ³⁶ F. Herrera and F. C. Spano, "Dark vibronic polaritons and the spectroscopy of organic microcavities," *Phys. Rev. Lett.* **118**, 223601 (2017).
- ³⁷ M. A. Zeb, P. G. Kirton, and J. Keeling, "Exact states and spectra of vibrationally dressed polaritons," *ACS Photonics* **5**, 249–257 (2017).
- ³⁸ P. Michetti and G. C. La Rocca, "Simulation of J-aggregate microcavity photoluminescence," *Phys. Rev. B* **77**, 195301 (2008).
- ³⁹ J. Bellessa, C. Bonnard, J. C. Plenet, and J. Mugnier, "Strong coupling between surface plasmons and excitons in an organic semiconductor," *Phys. Rev. Lett.* **93**, 036404 (2004).
- ⁴⁰ J. Chovan, I. E. Perakis, S. Ceccarelli, and D. G. Lidzey, "Controlling the interactions between polaritons and molecular vibrations in strongly coupled organic semiconductor microcavities," *Phys. Rev. B* **78**, 045320 (2008).
- ⁴¹ T. K. Hakala, J. J. Toppari, A. Kuzyk, M. Pettersson, H. Tikkanen, H. Kunttu, and P. Törmä, "Vacuum Rabi splitting and strong-coupling dynamics for surface-plasmon polaritons and rhodamine 6G molecules," *Phys. Rev. Lett.* **103**, 053602 (2009).
- ⁴² S. V. Baieva, T. K. Hakala, and J. J. Toppari, "Strong coupling between surface plasmon polaritons and sulforhodamine 101 dye," *Nanoscale Res. Lett.* **7**, 191 (2012).
- ⁴³ S. Baieva, O. Hakamaa, G. Groenhof, T. T. Heikkilä, and J. J. Toppari, "Dynamics of strongly coupled modes between surface plasmon polaritons and photoactive molecules: The effect of the Stokes shift," *ACS Photonics* **4**, 28–37 (2017).

III

MAGNOMECHANICS IN SUSPENDED MAGNETIC BEAMS

by

K. S. U. Kansanen, A. Asikainen, J. J. Toppari, G. Groenhof, T. T. Heikkilä

Physical Review B **104**, 214416 (2021)


Reproduced with permission. Copyright 2021 American Physical Society.

Magnomechanics in suspended magnetic beams

Kalle S. U. Kansanen^{1,*}, Camillo Tassi¹, Harshad Mishra², Mika A. Sillanpää², and Tero T. Heikkilä¹

¹*Department of Physics and Nanoscience Center, University of Jyväskylä, P.O. Box 35 (YFL), FI-40014 University of Jyväskylä, Finland*

²*Department of Applied Physics, Aalto University, P.O. Box 15100, FI-00076 Aalto, Finland*

 (Received 2 July 2021; revised 8 October 2021; accepted 29 November 2021; published 13 December 2021)

Cavity optomechanical systems have become a popular playground for studies of controllable nonlinear interactions between light and motion. Owing to the large speed of light, realizing cavity optomechanics in the microwave frequency range requires cavities up to several mm in size, hence making it hard to embed several of them on the same chip. An alternative scheme with much smaller footprint is provided by magnomechanics, where the electromagnetic cavity is replaced by a magnet undergoing ferromagnetic resonance, and the optomechanical coupling originates from magnetic shape anisotropy. Here, we consider the magnomechanical interaction occurring in a suspended magnetic beam, a scheme in which both magnetic and mechanical modes physically overlap and can also be driven individually. We show that a sizable interaction can be produced if the beam has some initial static deformation, as is often the case due to unequal strains in the constituent materials. We also show how the magnetism affects the magnetomotive detection of the vibrations, and how the magnomechanics interaction can be used in microwave signal amplification. Finally, we discuss experimental progress towards realizing the scheme.

DOI: [10.1103/PhysRevB.104.214416](https://doi.org/10.1103/PhysRevB.104.214416)

I. INTRODUCTION

In cavity optomechanical devices, the radiation pressure force mediates an interaction between mechanical modes and photons [1]. This has led to several developments, both fundamental and applied: ground-state cooling [2,3] and entanglement [4,5] of mechanical modes, quantum information storage in the mechanical excitation and interface, e.g. between superconducting qubits and flying optical photons [6], sensitive measurements with precision limits given by quantum mechanics; classical signal processing with tunable nonlinearities [7–11].

Several implementations of cavity optomechanics have been considered: mirrors on cantilevers and beams [12,13]; membranes in cavities [14,15]; atomic clouds [16]; beams and plate capacitors in microwave resonators [2,7,8,11,17,18]; photonic crystals patterned into beams [3].

Recently, the coupling between magnons and phonons has been considered to obtain an interaction similar to that in cavity optomechanics, but with the role of photons now played by magnons [19–22]. The interaction between magnons and phonons is mediated by the combination of the magnetic shape anisotropy and the magnetoelastic effect which make the frequency of the magnon, i.e., the ferromagnetic resonance (FMR), dependent on the strain. One interesting feature is that the speed of spin waves is substantially lower than that of electromagnetic waves, which can offer a much denser integration of similar functionalities. Moreover, enhanced tunability and richer interaction suggest additional possibilities for devices for fundamental studies and applications.

We propose and theoretically describe a scheme for magnomechanics that is a direct analog of a basic microwave

optomechanical system where a suspended conducting beam is capacitively coupled to a microwave resonator. We consider a suspended ferromagnetic beam that is subjected to an external in-plane magnetic field. This generates the FMR or magnon mode which is affected by the vibrations of the beam. However, as shown below, a simple doubly clamped beam does not give rise to the desired magnomechanical coupling. Since the FMR frequency changes as much to upward as to downward displacements of the beam, the analog of the radiation pressure force vanishes. Such symmetry may be broken by a static deformation as in Fig. 1(a).

Following Fig. 1(a), we consider a ferromagnetic beam, magnetized as a single domain and having a rectangular cross section with width w and height h . We assume that the coordinate system may be oriented so that the beam displacement is in the x direction and the beam axis is in the z direction. The clamps fix the ends of the beam to be in the xy plane parallel to one another with distance L in the z direction. The external and static magnetic field \mathbf{H}_0 is assumed to lay in the yz plane. The external field \mathbf{H}_0 fixes the static magnetization \mathbf{M}_0 around which magnons are generated.

The setup with a doubly clamped beam allows for separate driving of mechanical and ferromagnetic resonance modes. The measurement scheme is conceptually similar to microwave optomechanics. The mechanical mode can be driven by driving a current I_d through the beam, assuming that the beam is conducting, which generates a Lorentz force f on the beam due to the external field \mathbf{H}_0 . Similarly, the magnon mode can be driven by a time-dependent magnetic field \mathbf{h} , for instance, generated by a microwave antenna. These schemes are commensurate with the typical reflection and transmittance measurements performed with vector network analyzers. Moreover, the separate control over mechanics and magnons opens a perspective to signal transduction.

*kalle.s.u.kansanen@jyu.fi

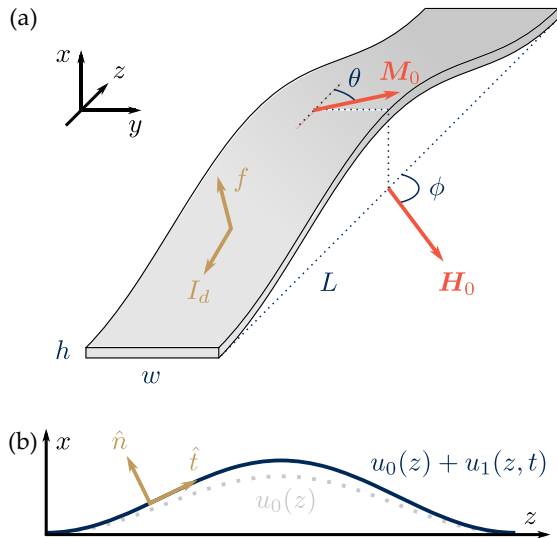


FIG. 1. Schematic drawings of a doubly clamped magnetic beam with a static deformation. (a) A three-dimensional perspective drawing of a static suspended beam with several useful definitions (see main text). (b) A simplified view of the deformation of the beam axis from the y direction. The gray dotted line represents the static deformation $u_0(z)$ and the blue solid line the total displacement $u = u_0 + u_1$ that includes the time-dependent vibrations u_1 . Here, \hat{t} and \hat{n} are tangent and normal vectors of the beam, corresponding to the local direction of the current I_d and the force f , respectively.

In contrast to recent experiments [19,22], this setup does not require a cavity to hybridize with the magnon mode, lessening the physical size of the magnomechanical system. Also, it does not require any magnetic field gradients as in a few recent theoretical works [20,21]; the fields \mathbf{H}_0 and \mathbf{h} are here considered to be homogeneous in space.

Magnomechanics is in many ways similar to optomechanics but there are several points of distinction. In the setup of Fig. 1, it is possible to modulate the optomechanical coupling by tuning either the strength or the direction of the external magnetic field \mathbf{H}_0 . This in turn changes the response of the system to driving. We also focus on a feature unique to magnetic systems: magnetic hysteresis and its effect on the magnomechanical coupling.

The layout of the paper is as follows. In Sec. II we derive the magnomechanical Hamiltonian for a statically deformed beam. In Sec. III we describe the driving of the mechanical and ferromagnetic resonances which is used in Sec. IV to describe possible experiments for the system. Section V discusses the first steps towards implementing a doubly clamped magnetic beam as a platform for magnomechanics.

II. MAGNOMECHANICAL HAMILTONIAN

To motivate the upcoming discussion, let us discuss the optomechanical Hamiltonian in detail. The simplest derivation of optomechanics follows from the assumption of a cavity, described by a bosonic mode \hat{c} , whose eigenfrequency ω_c depends on the position \hat{x}_b of some mechanical mode \hat{b}

(e.g., a mirror connected to a spring). The typical optomechanical Hamiltonian is then obtained by an expansion of the cavity frequency to first order in the position \hat{x}_b :

$$\begin{aligned} \hat{H}_{\text{optm}} &= \hbar\omega_m\hat{b}^\dagger\hat{b} + \hbar\omega_c(\hat{x}_b)\hat{c}^\dagger\hat{c} \\ &\simeq \hbar\omega_m\hat{b}^\dagger\hat{b} + \hbar\omega_c\hat{c}^\dagger\hat{c} + \hbar g_0\hat{c}^\dagger\hat{c}(\hat{b}^\dagger + \hat{b}), \end{aligned} \quad (1)$$

where ω_m is the eigenfrequency of the mechanical mode. The constant g_0 is called the optomechanical coupling and the corresponding term describes the radiation pressure force.

A similar mechanism can be found in ferromagnetic systems. Then, the cavity is replaced by a ferromagnetic resonance (FMR) and \hat{c} corresponds to a magnon mode. There are at least two distinct physical mechanisms that allow the FMR frequency to depend on a mechanical mode: On one hand, it is well known that the shape of the ferromagnet affects its FMR frequency [23]. On the other hand, the magnetoelasticity directly changes the ferromagnetic dynamics, providing an extraneous anisotropy field [24]. Therefore, the relevant mechanical mode \hat{b} is the vibration of the ferromagnet itself.

In this section, we start by describing the mechanical and ferromagnetic dynamics of a deformed beam from which we derive the magnomechanical coupling that corresponds to g_0 in Eq. (1).

A. Mechanical dynamics

We describe the deformations of the beam in Fig. 1 within the Euler-Bernoulli beam theory that is typically used to describe beam dynamics, even in the nanometer scale [25]. In order to describe the large static deformation [$h < \max u_0(z)$ in Fig. 1(b)] and vibrations around it, we include in the Euler-Bernoulli equation nonlinear terms that are typically neglected [26,27]. We assume that the beam material is homogeneous and isotropic. Then, vibrations in different directions do not generally couple, and the following analysis can be done separately for vibrations in the x and y directions. However, it turns out that the static deformation is needed for a finite magnomechanical coupling. In the following, we thus neglect the beam dynamics in the y direction. We also neglect shear modes, that is, modes where the displacement in the x direction depends on y , assuming that the width w is appreciably smaller than the length L . These assumptions are consistent with the actuation scheme of Lorentz force in Fig. 1. Without any external force, the beam displacement $u(z, t)$ in the x direction obeys the equation [27,28]

$$\rho A \frac{\partial^2 u}{\partial t^2} + EI_x \frac{\partial^4 u}{\partial z^4} = \left[T_0 + \frac{EA}{2L} \int_0^L dz \left(\frac{\partial u}{\partial z} \right)^2 \right] \frac{\partial^2 u}{\partial z^2}, \quad (2)$$

where T_0 is the initial tension, ρ is the mass density, E the Young modulus, $A = wh$ the area of the beam with a rectangular cross section, and $I_x = wh^3/12$ the corresponding bending modulus. Here, the terms on the right provide the nonlinear corrections related to tension whereas the usual Euler-Bernoulli kinetic and stress terms are on the left.

In order to describe the initially buckled beam and the flexural vibrations around it, we choose an approach similar to Ref. [28] and discuss it briefly here. Further details can be found in Appendix A.

A static deformation of the beam can be caused by a compressive stress that is, for instance, due to an external force on the clamping mechanism or due to the fabrication method of the beam. Here, we assume that this compression may be described by a negative tension $T_0 < 0$ in Eq. (2). We then divide the total mechanical deformation u into a static and dynamical part (u_0 and u_1 , respectively) as in Fig. 1(b) and assume that the dynamical deformation is small, that is,

$$u(z, t) = u_0(z) + u_1(z, t), \quad u_1 \ll u_0. \quad (3)$$

This allows for an expansion of the nonlinear Euler-Bernoulli equation (2) in the powers of u_1 . Together with the boundary conditions of a doubly clamped beam for both the static and dynamic deformations (∂_z denotes z derivative)

$$u_{0/1}(0) = u_{0/1}(L) = \partial_z u_{0/1}(0) = \partial_z u_{0/1}(L) = 0, \quad (4)$$

the mechanical system is now fully described.

The static deformation u_0 is solved from the zeroth-order equation in u_1 . We find a particularly simple expression

$$u_0(z) = u_m \frac{1 - \cos(2\pi z/L)}{2}, \quad (5)$$

where the parameter u_m gives the displacement at the midpoint of the beam as $u_0(L/2) = u_m$. This is also the point of the largest displacement. There is a one-to-one correspondence between u_m and the negative tension T_0 , which is why they can be used interchangeably.

From the first-order equation for the dynamic deformation u_1 , neglecting the terms that are of second order in u_1 , we can then find the flexural eigenmodes χ_n and the corresponding eigenfrequencies ω_n . These do not admit to simple expressions but a numerical solution is readily available [29]. We find that the dimensionless eigenfrequencies $\tilde{\omega}_n = \frac{L^2}{h} \sqrt{\frac{12\rho}{E}} \omega_n$ are determined by the ratio of the largest static deformation to the height of the beam u_m/h . Especially, the eigenfrequencies of symmetric eigenmodes ($n = 1, 3, \dots$) increase with u_m/h while the eigenfrequencies of antisymmetric modes ($n = 2, 4, \dots$) are constant (see Fig. 7 in Appendix A).

With the assumption of small dynamical deformation, the general solution can be expressed as a superposition

$$u_1(z, t) = \sum_n x_n(t) \chi_n(z) \quad (6)$$

with the dynamical amplitudes x_n and eigenmodes χ_n normalized as $\int_0^L \chi_n \chi_m dz = L \delta_{ij}$. This in turn gives the mechanical energy

$$H_{mc} = \sum_n \left[\frac{p_n^2}{2m} + \frac{1}{2} \omega_n^2 x_n^2 \right], \quad (7)$$

where the mass is given by $m = \rho LA$ and the momentum by $p_n = m \dot{x}_n$. Then, we can quantize the harmonic oscillators as usual:

$$\hat{x}_n = x_n^{\text{ZPM}} (\hat{b}_n^\dagger + \hat{b}_n), \quad (8a)$$

$$\hat{b}_n^\dagger = (x_n^{\text{ZPM}})^{-1} \left(\hat{x}_n - \frac{i}{m\omega_n} \hat{p}_n \right), \quad (8b)$$

where $x_n^{\text{ZPM}} = \sqrt{\frac{\hbar}{2m\omega_n}}$ is the zero-point motion amplitude and $\hat{b}_n^\dagger, \hat{b}_n$ are boson operators for each mode n .

B. Ferromagnetic resonance

We describe the magnetization \mathbf{M} and the magnon mode of the beam in Fig. 1 assuming that it is magnetized as a single domain, similar to the Stoner-Wohlfarth model [30]. The magnetization is driven by an effective field \mathbf{H}_{eff} that takes into account the external magnetic field \mathbf{H} , the demagnetizing field \mathbf{H}_{dm} , the magnetoelastic field \mathbf{H}_{me} , and intrinsic anisotropy field \mathbf{H}_{an} [31]. We consider the magnetization almost uniform, adiabatically following the beam geometry, and that the magnet is in the Landau-Lifshitz-Gilbert regime where $|\mathbf{M}| = M_S$ with M_S being the saturation magnetization. For the external magnetic field \mathbf{H} , we consider a strong static component \mathbf{H}_0 and a perturbation \mathbf{h} oscillating at a frequency close to the ferromagnetic resonance (FMR) frequency ω_K , although the latter plays a role only in the following section. Equivalently, the magnetization dynamics can be obtained from the magnetic free-energy density within the beam

$$\mathcal{F} = -\mu_0 \mathbf{H} \cdot \mathbf{M} + \mathcal{F}_{\text{dm}} + \mathcal{F}_{\text{me}} + \mathcal{F}_{\text{an}}, \quad (9a)$$

$$\mu_0 \mathbf{H}_{\text{eff}} = -\frac{\delta}{\delta \mathbf{M}} \int dx^3 \mathcal{F}[\mathbf{M}]. \quad (9b)$$

To obtain the total magnetic energy, the free-energy density \mathcal{F} must be integrated over the beam. Next, we describe the terms in the free-energy density in detail for the deformed beam. We first discuss the results arising from the assumption that there are no vibrations in y direction (meaning that the displacement u is only in x direction and it is a function of z). Then, we return to assess this assumption.

We calculate the demagnetizing field \mathbf{H}_{dm} in the thin plate limit $h \ll w \lesssim L$, which allows us to neglect the size-dependent terms in the demagnetizing field. It is obtained by requiring the continuity of the H -field components parallel to the beam, that is, H_y and the tangent field $H_t = [H_x \partial_z u(z) + H_z] / \sqrt{1 + (\partial_z u(z))^2}$, and the continuity of the B -field component normal to the beam, that is $B_n = [-B_x + B_z \partial_z u(z)] / \sqrt{1 + [\partial_z u(z)]^2}$ (see Fig. 1), where $\mathbf{B} = \mu_0 \mathbf{H}^{\text{out}}$ outside the beam and $\mathbf{B} = \mu_0 (\mathbf{H}^{\text{in}} + \mathbf{M})$ inside. The demagnetizing field \mathbf{H}_{dm} is within the beam and, thus, we set $\mathbf{H}^{\text{out}} = \mathbf{H}$ and $\mathbf{H}^{\text{in}} = \mathbf{H} + \mathbf{H}_{\text{dm}}$. Then, up to the second order in $\partial_z u$, we find its components

$$H_x^{\text{dm}} = -M_x [1 - (\partial_z u(z))^2] + M_z \partial_z u(z), \quad (10a)$$

$$H_y^{\text{dm}} = 0, \quad (10b)$$

$$H_z^{\text{dm}} = M_x \partial_z u(z) - M_z (\partial_z u(z))^2 \quad (10c)$$

from the continuity conditions. The corresponding free-energy density is given by

$$\frac{\mathcal{F}_{\text{dm}}}{\mu_0} = \frac{M_x^2}{2} - M_x M_z \partial_z u(z) + \frac{1}{2} (M_z^2 - M_x^2) (\partial_z u(z))^2. \quad (11)$$

It describes a hard axis parallel to \hat{n} , the (position-dependent) surface normal to the beam. Since we have to integrate the free-energy density due to the demagnetizing field over the beam volume, the component proportional to $\partial_z u(z)$ disappears in the case of a doubly clamped beam due to the boundary conditions $u(0) = u(L) = 0$ [32]. Moreover, for a small deformation the averaged surface normal aligns with the x direction, which is why the x axis is a hard axis for a uniform

magnetization. This means that for an in-plane magnetic field considered below, the magnetization also lies in the yz plane. On the other hand, deformations provide a position-dependent correction to this hard axis. These corrections are sensitive to vibrations and thus provide one contribution to the magnomechanical coupling.

In general, the magnetoelastic free-energy density is given by [24,33]

$$\mathcal{F}_{\text{me}} = \frac{B_1}{M_S^2} (M_x^2 \epsilon_{xx} + M_y^2 \epsilon_{yy} + M_z^2 \epsilon_{zz}) + \frac{2B_2}{M_S^2} (M_x M_y \epsilon_{xy} + M_x M_z \epsilon_{xz} + M_y M_z \epsilon_{yz}), \quad (12)$$

where B_1 and B_2 are the magnetoelastic coupling constants, and the strains ϵ_{ij} are given in the nonlinear Euler-Bernoulli theory by [26,34]

$$\epsilon_{ij} = \frac{1}{2} \left(\frac{\partial u_i}{\partial x_j} + \frac{\partial u_j}{\partial x_i} + \sum_k \frac{\partial u_k}{\partial x_i} \frac{\partial u_k}{\partial x_j} \right). \quad (13)$$

Here, u_i are the components of the general displacement vector at a given point. The last term in ϵ_{ij} is neglected in the linear elasticity theory but is here of importance.

Let us then consider, for convenience, the average of \mathcal{F}_{me} over the beam volume and denote it by $\bar{\mathcal{F}}_{\text{me}}$. Since $u_x \equiv u$ and $u_y = u_z = 0$, only the derivatives $\partial_z u$ and $\partial_y u$ are finite. Moreover, setting $\partial_y u = 0$ for now, only ϵ_{zz} and ϵ_{xz} are finite. However, in the process of averaging over the beam volume, we encounter the same situation as in the demagnetizing energy: first-order terms $\partial_z u$ average out due to boundary conditions. Thus, we find

$$\bar{\mathcal{F}}_{\text{me}} = \int \frac{dx^3}{LA} \mathcal{F}_{\text{me}} = \frac{B_1}{M_S^2} M_z^2 \bar{\epsilon}_{zz} \quad (14)$$

with the definition of averaged strain

$$\bar{\epsilon}_{zz} = \frac{1}{L} \int dz \epsilon_{zz} = \frac{1}{2L} \int dz (\partial_z u)^2. \quad (15)$$

Note that the total demagnetizing energy is also proportional to $\bar{\epsilon}_{zz}$ due to the last term in Eq. (11). Moreover, by using the expansion (3) of the displacement u into a static deformation and dynamical vibrations, the average strain can be expanded to first order by $\bar{\epsilon}_{zz} \simeq \bar{\epsilon}_{zz}^{(0)} + \bar{\epsilon}_{zz}^{(1)}$ with

$$\bar{\epsilon}_{zz}^{(0)} = \frac{1}{2L} \int_0^L dz (\partial_z u_0)^2, \quad (16a)$$

$$\bar{\epsilon}_{zz}^{(1)} = \frac{1}{L} \int_0^L dz (\partial_z u_0)(\partial_z u_1). \quad (16b)$$

Using the solution of the static deformation in Eq. (5), we obtain $\bar{\epsilon}_{zz}^{(0)} = \frac{\pi^2}{4} (u_m/L)^2$. Here, we expect that $u_m \ll L$, meaning that $\bar{\epsilon}_{zz}^{(0)} \ll 1$.

Finally, we assume that the magnetoelastic and demagnetizing fields dominate over the intrinsic (crystal) anisotropies, that is, the total free energy of the intrinsic anisotropies is small compared to the described free energies and may be neglected. At least, such an assumption is valid in the case of a polycrystalline magnet. This assumption may be lifted straightforwardly in favor of a specific crystal anisotropy

model; however, difficulties may arise when trying to take into account the possible direct effect of elasticity on the intrinsic anisotropies.

The average magnetic free-energy density, with the assumption of the displacements only in the x direction, is

$$\bar{\mathcal{F}} = -\mu_0 \mathbf{H} \cdot \mathbf{M} + \frac{B_1}{M_S^2} M_z^2 \bar{\epsilon}_{zz} + \mu_0 M_x^2 / 2 + \mu_0 (M_z^2 - M_x^2) \bar{\epsilon}_{zz}. \quad (17)$$

The addition of beam vibrations in the y direction only provides an additional term to $\bar{\epsilon}_{zz}$ that is proportional to $(\partial_z u_y)^2$. However, such term does not provide the correct form of optomechanical coupling as in Eq. (1): it is second order in the position operator. In contrast, the contribution of vibrations in the x direction around the static deformation u_0 is linear in position because of the expansion in Eq. (16) and $\bar{\epsilon}_{zz}^{(1)}$. Finally, we note that if $\partial_y u \neq 0$, both ϵ_{yz} and ϵ_{yy} are also finite. Without a static deformation in the y direction, $\bar{\epsilon}_{yy}$ does not provide magnomechanical coupling but $\bar{\epsilon}_{yz}$ will via the nonlinear term $(\partial_y u)(\partial_z u_0)$. Similar terms would appear from the demagnetizing field. Typically, such shear terms are neglected in optomechanics: this is justified if the beam width is much smaller than its length, or that only modes without shear are actuated. We follow the same assumption in this work.

We treat both cases of the metallic and insulator ferromagnets (e.g., a two-layer beam with a ferromagnetic insulating layer and a metal layer). To do so, we can observe that the current induced by a static field \mathbf{H}_0 and the flexural dynamics gives rise to a negligible screening effect for a thin film. Furthermore, the wavelength of the driving field \mathbf{h} , corresponding to a frequency close to the ferromagnetic resonance $c/\omega \sim 10^{-1}$ m, is much larger than the characteristic dimension of the typical micrometer-scale beam and, since we do not make particular assumptions on \mathbf{h} , we can write the quasistatic approximation

$$\nabla \times \mathbf{H}_0 \sim 0 \sim \nabla \times \mathbf{h}, \quad (18)$$

provided that we consider the screened \mathbf{h} in the conducting case.

Next, we derive the quantum mechanical Hamiltonian for the magnon mode assuming a static deformation of the beam. We express the magnetization as $\mathbf{M} = \mathbf{M}_0 + \mathbf{m}$, where \mathbf{M}_0 provides the direction of the static magnetization in the presence of a static external magnetic field \mathbf{H}_0 and \mathbf{m} is the deviation to be quantized. By using the assumptions of a single domain magnet and the external field in the yz plane, we have the situation depicted in Fig. 1:

$$\mathbf{H}_0 = H_0 (\cos \phi \hat{z} + \sin \phi \hat{y}), \quad \mathbf{M}_0 = M_S (\cos \theta \hat{z} + \sin \theta \hat{y}). \quad (19)$$

That is, the magnetization \mathbf{M}_0 is also in the yz plane, meaning that the static deformation of the beam does not remove the hard axis in the x direction. The magnetization angle θ depends on the direction and size of the field \mathbf{H}_0 . This dependence results from the competition between the external, the magnetoelastic, and the demagnetizing fields, as the angle θ is determined by the free-energy minimum from Eq. (17). Aside from the global free-energy minimum, there can exist a local

minimum corresponding to a metastable magnetization configuration. This describes magnetic hysteresis. Furthermore, the ferromagnetic resonance frequency depends on the effective field and, then, on $\bar{\epsilon}_{zz}$, giving rise to an optomechanicslike coupling. The magnetic anisotropy related with the strain also provides a coercive field which in the case of a magnetic field perpendicular to the beam is $H_c = 2|B_1|/(\mu_0 M_S^2) + 1|\bar{\epsilon}_{zz}^{(0)}| M_S$. For further details, see Appendix B 1.

We assume a Kittel-type magnon mode \mathbf{m} that is spatially uniform in the ferromagnetic beam and neglect the dynamics of finite momentum magnons. This follows from the magnon driving setup: we assume that the magnetic field \mathbf{h} is homogeneous in space and, thus, the spatially uniform mode is dominantly excited. In practice, however, the finite momentum magnons provide an effective thermal bath for the vibrations and the spatially uniform magnon mode. The spectrum of such a bath would then depend on the external magnetic field.

The quantum magnetization Hamiltonian can be obtained by substituting the Holstein-Primakoff relations in the total magnetic energy $H_{mg} = \int dx^3 \mathcal{F} = LA\bar{\mathcal{F}}$ (see Appendix B 2). Choosing the reference direction \hat{z}' along the static magnetization \mathbf{M}_0 ($\hat{z}' = \cos\theta\hat{z} + \sin\theta\hat{y}$), we can expand and get

$$M_{z'} = M_S - \frac{\hbar\gamma}{LA}\hat{m}^\dagger\hat{m}, \quad (20a)$$

$$M_{+'} = m_{ZPQ}\hat{m}, \quad M_{-'} = m_{ZPQ}\hat{m}^\dagger, \quad (20b)$$

where $m_{ZPQ} = \sqrt{\frac{2\hbar\gamma M_S}{LA}}$ and γ is the gyromagnetic ratio. The quantized magnetization components $M_{z'}$ and $M_{y'} = \frac{1}{2i}(M_{+'} - M_{-'})$ are related to those in the free-energy density $\bar{\mathcal{F}}$ in Eq. (17) by a rotation of the angle θ about the x axis which leaves the x component invariant, $M_x = M_{x'} = \frac{1}{2}(M_{+'} + M_{-'})$.

Without considering the driving terms \mathbf{h} and the coupling with the flexural dynamics $\epsilon_{zz}^{(0)}$, the magnetic Hamiltonian reads as, to the leading order in $1/M_S$,

$$\frac{\hat{H}_m}{\hbar} = \omega_1 \hat{m}^\dagger \hat{m} + \frac{\omega_2}{2} [\hat{m}^2 + (\hat{m}^\dagger)^2] + \omega_3 i \frac{\hat{m}^\dagger - \hat{m}}{\sqrt{2}}, \quad (21)$$

where

$$\omega_1 = \gamma\mu_0 \left[H_0 \cos(\phi - \theta) + \frac{M_S}{2} \right] - 3\bar{\epsilon}_{zz}^{(0)}\gamma\mu_0 M_S \cos^2\theta, \\ - \bar{\epsilon}_{zz}^{(0)} \frac{\gamma B_1}{M_S} (3\cos^2\theta - 1), \quad (22a)$$

$$\omega_2 = \gamma\mu_0 \frac{M_S}{2} - \bar{\epsilon}_{zz}^{(0)} \frac{\gamma B_1}{M_S} \sin^2\theta \\ - \bar{\epsilon}_{zz}^{(0)} \gamma\mu_0 M_S (\sin^2\theta + 1), \quad (22b)$$

$$\omega_3 = -\frac{\sqrt{2}\gamma M_S}{m_{ZPQ}} \left[\bar{\epsilon}_{zz}^{(0)} \left(\frac{B_1}{M_S} + \mu_0 M_S \right) \sin 2\theta \right. \\ \left. + \mu_0 H_0 \sin(\phi - \theta) \right]. \quad (22c)$$

The term proportional to $\hat{m}^\dagger \hat{m}$ is the sum of four components: one coming from the external magnetic field H_0 , the second and third from the hard axis, and the last from

the magnetoelastic coupling. On the other hand, ω_2 does not depend on the external magnetic field. This is a consequence of the assumption that \mathbf{H}_0 is parallel to the yz plane. Finally, the linear term ω_3 does not depend on the x -hard axis strength which is quadratic in M_x in Eq. (17).

\hat{H}_m is a highly tunable quadratic Hamiltonian which could be relevant in the continuous-variable quantum information processing [35]: the hard and easy axes produce a controlled squeezing. This leads to entanglement between the spins in the magnetic material [36]. Recently, it has been suggested that by tuning the frequency ω_1 close to ω_2 and coupling the magnon system to a microwave cavity, a magnon Schrödinger cat state (superposition of two coherent states) could be observed [37]. The fact that the magnon Hamiltonian is often not diagonal (i.e., $\hat{H}_m = \hbar\omega_K \hat{m}^\dagger \hat{m}$) should also have other signatures, e.g., in the shot noise of ferromagnet-conductor systems [38].

Let us diagonalize the Hamiltonian (21). For this task, it is useful to introduce dimensionless quadrature operators $\hat{x}_m = (\hat{m}^\dagger + \hat{m})/\sqrt{2}$ and $\hat{p}_m = i(\hat{m}^\dagger - \hat{m})/\sqrt{2}$ (the subscript indicates the corresponding bosonic mode). The Hamiltonian (21) may be expressed as

$$\frac{\hat{H}_m}{\hbar} = \frac{\omega_1 + \omega_2}{2} \hat{x}_m^2 + \frac{\omega_1 - \omega_2}{2} \hat{p}_m^2 + \omega_3 \hat{p}_m. \quad (23)$$

The diagonalization is achieved by first displacing \hat{p}_m and then scaling both \hat{x}_m and \hat{p}_m properly. That is, we define a new bosonic operator \hat{l} so that it has the quadrature operators $\hat{p}_l = \sqrt{c}(\hat{p}_m + d)$ and $\hat{x}_l = \hat{x}_m/\sqrt{c}$ where $c = \sqrt{(\omega_1 - \omega_2)/(\omega_1 + \omega_2)}$ and $d = \omega_3/(\omega_1 - \omega_2)$. In the validity range of the Euler-Bernoulli theory $\bar{\epsilon}_{zz}^{(0)} \ll 1$, we generally find that $c < 1$. Thus, we call c the squeezing factor. The variance of \hat{p}_l is smaller than the variance of \hat{p}_m by a factor of c ; the corresponding factor is $1/c > 1$ for the variances of \hat{x}_l and \hat{x}_m . The diagonalized Hamiltonian is then given by $\hat{H}_m = \hbar\omega_K \hat{l}^\dagger \hat{l}$ where the FMR frequency $\omega_K = \sqrt{\omega_1^2 - \omega_2^2}$ may be expressed as

$$\omega_K = \gamma\mu_0 [H_0 \cos(\theta - \phi) + \mathcal{M}_\epsilon \cos(2\theta)]^{\frac{1}{2}} \\ \times [H_0 \cos(\theta - \phi) + (1 - 2\bar{\epsilon}_{zz}^{(0)})M_S + \mathcal{M}_\epsilon \cos^2(\theta)]^{\frac{1}{2}}. \quad (24)$$

Here, $\mathcal{M}_\epsilon = -2\bar{\epsilon}_{zz}^{(0)}(\frac{B_1}{\mu_0 M_S^2} + 1)M_S = \pm H_c$ describes the anisotropy energy due to magnetoelastic and demagnetizing field terms. The sign of this term depends on the relative magnitude of the two effects in the typical situation with $B_1 < 0$. The corresponding bosonic transformation is given by

$$\hat{l} = \zeta_+ \hat{m} + \zeta_- \hat{m}^\dagger + i \frac{(\zeta_+ + \zeta_-)\omega_3}{\sqrt{2}\omega_K}, \quad (25a)$$

$$\zeta_\pm = \sqrt{\frac{1}{2} \left(\frac{\omega_1}{\omega_K} \pm 1 \right)}. \quad (25b)$$

Note that without strain, i.e., $\bar{\epsilon}_{zz}^{(0)} = 0$, we obtain $\omega_K = \gamma\mu_0 \sqrt{H_0(H_0 + M_S)}$ as expected while $c = \sqrt{H_0/(H_0 + M_S)}$ and $d = 0$. Therefore, the squeezing is inherent to the magnon system and produced by the out-of-plane hard axis while the displacement is due to the static deformation.

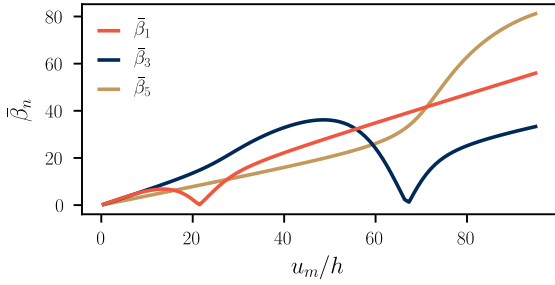


FIG. 2. The mechanical mode parameter $\bar{\beta}_n$ as a function of the static bending parameter u_m divided by the height h of the beam for the three first $n = \text{odd}$ modes.

C. Magnomechanical coupling

By introducing the flexural component of the strain $\bar{\epsilon}_{zz}^{(1)}$ via Eqs. (6) and (16) and replacing $\bar{\epsilon}_{zz}^{(0)}$ in Eq. (22) by the full $\bar{\epsilon}_{zz}$, we have both a magnomechanical and linear coupling.

The magnomechanical interaction Hamiltonian reads as

$$\begin{aligned} \hat{H}_{mm} = & \hbar \sum_n (g_n^{\text{me}} - g_n^{\text{dm}})(\hat{b}_n^\dagger + \hat{b}_n) \left[\hat{m}^\dagger \hat{m} (3 \cos^2 \theta - 1) \right. \\ & \left. + \frac{(\hat{m}^\dagger)^2 + \hat{m}^2}{2} \sin^2 \theta - \frac{M_S LA}{\hbar \gamma} \cos^2 \theta - \frac{\sin^2 \theta}{2} \right] \\ & - \hbar \sum_n g_n^{\text{dm}} (\hat{b}_n^\dagger + \hat{b}_n) \left[\hat{m}^\dagger \hat{m} + \frac{(\hat{m}^\dagger)^2 + \hat{m}^2}{2} + 1 \right], \end{aligned} \quad (26a)$$

$$g_n^{\text{me}} = -\bar{\beta}_n \frac{\hbar \chi_n^{\text{ZPM}}}{L^2} \frac{\gamma B_1}{M_S}, \quad (26b)$$

$$g_n^{\text{dm}} = \bar{\beta}_n \frac{\hbar \chi_n^{\text{ZPM}}}{L^2} \gamma \mu_0 M_S, \quad (26c)$$

$$\bar{\beta}_n = \frac{L}{\hbar} \int_0^L dz (\partial_z u_0)(\partial_z \chi_n), \quad (26d)$$

where g_n^{me} and g_n^{dm} refer to magnetoelastic and demagnetizing coupling, respectively. From the dimensionless mode parameters $\bar{\beta}_n$ we get a selection rule: only the modes with odd $n = 1, 3, \dots$ corresponding to even mode functions give rise to a coupling. In Fig. 2, we plot $\bar{\beta}_n$ for the three lowest even modes as a function of the static bending parameter u_m . We note that the change in the eigenmode shape χ_n is as a function of u_m so drastic that, at certain points, χ_n becomes orthogonal to the static deformation u_0 (for further details, see Appendix A). At these points, the magnomechanical coupling vanishes. Also, rather surprisingly, there is no clear hierarchy of the parameters $\bar{\beta}_n$ but rather, they depend strongly on the static deformation. It may hence be that a higher-frequency mode couples stronger to the magnetization dynamics.

There is also a linear coupling

$$\hat{H}_l = \hbar \sum_n g_n^{(l)} i \frac{\hat{m}^\dagger - \hat{m}}{\sqrt{2}} \frac{\hat{b}_n^\dagger + \hat{b}_n}{\sqrt{2}} \sin 2\theta, \quad (27a)$$

$$g_n^{(l)} = \bar{\beta}_n \frac{\hbar \chi_n^{\text{ZPQ}}}{\sqrt{12} L^2} \frac{M_S}{m_{\text{ZPQ}}} \gamma \mu_0 \mathcal{M}_\epsilon. \quad (27b)$$

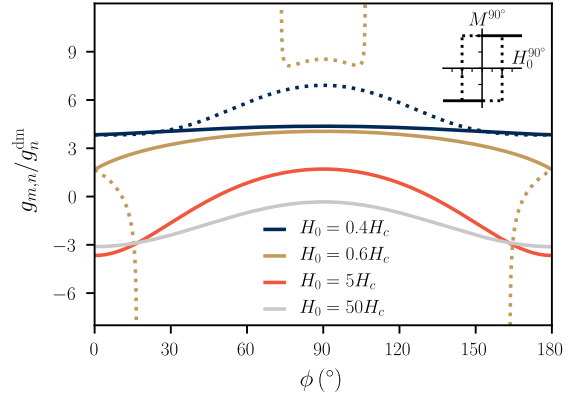


FIG. 3. Magnomechanical coupling constant $g_{m,n}$ as a function of the external field direction ϕ . The different curves represent different magnetic field strengths H_0 , characterized by the coercive field H_c at $\phi = 90^\circ$: the dotted lines correspond to the metastable magnetization configuration when $H_0 < H_c$. Note that this metastable state does not necessarily exist for all ϕ . Here, we set $u_m/L = 0.1$ and $B_1 = -0.6 \mu_0 M_S^2$ so that $50 H_c \approx M_S$. The inset shows the corresponding hysteresis curve for $\phi = 90^\circ$.

It also depends on the mechanical mode parameter $\bar{\beta}_n$ and is directly proportional to the coercive field $H_c = |\mathcal{M}_\epsilon|$ measured perpendicular to the beam. In this work, however, we concentrate on a situation in which the FMR and mechanical frequencies are strongly detuned and the linear coupling will therefore play no further role.

Note that the interaction terms in Eqs. (26) and (27) are written in the original nondiagonalized basis, and therefore are not yet the relevant ones for magnomechanical measurements. Using the transformation (25) allows us to write this in the diagonal basis. Neglecting doubly rotating terms, the result for the magnomechanical coupling Hamiltonian is $\hat{H}_{mm} = \hbar \sum_n g_{m,n} (\hat{b}_n^\dagger + \hat{b}_n) \hat{I}^\dagger \hat{I}$ with

$$g_{m,n} = 2(g_n^{\text{me}} - g_n^{\text{dm}}) \left(c \cos^2 \theta + \frac{1}{c} \cos 2\theta \right) - 2c g_n^{\text{dm}}. \quad (28)$$

The squeezing factor

$$c = \sqrt{\frac{H_0 \cos(\theta - \phi) + \mathcal{M}_\epsilon \cos(2\theta)}{H_0 \cos(\theta - \phi) + (1 - 2\bar{\epsilon}_{zz}^{(0)}) M_S + \mathcal{M}_\epsilon \cos^2(\theta)}}$$

depends on the direction of the magnetic field in a nontrivial way which is why the magnomechanical coupling depends not only on the direction of the field, but also its precise magnitude setting the direction of the magnetization. Moreover, the magnitude is different for the stable and metastable magnetizations for fields below the coercive field.

We illustrate the dependence of the magnomechanical coupling on the magnetic field direction in Fig. 3, assuming that the z axis is a hard axis ($|B_1| < \mu_0 M_S^2$). We observe that, in general, as the magnitude of the external field H_0 is increased, the magnomechanical coupling decreases. Focusing on the angle $\phi = 90^\circ$, the magnomechanical coupling changes sign as a function of the external magnetic field strength H_0 and approaches the value $g_{m,n} \rightarrow -2g_n^{\text{me}}$ as $M_S/H_0 \rightarrow 0$. Lastly, we

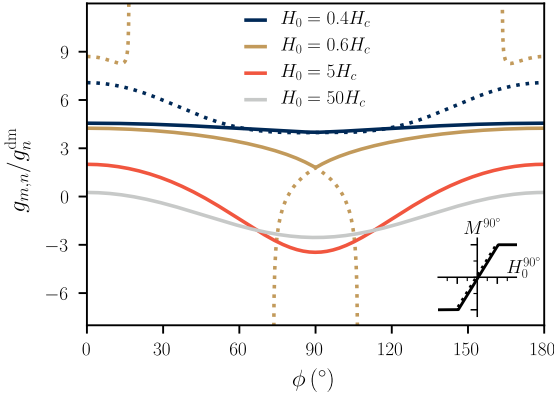


FIG. 4. Magnomechanical coupling constant $g_{m,n}$ as a function of the external field direction ϕ that is otherwise identical to Fig. 3 except we set $B_1 = -1.4\mu_0 M_S^2$. With this value, the coercive field at 90° remains the same but the z axis becomes an easy axis, changing both the hysteresis curve as well as the magnomechanical coupling.

find that $H_0 = H_c/2$ represents the point where the metastable magnetization ceases to exist for some values of ϕ . For external fields H_0 that are between $H_c/2$ and H_c , this shows up in the magnomechanical coupling as divergences; it should be noted, however, that the free-energy barrier is very small at these points.

An interesting consequence of our choices for the magnetization free energy is that there are always two values of B_1 that correspond to a given coercive field H_c . This changes the magnomechanical coupling constant as shown in Fig. 4. There, the magnetoelastic energy is negative ($B_1 < 0$) and dominates, that is, $|B_1| > \mu_0 M_S^2$. At the same time, the z axis becomes an easy axis. Thus, a hysteresis measurement separates these two situations with the same coercive field; see the insets of both Figs. 3 and 4 which describe the hysteresis curves obtained for an external magnetic field pointing perpendicular to the beam at $\phi = 90^\circ$.

Finally, we note that interesting physics remains even if the magnomechanical coupling vanishes, $g_{m,n} = 0$. In such a case, a second-order cross-Kerr-type term, i.e., a term quadratic in the deformation, may remain finite. The situation is analogous to the “membrane in the middle” optomechanics setup with a vibrating semitransparent mirror in the center of the cavity which is proposed as a way of measuring the phonon number in the mechanical mode [14]. In the doubly clamped magnetic beam, such terms are always present as discussed below Eq. (17). Interestingly, they can be finite without ($u_0 = 0$) and with the static deformation. The strength of the cross-Kerr terms may also depend on the external field H_0 . Especially in the beam with a static deformation, there are multiple values for H_0 and ϕ which give $g_{m,n} = 0$ as shown in Figs. 3 and 4. However, the analysis of the cross-Kerr terms is beyond the scope of this work.

III. DRIVING INDIVIDUAL RESONANCES

In order to experimentally see the magnomechanical coupling and its effects, it is necessary to consider the ways the

magnomechanical system may be driven. At the same time, dissipation to the environment is still to be taken into account. Here, we discuss some general features of the driving while showing an example of a possible scheme together with a model for its description using the input-output formalism [39]. For brevity, we focus only on reflection measurements.

The driving of the magnon mode \hat{m} is achieved by applying an alternating magnetic field \mathbf{h} that is perpendicular to the static field \mathbf{H}_0 . Here, it is convenient to choose \mathbf{h} in the direction of the displacement u , i.e., in the x direction. Then, \mathbf{h} is independent of the direction ϕ of the static field \mathbf{H}_0 . This produces an extra term in the Hamiltonian, proportional to $\mu_0 |\mathbf{h}| M_x$ or $|\mathbf{h}| (\hat{m} + \hat{m}^\dagger)$. The coupling rate of a similar drive is described and measured in Ref. [40]; importantly, it is directly proportional to the spatial overlap of the magnon mode and the driving field.

Within the input-output formalism, we do not include such driving to the closed-system Hamiltonian, but rather assume that there exists a bath of free electromagnetic modes to which the magnon mode \hat{m} is coupled. Integrating out these free modes gives rise to dissipation and the possibility of the bath exciting the system, either via thermal noise or an external drive. In the diagonalized frame, the squeezing factor c is introduced to the coupling between the bath and the magnon which modifies the dissipation rate.

Since the alternating magnetic field can be produced by an alternating current, we can readily associate the input and output fields of the magnon mode to ingoing and outgoing voltage signals on a transmission line. If we now denote the driving field by \hat{l}_{in} , we have the input-output relation $\hat{l}_{\text{out}} - \hat{l}_{\text{in}} = \sqrt{\kappa_e} \hat{l}$ in the diagonalized frame. The dynamics is then determined by

$$\dot{\hat{l}} = \frac{i}{\hbar} [\hat{H}_S, \hat{l}] - \frac{\kappa}{2} \hat{l} - \sqrt{\kappa_e} \hat{l}_{\text{in}}, \quad (29)$$

where $\hat{H}_S = \hat{H}_m + \hat{H}_{mm} + \hat{H}_{mc}$ is the system Hamiltonian, κ the total effective magnon linewidth, and κ_e the dissipation rate related to external driving. In the proposed setup, we expect that $\kappa_e/\kappa \ll 1$ due to only a small proportion of the external field residing within the beam.

Similar to traditional optomechanics, the mechanical mode does not necessarily need to be actuated. However, it may still be driven and characterized, for instance, within the magnetomotive scheme [41–43] by utilizing the static field \mathbf{H}_0 . If an alternating current I_d goes through the beam, a Lorentz force of magnitude $f = I_d \mu_0 (H_0 \sin \phi + M_S \sin \theta)$ per unit length acts on the beam to the direction $\hat{n}(z)$ that is locally perpendicular to the beam as in Fig. 1(b). We may neglect the dynamical magnetization in this force as we assume its characteristic frequency to be much larger than those of the vibrational eigenmodes. Likewise, the flexural (dynamic vibrational) modes should have a negligible effect on the direction $\hat{n}(z)$ and, thus, we can consider only the normal of the static deformation u_0 here. It is possible to find the x component of the force $f_x(z)$, which in turn must be projected to the eigenmodes χ_n to determine its effect on the amplitude x_n . The effective force per unit length on x_n is

$$f_{\text{eff}} = \int_0^L \frac{dz}{L} \chi_n f_x = f \int_0^L \frac{dz}{L} \frac{\chi_n}{\sqrt{1 + (\partial_z u_0)^2}}. \quad (30)$$

It is possible to redefine the mass m in Eq. (7) to contain the integral term; this gives the so-called effective mass [1]. Due to the mirror symmetry of the static beam, only the symmetric vibrational eigenmodes couple to this force. Note that a similar analysis holds for the force in the z direction: such force f_z is negligible when $\partial_z u_0 \ll 1$ and it only couples to the antisymmetric vibrational eigenmodes. By changing the frequency of the drive I_d , we may then drive individual flexural modes on resonance if the vibrations are of high quality.

What is then observed is the induced voltage, as the beam vibrates and thus changes a magnetic flux through a circuit in the xz plane. This induced voltage is

$$V_{\text{emf}} = \mu_0 H_0 \sin(\phi) \int_0^L dz \frac{\partial u(z)}{\partial t} = \mu_0 H_0 \sin(\phi) L \sum_n \dot{x}_n. \quad (31)$$

That is, all flexural modes contribute to the voltage. The static magnetization \mathbf{M}_0 may be neglected as it does not provide a change in the magnetic flux in the first order while the dynamical magnetization changes at much higher frequency than the vibrations.

The modeling of the magnetomotive scheme can be done within the input-output formalism. First, we define formally the input and output fields for each vibration mode \hat{b}_n by the usual relation $\hat{b}_{n,\text{out}} - \hat{b}_{n,\text{in}} = \sqrt{\gamma_{n,e}} \hat{b}_n$ where γ_n refers to the total dissipation rate of the vibration mode n whereas $\gamma_{n,e}$ refers to external losses. One may then transform this formal input-output relation to match the induced voltage in Eq. (31) by multiplying by $H_0 L \sin \phi$, using $\hat{x}_n \propto (\hat{b}_n + \hat{b}_n^\dagger)$, and taking the time derivative. These transformations also define new input and output fields. However, in the Fourier space, these are linear transformations so we may equally well consider the original input-output relation, as long as we remember that all the fields are in fact proportional to $\sin \phi$ and that $\gamma_{n,e}$ depends on the force projection on the eigenmodes. The dynamics of the flexural modes is obtained by

$$\dot{\hat{b}}_n = \frac{i}{\hbar} [\hat{H}_S, \hat{b}_n] - \frac{\gamma_n}{2} \hat{b}_n - \sqrt{\gamma_{n,e}} \hat{b}_{n,\text{in}} \quad (32)$$

from which it is straightforward to obtain the output $\hat{b}_{n,\text{out}}$.

Lastly, it should be noted that there is ‘‘cross driving,’’ i.e., the different drives exemplified here interact if they are applied simultaneously. The alternating current I_d through the beam causes a force proportional to $\mu_0 |\mathbf{h}| I_d$ to the beam. Likewise, it causes an extraneous magnetic flux which generates induced voltage proportional to the magnitude of current I_d . These effects are negligible in most cases with a frequency mismatch of the magnon and flexural modes.

IV. MAGNOMECHANICS

With the magnomechanical Hamiltonian and the scheme to drive and observe such a system, we may describe an example magnomechanics experiment. The wealth of literature on optomechanical systems can be used straightforwardly due to the similar form of the Hamiltonian. However, there are a few issues that are important for magnomechanics specifically.

The relevant magnitude of the eigenfrequencies and dissipation rates of the magnon and mechanical system affect the possible measurements. As mentioned in the derivation of the magnomechanical Hamiltonian, we assume that the mechanical frequency is much smaller than the FMR frequency $\omega_m \ll \omega_K$. These systems are also assumed underdamped, meaning that for each system the eigenfrequency is larger than the dissipation rate $\omega_m > \gamma$ and $\omega_K > \kappa$. The only question left is thus whether the mechanical eigenfrequency ω_m is larger than the FMR linewidth κ or not. The case $\omega_m > \kappa$ is called the resolved sideband regime which, in optomechanics, has allowed for ground-state cooling of the mechanical oscillator [2,3,44] and amplification of microwave signals at the quantum limit [45]. This is also the regime of experiments in Refs. [19,22] performed with microwave cavities and YIG spheres. However, for many other ferromagnetic materials, it may be expected that $\omega_m < \kappa$. Although the analysis could proceed either way, we focus on results in this nonresolved sideband regime where the FMR linewidth κ dominates.

Next, we describe in detail an amplification scheme for microwave signals in the nonresolved sideband regime which is both theoretically known [46] and experimentally observed [47] in optomechanical systems. Especially, we focus on the aspect that is not present in optomechanics: the tunability of the magnomechanical coupling as well as the magnon eigenfrequency with respect to the external static field \mathbf{H}_0 .

The derivation of the reflection coefficient, often called S_{11} , follows the lines of Ref. [46]. First, we assume a strong drive on the magnon system at a frequency ω_d and focus on the deviations around the driven system. That is, we replace $\hat{l} \rightarrow (\sqrt{n} + \hat{l})e^{-i\omega_d t}$, where we identify n as the number of magnons, in the Hamiltonians of Eqs. (21), (26), and (27), using the transformation in Eq. (25). Note that the Holstein-Primakoff transformation gives an upper limit to the strength of the drive, given by $M_S \gg \hbar \gamma_n / (LA)$. Then, we may neglect the second-order terms of the deviations as well as the terms that rotate at frequency ω_d or faster. The dynamical part of the Hamiltonian then reads as in the diagonalized frame

$$\hat{H}_S / \hbar = \omega_K \hat{l}^\dagger \hat{l} + \sum_j \omega_j \hat{b}_j^\dagger \hat{b}_j + \sum_j G_j \hat{x}_j \hat{x}_{b,j}, \quad (33)$$

where $\hat{x}_{b,j} = (\hat{b}_j + \hat{b}_j^\dagger) / \sqrt{2}$ and the effective coupling constant follows from Eq. (28) by $G_j = 2\sqrt{n} g_{m,j}$, that is,

$$G_j = 4\sqrt{n} \left[(g_j^{\text{me}} - g_j^{\text{dm}}) \left(c \cos^2 \theta + \frac{1}{c} \cos 2\theta \right) - c g_j^{\text{dm}} \right]. \quad (34)$$

The effective magnomechanical coupling is thus enhanced by the number n of magnons and is tunable by the external field \mathbf{H}_0 , as it determines the direction of the magnetization θ and the squeezing factor c .

The response matrix of the magnomechanical system is obtained by utilizing the input-output equations in the Fourier space and the transformation between the bosonic operators \hat{l} and \hat{b}_j and their respective quadratures. For simplicity, let us focus on a single flexural mode j and denote $\omega_j = \omega_m$ while

dropping the other subscripts. We find now the linear response

$$\begin{pmatrix} \hat{l}(\omega) \\ \hat{l}^\dagger(\omega) \\ \hat{b}(\omega) \\ \hat{b}^\dagger(\omega) \end{pmatrix} = T \begin{pmatrix} \hat{l}_{\text{in}}(\omega) \\ \hat{l}_{\text{in}}^\dagger(\omega) \\ \hat{b}_{\text{in}}(\omega) \\ \hat{b}_{\text{in}}^\dagger(\omega) \end{pmatrix}, \quad (35)$$

where all elements of the matrix T may be nonzero (further details given in Appendix C). Here, it should be noted that \hat{l} is now defined in a frame that corotates with the drive so the frequencies are defined with respect to the drive frequency ω_d . For example, $\hat{l}_{\text{in}}(\omega_p)$ corresponds to an input at frequency $\omega_d + \omega_p$ whereas $\hat{l}_{\text{in}}^\dagger(\omega_p)$ corresponds to $\omega_d - \omega_p$.

The output fields are readily obtained from the relations $\hat{l}_{\text{out}} = \hat{l}_{\text{in}} + \sqrt{\kappa_e} \hat{l}$ and $\hat{b}_{\text{out}} = \hat{b}_{\text{in}} + \sqrt{\gamma_e} \hat{b}$. Especially, we can define now the reflection coefficients for the magnon and mechanical systems as $S_{11}^l = 1 + \sqrt{\kappa_e} T_{11}$ and $S_{11}^b = 1 + \sqrt{\gamma_e} T_{33}$. Likewise, the transduction coefficients may be defined as $S_{lb} = \sqrt{\kappa_e} T_{13}$ (from mechanics to magnons) and $S_{bl} = \sqrt{\gamma_e} T_{31}$ (vice versa).

The amplification of the probe signals may be observed by calculating the reflection coefficient. Assuming that the magnon dissipation rate κ is large compared to ω_m and γ , we obtain for $\omega_d = \omega_K$ and $\omega = \pm\omega_m$

$$S_{11}^l = 1 - 2 \frac{\kappa_e}{\kappa} \left(1 \pm \frac{G^2}{\kappa\gamma} \right) \quad (36)$$

for high-quality vibrations $\omega_m \gg \gamma$. Thus, if the coupling G is large enough, we find $|S_{11}^l| \gg 1$. At the same time, the mechanical response is sharply peaked at approximately $\tilde{\omega}_m \approx \omega_m - \text{Re } \Lambda$ where

$$\Lambda = \frac{i\omega_m \Delta G^2}{[i(\tilde{\omega}_m + \omega_m) - \frac{\gamma}{2}][\Delta^2 + (i\tilde{\omega}_m - \frac{\kappa}{2})^2]} \quad (37)$$

and $\Delta = \omega_K - \omega_d$. This change in the resonant frequency corresponds to the optical spring effect of optomechanics. At this frequency, the reflection coefficient for the force driving the mechanics is given by $S_{11}^b = 1 - \gamma_e / (\frac{\gamma}{2} + \text{Im } \Lambda)$. Thus, the current through the beam may be modified by the magnomechanical coupling.

The reflection coefficients for different angles ϕ of the external field \mathbf{H}_0 are graphed in Fig. 5. With the chosen parameters, the effective coupling constant (34) vanishes at $\phi \approx 43^\circ$ (see also the orange line in Fig. 3) and, thus, the responses match those of the uncoupled systems (blue line). It would be possible to obtain larger values of the coupling constant with values $\phi \approx 0$ but, as discussed in Sec. III, this would not be commensurate with the magnetomotive scheme for which the input and output amplitudes depend on $\sin \phi$.

V. EXPERIMENT ON A MAGNETIC BEAM

Already in some experiments, magnetic beams and cantilevers have been considered [48–50]. Here we demonstrate successful fabrication and characterization of a magnetic beam made out of CoFeB, which exhibits a large magnetostriction, and is promising for the upcoming magnomechanics experiments. The beam is a bilayer system, consisting of nonmagnetic aluminum and the CoFeB layer. Using a

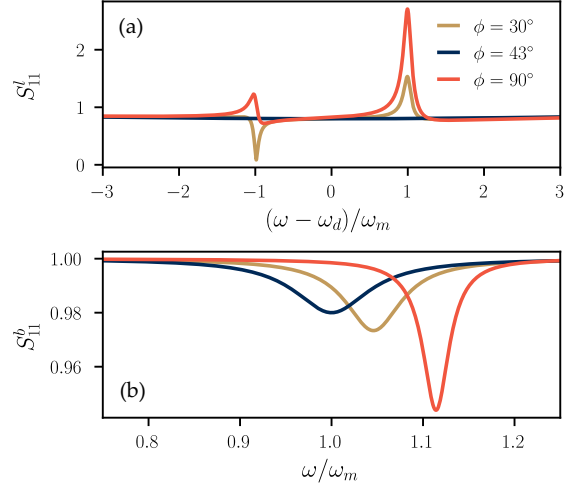


FIG. 5. Reflection coefficients of the magnon (a) and flexural (b) systems for three different angles ϕ while the magnitude of the external field $H_0 = 5H_c \approx 0.1M_S$ is fixed. In (a), we set $\Delta = 0$ whereas in (b) $\Delta = -\omega_m$ for all angles. The magnitude of the effective coupling rate is given by $2\sqrt{n}g_j^{\text{dm}} = 0.8\omega_m$, and the dissipation rates are $\kappa = 15\omega_m$, $\gamma = 0.1\omega_m$, $\kappa_e/\kappa = 0.1$, and $\gamma_e/\gamma = 0.01$. We choose here relatively low-quality vibrations for visual clarity. Otherwise, the parameters match those of Fig. 3 so that the orange line there characterizes the angular dependence of the magnomechanical coupling constant.

combination of electron-beam lithography, evaporation, dc sputtering, and a lift-off-based process, we first fabricated the beam structures over a silicon substrate. Subsequently, using reactive ion etching, we created the suspended bridge structures. The final fabricated bridges had a length of 50 μm and a width of 10 μm . The aluminum layer had a thickness of 100 nm while the CoFeB layer was 50 nm thick (with a Ta capping layer of 3 nm). Consequent to the fabrication steps, an asymmetric deformation is observed in the bridge at room temperature as seen in Fig. 6. This deformation may be attributed to a compressive stress owing to a mismatch of the elastic constants in the different layers. Since the thermal expansion coefficients of these layers are also different, it is expected that the compressive stresses observed at room temperature may be changed at cryogenic temperatures. Nevertheless, as pointed out in the above sections, the presence of the asymmetric deformation is necessary for providing a sizable magnomechanical coupling.

We also characterized the magnetic hysteresis of the suspended beam and found the low-temperature switching field $H_{\text{sw}} = 30\text{ mT}$ in the presence of a field in the y direction, i.e., perpendicular to the wire. This hence corresponds to the case considered in Fig. 3. Using the saturation magnetization of CoFeB, $M_S \approx 1200\text{ emu/cm}^3$ corresponding to $\mu_0 M_S \approx 1.5\text{ T}$ or $\gamma\mu_0 M_S \approx 42\text{ GHz}$, this H_{sw} would be obtained with $\tilde{\epsilon}_{zz}^{(0)} [1 + B_1/(\mu_0 M_S^2)] = 0.01$ assuming that $|B_1| \ll \mu_0 M_S^2$. This corresponds to the maximum deformation $u_m \approx 0.06L$, quite well in line with what is seen in Fig. 6. It should, however, be noted that the magnetoelastic constant B_1

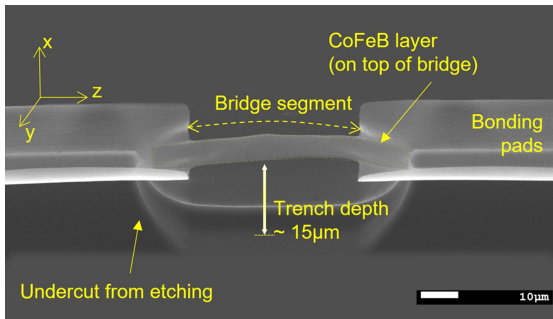


FIG. 6. Scanning electron micrograph of a doubly clamped beam fabricated in our laboratory (see main text for further details). A close inspection of the beam or bridge segment reveals that the beam is deformed but its structure differs slightly from the idealized beam in Fig. 1. The process of reactive ion etching during the fabrication also leads to the formation of an undercut, further contributing to the asymmetry.

does not only depend on the material but also on the details of fabrication [33,51]. To our knowledge, there are no accurate estimates available in the literature that would correspond to our system.

The mechanical eigenfrequency may be estimated by using the solved dimensionless eigenfrequencies in Fig. 7 (see Appendix A) and, for simplicity, by using the characteristic values for a beam fully made of aluminum, $\rho = 2.7 \text{ g/cm}^3$ and $E = 70 \text{ GPa}$. Since $u_m/h \approx 20$ according to the analysis based on the switching field, we find that the eigenfrequency of the first mode is $\omega_1/(2\pi) \approx 1 \text{ MHz}$. This corresponds to the zero-point motion amplitude $x_1^{\text{ZPM}} \approx 6 \times 10^{-15} \text{ m}$. In contrast, if $u_m/h = 10$, we would find the eigenfrequency 0.5 MHz as the conversion from Fig. 7 is given by $\omega_n \approx (88 \text{ kHz}) \times \bar{\omega}_n$.

Finally, let us estimate the expected size of the magnomechanical coupling for this setup. Using $u_m/h \approx 20$, which gives the mechanical mode parameter $\bar{\beta}_1 \approx 3$, we get $g_1^{\text{dm}} \approx 50 \text{ mHz}$. This is the scale used in Figs. 3 and 4 and depending

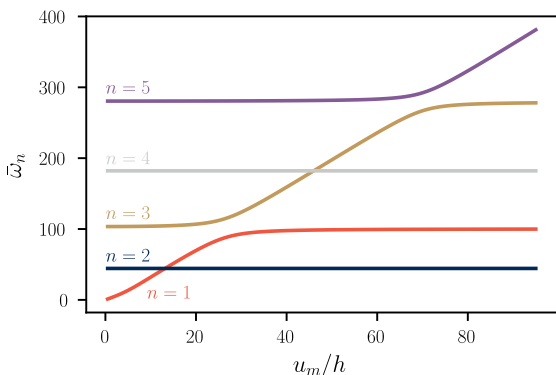


FIG. 7. The dimensionless eigenfrequencies of the dynamical mode \bar{u}_1 .

on the precise magnetic field the actual magnomechanical coupling may be somewhat larger. Due to the nonlinear nature of the Euler-Bernoulli equation used, if the static deformation was half as large, $u_m/h = 10$, we would find $g_1^{\text{dm}} \approx 0.15 \text{ Hz}$. These couplings are comparable to what was found for the magnomechanical coupling in [19,22] for YIG spheres and somewhat smaller than the optomechanical coupling in our setups (e.g., $g \sim 100 \text{ Hz}$ in [8]).

Experimental preparations on realizing the magnomechanical physics are currently ongoing in our laboratory.

VI. CONCLUSIONS

We present a detailed analysis of magnetoelastic interactions in suspended micromechanical beams made out of ferromagnetic materials. We find the mechanical vibrations of the beam, and its ferromagnetic resonance, exhibit nonlinear interactions reminiscent of radiation-pressure coupling in cavity optomechanics or in microwave optomechanics. The interaction, however, is more versatile and easily configurable. Part of the interaction arises via magnetoelasticity, where the vibrations modulate the frequency of the magnetic resonance. The dominant coupling under typical conditions, however, is due to demagnetizing field of the beam, which is affected by the instantaneous shape of the vibrating beam. The predicted radiation-pressure coupling rates are smaller than in microwave optomechanics, but still sizable enough that optomechanical physics such as cooling, amplification, and lasing are within experimental reach. In comparison to optomechanics, our system has the assets of a small footprint, a reconfigurable interaction, and a high-power tolerance of the magnon resonance.

ACKNOWLEDGMENTS

We thank R. Holländer, H. Qin, and S. van Dijken for useful discussions. This work was supported by the Academy of Finland (Contracts No. 307757, No. 312057, No. 317118, and No. 321981), by the European Research Council (Contract No. 615755), and by the Centre for Quantum Engineering at Aalto University. K.S.U.K. acknowledges the financial support of the Magnus Ehrnrooth foundation. We acknowledge funding from the European Union's Horizon 2020 research and innovation program under Grant Agreement No. 732894 (FETPRO HOT). We acknowledge the facilities and technical support of Otaniemi research infrastructure for Micro and Nanotechnologies (OtaNano) that is part of the European Microkelvin Platform.

APPENDIX A: BEAM DYNAMICS

From the nonlinear Euler-Bernoulli equation (2) one can find a beam configuration that has a static deformation as well as the eigenmodes in which the beam vibrates [28]. These eigenmodes depend directly on the static deformation which is caused in our description by a negative tension T_0 . That is, there is a constant compressive stress or “load” which we denote by $P = -T_0 > 0$.

For the following analysis, it is useful to make Eq. (2) dimensionless by introducing the relations

$$\bar{u} = \sqrt{\frac{A}{I_x}} u, \quad \bar{z} = \frac{z}{L}, \quad \bar{t} = \sqrt{\frac{EI_x}{\rho AL^4}} t, \quad (\text{A1a})$$

$$\bar{T}_0 = \frac{L^2}{EI_x} T_0, \quad \bar{f} = \frac{A^{1/2} L^4}{EI_x^{3/2}} f, \quad (\text{A1b})$$

where $f = f(z)$ is the external force per unit length on the beam. The dimensionless nonlinear Euler-Bernoulli equation reads as ($\bar{P} = -\bar{T}_0$)

$$\frac{\partial^2 \bar{u}}{\partial \bar{t}^2} + \frac{\partial^4 \bar{u}}{\partial \bar{z}^4} + \left[\bar{P} - \frac{1}{2} \int_0^1 d\bar{z} \left(\frac{\partial \bar{u}}{\partial \bar{z}} \right)^2 \right] \frac{\partial^2 \bar{u}}{\partial \bar{z}^2} = \bar{f}. \quad (\text{A2})$$

We set the force to vanish, $\bar{f} = 0$, as we are interested in the static deformation and the eigenmodes of vibrations around it.

Let us now assume $\bar{u}(\bar{z}, \bar{t}) = \bar{u}_0(\bar{z}) + \bar{u}_1(\bar{z}, \bar{t})$ where $\bar{u}_0 \gg \bar{u}_1$ as in the main text. Using this assumption, we may insert the relation for $\bar{u}(\bar{z}, \bar{t})$ to Eq. (A2) and separate the resulting equation into two by considering the zeroth and first power of \bar{u}_1 . We find that the static deformation \bar{u}_0 is determined by the zeroth-order equation which reads as

$$\partial_{\bar{z}\bar{z}\bar{z}\bar{z}} \bar{u}_0 + \bar{\alpha}^2 \partial_{\bar{z}\bar{z}} \bar{u}_0 = 0, \quad \bar{\alpha}^2 = \bar{P} - \frac{1}{2} \int_0^1 d\bar{z} (\partial_{\bar{z}} \bar{u}_0)^2. \quad (\text{A3})$$

A static deformation is possible only if $\bar{\alpha}^2 > 0$; otherwise, $\bar{u}_0 = 0$ is the only solution. This is known as the buckling transition.

We may begin solving Eq. (A3) by assuming that $\bar{\alpha}^2$ is independent of \bar{u}_0 . If indeed $\bar{\alpha}^2 > 0$, one can provide a general solution of the differential equation in terms of trigonometric and linear functions. However, the boundary conditions (4) fix $\bar{\alpha} = 2\pi$ for a single antinode solution which reads as

$$\bar{u}_0(\bar{z}) = \bar{u}_m \frac{1 - \cos(\bar{\alpha}\bar{z})}{2}. \quad (\text{A4})$$

Here, the parameter $\bar{u}_m = \pm 4\sqrt{\frac{\bar{P}}{\bar{\alpha}^2} - 1}$ is fixed self-consistently by inserting the solution to the definition of $\bar{\alpha}^2$. It also describes the value \bar{u}_0 of deformation in the middle of the beam $\bar{z} = \frac{1}{2}$. Note that \bar{P} may be removed in favor of \bar{u}_m if the condition for buckling $\bar{P} > \bar{\alpha}^2 = 4\pi^2$ holds true.

In the first order of \bar{u}_1 , its dynamics is described by

$$\partial_{\bar{t}\bar{t}} \bar{u}_1 + \partial_{\bar{z}\bar{z}\bar{z}\bar{z}} \bar{u}_1 + \bar{\alpha}^2 \partial_{\bar{z}\bar{z}} \bar{u}_1 - \bar{\beta} \partial_{\bar{z}\bar{z}} \bar{u}_0 = 0, \quad (\text{A5a})$$

$$\bar{\beta} = \int_0^1 d\bar{z} (\partial_{\bar{z}} \bar{u}_0) (\partial_{\bar{z}} \bar{u}_1). \quad (\text{A5b})$$

We can now find the flexural eigenmodes by Fourier transforming $\bar{u}_1(\bar{z}, \bar{t}) = \bar{u}_1(\bar{z}) e^{-i\bar{\omega}\bar{t}}$ which gives

$$\partial_{\bar{z}\bar{z}\bar{z}\bar{z}} \bar{u}_1 + \bar{\alpha}^2 \partial_{\bar{z}\bar{z}} \bar{u}_1 - \bar{\omega}^2 \bar{u}_1 = \bar{\beta} \partial_{\bar{z}\bar{z}} \bar{u}_0. \quad (\text{A6})$$

Here, the dimensionless frequency $\bar{\omega}$ is related to the physical one with $\omega = \sqrt{\frac{EI_x}{\rho AL^4}} \bar{\omega}$. The differential equation (A6) is written so that the left-hand side is the homogeneous equation while the right-hand side provides the nonhomogeneous term. It is straightforward to check that setting $\bar{u}_1 \propto \partial_{\bar{z}\bar{z}} \bar{u}_0$ gives a particular solution. Thus, the general solution may be

written as

$$\begin{aligned} \bar{u}_1(\bar{z}) = & C_1 \cos(\delta_+ \bar{z}) + C_2 \sin(\delta_+ \bar{z}) + C_3 \cosh(\delta_- \bar{z}) \\ & + C_4 \sinh(\delta_- \bar{z}) + C_5 \frac{\bar{\alpha}^2 \bar{u}_m}{2} \cos \bar{\alpha} \bar{z}, \end{aligned} \quad (\text{A7})$$

where

$$\delta_{\pm} = \frac{\sqrt{\sqrt{\bar{\alpha}^4 + 4\bar{\omega}^2} \pm \bar{\alpha}^2}}{\sqrt{2}}. \quad (\text{A8})$$

Here, the terms with $C_1 \dots C_4$ specify the solution of the homogeneous equation.

The constants $C = (C_1, C_2, C_3, C_4, C_5)$ may be fixed in the following manner: The boundary conditions for \bar{u}_1 give in total four equations. The last equation is obtained by inserting the full general solution into Eq. (A6) where we use the definition (A5b) for $\bar{\beta}$. This set of equations can be rearranged into a linear equation $\mathbf{M}_{\text{nl}} C = \mathbf{0}$, where the matrix \mathbf{M}_{nl} depends on frequency $\bar{\omega}$. One can then solve the equation numerically in many ways: we use the singular value decomposition to minimize the smallest singular value and use the corresponding vector C belonging into the null space of \mathbf{M}_{nl} . We then normalize the found solution for \bar{u}_1 so that it corresponds to the eigenmode χ_n , that is, $\int_0^1 d\bar{z} \chi_n^2 = 1$.

We note that it would be possible to remove C_5 by setting $C_5 = -\bar{\beta}/\bar{\omega}^2$ which gives the correct particular solution and, then, self-consistently solve for $\bar{\beta}$. However, the division by the unknown frequency is numerically problematic since values $\bar{\omega} \approx 0$ are needed. Even with finite frequencies, this method did not produce orthogonal modes. With the method described above, we find the eigenmodes χ_n to be orthonormal to a reasonable numerical accuracy, meaning that $\int_0^1 d\bar{z} \chi_n \chi_m \approx \delta_{nm}$.

In Fig. 7 we have plotted the five first eigenfrequencies. The structure of eigenfrequencies as a function of the static deformation u_m is that of crossings and avoided crossings. We find, as in Ref. [28], that the antisymmetric modes with $n = 2, 4, \dots$ do not depend on the static deformation. This is because the static deformation is symmetric and, thus, $\bar{\beta} = 0$ for these modes. As u_m increases, there is a crossing in eigenfrequencies between the symmetric and antisymmetric mode, followed by an avoided crossing with the next symmetric mode.

A few examples of the eigenmodes χ_n for different static deformations u_m are plotted in Fig. 8. In general, we note that the eigenmodes χ_n with odd n are changed by the static deformation while χ_n with even n remain the same. More specifically, the first mode χ_1 is plotted in Fig. 8(a). After the crossing in eigenfrequencies ω_1 and ω_2 around $u_m/h \approx 14$ the eigenmode χ_1 starts to resemble the third mode at small u_m : it has three antinodes. The same can be observed for χ_3 in Fig. 8(c) where the eigenmodes have either three or five antinodes. On the other hand, the eigenmode χ_2 remains independent of u_m/h as can be seen in Fig. 8(b).

APPENDIX B: MAGNETIC DYNAMICS

1. Magnetic hysteresis

The static component of the magnetization \mathbf{M}_0 can be determined for a given external field \mathbf{H}_0 , knowing the saturation

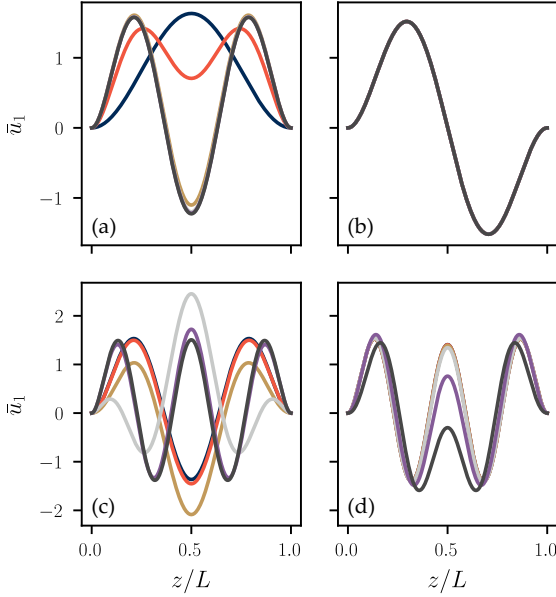


FIG. 8. Eigenmodes χ_n for (a) $n = 1$, (b) $n = 2$, (c) $n = 3$, and (d) $n = 5$. Here, u_m/h are chosen from approximately $\{0.5, 19, 37, 55, 73, 91\}$.

magnetization M_S , the magnetoelastic constant B_1 , and the static strain $\bar{\epsilon}_{zz}^{(0)}$.

For simplicity, we assume that the static component of the magnetic field is parallel to the yz plane: $\mathbf{H}_0 = H_0(\cos\phi\hat{z} + \sin\phi\hat{y})$ with $H_0 > 0$. In this case, the static magnetization \mathbf{M}_0 is obtained by minimizing the magnetic free energy, proportional to Eq. (17) with $\mathbf{H} = \mathbf{H}_0$ and $\mathbf{M} = \mathbf{M}_0$, which is up to a constant

$$\mathcal{F}_0 = -\mu_0 \mathbf{H}_0 \cdot \mathbf{M}_0 + \mu_0 \left(\frac{1}{2} - \bar{\epsilon}_{zz}^{(0)} \right) M_x^2 + \mu_0 \left(\frac{B_1}{\mu_0 M_S^2} + 1 \right) \bar{\epsilon}_{zz}^{(0)} M_z^2. \quad (\text{B1})$$

In the validity range of the Euler-Bernoulli theory $\partial_z u(z) \ll 1$ and $\bar{\epsilon}_{zz}^{(0)} \ll 1$, we must have $M_{0x} = 0$. Thus, we can make the ansatz $\mathbf{M}_0 = M_S(\cos\theta\hat{z} + \sin\theta\hat{y})$ where the angle θ is obtained by minimizing

$$\frac{\mathcal{F}_0}{\mu_0 M_S H_0} = -\cos(\theta - \phi) + \left(\frac{B_1}{\mu_0 M_S^2} + 1 \right) \frac{M_S}{H_0} \bar{\epsilon}_{zz}^{(0)} \cos^2 \theta. \quad (\text{B2})$$

Since, in general, the magnetoelastic constant B_1 can be positive or negative, the solution of θ depends on this choice. More precisely, the sign of $B_1/(\mu_0 M_S^2) + 1$ determines the behavior of the magnetic free energy \mathcal{F}_0 when H_0 and $\bar{\epsilon}_{zz}^{(0)}$ are fixed and nonzero. In either case, the competition between the external magnetic field, the demagnetizing field, and the magnetoelastic field gives rise to hysteresis that is similar to the Stoner-Wohlfarth hysteresis [30,52].

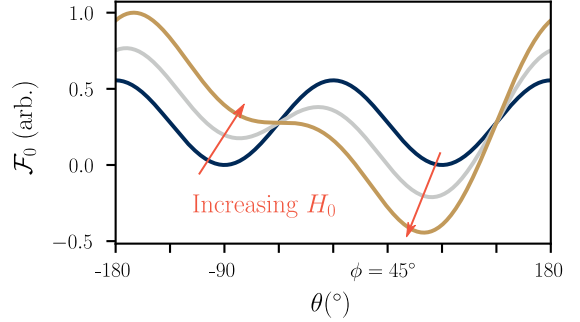


FIG. 9. The static magnetic free energy derived in Eq. (B2) for $B_1 > -\mu_0 M_S^2$ (corresponding to a hard z axis) as a function of the angle θ , as the magnitude H_0 of the external field pointing at $\phi = 45^\circ$ is increased (orange arrows). The blue line corresponds to $H_0 = 0$. As H_0 is increased, the metastable local minimum of \mathcal{F}_0 disappears and the global minimum approaches ϕ .

If $B_1 > -\mu_0 M_S^2$, the prefactor of $\cos^2\theta$ term in Eq. (B2) is positive and, therefore, the z axis is a hard axis of the magnetic system. The magnetic free energy in this situation is depicted in Fig. 9 as a function of θ . Without any external field (blue line), the minima are found at $\theta = \pm 90^\circ$. When the external field magnitude H_0 is increased, at first, one of the minima becomes a global minimum and, eventually, the second metastable local minimum disappears. At the same time, the magnetization angle θ corresponding to a global minimum approaches $\phi = 45^\circ$.

The case with $B_1 < -\mu_0 M_S^2$ corresponds to an easy z axis, as the sign of $B_1/(\mu_0 M_S^2) + 1$ is negative. Mathematically, this case can be mapped exactly to the previous hard z axis case with the transformations $\theta \rightarrow \theta + 180^\circ$ and $\mathcal{F}_0 \rightarrow -\mathcal{F}_0$. Thus, comparing to Fig. 9, the maxima correspond to the minima after a shift in θ in this case.

For $\phi = 90^\circ$, i.e., magnetic field perpendicular to the beam, the problem can be solved analytically. For low fields, the (meta)stable magnetization directions depend on the sign of the anisotropy term, i.e., the sign of $B_1/(\mu_0 M_S^2) + 1$, because when this term is positive, the beam axis is a hard axis and the magnetization prefers to lie along the magnetic field. For the opposite sign of the anisotropy, the static magnetization is along the beam for low fields and along the field for high fields. The coercive field, i.e., the size of the magnetic field where the second relative minimum disappears is, however, in both cases

$$H_c = 2 \left| \frac{B_1}{\mu_0 M_S^2} + 1 \right| \bar{\epsilon}_{zz}^{(0)} M_S. \quad (\text{B3})$$

This field can be accessed in magnetic hysteresis measurements, but it is also related with the size of the magnomechanical coupling.

In Fig. 10 we show the solution of θ as a function of ϕ for different external field magnitudes H_0 . The magnetization angle θ is fully characterized by ϕ and H_0/H_c if the z axis being a hard or easy axis is given [the sign of $B_1/(\mu_0 M_S^2) + 1$].

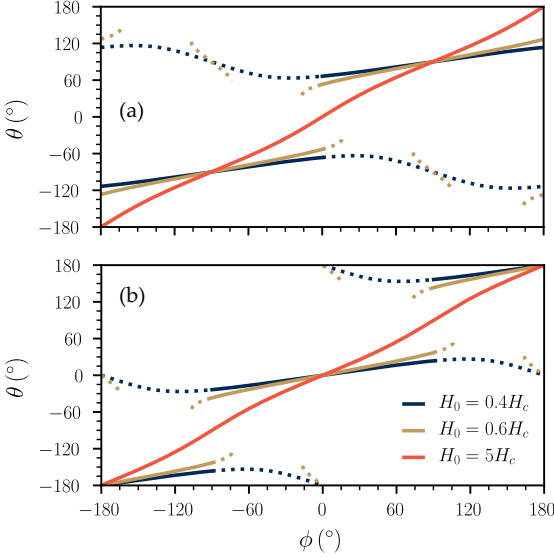


FIG. 10. The magnetization angle θ as a function of ϕ . In (a) $B_1 < -\mu_0 M_S^2$ and in (b) $B_1 > -\mu_0 M_S^2$ corresponding to the z axis being a hard and easy axis, respectively. The dotted lines represent the metastable free-energy minimum. For $H_0 > H_c$, the metastable minimum disappears, and for large H_0 we find $\theta \approx \phi$ as expected.

2. Magnetic Hamiltonian

The magnetization dynamics is given by the Landau-Lifshitz equation that can be written in the Hamiltonian formalism [53]

$$\dot{a} = i \frac{\partial H_{mg}}{\partial a^*}, \quad \dot{a}^* = -i \frac{\partial H_{mg}}{\partial a}, \quad (\text{B4})$$

where

$$M_{z'} = M_S - \frac{\gamma}{LA} a^* a, \quad (\text{B5a})$$

$$M_{+'} = \sqrt{\frac{2\gamma M_S}{LA}} \sqrt{1 - \frac{\gamma}{2M_S LA} a^* a}, \quad (\text{B5b})$$

$$M_{-'} = \sqrt{\frac{2\gamma M_S}{LA}} a^* \sqrt{1 - \frac{\gamma}{2M_S LA} a^* a}, \quad (\text{B5c})$$

$$H_{mg} = LA\mathcal{F}, \quad M_{\pm'} = M_{x'} \pm i M_{y'} \quad (\text{B5d})$$

and the conjugate variables are $a = (q + ip)/\sqrt{2}$, $a = (q - ip)/\sqrt{2}$. The quantization can be achieved with $[\hat{a}, \hat{a}^\dagger] = i\hbar \{a, a^*\} = \hbar$, where the braces represent the Poisson brackets. This corresponds to the Holstein-Primakoff bosonization, where $\hat{m}^\dagger =: \hat{a}^\dagger/\sqrt{\hbar}$ creates a boson.

If we assume $\mathbf{M}_0 = M_S \hat{z}'$ and $H_0 \gg h$, we can obtain the linearized Landau-Lifshitz equation by retaining only the quadratic terms in a, a^* in Eq. (B5). After a linear transformation $a \rightarrow \tilde{a}$, having the same form as Eq. (25), the Hamiltonian reads as $H_{mg} = \omega_K \tilde{a}^* \tilde{a} - (\tilde{h}^* \tilde{a} + \tilde{h} \tilde{a}^*)$, where

$$\tilde{h} = \mu_0 \sqrt{\frac{\gamma M_S LA}{2}} [h_{x'}(\zeta_+ - \zeta_-) + ih_{y'}(\zeta_+ + \zeta_-)] \quad (\text{B6})$$

and ω_K, ζ_{\pm} are defined in the main text in Eqs. (24) and (25). Then, by Fourier transforming $\tilde{a} \rightarrow e^{-i\omega t} \tilde{a}$, $h_{x',y'} \rightarrow e^{-i\omega t} h_{x',y'}$, the dynamic equations for the magnetization (B4) are

$$\begin{pmatrix} \dot{\tilde{h}}^* \\ \dot{\tilde{h}} \end{pmatrix} = \begin{pmatrix} \omega_K - \omega & 0 \\ 0 & \omega_K - \omega \end{pmatrix} \begin{pmatrix} \tilde{a}^* \\ \tilde{a} \end{pmatrix} \quad (\text{B7})$$

from which we can see that ω_K is the FMR resonance frequency.

APPENDIX C: DERIVATION OF THE LINEAR RESPONSE

As in the main text, let us focus on the case of a single flexural mode. Using the input-output equations given in Eqs. (29) and (32) with the Hamiltonian (33), we obtain a system of equations

$$\begin{pmatrix} \dot{\hat{x}}_l \\ \dot{\hat{p}}_l \\ \dot{\hat{x}}_b \\ \dot{\hat{p}}_b \end{pmatrix} = M \begin{pmatrix} \hat{x}_l \\ \hat{p}_l \\ \hat{x}_b \\ \hat{p}_b \end{pmatrix} - C \begin{pmatrix} \hat{x}_{l,\text{in}} \\ \hat{p}_{l,\text{in}} \\ \hat{x}_{b,\text{in}} \\ \hat{p}_{b,\text{in}} \end{pmatrix}, \quad (\text{C1})$$

where $C = \text{diag}(\sqrt{\kappa_e}, \sqrt{\kappa_e}, \sqrt{\gamma_e}, \sqrt{\gamma_e})$ is a diagonal matrix containing the external coupling rates and

$$M = \begin{pmatrix} -\kappa/2 & \Delta & 0 & 0 \\ -\Delta & -\kappa/2 & G & 0 \\ 0 & 0 & -\gamma/2 & \omega_m \\ G & 0 & -\omega_m & -\gamma/2 \end{pmatrix}, \quad (\text{C2})$$

where $\Delta = \omega_K - \omega_d$. The quadrature operators are connected to their bosonic counterparts by a unitary transformation. Let us now denote this transformation by U and define it such that

$$\begin{pmatrix} \hat{x}_l \\ \hat{p}_l \\ \hat{x}_b \\ \hat{p}_b \end{pmatrix} = U \begin{pmatrix} \hat{l} \\ \hat{l}^\dagger \\ \hat{b} \\ \hat{b}^\dagger \end{pmatrix}, \quad U = \frac{1}{\sqrt{2}} \begin{pmatrix} 1 & 1 & 0 & 0 \\ -i & i & 0 & 0 \\ 0 & 0 & 1 & 1 \\ 0 & 0 & -i & i \end{pmatrix}. \quad (\text{C3})$$

The same relation holds for the input operators. Now, we can apply the Fourier transformation $\hat{x}^{(\dagger)}(\omega) = \int \hat{x}^{(\dagger)}(t) e^{i\omega t} dt$ to Eq. (C1) and use the transformation (C3) to express the linear response matrix T as

$$T(\omega) = U^{-1}(i\omega I + M)^{-1} C U, \quad (\text{C4})$$

where I is the 4×4 identity matrix. Due to the complex structure of the response matrix T , there are only six independent components which read as

$$T_{11} = -\frac{i\sqrt{\kappa_e}}{D} \left[\frac{\omega_m}{2} G^2 + i\chi_\gamma(-\omega_m)\chi_\gamma(\omega_m)\chi_\kappa(-\Delta) \right], \quad (\text{C5a})$$

$$T_{12} = -\frac{i\sqrt{\kappa_e}\omega_m}{D} G^2, \quad (\text{C5b})$$

$$T_{13} = -\frac{i\sqrt{\gamma_e}G}{D} \chi_\gamma(-\omega_m)\chi_\kappa(-\Delta), \quad (\text{C5c})$$

$$T_{14} = -\frac{i\sqrt{\gamma_e}G}{D} \chi_\gamma(\omega_m)\chi_\kappa(-\Delta), \quad (\text{C5d})$$

$$T_{33} = -\frac{i\sqrt{\gamma_e}}{D} \left[\frac{\Delta}{2} G^2 + i\chi_\gamma(-\omega_m)\chi_\kappa(\Delta)\chi_\kappa(-\Delta) \right], \quad (\text{C5e})$$

$$T_{34} = -\frac{i\sqrt{\gamma_e}\Delta}{D} G^2, \quad (\text{C5f})$$

where $\chi_\eta(\omega_0) = i(\omega - \omega_0) - \eta/2$ and

$$D = \chi_Y(\omega_m)\chi_Y(-\omega_m)\chi_\kappa(\Delta)\chi_\kappa(-\Delta) - \Delta\omega_m G^2 \quad (C6)$$

is the determinant of the matrix $i\omega I + M$. The full linear response matrix T may now be written as

$$T = \begin{pmatrix} T_{11}(\omega) & T_{12}(\omega) & T_{13}(\omega) & T_{14}(\omega) \\ T_{12}^*(\omega) & T_{11}(-\omega) & T_{14}^*(\omega) & T_{13}^*(-\omega) \\ \sqrt{\frac{\kappa_c}{\gamma_e}} T_{13}(\omega) & \sqrt{\frac{\kappa_c}{\gamma_e}} T_{14}(\omega) & T_{33}(\omega) & T_{34}(\omega) \\ \sqrt{\frac{\kappa_c}{\gamma_e}} T_{14}^*(\omega) & \sqrt{\frac{\kappa_c}{\gamma_e}} T_{13}^*(-\omega) & T_{34}^*(\omega) & T_{33}^*(-\omega) \end{pmatrix}. \quad (C7)$$

That is, the other elements are obtained by conjugation, multiplying by a prefactor $\sqrt{\frac{\kappa_c}{\gamma_e}}$, and setting $\omega \rightarrow -\omega$.

-
- [1] M. Aspelmeyer, T. J. Kippenberg, and F. Marquardt, Cavity optomechanics, *Rev. Mod. Phys.* **86**, 1391 (2014).
- [2] J. D. Teufel, T. Donner, D. Li, J. W. Harlow, M. S. Allman, K. Cicak, A. J. Sirois, J. D. Whittaker, K. W. Lehnert, and R. W. Simmonds, Sideband cooling of micromechanical motion to the quantum ground state, *Nature (London)* **475**, 359 (2011).
- [3] J. Chan, T. P. M. Alegre, A. H. Safavi-Naeini, J. T. Hill, A. Krause, S. Gröblacher, M. Aspelmeyer, and O. Painter, Laser cooling of a nanomechanical oscillator into its quantum ground state, *Nature (London)* **478**, 89 (2011).
- [4] C. F. Ockeloen-Korppi, E. Damskägg, J. M. Pirkkalainen, M. Asjad, A. A. Clerk, F. Massel, M. J. Woolley, and M. A. Sillanpää, Stabilized entanglement of massive mechanical oscillators, *Nature (London)* **556**, 478 (2018).
- [5] R. Riedinger, A. Wallucks, I. Marinković, C. Löschnauer, M. Aspelmeyer, S. Hong, and S. Gröblacher, Remote quantum entanglement between two micromechanical oscillators, *Nature (London)* **556**, 473 (2018).
- [6] M. Mirhosseini, A. Sipahigil, M. Kalaei, and O. Painter, Superconducting qubit to optical photon transduction, *Nature (London)* **588**, 599 (2020).
- [7] F. Lecocq, J. B. Clark, R. W. Simmonds, J. Aumentado, and J. D. Teufel, Mechanically Mediated Microwave Frequency Conversion in the Quantum Regime, *Phys. Rev. Lett.* **116**, 043601 (2016).
- [8] C. F. Ockeloen-Korppi, E. Damskägg, J.-M. Pirkkalainen, T. T. Heikkilä, F. Massel, and M. A. Sillanpää, Low-Noise Amplification and Frequency Conversion with a Multiport Microwave Optomechanical Device, *Phys. Rev. X* **6**, 041024 (2016).
- [9] F. Ruesink, M.-A. Miri, A. Alù, and E. Verhagen, Nonreciprocity and magnetic-free isolation based on optomechanical interactions, *Nat. Commun.* **7**, 13662 (2016).
- [10] Z. Shen, Y.-L. Zhang, Y. Chen, C.-L. Zou, Y.-F. Xiao, X.-B. Zou, F.-W. Sun, G.-C. Guo, and C.-H. Dong, Experimental realization of optomechanically induced non-reciprocity, *Nat. Photon.* **10**, 657 (2016).
- [11] L. Mercier de Lépinay, C. F. Ockeloen-Korppi, D. Malz, and M. A. Sillanpää, Nonreciprocal Transport Based on Cavity Floquet Modes in Optomechanics, *Phys. Rev. Lett.* **125**, 023603 (2020).
- [12] C. H. Metzger and K. Karrai, Cavity cooling of a microlever, *Nature (London)* **432**, 1002 (2004).
- [13] S. Gigan, H. R. Böhm, M. Paternostro, F. Blaser, G. Langer, J. B. Hertzberg, K. C. Schwab, D. Bäuerle, M. Aspelmeyer, and A. Zeilinger, Self-cooling of a micromirror by radiation pressure, *Nature (London)* **444**, 67 (2006).
- [14] J. Thompson, B. Zwickl, A. Jayich, F. Marquardt, S. Girvin, and J. Harris, Strong dispersive coupling of a high-finesse cavity to a micromechanical membrane, *Nature (London)* **452**, 72 (2008).
- [15] M. Rossi, D. Mason, J. Chen, Y. Tsaturyan, and A. Schliesser, Measurement-based quantum control of mechanical motion, *Nature (London)* **563**, 53 (2018).
- [16] T. P. Purdy, D. W. C. Brooks, T. Botter, N. Brahm, Z.-Y. Ma, and D. M. Stamper-Kurn, Tunable Cavity Optomechanics with Ultracold Atoms, *Phys. Rev. Lett.* **105**, 133602 (2010).
- [17] C. A. Regal, J. D. Teufel, and K. W. Lehnert, Measuring nanomechanical motion with a microwave cavity interferometer, *Nat. Phys.* **4**, 555 (2008).
- [18] T. Rocheleau, T. Ndukum, C. Macklin, J. B. Hertzberg, A. A. Clerk, and K. C. Schwab, Preparation and detection of a mechanical resonator near the ground state of motion, *Nature (London)* **463**, 72 (2010).
- [19] X. Zhang, C.-L. Zou, L. Jiang, and H. X. Tang, Cavity magnomechanics, *Sci. Adv.* **2**, e1501286 (2016).
- [20] C. Gonzalez-Ballester, D. Hümmer, J. Gieseler, and O. Romero-Isart, Theory of quantum acoustomechanics and acoustomechanics with a micromagnet, *Phys. Rev. B* **101**, 125404 (2020).
- [21] C. Gonzalez-Ballester, J. Gieseler, and O. Romero-Isart, Quantum Acoustomechanics with a Micromagnet, *Phys. Rev. Lett.* **124**, 093602 (2020).
- [22] C. A. Potts, E. Varga, V. A. S. V. Bittencourt, S. V. Kusminskiy, and J. P. Davis, Dynamical Backaction Magnomechanics, *Phys. Rev. X* **11**, 031053 (2021).
- [23] C. Kittel, On the theory of ferromagnetic resonance absorption, *Phys. Rev.* **73**, 155 (1948).
- [24] C. Kittel, Physical theory of ferromagnetic domains, *Rev. Mod. Phys.* **21**, 541 (1949).
- [25] T. T. Heikkilä, *The Physics of Nanoelectronics: Transport and Fluctuation Phenomena at Low Temperatures* (Oxford University Press, Oxford, 2013).
- [26] L. Landau, E. Lifshitz, A. Kosevich, J. Sykes, L. Pitaevskii, and W. Reid, *Theory of Elasticity: Volume 7*, Course of Theoretical Physics (Elsevier, Amsterdam, 1986).

- [27] J. Reddy and P. Mahaffey, Generalized beam theories accounting for von Kármán nonlinear strains with application to buckling, *J. Coupled Syst. Multiscale Dyn.* **1**, 120 (2013).
- [28] A. H. Nayfeh and S. A. Emam, Exact solution and stability of postbuckling configurations of beams, *Nonlinear Dyn.* **54**, 395 (2008).
- [29] All numerics was constructed with Python and, more precisely, with numpy-, scipy-, and matplotlib-packages. The scripts to produce Figs. 2–10 are available at <https://gitlab.jyu.fi/jyucmt/suspended-beam-magnomechanics>.
- [30] E. C. Stoner and E. Wohlfarth, A mechanism of magnetic hysteresis in heterogeneous alloys, *Philos. Trans. R. Soc. A* **240**, 599 (1948).
- [31] T. L. Gilbert, A phenomenological theory of damping in ferromagnetic materials, *IEEE Trans. Magn.* **40**, 3443 (2004).
- [32] In a cantilever, the free-energy term $\mu_0 M_x M_z u'(z)$ due to demagnetizing field (11) does not disappear. Rather, averaging over the length gives an additional free-energy term $-M_x M_z [u(L) - u(0)]/L$ to Eq. (9) which may change the form of the magnomechanical coupling.
- [33] D. Sander, The correlation between mechanical stress and magnetic anisotropy in ultrathin films, *Rep. Prog. Phys.* **62**, 809 (1999).
- [34] The strain tensor ϵ_{ij} connects the lengths of line elements before and after displacement [26]: Let $dL = \sqrt{dx_1^2 + dx_2^2 + dx_3^2}$ be the infinitesimal distance between two points on the beam at \mathbf{r} . Then, after displacing the beam by a vector field \mathbf{u} , the points are at $\mathbf{r}' = \mathbf{r} + \mathbf{u}(\mathbf{r})$ and the lengths of the line elements are changed to $dx'_i = dx_i + (\nabla \mathbf{u} \cdot d\mathbf{x})_i$. Consequently, $dL'^2 = dL^2 + 2 \sum_{ij} \epsilon_{ij} dx_i dx_j$ with ϵ_{ij} as defined in the main text.
- [35] A. Serafini, *Quantum Continuous Variables: A Primer of Theoretical Methods* (CRC Press, Boca Raton, FL, 2017).
- [36] J. Zou, S. K. Kim, and Y. Tserkovnyak, Tuning entanglement by squeezing magnons in anisotropic magnets, *Phys. Rev. B* **101**, 014416 (2020).
- [37] S. Sharma, V. A. S. V. Bittencourt, A. D. Karenowska, and S. V. Kusminskiy, Spin cat states in ferromagnetic insulators, *Phys. Rev. B* **103**, L100403 (2021).
- [38] A. Kamra and W. Belzig, Super-Poissonian Shot Noise of Squeezed-Magnon Mediated Spin Transport, *Phys. Rev. Lett.* **116**, 146601 (2016).
- [39] C. W. Gardiner and M. J. Collett, Input and output in damped quantum systems: Quantum stochastic differential equations and the master equation, *Phys. Rev. A* **31**, 3761 (1985).
- [40] L. McKenzie-Sell, J. Xie, C.-M. Lee, J. W. A. Robinson, C. Ciccarelli, and J. A. Haigh, Low-impedance superconducting microwave resonators for strong coupling to small magnetic mode volumes, *Phys. Rev. B* **99**, 140414(R) (2019).
- [41] A. N. Cleland and M. L. Roukes, Fabrication of high frequency nanometer scale mechanical resonators from bulk Si crystals, *Appl. Phys. Lett.* **69**, 2653 (1996).
- [42] D. S. Greywall, B. Yurke, P. A. Busch, and S. C. Arney, Low-temperature anomalies in the dissipation of small mechanical resonators, *Europhys. Lett.* **34**, 37 (1996).
- [43] T. F. Li, Y. A. Pashkin, O. Astafiev, Y. Nakamura, J. S. Tsai, and H. Im, High-frequency metallic nanomechanical resonators, *Appl. Phys. Lett.* **92**, 043112 (2008).
- [44] F. Marquardt, J. P. Chen, A. A. Clerk, and S. M. Girvin, Quantum Theory of Cavity-Assisted Sideband Cooling of Mechanical Motion, *Phys. Rev. Lett.* **99**, 093902 (2007).
- [45] F. Massel, T. T. Heikkilä, J.-M. Pirkkalainen, S. U. Cho, H. Saloniemi, P. J. Hakonen, and M. A. Sillanpää, Microwave amplification with nanomechanical resonators, *Nature (London)* **480**, 351 (2011).
- [46] T. Botter, D. W. C. Brooks, N. Brahm, S. Schreppler, and D. M. Stamper-Kurn, Linear amplifier model for optomechanical systems, *Phys. Rev. A* **85**, 013812 (2012).
- [47] M. A. Cohen, D. Bothner, Y. M. Blanter, and G. A. Steele, Optomechanical Microwave Amplification Without Mechanical Amplification, *Phys. Rev. Appl.* **13**, 014028 (2020).
- [48] J. Losby, J. A. J. Burgess, C. M. B. Holt, J. N. Westwood, D. Mitlin, W. K. Hiebert, and M. R. Freeman, Nanomechanical torque magnetometry of permalloy cantilevers, *J. Appl. Phys.* **108**, 123910 (2010).
- [49] H. Arisawa, S. Daimon, Y. Oikawa, Y.-J. Seo, K. Harii, K. Oyanagi, and E. Saitoh, Magnetomechanical sensing based on delta-E effect in $\text{Y}_3\text{Fe}_5\text{O}_{12}$ micro bridge, *Appl. Phys. Lett.* **114**, 122402 (2019).
- [50] F. Heyroth, C. Hauser, P. Trempler, P. Geyer, F. Syrowatka, R. Dreyer, S. G. Ebbinghaus, G. Woltersdorf, and G. Schmidt, Monocrystalline Freestanding Three-Dimensional Yttrium-Iron-Garnet Magnon Nanoresonators, *Phys. Rev. Appl.* **12**, 054031 (2019).
- [51] P. G. Gowtham, G. M. Stiehl, D. C. Ralph, and R. A. Buhrman, Thickness-dependent magnetoelasticity and its effects on perpendicular magnetic anisotropy in Ta/CoFeB/MgO thin films, *Phys. Rev. B* **93**, 024404 (2016).
- [52] E. P. Wohlfarth, Relations between different modes of acquisition of the remanent magnetization of ferromagnetic particles, *J. Appl. Phys.* **29**, 595 (1958).
- [53] D. Stancil and A. Prabhakar, *Spin Waves: Theory and Applications* (Springer, New York, 2009).

IV

CAVITY-INDUCED BIFURCATION IN CLASSICAL RATE THEORY

by

K. S. U. Kansanen and T. T. Heikkilä

Manuscript, submitted to the arXiv-repository (2202.12182v2)

Copyright 2022 the Authors

Cavity-induced bifurcation in classical rate theory

Kalle S. U. Kansanen^{1,*} and Tero T. Heikkilä¹

¹*Department of Physics and Nanoscience Center, University of Jyväskylä,
P.O. Box 35 (YFL), FI-40014 University of Jyväskylä, Finland
(Dated: August 5, 2022)*

We show how coupling an ensemble of bistable systems to a common cavity field affects the collective stochastic behavior of this ensemble. In particular, the cavity provides an effective interaction between the systems, and parametrically modifies the transition rates between the metastable states. We predict that for a coupling strength exceeding a certain threshold, the cavity induces a spontaneous symmetry breaking where the stationary states of the bistable system bifurcate and the systems coalesce preferentially in one of the states. The effect crucially depends on the distribution of system–cavity coupling strengths. In the case of alternating signs of the couplings, the bifurcation shows up as a phase separation. Our results are of particular relevance in polaritonic chemistry where the presence of a cavity has been suggested to affect chemical reactions.

Classical rate theory provides a stochastic framework for investigations in natural and social sciences [1–6]. It has been used to describe a wide variety of phenomena in different fields: the spreading of diseases in epidemiology [7, 8], the growth and decline of companies in economics [9] and of populations in ecology [10], and disintegration of radioactive nuclei in atomic physics, to name a few. In chemistry, rate equations provide a quantitative way of understanding chemical reactions [11].

There have been several recent indications of chemical reactions being altered by the formation of vibrational polaritons, hybrid excitations formed by the coupling of molecular vibrations to vacuum electromagnetic field of an optical cavity [12–14]. The vacuum field has been reported to work both as a catalyst [15, 16] and an inhibitor [17–19] in different reactions. However, the current theoretical understanding seems to contradict these experimental results. The conventional approach that concentrates on the cavity-induced modification of the individual reaction rates within the transition state theory finds that all the polaritonic effects should disappear when the number of molecules forming the polariton increases [20–23]. Furthermore, very recently, there have been reports of failed replication experiments [24, 25], adding to the confusion.

The cavity effect on the chemistry poses an interesting stochastic problem, regardless of the current experimental knowledge on the subject. Its fundamental notion is that of collectivity: a large number of molecules participate in the polaritons. At the same time, the strength of the light-matter coupling may vary from molecule to molecule.

In this Letter, we concentrate on the effect of the indirect interactions between molecules mediated by the cavity field in the classical limit. We show that such an interaction can be taken into account in the classical rate theory as transition rates that depend parametrically on the state of the molecules. The rate equation describing the macroscopic state of the many molecule system is consequently non-linear. We find an order pa-

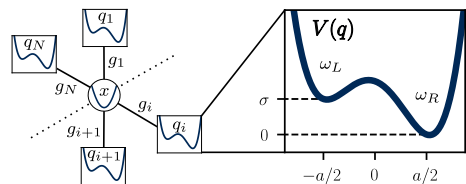


FIG. 1. Interactions between a harmonic cavity mode x and N identical modes q_i , described by a bistable potential $V(q)$. In the harmonic approximation, $\partial_q^2 V(a/2) = \omega_R^2$ and $\partial_q^2 V(-a/2) = \omega_L^2$ define the relevant frequencies.

rameter for the polaritonic system and show that, in an attainable parameter regime, it bifurcates so that it can have multiple solutions in the stationary state. Furthermore, we show that the distribution of the light-matter couplings dictates whether this bifurcation may be seen in the macroscopic state or whether it corresponds to a “hidden” order; a phase separation. Even before the bifurcation, the cavity-mediated interaction may slow down the effective transition rates, suggesting that the collectivity of the many molecule system must be considered on the level of the rate equations, not only on the level of the rates themselves.

Rate theory. Let us first consider a one-dimensional and bistable system described by a potential $V(q)$ as in Fig. 1. Here, q is a position quadrature which can describe, e.g., a vibrational mode of the molecule. Classical rate theory then relates the probability p to find the system in one of the wells to the transition rates $\Gamma_{\mu\nu}$ between the wells. We adopt a terminology of left and right wells corresponding to the minima of $V(q)$ at $q < 0$ and $q > 0$, respectively. Thus, if p_j is the probability to find the j th system in the left well, its rate equation [26] reads as

$$\frac{d}{dt} p_j = -\Gamma_{LR}^j p_j + \Gamma_{RL}^j [1 - p_j]. \quad (1)$$

The macroscopic behaviour is obtained from Eq. (1) by

noting that the expectation value of the number of systems in the left well is given by $N_L = \sum_j p_j$. If the transition rates are independent of the system j , we find

$$\frac{d}{dt} \frac{N_L}{N} = -\Gamma_{LR} \frac{N_L}{N} + \Gamma_{RL} \left[1 - \frac{N_L}{N} \right]. \quad (2)$$

In the following, we show that this approach has to be extended when the molecules have varying couplings to the cavity.

Often, the transition rates are assumed to be independent of p_j and time, i.e., constants. In such a case, to comply with thermodynamics, the rates must obey the detailed balance $\Gamma_{LR}/\Gamma_{RL} = e^{\beta\sigma}$ where $\beta = 1/k_B T$ is the inverse temperature and $\sigma = V(-a/2) - V(a/2)$ corresponds to the potential bias between the different states (Fig. 1). The rate equation then describes thermalization to the Boltzmann distribution.

The coupling of the molecules to the vacuum field leads to a state-dependent modification of the rates in Eq. (1). This is caused by the effective interaction between the different molecules mediated by the cavity. Before deriving the modification explicitly, we write this statement formally as $\Gamma_{\mu\nu} = \Gamma_{\mu\nu}^0 r_{\mu\nu}(N_L)$ where $r_{\mu\nu}(N_L)$ represents the rate modification caused by the vacuum field which may be expected to be a function of N_L and not of the individual p_j 's. The subsequent solution of the rate modifications $r_{\mu\nu}$ is the main result of this work from which the polaritonic effects follow.

State-dependent rate modification. Consider N systems with coordinates q_j coupled to an external collective mode as in Fig. 1. In what follows, we call those N systems ‘‘molecules’’ and the collective mode is a ‘‘cavity’’, in analogy to the systems studied in polaritonic chemistry. However, this approach works also for example in the case of a large number of superconducting flux qubits coupled to a single microwave cavity, or bistable atoms in a cold-atom arrangement, coupled to a common cavity mode [27].

We derive the state-dependent transition rates from the detailed balance. That is, if the stationary state of the total system thermalizes in the presence of the cavity, the rates for the molecule j obey

$$\frac{\Gamma_{LR}^j}{\Gamma_{RL}^j} = \exp\{\beta[V_{\text{tot}}(q_j < 0) - V_{\text{tot}}(q_j > 0)]\}, \quad (3)$$

when V_{tot} is the potential energy for a polaritonic state and the notation is understood so that all the other modes $q_{k \neq j}$ are fixed.

Motivated by quantum electrodynamics (QED), we introduce a single cavity mode of frequency ω_c and its position quadrature x and choose the classical potential energy of a polaritonic system [28] as

$$V_{\text{tot}} = \sum_{i=1}^N V(q_i) + \frac{1}{2} \omega_c^2 x^2 + \sum_{i=1}^N d_i(q_i)x, \quad (4)$$

where d_i represents the molecular dipole moment component in the direction of the cavity mode’s polarization vector.

We focus on a linear dipole moment $d_j(q_j) = \sqrt{\omega_c \omega_m} g_j q_j$ to gain insight on the effect of the cavity on the transition rates. Here, $\omega_m^2 = (\omega_L^2 + \omega_R^2)/2$ represents the mean frequency of the potential $V(q)$, and the square root term normalizes the light-matter coupling constant g_j . These choices allow mapping this model potential to the Dicke Hamiltonian in which case g_j follows directly from the QED derivation [29]. However, our approach works for an arbitrary dipole function $d_i(q_i)$.

The light-matter coupling g_j typically depends on both the position of the molecule within the cavity and the alignment of its dipole moment [29–31]. Importantly, g_j can be either positive or negative which has physical consequences. The strength of the collective coupling is indicated by the Rabi splitting frequency $\Omega \propto \sqrt{\sum_j g_j^2}$, defined as the difference of the eigenfrequencies of the total potential on resonance $\omega_L = \omega_R = \omega_c$ [32, 33]. We assume that $g_j \ll \omega_c, \omega_m$ while Ω is a small fraction of ω_c and ω_m due to $N \gg 1$.

The effective interaction mediated by the cavity can be understood by a force analysis. For a system in a stationary state, displacing the mode q_j by δq_j causes a force proportional to $-g_j \delta q_j$ to the cavity mode x . This leads to a displacement δx proportional to the force to the cavity mode. The force applied on another mode q_k is then proportional to $-g_k \delta x$ which reads as $g_k g_j \delta q_j$ in terms of the original displacement on mode q_j . Whenever the coupling constants of two different molecules share the same sign, the force between them is attractive and for opposite signs repulsive. The cavity-induced interaction resembles the phonon-mediated interaction between electrons in superconductivity [34].

We solve the stationary states of V_{tot} within the harmonic approximation which holds when $g_j \ll \omega_c, \omega_m$ and, thus, the cavity-induced change to the local minimum points of $V(q_j)$ is small. Technically, we first solve the values of q_j 's and x from the conditions $\partial_x V_{\text{tot}} = \partial_{q_j} V_{\text{tot}} = 0$ by treating the signs of q_j as variables, representing whether the molecule j is in the left or the right well. We find that all the stationary points may be expressed by using the collective order parameter

$$\Delta = \frac{1}{N} \sum_{i=1}^N \frac{g_i}{\sqrt{\langle g^2 \rangle}} \text{sign}(q_i), \quad (5)$$

where $\langle g^2 \rangle = \sum_i g_i^2 / N$ represents the average over the molecules and $\text{sign}(q_i)$ is the sign function. If there is no variation in the coupling constants g_i , Δ becomes the normalized difference between the number of molecules in the right and the left well, $\Delta \rightarrow \delta N / N = (N_R - N_L) / N$. Finally, we calculate the value of V_{tot} using Eq. (4) at these stationary points. The details of this algebraic calculation are relegated to the Supplemental Material [27].

We find that the stationary states of the full N molecule system have the potential energy

$$\frac{V_{\text{tot}}}{N} = -E_b P \Delta^2 - \frac{\sigma}{2} \frac{\delta N}{N}. \quad (6)$$

The first term is caused by the effective interaction via the cavity mode while the second term describes the potential bias of $V(q)$. The magnitude of the interaction is determined by the product of an effective potential barrier $E_b = \frac{1}{2}\omega_m^2(a/2)^2$ [35] and a polaritonic coefficient

$$P = \frac{N \langle g^2 \rangle}{\omega_c \omega_m - \sum_i (\frac{\omega_m}{\omega_i} g_i)^2}. \quad (7)$$

Here, ω_i equals ω_L for $q_i < 0$ and ω_R for $q_i > 0$. The coefficient P can be related to the Rabi splitting Ω using $N \langle g^2 \rangle \propto \Omega^2$. We assume that Ω is a small fraction of $\sqrt{\omega_c \omega_m}$ and $P \ll 1$. Consequently, P may be treated as a state-independent constant since its variation is proportional to P^2 [27].

Using the detailed balance (3) and Eq. (6), we find in the lowest order of P that

$$\frac{\Gamma_{LR}^j}{\Gamma_{RL}^j} = \frac{\Gamma_{LR}^0 r_{LR}^j}{\Gamma_{RL}^0 r_{RL}^j} = \exp\left(\beta\sigma + 2\alpha \frac{g_j}{\sqrt{\langle g^2 \rangle}} \Delta\right), \quad (8)$$

where $\alpha = 2P\beta E_b$ plays the role of a control parameter. It should be noted that, even though $P \ll 1$, the effective potential barrier E_b can be much larger than the temperature so that α can be of the order of unity.

Equation (8) expresses the relative change of the rates due to the change of the number of molecules in the left and right wells. To find the individual rates, we use the fact that reversing all coordinates also interchanges the rates. That is, we impose that r_{RL} must be equal to r_{LR} if we at the same time transform $q_i \rightarrow -q_i$, $\sigma \rightarrow -\sigma$, and $\omega_{L/R} \rightarrow \omega_{R/L}$. The control parameter α retains its value in this parity transformation. By using this equality in Eq. (8) and expanding the exponent of r_{LR} in the powers of Δ , we find that

$$r_{LR}^j = C \exp\left(\alpha \frac{g_j}{\sqrt{\langle g^2 \rangle}} \Delta + f\right), \quad (9)$$

where f is a function of Δ that stays invariant in the parity transformation. A few examples of such functions are Δ^2 and $\sigma\Delta$. C is a constant that describes a state-independent cavity-induced modification that may be acquired in, e.g., the transition state theory. Here, we assume that such modifications are small and $C = 1$. The function f , although not forbidden by the symmetry, we neglect as there is no clear physical origin for such terms. That is, we set $f = 0$. In this case, $r_{RL}^j = 1/r_{LR}^j$.

Next, we use Eq. (8) to evaluate the stationary state of the macroscopic system. The separate rate modifications (9) allow for a continuous-time Markov chain simulation of Eq. (1) from which dynamics can also be investigated and compared to an analytical approach [27, 36].

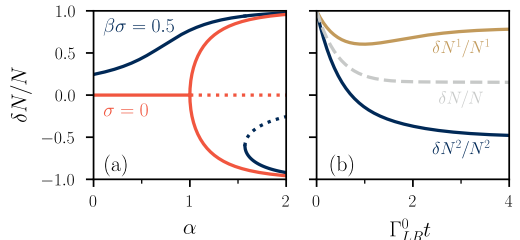


FIG. 2. (a) Steady state solutions of Eq. (2) exhibiting bifurcation for equal couplings. The dotted line represents an unstable solution whereas the solid lines are stable; the average tends to one of the stable solutions after a long time. (b) Phase separation of a system that is divided into two equally large partitions ($N^1 = N^2 = N/2$) with couplings related by $g_1 = -2g_2$. The solid lines represent the dynamics of the partitions alone whereas the dashed line describes the dynamics of the full system. Here, $\Gamma_{LR}^0 = \Gamma_{RL}^0$, $\alpha = 1.3$ and $\sigma = 0$.

Equal coupling strengths. We illustrate some qualitative consequences of the parametric rate modifications by taking a simplifying limit of identical couplings as in [32]; we set $g_j = g_0$ for all j . In this case, the transition rates become independent of the molecule in question. The set of rate equations can be mapped to a master equation describing the probability to find exactly N_L molecules in the left well. Interestingly, a similar state-dependent master equation has been used to model the formation of time crystals in magneto-optical traps [37]. We confirm numerically that such a master equation and the macroscopic rate equation (2) produce the same results as long as $N \gg 1$ [27].

We find the stationary state of the full N molecule system by inserting Eq. (8) into the macroscopic rate equation (2) together with $\frac{d}{dt} N_L = 0$. It gives

$$\frac{\delta N}{N} = \tanh\left(\beta \frac{\sigma}{2} + \alpha \frac{\delta N}{N}\right). \quad (10)$$

The solutions for δN determine the long-time behaviour of the macroscopic system.

First, let us consider $\sigma = 0$. If there is no coupling to light, the only stationary state is $N_L = N_R = N/2$ due to the left/right symmetry. For small values of $\alpha = 2P\beta E_b$, there is no change to this stationary state. However, as soon as $\alpha > 1$, we find two new stationary states while the state $N_L = N_R$ becomes unstable. The stationary states are represented in Fig. 2(a) as a function of the control parameter α . As this configuration is possible only if the coupling is large enough, we call it the cavity-induced bifurcation of the stationary state.

The cavity-induced bifurcation remains in the presence of a finite bias σ . However, the critical value of α increases as σ increases. For a very large bias $\beta\sigma \gg \alpha$, all the systems eventually end up in the right well which is

lower in energy. This is expected, as biasing the potential pushes the molecules towards the right well whereas the attractive interaction tries to keep the molecules in the same well. Before the bifurcation, one can also see the effect of the cavity-mediated attraction in that more molecules can be found in the right well than without the cavity. This seems as if the cavity increased the potential bias.

The mere state-dependent light-matter coupling — caused by a nonlinear $d_i(q_i)$ — may bias the polaritonic system. Similar to a potential bias, the molecules prefer the state with the larger coupling strength even with a single stationary state, and the larger the coupling difference, the larger the critical value of α [27].

Effect of coupling strength distribution. If there is only a partial control of the coupling constants as in polaritonic chemistry, one must include the variation of the couplings. We argue that this can but does not necessarily remove the cavity induced effects. Especially, the role of the average $\langle g \rangle$ is important. This average is independent of the optically observed Rabi splitting which is proportional to $\sqrt{N \langle g^2 \rangle}$ [12–14, 38, 39] and hence does not depend on the sign of the individual g_j 's.

The order parameter Δ determines the individual rates in Eq. (8). If we consider a partition of the N molecules such that all molecules within the partition share the same coupling constant g_j , they also share the same transition rates $\Gamma_{\mu\nu}^j$. Macroscopic rate equations similar to Eq. (2) can be derived for each partition but deriving a closed-form differential equation for Δ is impossible. Consequently, the full macroscopic rate equation cannot be evaluated. However, the stationary states of the partitions can be solved in terms of Δ . This leads to a self-consistency equation [27]

$$\Delta = \left\langle \frac{g}{\sqrt{\langle g^2 \rangle}} \tanh \left(\beta \frac{\sigma}{2} + \alpha \frac{g}{\sqrt{\langle g^2 \rangle}} \Delta \right) \right\rangle \quad (11)$$

whose solution can be used to find

$$\frac{\delta N}{N} = \left\langle \tanh \left(\beta \frac{\sigma}{2} + \alpha \frac{g}{\sqrt{\langle g^2 \rangle}} \Delta \right) \right\rangle \quad (12)$$

given a distribution of coupling constants g .

We specifically discuss the case $\sigma = 0$. By expanding Eq. (11) to the third order in Δ , one finds the solutions $\Delta \propto \pm \sqrt{\alpha - 1}$ and $\Delta = 0$. Thus, $\alpha = 1$ is the critical value for the bifurcation of the order parameter Δ . This agrees with Fig. 2 in which $\Delta = \delta N/N$. At the same time, Eq. (12) may be linearized giving $\delta N \propto \langle g \rangle \Delta$. Whenever $\langle g \rangle = 0$, we find $\delta N = 0$ or $N_L = N_R$. Thus, even if Δ bifurcates, it is possible that no change in the macroscopic state is seen.

The bifurcation of Δ indicates formation of a new polaritonic phase; the coupling constants g_j and the corresponding modes q_j become strongly correlated. This is

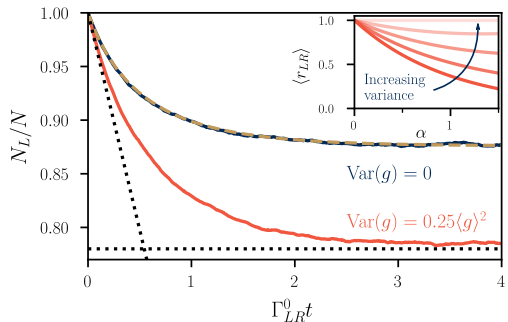


FIG. 3. Kinematics for different Gaussian distributions of coupling constants g_j . The other parameters are as in Fig. 2(b). The solid lines are obtained by the Markov chain simulation of 1000 molecules averaged over 100 realizations, the dashed line by evaluating Eq. (2), while the dotted black lines represent both the stationary state [Eqs. (11)–(12)] and the initial behaviour [Eq. (13)]. Inset: The rate modification in the initial state $N_L = N$ [Eq. (13)] as a function of α . From bottom to top, the different lines are obtained by setting $\langle g \rangle^2 = c \langle g^2 \rangle$ with $c = 1, 0.75, 0.5, 0.25, 0$.

exemplified in Fig. 2(b) in a simple case of two equally large partitions with two different couplings. The partitions have distinctly different dynamical behaviors and, in the stationary state, the molecules are found mostly in the right well for one partition and in the left well for the other. Such a correlation may be observed even if all the couplings are different [27].

Finally, let us consider the dynamics of thermalization, i.e., reaction kinematics. To this end, consider an experiment where every molecule is initialized in the left well (“reactant”) and, at a time t later, the percentage of the molecules in the right well (“product”) is measured. The thermalization (or reaction) rate is initially controlled by Γ_{LR} alone. Averaging over Eq. (9), this initial rate is modified from Γ_{LR}^0 by a factor

$$\langle r_{LR} \rangle \approx \exp \left(-\alpha \frac{\langle g \rangle^2}{\langle g^2 \rangle} + \frac{\alpha^2 \langle g \rangle^2}{2 \langle g^2 \rangle} \left[1 - \frac{\langle g \rangle^2}{\langle g^2 \rangle} \right] \right) \quad (13)$$

in the leading order of $1/N$ and to the second order in the cumulant expansion [27]. This result is independent of the bias σ . In the inset of Fig. 3, we show the effect of α and the variance of the coupling distribution. The effective transition rate becomes always slower due to the presence of the cavity — the cavity is an inhibitor — and the effect is stronger the less varied the couplings are.

The agreement between our theoretical approach and the Markov chain simulation is shown in Fig. 3. For equal couplings, $\text{Var}(g) = 0$, we use the macroscopic rate equation (2) directly and the results are nearly indistinguishable. Our solutions for the stationary and transient behavior also agree well with the simulation.

To summarize, we have shown how a cavity-mediated interaction between molecules can cause a collective change in their stochastic behavior. The cavity may cause a slowdown of the thermalization rate of the full system and a bifurcation in the stationary state. The polaritonic effect depends on the number of molecules and the distribution of the light-matter couplings. The bifurcation can even show up as a phase separation without altering the macroscopic state. In polaritonic chemistry, our approach is straightforward to extend to studies of multiple cavity modes, molecular symmetries [40], and cavity-induced reaction selectivity [19]. Due to the ubiquitous nature of polaritonics, our results can be used to describe other systems such as electric circuits and cold atoms in optical traps.

We thank Mark Dykman, Jussi Toppari, and Gerrit Groenhof for the insightful discussions. This project was supported by the Magnus Ehrnrooth foundation and the Academy of Finland (project numbers 317118 and 321982).

* kalle.kansanen@gmail.com

- [1] C. Gardiner, *Stochastic methods: A handbook for the natural and social sciences*, 4th ed., Springer Series in Synergetics (Springer, Berlin, 2009).
- [2] N. G. Van Kampen, *Stochastic processes in physics and chemistry*, 3rd ed. (Elsevier, Oxford, 2007).
- [3] C. Castellano, S. Fortunato, and V. Loreto, Statistical physics of social dynamics, *Rev. Mod. Phys.* **81**, 591 (2009).
- [4] W. Weidlich, Physics and social science — the approach of synergetics, *Phys. Rep.* **204**, 1 (1991).
- [5] J. Schnakenberg, Network theory of microscopic and macroscopic behavior of master equation systems, *Rev. Mod. Phys.* **48**, 571 (1976).
- [6] M. F. Weber and E. Frey, Master equations and the theory of stochastic path integrals, *Rep. Prog. Phys.* **80**, 046601 (2017).
- [7] N. T. J. Bailey, A simple stochastic epidemic, *Biometrika* **37**, 193 (1950).
- [8] K. Rock, S. Brand, J. Moir, and M. J. Keeling, Dynamics of infectious diseases, *Rep. Prog. Phys.* **77**, 026602 (2014).
- [9] R. R. Nelson and S. G. Winter, *An Evolutionary Theory of Economic Change* (Harvard University Press, Cambridge, 1985).
- [10] A. Hastings, K. C. Abbott, K. Cuddington, T. Francis, G. Gellner, Y.-C. Lai, A. Morozov, S. Petrovskii, K. Scranton, and M. L. Zeeman, Transient phenomena in ecology, *Science* **361**, eaat6412 (2018).
- [11] P. Hänggi, P. Talkner, and M. Borkovec, Reaction-rate theory: fifty years after Kramers, *Rev. Mod. Phys.* **62**, 251 (1990).
- [12] F. J. Garcia-Vidal, C. Ciuti, and T. W. Ebbesen, Manipulating matter by strong coupling to vacuum fields, *Science* **373**, eabd0336 (2021).
- [13] F. Herrera and J. Owrutsky, Molecular polaritons for controlling chemistry with quantum optics, *J. Chem. Phys.* **152**, 100902 (2020).
- [14] R. F. Ribeiro, L. A. Martínez-Martínez, M. Du, J. Campos-Gonzalez-Angulo, and J. Yuen-Zhou, Polariton chemistry: controlling molecular dynamics with optical cavities, *Chem. Sci.* **9**, 6325 (2018).
- [15] J. Lather, P. Bhatt, A. Thomas, T. W. Ebbesen, and J. George, Cavity catalysis by cooperative vibrational strong coupling of reactant and solvent molecules, *Angew. Chem. Int. Ed.* **58**, 10635 (2019).
- [16] J. Lather and J. George, Improving enzyme catalytic efficiency by co-operative vibrational strong coupling of water, *J. Phys. Chem. Lett.* **12**, 379 (2020).
- [17] A. Thomas, J. George, A. Shalabney, M. Dryzhakov, S. J. Varma, J. Moran, T. Chervy, X. Zhong, E. Devaux, C. Genet, J. A. Hutchison, and T. W. Ebbesen, Ground-state chemical reactivity under vibrational coupling to the vacuum electromagnetic field, *Angew. Chem. Int. Ed.* **55**, 11462 (2016).
- [18] R. M. A. Vergauwe, A. Thomas, K. Nagarajan, A. Shalabney, J. George, T. Chervy, M. Seidel, E. Devaux, V. Torbeev, and T. W. Ebbesen, Modification of enzyme activity by vibrational strong coupling of water, *Angew. Chem. Int. Ed.* **58**, 15324 (2019).
- [19] A. Thomas, L. Lethuillier-Karl, K. Nagarajan, R. M. A. Vergauwe, J. George, T. Chervy, A. Shalabney, E. Devaux, C. Genet, J. Moran, and T. W. Ebbesen, Tilting a ground-state reactivity landscape by vibrational strong coupling, *Science* **363**, 615 (2019).
- [20] V. P. Zhdanov, Vacuum field in a cavity, light-mediated vibrational coupling, and chemical reactivity, *Chem. Phys.* **535**, 110767 (2020).
- [21] J. A. Campos-Gonzalez-Angulo and J. Yuen-Zhou, Polaritonic normal modes in transition state theory, *J. Chem. Phys.* **152**, 161101 (2020).
- [22] T. E. Li, A. Nitzan, and J. E. Subotnik, On the origin of ground-state vacuum-field catalysis: Equilibrium consideration, *J. Chem. Phys.* **152**, 234107 (2020).
- [23] D. S. Wang and S. F. Yelin, A roadmap toward the theory of vibrational polariton chemistry, *ACS Photon.* **8**, 2818 (2021).
- [24] M. V. Imperatore, J. B. Asbury, and N. C. Giebink, Reproducibility of cavity-enhanced chemical reaction rates in the vibrational strong coupling regime, *J. Chem. Phys.* **154**, 191103 (2021).
- [25] G. D. Wiesehan and W. Xiong, Negligible rate enhancement from reported cooperative vibrational strong coupling catalysis, *J. Chem. Phys.* **155**, 241103 (2021).
- [26] We use the term "rate equation" as it fits the context of the Letter. In other contexts, at least the names "Kolmogorov equation" and "master equation" have been used to describe the same approach.
- [27] Supplemental material available at URL. It contains additional references [41–48].
- [28] The quadratures are chosen so that the corresponding kinetic energy is $(p_x^2 + \sum_i p_i^2)/2$, i.e., all the information about polaritonics resides in the potential alone.
- [29] D. F. Walls and G. J. Milburn, *Quantum Optics* (Springer, Berlin, 2008).
- [30] R. Chikkaraddy, B. De Nijs, F. Benz, S. J. Barrow, O. A. Scherman, E. Rosta, A. Demetriadou, P. Fox, O. Hess, and J. J. Baumberg, Single-molecule strong coupling at room temperature in plasmonic nanocavities, *Nature* **535**, 127 (2016).
- [31] W. Ahn, I. Vurgaftman, A. D. Dunkelberger, J. C.

- Owrutsky, and B. S. Simpkins, Vibrational strong coupling controlled by spatial distribution of molecules within the optical cavity, *ACS Photon.* **5**, 158 (2018).
- [32] M. Tavis and F. W. Cummings, Exact solution for an N -molecule–radiation-field Hamiltonian, *Phys. Rev.* **170**, 379 (1968).
- [33] K. S. U. Kansanen, A. Asikainen, J. J. Toppari, G. Groenhof, and T. T. Heikkilä, Theory for the stationary polariton response in the presence of vibrations, *Phys. Rev. B* **100**, 245426 (2019).
- [34] G. Eliashberg, Interactions between electrons and lattice vibrations in a superconductor, *Sov. Phys. JETP* **11**, 696 (1960).
- [35] Note that E_b is typically larger than the true potential barrier energy that determines the transition rates $\Gamma_{\mu\nu}^0$ in the absence of the cavity.
- [36] The numerical simulation code and all plotting scripts are based on Python (especially, numpy-, scipy, and matplotlib-packages) and can be found at <https://gitlab.jyu.fi/jyucmt/prt2022>.
- [37] M.-S. Heo, Y. Kim, K. Kim, G. Moon, J. Lee, H.-R. Noh, M. I. Dykman, and W. Jhe, Ideal mean-field transition in a modulated cold atom system, *Phys. Rev. E* **82**, 031134 (2010).
- [38] B. S. Simpkins, K. P. Fears, W. J. Dressick, B. T. Spann, A. D. Dunkelberger, and J. C. Owrutsky, Spanning strong to weak normal mode coupling between vibrational and Fabry–Pérot cavity modes through tuning of vibrational absorption strength, *ACS Photon.* **2**, 1460 (2015).
- [39] P. Törmä and W. L. Barnes, Strong coupling between surface plasmon polaritons and emitters: a review, *Rep. Prog. Phys.* **78**, 013901 (2014).
- [40] Y. Pang, A. Thomas, K. Nagarajan, R. M. A. Ver-gauwe, K. Joseph, B. Patraha, K. Wang, C. Genet, and T. W. Ebbesen, On the role of symmetry in vibrational strong coupling: The case of charge-transfer complexation, *Angew. Chem. Int. Ed.* **59**, 10436 (2020).
- [41] S. Shin and H. Metiu, Nonadiabatic effects on the charge transfer rate constant: A numerical study of a simple model system, *J. Chem. Phys.* **102**, 9285 (1995).
- [42] J. Galego, C. Climent, F. J. Garcia-Vidal, and J. Feist, Cavity Casimir-Polder forces and their effects in ground-state chemical reactivity, *Phys. Rev. X* **9**, 021057 (2019).
- [43] X. Li, A. Mandal, and P. Huo, Cavity frequency-dependent theory for vibrational polariton chemistry, *Nat. Commun.* **12**, 1 (2021).
- [44] J. George, T. Chervy, A. Shalabney, E. Devaux, H. Hiura, C. Genet, and T. W. Ebbesen, Multiple Rabi splittings under ultrastrong vibrational coupling, *Phys. Rev. Lett.* **117**, 153601 (2016).
- [45] J. A. Zasadzinski, R. Viswanathan, L. Madsen, J. Garnæs, and D. K. Schwartz, Langmuir-Blodgett films, *Science* **263**, 1726 (1994).
- [46] J. J. Gooding and S. Ciampi, The molecular level modification of surfaces: from self-assembled monolayers to complex molecular assemblies, *Chem. Soc. Rev.* **40**, 2704 (2011).
- [47] T. Orlando, J. Mooij, L. Tian, C. H. Van Der Wal, L. Levitov, S. Lloyd, and J. Mazo, Superconducting persistent-current qubit, *Phys. Rev. B* **60**, 15398 (1999).
- [48] A. Kruckenhauser, L. M. Sieberer, L. De Marco, J.-R. Li, K. Matsuda, W. G. Tobias, G. Valtolina, J. Ye, A. M. Rey, M. A. Baranov, and P. Zoller, Quantum many-body physics with ultracold polar molecules: Nanostructured potential barriers and interactions, *Phys. Rev. A* **102**, 023320 (2020).

Supplemental Material for “Cavity-induced bifurcation in classical rate theory”

Kalle S. U. Kansanen¹ and Tero T. Heikkilä¹

¹*Department of Physics and Nanoscience Center, University of Jyväskylä,
P.O. Box 35 (YFL), FI-40014 University of Jyväskylä, Finland*

(Dated: August 5, 2022)

This supplement is organized as follows: First, we calculate the stationary states of a polaritonic potential in Section I. Then, we use these results to obtain the transition rates using the detailed balance in Section II. In this section, the cumulant expansion of the transition rates is also presented. In Section III, we derive the self-consistency equation for the order parameter Δ of the polaritonic system. Section IV discusses a special case of the polaritonic model, that of equal couplings. In this case, the rate equation approach presented in the main text can be mapped to a master equation. The continuous-time Markov chain simulation method is presented in Section V. We then show some consequences of state-dependent light-matter coupling, caused by a nonlinear dipole moment, in Section VI using a numerical example. Finally, in Section VII, we discuss possible realizations of the cavity-induced bifurcation. We discuss the specific experimental details of polaritonic chemistry in a detailed manner, present an electric circuit model using flux qubits, and briefly discuss the possibilities of cold atoms.

I. CALCULATION OF THE STATE-DEPENDENT POTENTIAL ENERGY

Here, we present how we calculate the potential energies of the classical states, starting from the total potential

$$V_{\text{tot}} = \sum_{i=1}^N V(q_i) + \frac{1}{2}\omega_c^2 x^2 + \sum_{i=1}^N d_i(q_i)x, \quad (\text{S1})$$

where $V(q_i)$ is a bistable potential and $d_i(q_i)$ characterizes the dipole moment of the molecule j projected on the polarization vector of the cavity mode. We point out that the following calculation is very similar to the Caldeira–Leggett model except that the typical bath of harmonic oscillators is replaced by a single mode. Consequently, instead of dissipation, integration over the cavity mode x leads to effective interaction between the molecular coordinates q_i .

First, we solve the stationary points dictated by the conditions $\partial_x V_{\text{tot}} = 0 = \partial_{q_i} V_{\text{tot}}$. We work here in the harmonic approximation, assuming that the coupling to the cavity quadrature x induces a small change in the positions of the stationary points q_i^* which fulfill $\partial_{q_i} V(q_i)|_{q_i=q_i^*} = 0$. We choose the coordinate system so that $q_i^* = \pm a/2$ without the presence of the cavity field. Thus, a is the distance between the (local) minimum points. To characterize the displacement of the minimum points, we introduce a variable $\delta q_i = q_i - \frac{a}{2}\text{sign}(q_i)$. We can now write the potential in the harmonic approximation as

$$V(q_i) \approx -\frac{\sigma}{2}\text{sign}(q_i) + \frac{1}{2}\omega_i^2 \delta q_i^2, \quad (\text{S2})$$

where σ represents the energy difference between the left and right well and ω_i^2 is a shorthand notation for

$$\omega^2(q_i) = \frac{\omega_R^2 + \omega_L^2}{2} + \frac{\omega_R^2 - \omega_L^2}{2}\text{sign}(q_i), \quad (\text{S3})$$

which alternates between ω_L^2 and ω_R^2 depending on the sign of q_i . Similarly, we assume that the dipole moment can be linearized near $q = \pm a/2$

$$d_i(q_i) \approx \lambda_i^2 \left[\delta q_i + \frac{q_0}{2}\text{sign}(q_i) \right], \quad (\text{S4})$$

where $\lambda_i^2 \equiv \lambda_i^2[\text{sign}(q_i)]$ describes the strength of the light-matter coupling and q_0 additionally characterizes the difference in the dipole moment between right and left well. The coupling constants λ_i^2 can generally vary both due to the state, similar to the frequencies ω_i^2 , and due to disorder in the polarization vectors and positions. The results of the main paper are obtained by replacing $q_0 = a$ and $\lambda_i^2 \rightarrow \sqrt{\omega_m \omega_c} g_i$ where g_i is independent of the molecular state. The presence of the square root term is due to the choice of coordinates q_i and x so that, for a harmonic potential $V(q_i)$, we retain the light-matter interaction with constants g_i as $g_i(a^\dagger + a)(b_i^\dagger + b_i)$ after quantization as in the Dicke model.

As the derivative of the sign function $\text{sign}(q_i)$ vanishes everywhere except at $q_i = 0$, and q_i obtains values only near $\pm a/2$ by assumption, we find

$$0 = \frac{\partial V_{\text{tot}}}{\partial x} = \omega_c^2 x + \sum_i \lambda_i^2 \left[\delta q_i + \frac{q_0}{2} \text{sign}(q_i) \right], \quad (\text{S5a})$$

$$0 = \frac{\partial V_{\text{tot}}}{\partial q_i} = \omega_i^2 \delta q_i + \lambda_i^2 x. \quad (\text{S5b})$$

This set of equations can be solved by noting that Eq. (S5a) depends on $Q = \sum_i \lambda_i^2 \delta q_i$ and, at the same time, we can derive from Eq. (S5b) an equation

$$0 = Q + \sum_i \frac{\lambda_i^4}{\omega_i^2} x \quad (\text{S6})$$

for the collective variable Q . Inserting the solution of Q in terms of x to Eq. (S5a) gives

$$x = -\frac{\frac{q_0}{2} \sum_i \lambda_i^2 \text{sign}(q_i)}{\omega_c^2 - \sum_i \frac{\lambda_i^4}{\omega_i^2}} = -\frac{\omega_m^2}{\sqrt{\langle \lambda^4 \rangle}} P \Delta \frac{q_0}{2}. \quad (\text{S7})$$

In the latter equality, we introduce the useful notations from the main text — which we gather here for convenience

$$\omega_m^2 = \frac{\omega_R^2 + \omega_L^2}{2}, \quad \langle \lambda^4 \rangle = \frac{1}{N} \sum_i \lambda_i^4, \quad P = \frac{N \langle \lambda^4 \rangle}{\omega_c^2 \omega_m^2 - \sum_i \frac{\omega_m^2}{\omega_i^2} \lambda_i^4}, \quad \Delta = \frac{1}{N} \sum_i \frac{\lambda_i^2}{\sqrt{\langle \lambda^4 \rangle}} \text{sign}(q_i). \quad (\text{S8})$$

Though, here, the coupling λ_i^2 still depends on the state of the molecule i . The solution of x allows for the solutions of individual δq_i which are simply $\delta q_i = -\frac{\lambda_i^2}{\omega_i^2} x$. Note that the solution is consistent with the harmonic approximation as long as the dimensionless constant P is well below unity and $|\omega_L^2 - \omega_R^2| \ll (1 - P)(\omega_L^2 + \omega_R^2)$.

Finding the potential minima is now straightforward. We insert the obtained local minimum points into the expression of total potential V_{tot} . The potential energies found in this way still depend on the state of the system in the sense that the variables $\text{sign}(q_i)$ are not fixed. Within the harmonic approximation it holds that $|\delta q_i| < a/2$ and it is clear that the signs of q_i indicate whether the system is in the left ($q_i < 0$) or right ($q_i > 0$) well. We find

$$\begin{aligned} V_{\text{tot}} &= -\frac{\sigma}{2} \delta N + \sum_{i=1}^N \frac{1}{2} \omega_i^2 \delta q_i^2 + \frac{1}{2} \omega_c^2 x^2 + \sum_{i=1}^N \lambda_i^2 x \left[\delta q_i + \frac{q_0}{2} \text{sign}(q_i) \right] \\ &= -\frac{\sigma}{2} \delta N + \frac{1}{2} \left(\omega_c^2 - \sum_i \frac{\lambda_i^4}{\omega_i^2} \right) x^2 + \frac{q_0}{2} x \sum_{i=1}^N \lambda_i^2 \text{sign}(q_i) \\ &= -\frac{\sigma}{2} \delta N - \frac{N}{2} \omega_m^2 \left(\frac{q_0}{2} \right)^2 P \Delta^2, \end{aligned} \quad (\text{S9})$$

which matches with the result of the main text when $E_b = \frac{1}{2} \omega_m^2 \left(\frac{q_0}{2} \right)^2$ is identified in the latter term. Since E_b has the dimension of energy, we call it the effective potential barrier.

In the main text and the remainder of this supplement, we assume, for simplicity, that the dipole moment function $d_i(q_i)$ can be written as a linear function over the whole range of q_i . Physically, this assumption means that both states are equally coupled to the cavity. The condition is easily relaxed to investigate a multitude of possible polaritonic systems — we briefly discuss one example in Sec. VI. In terms of the model at hand, it means that $d_i(q_i) = \lambda_i^2 q_i$ where λ_i^2 is a constant for each molecule i . Thus, the average $\langle \lambda^4 \rangle$ is state independent and, as seen in the next section, P can be regarded as a constant in the lowest order of the light–matter coupling. In addition, if also $\omega_L = \omega_R$, E_b simply describes the potential energy $V(q = 0)$ within the harmonic approximation since $q_0 = a$.

II. DETAILED BALANCE AND CUMULANT EXPANSION

The detailed balance states that the transition rates must obey

$$\frac{\Gamma_{LR}^j}{\Gamma_{RL}^j} = \exp\{\beta[V_{\text{tot}}(q_j < 0) - V_{\text{tot}}(q_j > 0)]\} = \exp(\beta \delta V_{\text{tot}}) \quad (\text{S10})$$

in order for the system to thermalize to the Boltzmann distribution. The above notation refers to the other systems being fixed while j th system moves from one well to another. We assume here that the light-matter coupling is state independent.

First, we calculate the difference in P due to one system moving. It is useful to denote $K = \frac{1}{N} \sum_i \frac{\lambda_i^4}{\langle \lambda^4 \rangle} \frac{\omega_m^2}{\omega_i}$. Note that $K = 1$ if $\omega_L = \omega_R$. Thus, we formally can expand P around $K = 1$ which leads to

$$P = \sum_{n=0}^{\infty} \left(\frac{N \langle \lambda^4 \rangle}{\omega_c^2 \omega_m^2 - N \langle \lambda^4 \rangle} \right)^{n+1} (K - 1)^n \equiv \sum_{n=0}^{\infty} P_0^{n+1} (K - 1)^n. \quad (\text{S11})$$

Since we assume that $N \langle \lambda^4 \rangle / (\omega_c^2 \omega_m^2)$ is small and $P_0 \ll 1$, $P \approx P_0 + P_0^2 (K - 1)$ to a good approximation. The higher powers of K also scale in the powers of $1/N$. Finding the difference due to moving one system is now straightforward and results in

$$\delta P \approx \frac{1}{N} P^2 \frac{\lambda_j^4}{\langle \lambda^4 \rangle} \left(\frac{\omega_m^2}{\omega_L^2} - \frac{\omega_m^2}{\omega_R^2} \right) + \mathcal{O}(P^3/N^2). \quad (\text{S12})$$

In the main text, we neglect the second order contribution of P and, thus, the state dependency of P .

Since P can be regarded as a constant in the calculation of the difference in potential energies, the calculation simplifies greatly and we obtain

$$\delta V_{\text{tot}} = \sigma - N E_b P \left[\left(\frac{-\frac{\lambda_j^2}{\sqrt{\langle \lambda^4 \rangle}} + \sum_{i \neq j} \frac{\lambda_i^2}{\sqrt{\langle \lambda^4 \rangle}} \text{sign}(q_i)}{N} \right)^2 - \left(\frac{\frac{\lambda_j^2}{\sqrt{\langle \lambda^4 \rangle}} + \sum_{i \neq j} \frac{\lambda_i^2}{\sqrt{\langle \lambda^4 \rangle}} \text{sign}(q_i)}{N} \right)^2 \right] \quad (\text{S13})$$

$$= \sigma + 4 P E_b \frac{\lambda_j^2}{\sqrt{\langle \lambda^4 \rangle}} \frac{\sum_{i \neq j} \frac{\lambda_i^2}{\sqrt{\langle \lambda^4 \rangle}} \text{sign}(q_i)}{N}. \quad (\text{S14})$$

However, we still have to connect this to what would be observed in experiments which deal with macroscopic numbers of N .

With the value of δV_{tot} , the detailed balance states that

$$\frac{\Gamma_{LR}^j}{\Gamma_{RL}^j} = \frac{\Gamma_{LR}^0}{\Gamma_{RL}^0} \frac{r_{LR}^j}{r_{RL}^j} = e^{\beta \sigma} \exp \left(4 P \beta E_b \frac{\lambda_j^2}{\sqrt{\langle \lambda^4 \rangle}} \frac{\sum_{i \neq j} \frac{\lambda_i^2}{\sqrt{\langle \lambda^4 \rangle}} \text{sign}(q_i)}{N} \right). \quad (\text{S15})$$

Here, one can readily identify the ratio of the rate modification factors which is the latter exponent.

Now, we can appeal to symmetry: if we interchange left and right everywhere in the potential $V(q)$, the rate modifications should remain the same. Thus,

$$r_{LR}^j(\{q_i\}; \sigma, \omega_L^2, \omega_R^2) = r_{RL}^j(\{-q_i\}; -\sigma, \omega_R^2, \omega_L^2). \quad (\text{S16})$$

where $\{q_i\}$ refers to the set of all q_i 's. One can confirm that P remains invariant in this transformation (the relevant quantity in P is $\sum_i \lambda_i^4 \frac{\omega_m^2}{\omega_i^2} = \sum_i \lambda_i^4 \frac{\omega_m^2}{1 + (\omega_R^2 - \omega_L^2) \text{sign}(q_i) / (\omega_R^2 + \omega_L^2)}$). Following the line of deduction as in the main text, we can thus write

$$r_{LR}^j = \exp \left(2 P \beta E_b \frac{\lambda_j^2}{\sqrt{\langle \lambda^4 \rangle}} \frac{\sum_{i \neq j} \frac{\lambda_i^2}{\sqrt{\langle \lambda^4 \rangle}} \text{sign}(q_i)}{N} \right) \quad (\text{S17})$$

and $r_{RL}^j = 1/r_{LR}^j$. We may also replace the sum in this expression with Δ as the error made is of the order of $1/N$.

Next, we treat the coupling constants λ_j^2 as independent random variables — instead of considering them to have some fixed values — and average the detailed balance relation over all realizations. Furthermore, we assume that the sign of q_j is independent of λ_j^2 which does not necessarily hold for a dynamical system but may be assumed to hold for the initial state, for instance. The average of the exponent gives rise to the cumulant expansion. To calculate the

cumulants, we first calculate the raw moments of the term in the exponent. Taking only the leading order in $1/N$, we find

$$\left\langle \left[\frac{\lambda_j^2}{\sqrt{\langle \lambda^4 \rangle}} \frac{\sum_{i \neq j} \frac{\lambda_i^2}{\sqrt{\langle \lambda^4 \rangle}} \text{sign}(q_i)}{N} \right]^n \right\rangle \approx \left\langle \left(\frac{\lambda^2}{\sqrt{\langle \lambda^4 \rangle}} \right)^n \right\rangle \left[\frac{\langle \lambda^2 \rangle}{\sqrt{\langle \lambda^4 \rangle}} \frac{\delta N}{N} \right]^n. \quad (\text{S18})$$

Since all cumulants may be expressed using only raw moments in a specific polynomial manner [1], we can deduce from this result that the n th cumulant K_n of the term in the exponent of r_{LR}^j is

$$K_n = \left[2P\beta E_b \frac{\langle \lambda^2 \rangle}{\sqrt{\langle \lambda^4 \rangle}} \frac{\delta N}{N} \right]^n K_n \left(\lambda^2 / \sqrt{\langle \lambda^4 \rangle} \right). \quad (\text{S19})$$

That is, we have related the cumulants of the sum to the cumulant of its individual elements. Using the cumulant expansion to second order, we have that

$$\ln \langle r_{LR} \rangle \approx 2P\beta E_b \frac{\langle \lambda^2 \rangle^2}{\langle \lambda^4 \rangle} \frac{\delta N}{N} + \frac{1}{2} (2P\beta E_b)^2 \frac{\langle \lambda^2 \rangle^2}{\langle \lambda^4 \rangle} \left[1 - \frac{\langle \lambda^2 \rangle^2}{\langle \lambda^4 \rangle} \right] \left(\frac{\delta N}{N} \right)^2. \quad (\text{S20})$$

Here, the first term follow from the average and the second from the variance. We emphasize that the approximation is valid when $N \gg 1$. The cumulant expansion is otherwise exact if the distribution of λ_j^2 's is Gaussian; only the first two cumulants may be finite for a Gaussian distribution.

III. DERIVATION OF THE SELF-CONSISTENCY EQUATION

One can derive a self-consistency equation for Δ in the stationary state. Let us assume that, even though there are N systems, there are $M < N$ different values for the coupling constants λ_j^2 . Let us denote $c_j = \frac{\lambda_j^2}{\sqrt{\langle \lambda^4 \rangle}}$ and $\alpha = 2P\beta E_b$ here, for brevity. Then, if there are $N^j, j \in \{1, 2, \dots, M\}$ subsystems ($N = \sum_j N^j$) with the constant c_j , we can write $\Delta = \frac{1}{N} \sum_j c_j (N^j - 2N_L^j)$ where N_L^j is the number of systems in the left well having a coupling constant c_j . Following the main text, we assume that we can write for each subsystem j the macroscopic equation

$$\frac{d}{dt} N_L^j = -\Gamma_{LR}^j N_L^j + \Gamma_{RL}^j (N^j - N_L^j). \quad (\text{S21})$$

We assume that each subsystem has a stationary value. We may then solve, using Eq. (S15),

$$\frac{N_L^j}{N^j} = \frac{1}{1 + \exp(\beta\sigma + 2\alpha c_j \Delta)}. \quad (\text{S22})$$

Inserting this solution to the definition of Δ and δN leads to

$$\frac{\delta N}{N} = 1 - 2 \frac{\sum_j N_L^j}{N} = \sum_j \frac{N^j}{N} \tanh\left(\beta \frac{\sigma}{2} + \alpha c_j \Delta\right) \equiv \left\langle \tanh\left(\beta \frac{\sigma}{2} + \alpha c \Delta\right) \right\rangle, \quad (\text{S23})$$

$$\Delta = \sum_j \frac{c_j}{N} (N^j - 2N_L^j) = \sum_j \frac{N^j}{N} c_j \tanh\left(\beta \frac{\sigma}{2} + \alpha c_j \Delta\right) \equiv \left\langle c \tanh\left(\beta \frac{\sigma}{2} + \alpha c \Delta\right) \right\rangle. \quad (\text{S24})$$

In both equations, we identified the structure of $\sum_j (N^j/N) f(c_j)$ as an average over the distribution of c 's which follows from the fact that there are exactly N^j values of c_j . In the limit $N \rightarrow \infty$, we may construct a continuous distribution of the coupling constants which we use here as an approximation for systems of finite size.

It should be noted that we treat Δ and δN as numbers, not stochastic variables, even though the underlying stochastic processes determine their realizations and the possible values of Δ are constrained by the distribution of the coupling constants.

Here, we have neglected the possible variation of α with the macroscopic state. This arises from the variation of P , as discussed in Section II. In principle, this is remedied by including an equation for $\alpha = \alpha(\Delta)$ and solving all three equations self consistently. It should be noted that the variation of P with the macroscopic state is a second order effect in P and, thus, one should also calculate δV_{tot} to the same order.

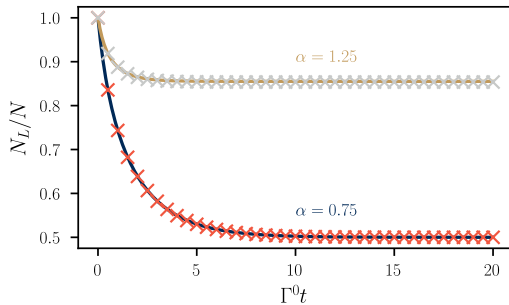


FIG. S1. Comparison of the macroscopic rate equation (solid lines) and master equation (crosses). Here, $\Gamma_{LR}^0 = \Gamma_{RL}^0 = \Gamma^0$ and $N = 1000$.

IV. RELATION TO THE FULL MASTER EQUATION OF THE N MOLECULE SYSTEM

If all the coupling constants g_j are equal, the potential difference δV_{tot} is independent of the system index j . In this case, the full N molecule system is readily described by the probability $P(N_L)$ to find N_L systems in the left well. The master equation for these probabilities reads as

$$\frac{d}{dt}P(N_L) = \mu_{N_L+1}P(N_L+1) + \nu_{N_L-1}P(N_L-1) - (\mu_{N_L} + \nu_{N_L})P(N_L), \quad (\text{S25})$$

where $\mu_M = M\Gamma_{LR}^0 r_{LR}(M)$ describes the removal rate of particles from the left well to the right well and $\nu_M = (N-M)\Gamma_{RL}^0 r_{RL}(M)$ the inverse process. Now, the expectation value of N_L is given by $\langle N_L \rangle = \sum_{N_L} N_L P(N_L)$. Using this definition, one can derive from the master equation an equation for the average as

$$\frac{d}{dt}\langle N_L \rangle = -\Gamma_{LR}^0 \langle r_{LR} N_L \rangle + \Gamma_{RL}^0 \langle r_{RL} (N - N_L) \rangle. \quad (\text{S26})$$

This matches exactly to the macroscopic rate equation presented in the main text if $\langle r_{LR} N_L \rangle = \langle r_{LR} \rangle \langle N_L \rangle$ and $\langle r_{RL} (N - N_L) \rangle = \langle r_{RL} \rangle (N - \langle N_L \rangle)$, and the resulting rate modification factors may be understood as a function of the mean value of N_L only. Due to the non-linearity of the rate modifications, this can be used as a valid approximation only when the fluctuations of N_L are small compared to some characteristic scale given by the rate modifications.

This assumption can be checked numerically. First, we note that the transition rates are independent of time. The master equation (S25) can thus be written in a matrix form as $\partial_t \vec{P} = W \vec{P}$ where W is independent of time. Given an initial state $\vec{P}(t=0)$, we formally have $\vec{P}(t) = e^{Wt} \vec{P}(t=0)$. The numerical problem is then to calculate the matrix exponential e^{Wt} . Fig. S1 shows that the macroscopic rate equation and the master equation produces the same mean behavior for N_L as N is large enough.

We note that even though the rate equations are state dependent and consequently non-linear, the macroscopic behaviour fits well to the typical exponential behaviour $N_L(t) = N_L(\infty) + [N_L(0) - N_L(\infty)]e^{-\gamma t}$ with a suitable fitting constant γ . This observation seems to hold even when the variation of couplings is included which is possible by the numerical method presented in the next section.

V. NUMERICAL METHOD

Here, we shortly describe the Markov chain algorithm we use in this work. The main motivation is to simulate a set of rate equations

$$\frac{d}{dt}p_j = -\Gamma_{LR}^j p_j + \Gamma_{RL}^j (1 - p_j) \quad (\text{S27})$$

where $\Gamma_{\mu\nu}^j$ depend on the state of the system. In our formulation, these states are $s_j = \text{sign}(q_j) \in \{-1, +1\}$. The rate equation describes that in a small time step Δt , the probability to change the system from $s_j = -1$ to $s_j = +1$ is given by $\Gamma_{LR}^j \Delta t$ while the converse process has the probability $\Gamma_{RL}^j \Delta t$. The algorithm is as follows:

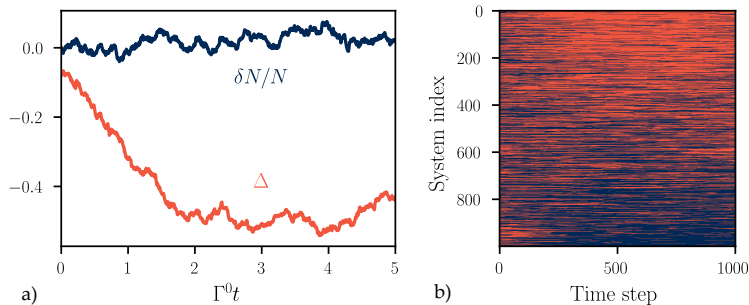


FIG. S2. A single realization of the Markov chain simulation for $N = 1000$ systems and 1000 time steps ($\Gamma^0 \Delta t = 0.01$). Other parameters are $\alpha = 1.3$, $\sigma = 0$, and $\Gamma_{LR}^0 = \Gamma_{RL}^0 = \Gamma^0$. Here, the coupling constants are sampled from a Gaussian distribution with zero mean. a) The time evolution of the quantities δN and Δ . As mentioned in the main text, Δ has a solution other than zero when $\alpha > 1$ while δN fluctuates around zero. b) As a visual representation, the states "left" and "right" are here represented by blue and orange, respectively, for each time step. Here, the different systems are indexed in the ascending order in the coupling constant (i.e. $g_1 \leq g_j \leq g_N$). The correlation becomes visible; the systems with largest values of coupling are predominantly found in the left well after a transient period.

1. Initialize the states $\{s_j\}$ at time t if necessary.
2. Draw N random numbers $u_j \sim \text{Uniform}(0, 1)$.
3. For each $j \in \{1, 2, \dots, N\}$ calculate $A_j = \Gamma_{LR}^j \Delta t$ if $s_j = -1$ and $A_j = \Gamma_{RL}^j \Delta t$ if $s_j = +1$ using the system state at time t .
4. For each $j \in \{1, 2, \dots, N\}$ compare u_j and A_j . If $u_j < A_j$, set the system state at time $t + \Delta t$ to be $s_j(t + \Delta t) = -s_j(t)$. Otherwise, set $s_j(t + \Delta t) = s_j(t)$.
5. Return to step 1 with $t \rightarrow t + \Delta t$.

Thus, when an appropriate amount of time steps is taken, we have a list of system states $s_j(t)$ at the chosen time points. These states can be used to calculate e.g. Δ or δN . This is exemplified in Fig. S2.

Practically, we choose N to be large enough so that there are no spurious $1/N$ effects and correspondence with the master equation approach holds. The time step we choose so that $\Gamma_{\mu\nu}^0 \Delta t$ is below or of the order of 1 percent. The initial state is chosen according to how many systems are wanted to be found in the left well and then the states are shuffled.

VI. EFFECT OF NONLINEAR DIPOLE MOMENT IN A SYMMETRIC POTENTIAL

We shortly describe how the physics changes when the assumption of equal light-matter coupling strength in both wells is lifted. Now, we have to specify two coupling constants λ_{iL}^2 and λ_{iR}^2 for each molecule in Eq. (S4) based on its state [$\text{sign}(q_i) = \pm 1$]. Furthermore, the average coupling on different states may differ, that is $\langle \lambda_L^2 \rangle \neq \langle \lambda_R^2 \rangle$. For simplicity, we assume here a symmetric potential with $\omega_L = \omega_R$ and $\sigma = 0$.

Physically, breaking the (anti)symmetry of the dipole moment leads to a preference or a lower energy on the state that is coupled more strongly to light. This is relevant for engineering state or reaction selectivity by vacuum fields. The bifurcation behavior presented in the main text also changes. Here, we investigate this numerically with the help of the Monte Carlo algorithm presented in the previous section.

The main mathematical difficulty in the case of a state-dependent light-matter coupling is that the quantity P is no longer a constant. For a linear dipole moment, this dimensionless parameter effectively describes the strength of the Rabi splitting. Now, assuming relatively small couplings and thus taking only the lowest order in $\sqrt{\langle \lambda^4 \rangle} / (\omega_c \omega_m)$, it is useful to write P in terms of an auxiliary constant $\tilde{\lambda}^4$

$$P = \frac{N \langle \lambda^4 \rangle}{\omega_c^2 \omega_m^2 - \sum_i \frac{\omega_m^2}{\omega_i^2} \lambda_i^4} \approx \frac{N \langle \lambda^4 \rangle}{\omega_c^2 \omega_m^2} = \frac{\langle \lambda^4 \rangle}{\tilde{\lambda}^4} \frac{N \tilde{\lambda}^4}{\omega_c^2 \omega_m^2} \equiv \frac{\langle \lambda^4 \rangle}{\tilde{\lambda}^4} \tilde{P}. \quad (\text{S28})$$

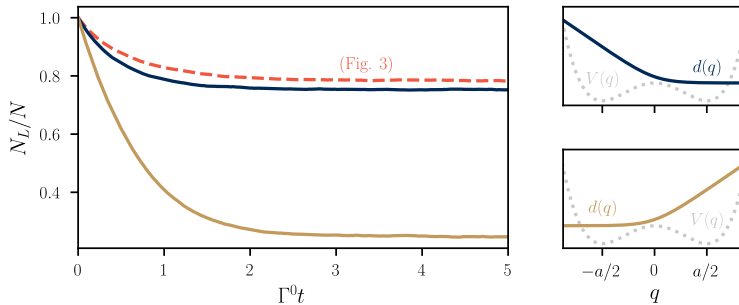


FIG. S3. Monte Carlo simulation of a polaritonic system with nonlinear dipole moments, schematized on the right side of the figure. The transition dipole moment vanishes on the right state in the blue line and on the left state in the brown line. The orange line from Fig. 3 is the dashed line here for reference. The simulation uses $N = 1000$ molecules averaged over 100 realizations, and $\Gamma_{LR}^0 = \Gamma_{RL}^0 = \Gamma^0$.

Recall that $\langle \lambda^4 \rangle$ depends on the state of the molecules as well. Now, \tilde{P} can characterize the total coupling strength if we choose, for instance, $\tilde{\lambda}^4 = (\langle \lambda_R^4 \rangle + \langle \lambda_L^4 \rangle)/2$ or simply $\tilde{\lambda}^4 = \langle \lambda_{L/R}^4 \rangle$.

The calculation of the energy difference between left and right states δV_{tot} follows as in Sec. II. In the lowest order of $1/N$, we find

$$\frac{\Gamma_{LR}^j}{\Gamma_{RL}^j} = e^{\beta \delta V_{\text{tot}}} = \exp \left[2\tilde{\alpha} \frac{\langle \lambda^4 \rangle}{\tilde{\lambda}^4} \frac{\lambda_{jL}^2 + \lambda_{jR}^2}{2\sqrt{\langle \lambda^4 \rangle}} \left(\Delta - \frac{\lambda_{jL}^2 - \lambda_{jR}^2}{2\sqrt{\langle \lambda^4 \rangle}} \Delta^2 \right) \right], \quad (\text{S29})$$

where $\tilde{\alpha} = 2\tilde{P}\beta E_b$ now functions as a control parameter. It is noteworthy that the nonlinearity of the dipole moment is connected with a Δ^2 -term in the energy difference. This term shows that the different light-matter coupling constants generate an effective energy gradient to the molecular states. Furthermore, the collective coupling always vanishes if the dipole moment is fully symmetric so that $\lambda_{jR}^2 = -\lambda_{jL}^2$.

Here, we concentrate on a numerical example, even though one could proceed with a similar kind of argumentation as in Sec. II. Let us choose a light-matter coupling that vanishes on one state and is finite on the other. How does the polaritonic system relax, if all the molecules are initially in the left state, and what is the stationary state? To further connect this setup to Fig. 3 in the main text, we choose $\tilde{\lambda}^4$ so that it is the larger one of $\langle \lambda_R^4 \rangle$ and $\langle \lambda_L^4 \rangle$, choose the couplings from a normal distribution with $\text{Var}(g) = 0.25 \langle g \rangle^2$ (in the description $\lambda_i^2 = \sqrt{\omega_m \omega_c} g_i$), and set $\tilde{\alpha} = 1.3$. That is, in the case in which only the molecules on the left state couple to light, the situation is initially the same as in Fig. 3 (orange line).

The result of the numerical simulation is plotted in Fig. S3. As expected, the initial evolution of the macroscopic state is very similar in the case where the left state couples to light as to when both states are coupled to light. The stationary state changes only in a minor way.

Much more interesting is the case where the coupling to light is on the right state only. Initially, there is no light-matter coupling and the polaritonic system starts to thermalize towards an even split between the states. This initial rate is similar to that without any coupling. The stationary state however changes notably as more of the molecules prefer the right state. This again shows the effective attractive interaction mediated by the cavity. Finally, because of symmetry in the potential and the mirror symmetry of the nonlinear dipole moment, the stationary states of these two plotted scenarios are related. One gets from one to the other by simply interchanging the labels for left and right.

Finally, we note that Eq. (S29) allows solving the stationary states analytically. This is the most straightforward in the case in which there is no variation in the left and right coupling constants, that is, $\lambda_{iL}^2 = \lambda_L^2$ and $\lambda_{iR}^2 = \lambda_R^2$. Focusing still on the symmetric potential, the relevant parameter is the ratio $\lambda_R^2/\lambda_L^2 = g_R/g_L$. The effect on the bifurcation diagram, comparing to Fig. 2(a) in the main text, is similar to having a bias in the potential as shown in Fig. S4. That is, the critical value of $\tilde{\alpha}$ at which the bifurcation happens increases as the ratio g_R/g_L deviates from unity. Similar to the effect of bias, there is a measurable effect before the critical value as more molecules are found in the state with the larger coupling.

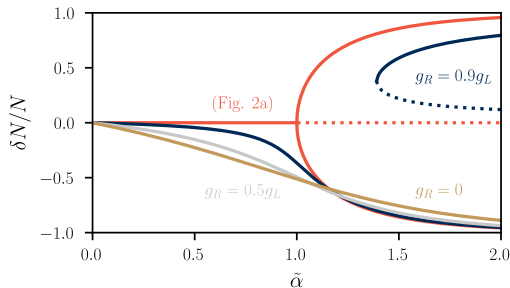


FIG. S4. Bifurcation diagram for a symmetric potential without any variation in the left and right light-matter couplings. Here, we fix $\lambda^4 = \lambda_L^4$ within $\tilde{\alpha}$ and the different curves represent different values of λ_R^2 .

VII. REALIZATIONS OF CAVITY-INDUCED BIFURCATION

A. Polaritonic chemistry

Let us discuss the validity range of the approach in the main text in the context of polaritonic chemistry. As we derive the rate constant modification from detailed balance, our results disregard quantum effects. That is, the temperature must be above a certain threshold frequency that is related to $\omega_c, \omega_L, \omega_R$ [2]. This limits the systems mostly to vibrational strong coupling where these frequencies are typically of the order of 100 meV and not in the range of several eV as in electronic strong coupling (at room temperature $k_B T \sim 25$ meV). More notably, we treat the molecules as one-dimensional systems and assume a constant bilinear coupling to the (single mode) cavity. We believe that even though this choice neglects many details of molecules used in recent experiments, it gives an important analytical insight which can be improved upon with specific molecular models.

We note that the potential $V(q)$ with $\sigma = 0$ and $\omega_L = \omega_R$ is similar to the ground state potential of the Shin-Metiu model describing proton-coupled electron transfer [3]. Recently, it has been used in other works in polaritonic chemistry [4, 5]. In these works, the typical barrier energy is of the order of 1 eV; although it depends on the exact choice of model parameters. Since the effective potential barrier E_b is typically larger than the barrier energy, our order of magnitude estimate is that $E_b/(k_B T)$ may range from tens to hundreds.

To identify the strong coupling, the Rabi splitting Ω must be large enough to be observed. This means that $\Omega \gtrsim (\kappa + \gamma)/2$ where κ and γ refer to the dissipation rates of the cavity and the molecular mode, respectively. We have assumed the collective strong coupling regime where $\Omega/\omega_m \sim 0.1$ leading to $P \sim 0.01$. Thus, all the results are given in the first order of P and higher order corrections are yet to be found. Experimentally, it has been shown that it is possible to reach the so-called ultrastrong coupling regime in vibrational strong coupling; $\Omega/\omega_m \approx 0.24$ in Ref. 6.

Therefore, the control parameter $\alpha = 2P\beta E_b$ can be of the order of unity in experiments of polaritonic chemistry. For example, if $P = 0.01$ and $\beta E_b = 100$, we have $\alpha = 2$. In the main text, we find that cavity induced bifurcation is possible only if $\alpha > 1$.

We emphasize the fact that the coupling constants can differ from molecule to molecule which, somewhat surprisingly, is often neglected in the seminal theoretical works [7]. To further complicate the picture, the couplings may truly be time dependent if the molecules can diffuse within the cavity. However, such time dependent variation is much faster than the typical reaction rates, and thus, we can deal with only the averages of coupling constants. There are at least two types of randomness in the couplings: 1) "orientation disorder" due to the varying directions of transition dipole moments with respect to the cavity polarization vector(s), and 2) "position disorder" due to the varying positions of the molecules within the cavity. These disorders have been shown and studied in several experiments, for instance, in plasmonic picocavities [8] and in optical cavities [9]. In the main text, we find that the average of the coupling constants determines the macroscopic properties of the N molecule polaritonic system, for instance the stationary state and the rate modification. The detailed understanding of these disorders is thus important.

It is speculated in Ref. 10 that the orientation disorder must be negligible in order to see polaritonic chemistry. This indeed corresponds to the rate modification analysis in the main text, as assuming that the transition dipole moments are distributed isotropically would lead to the average of the coupling constants being zero and leaving the rate unchanged. However, it is not clear to us what processes would cause the alignment of molecules in the experiments. There are fabrication techniques to construct such aligned molecular assemblies [11, 12] but they represent a departure from the microfluidistic cavity approach detailed in Ref. 10. We hope that our work could motivate theoretical and

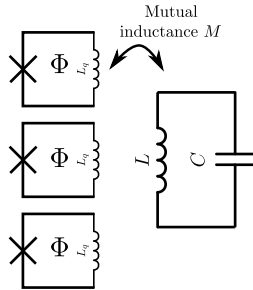


FIG. S5. Electronic circuit model of an LC oscillator coupled to a set of flux qubits, where the Josephson junctions are marked with the triangle. There is a flux $\Phi = h/(2e) + \delta\Phi$ applied across each loop.

experimental inquiries into this kind of disorder.

The effect of the positions of the molecules within the cavity has been investigated experimentally [9]. The experimental findings agree well with the current theoretical understanding presented here and in the main text. That is, local variations in the cavity field strength affect the couplings. We also know from Maxwell's equations that such vacuum electromagnetic fields may change sign as a function of position within the cavity. This is often neglected since observables such as the energy and the absorption/fluorescence spectrum are independent of the sign. Also, for a single molecule, the sign is always an irrelevant phase factor of the cavity field. The phase difference between different positions is important for the chemistry because one would expect that the molecules are distributed somewhat uniformly within the cavity. The average of the coupling constants should be zero for antisymmetric cavity modes and decreases as the order of the cavity mode is increased for symmetric modes. Thus, it would seem beneficial to limit the variation in the molecule positions by cavity design and/or using the lowest order cavity mode. The reader should be aware that this message is in contradiction with the published experiments in polaritonic chemistry (see main text for references); for instance, the second-order cavity mode was put in resonance with a vibrational mode in Ref. 13 and the tenth-order mode was used in Ref. 14. It is an intriguing possibility that some effects would be, in fact, caused by coupling to the highly detuned first cavity mode and, consequently, the interpretation of polaritonic chemistry as a resonant effect would be challenged.

In the presence of great position and orientation disorder, we expect no change in the rates. Nevertheless, if Rabi splitting is large enough and $\alpha > 1$, a phase separation based on the value of coupling constants is possible. If we imagine a case where we have somehow aligned the transition dipole moments and the relevant cavity mode is the second lowest order mode, the phase separation would manifest as a physical separation. The molecules on one side of the cavity would then go to another state than those on the other side. This could be achieved, alternatively, with two films of oriented dipole moments using the same measurement setup as in Ref. 9 so that the films are at the opposite sides of the cavity (that is, mirror-film-spacer-film-mirror).

B. Coupled anharmonic LC oscillators

Although our work was initially motivated by polaritonic chemistry, our generic stochastic model is applicable to a large variety of systems. Here we illustrate how similar physics could be studied in an ensemble of superconducting flux qubits all coupled to the same cavity. We also show how in this setup one can in principle realize the alternating sign of the couplings.

Consider the electronic circuit drawn in Fig. S5. It describes an LC circuit coupled via mutual inductance with N (ideally identical) flux qubits [15]. The figure depicts a simplified version of the flux qubit, but the idea can be generalized to the usually used configurations where the inductance L_q is replaced by several Josephson junctions. Such systems have two macroscopic quantum states corresponding to clockwise and counterclockwise persistent currents, used as the logical qubit states. When the flux $\Phi \approx h/2e[1 + f/(2\pi)]$, the flux qubit Hamiltonian is

$$H = \frac{\hat{Q}_q^2}{2C_q} + E_J \underbrace{[b\phi^2 + \cos(\phi - f)]}_{V(\phi)}. \quad (\text{S30})$$

Here \hat{Q}_q is the displacement charge operator of the capacitor with capacitance C_q . \hat{Q}_q is canonically conjugate with

the phase difference ϕ across the junction. They thus take the roles of canonical momentum and position in the electronic circuit. E_J is the Josephson energy of the junction and $b = 2\pi^2\hbar^2/(2eLE_J)$ is a dimensionless parameter characterizing the inductor with inductance L . For $f \ll \pi$ and $b < 0.5$, the effective potential $V(\phi)$ has two minima corresponding to the two directions of the persistent current. The relative bias between the minima can be controlled with f such that the two minima are degenerate for $f = 0$. For small b and f , the minima are around $\phi_{\pm} \equiv \frac{\pm\pi}{1+2b} + f$, and both have eigenfrequencies $\omega_L = \omega_R \approx \omega_p\sqrt{1+2b}$, where $\omega_p = 2e\sqrt{E_J/C_q}/\hbar$ is the Josephson plasma frequency. Then, the effective barrier height is $E_b = \frac{1}{2}E_J(1+2b)[(\phi_+ - \phi_-)/2]^2 = \frac{\pi^2}{2}\frac{E_J}{1+2b}$.

Flux qubits operate in the regime where the potential barrier between the states is low, $E_b \sim \hbar\omega_{L/R}$, and thereby the tunnel coupling is large, providing coherent oscillations of the quantum state between the two minima. This limit is reached when the charging energy $E_C = e^2/(2C_q)$ is not much smaller than the Josephson energy E_J . On the contrary, we assume $E_J \gg E_C$ and thereby a high barrier, such that the transitions between the minima are rare and mostly driven by thermal noise in the environment of the system.

In such systems, the mutual inductance coupling of the individual qubits to a common LC circuit has been used as a means to realize controllable coupling between the qubits, as they are tuned on and off resonance with each other [15]. However, there the resonance condition derives from the resonance of the qubit energy splitting, whereas we assume that the resonance is between the bistable energy minima. Let us then consider a mutual inductance coupling of the flux qubits to a common LC circuit. We model this coupling in the limit where the qubits are in one of their minima, in which case we describe them as LC oscillators. The Lagrangian of the system is thus

$$\begin{aligned} \mathcal{L} &= \frac{1}{2}L\dot{Q}_c^2 + \frac{1}{2}L_p \sum_{j=1}^N \dot{Q}_j^2 + \sum_{j=1}^N M_j \dot{Q}_j \dot{Q}_c - \frac{1}{2C}Q_c^2 - \frac{1}{2C_p} \sum_{j=1}^N Q_j^2 \\ &\equiv \frac{1}{2}\dot{\vec{Q}}^T \mathbf{L} \dot{\vec{Q}} - \frac{1}{2}\vec{Q}^T \mathbf{C}^{-1} \vec{Q}, \end{aligned} \quad (\text{S31})$$

where we have introduced capacitance C_p and inductance L_p such that $\omega_p = 1/\sqrt{L_p C_p}$ for the flux qubits. Note that this form of expression is possible because $\omega_L = \omega_R = \omega_p$; otherwise the state of the flux qubits affects the capacitance and inductance. The mutual inductance M_j can be characterized by a dimensionless parameter $k_j \in [-1, 1]$ so that $M_j = k_j\sqrt{LL_p}$. Here, one can understand the possibility of a negative k_j as a phase shift of the induced current; the sign depends on the details of the inductive coupling.

We define the conjugate momentum using the notation of the flux quantum $\Phi_0 = h/2e$ as

$$\frac{\Phi_0}{2\pi}\varphi_i = \frac{\partial \mathcal{L}}{\partial \dot{Q}_i} = \begin{cases} L\dot{Q}_c + \sum_j M_j \dot{Q}_j, \\ L_p \dot{Q}_i + M_i \dot{Q}_c, \end{cases} \quad (\text{S32})$$

which can be also formally written as $\vec{\varphi} \propto \mathbf{L}\dot{\vec{Q}}$. With this definition, the left hand side represents magnetic flux. The Hamiltonian of the full systems is obtained by the Legendre transform. We find

$$H_{\text{tot}} = \frac{1}{2} \left(\frac{\Phi_0}{2\pi} \right)^2 \vec{\varphi}^T \mathbf{L}^{-1} \vec{\varphi} + \frac{1}{2} \vec{Q}^T \mathbf{C}^{-1} \vec{Q}. \quad (\text{S33})$$

The inversion of the inductance matrix \mathbf{L} presents a difficult analytical problem. If the mutual inductances M_j are large, that is $|k_j| \approx 1$, every element of the matrix \mathbf{L}^{-1} is generally non-zero. However, we assume that they are small. To first order, the solution is obtained by noting that we can obtain the conjugate relation for φ only in the zeroth order of M 's and substitute the result in the original Lagrangian \mathcal{L} in Eq. (S31) as it is first order in M 's. We find for an LC circuit of resonant frequency $\omega_c = 1/\sqrt{LC}$

$$\begin{aligned} H_{\text{tot}} &\approx \frac{Q_c^2}{2C} + \sum_j \frac{Q_j^2}{2C_p} + \left(\frac{\Phi_0}{2\pi} \right)^2 \left[\frac{1}{2} \frac{\varphi_c^2}{L} + \frac{1}{2} \sum_j \frac{\varphi_j^2}{L_p} + \sum_j \frac{k_j}{\sqrt{LL_p}} \varphi_c \varphi_j \right] \\ &\equiv \frac{P_c^2}{2} + \sum_j \frac{P_j^2}{2} + \frac{1}{2} \omega_c^2 X_c^2 + \frac{1}{2} \sum_j \omega_p^2 X_j + \omega_c \omega_p \sum_j k_j X_c X_j, \end{aligned} \quad (\text{S34})$$

where, in the last step, we denoted $P_j = Q_j/\sqrt{C_p}$ and $P_c = Q_c/\sqrt{C}$ and correspondingly $X_c = \frac{\Phi_0}{2\pi}\sqrt{C}\varphi_c$ and $X_j = \frac{\Phi_0}{2\pi}\sqrt{C_p}\varphi_j$. Thus, in the lowest order approximation, the Hamiltonian corresponds to the potential we chose to describe in Eq. (S1) with $\lambda_j^2 = k_j\omega_c\omega_p$. Note that both of these models are within the harmonic approximation, as we expanded the flux qubit Hamiltonian around a minimum point.

In other words, the cavity induced bifurcation could be observed in flux qubits by studying their collective evolution towards a state where even in the absence of a bias f , a majority of the qubits would be in the state with, say, clockwise circulating persistent current.

C. Cold atoms

Recently, there has notable progress in the field of cold polar molecules [16]. Following the long tradition of optical trapping of cold molecules, this field provides an interesting opportunity to realize a controllable polaritonic system. This is because the many internal degrees of freedom in molecules allow for metastability in the energy, as described in this supplement and in the main text. Thus, in the future, it would seem possible to manufacture a system that is topologically the same as in polaritonics but with controllable coupling constants, and then investigate the noise activated processes or even quantum tunneling between the possible molecular states.

-
- [1] C. Gardiner, *Stochastic methods: A handbook for the natural and social sciences*, 4th ed., Springer Series in Synergetics (Springer, Berlin, 2009).
 - [2] P. Hänggi, P. Talkner, and M. Borkovec, Reaction-rate theory: fifty years after Kramers, *Rev. Mod. Phys.* **62**, 251 (1990).
 - [3] S. Shin and H. Metiu, Nonadiabatic effects on the charge transfer rate constant: A numerical study of a simple model system, *J. Chem. Phys.* **102**, 9285 (1995).
 - [4] J. Galego, C. Climent, F. J. Garcia-Vidal, and J. Feist, Cavity Casimir-Polder forces and their effects in ground-state chemical reactivity, *Phys. Rev. X* **9**, 021057 (2019).
 - [5] X. Li, A. Mandal, and P. Huo, Cavity frequency-dependent theory for vibrational polariton chemistry, *Nat. Commun.* **12**, 1 (2021).
 - [6] J. George, T. Chervy, A. Shalabney, E. Devaux, H. Hiura, C. Genet, and T. W. Ebbesen, Multiple Rabi splittings under ultrastrong vibrational coupling, *Phys. Rev. Lett.* **117**, 153601 (2016).
 - [7] M. Tavis and F. W. Cummings, Exact solution for an N -molecule-radiation-field Hamiltonian, *Phys. Rev.* **170**, 379 (1968).
 - [8] R. Chikkaraddy, B. De Nijs, F. Benz, S. J. Barrow, O. A. Scherman, E. Rosta, A. Demetriadou, P. Fox, O. Hess, and J. J. Baumberg, Single-molecule strong coupling at room temperature in plasmonic nanocavities, *Nature* **535**, 127 (2016).
 - [9] W. Ahn, I. Vurgaftman, A. D. Dunkelberger, J. C. Owrutsky, and B. S. Simpkins, Vibrational strong coupling controlled by spatial distribution of molecules within the optical cavity, *ACS Photon.* **5**, 158 (2018).
 - [10] F. J. Garcia-Vidal, C. Ciuti, and T. W. Ebbesen, Manipulating matter by strong coupling to vacuum fields, *Science* **373**, eabd0336 (2021).
 - [11] J. A. Asadzinski, R. Viswanathan, L. Madsen, J. Garnæs, and D. K. Schwartz, Langmuir-Blodgett films, *Science* **263**, 1726 (1994).
 - [12] J. J. Gooding and S. Ciampi, The molecular level modification of surfaces: from self-assembled monolayers to complex molecular assemblies, *Chem. Soc. Rev.* **40**, 2704 (2011).
 - [13] A. Thomas, J. George, A. Shalabney, M. Dryzhakov, S. J. Varma, J. Moran, T. Chervy, X. Zhong, E. Devaux, C. Genet, J. A. Hutchison, and T. W. Ebbesen, Ground-state chemical reactivity under vibrational coupling to the vacuum electromagnetic field, *Angew. Chem. Int. Ed.* **55**, 11462 (2016).
 - [14] J. Lather, P. Bhatt, A. Thomas, T. W. Ebbesen, and J. George, Cavity catalysis by cooperative vibrational strong coupling of reactant and solvent molecules, *Angew. Chem. Int. Ed.* **58**, 10635 (2019).
 - [15] T. Orlando, J. Mooij, L. Tian, C. H. Van Der Wal, L. Levitov, S. Lloyd, and J. Mazo, Superconducting persistent-current qubit, *Phys. Rev. B* **60**, 15398 (1999).
 - [16] A. Kruckenhauser, L. M. Sieberer, L. De Marco, J.-R. Li, K. Matsuda, W. G. Tobias, G. Valtolina, J. Ye, A. M. Rey, M. A. Baranov, and P. Zoller, Quantum many-body physics with ultracold polar molecules: Nanostructured potential barriers and interactions, *Phys. Rev. A* **102**, 023320 (2020).

V

THEORY FOR POLARITONIC QUANTUM TUNNELING

by

K. S. U. Kansanen

Manuscript, submitted to the arXiv-repository (2204.13490v1)

Copyright 2022 the Author

Theory for polaritonic quantum tunneling

Kalle S. U. Kansanen*

Department of Physics and Nanoscience Center, University of Jyväskylä,
P.O. Box 35 (YFL), FI-40014 University of Jyväskylä, Finland

(Dated: April 28, 2022)

I investigate the tunneling decay rate of a polaritonic system formed by a strong coupling between a vacuum cavity mode and N metastable systems. Using a simple model potential, I find the instanton solutions controlling the low-temperature tunneling rate. The resulting rate modification due to the cavity is proportional to the mean of the second power of the light-matter coupling. No collective effect that would enhance the rates by a factor of \sqrt{N} is present, which is in line with the results in the thermal activation regime.

I. INTRODUCTION

Tunneling is a manifestation of quantum coherence: quantum systems are able to surmount barriers they energetically should not due to their wave-like properties [1]. The range of tunneling systems is broad: elementary particles in nuclear matter [2], electrons in conductors [3, 4], magnetization in nanomagnets [5], and superconducting phase in superconducting circuits [6]. Theoretically, tunneling can be understood as the quantum mechanical counterpart to classical thermal activation describing, for instance, chemical reactions [7–9].

Another type of quantum coherence can be seen when a coherent exchange of energy between two quantum mechanical systems happens. A prime example of such coherent systems is polaritons which are the hybrid excitations of the vacuum electromagnetic field and molecular degrees of freedom. Recently, it has been suggested that the formation of such coherent systems could affect chemistry which is still poorly understood [10–13]. In fact, a transition state theory calculation shows that all the polaritonic enhancements to the reaction rate scale as $1/N$ where N is the number of molecules participating in the polariton [14–16]. This is often attributed to the fact that the coupling to light induces only two energetically different polaritonic states, separated in energy by the Rabi splitting proportional to \sqrt{N} , while $N - 1$ molecular states, the so-called dark states, remain energetically the same.

Motivated by the idea of polaritonic chemistry, I focus on a related question whether there can be a genuine polaritonic quantum tunneling effect. This question arises naturally as the light-matter coupling changes the coherence properties of the system at hand. It also induces collective behavior through the formation of polaritons. In fact, the $N - 1$ dark states are superpositions over the molecular states even though their energy does not change.

In this article, I present a model of N metastable systems coupled to a cavity mode and investigate the effect of the common cavity mode on the low-temperature

tunneling decay rate. For a simple model potential, I analytically solve the polaritonic rate modification using path integral techniques in the semiclassical approximation. Such solvable models are rare; there are only a few truly multidimensional problems in quantum tunneling that have been solved analytically [1, 17].

In the low-temperature regime, the tunneling decay rate is dominated by *instantons*. I find the instanton solutions for the polaritonic system without friction. As the main result, I find the polaritonic rate modification as a function of the number N of metastable systems. The tunneling decay rate is modified by a factor proportional to the single-molecule coupling constant and not by the Rabi splitting. This shows that the cavity indeed induces a coherence effect but it is not a collective effect. Similar to the transition state theory calculation [14, 15], the polaritonic enhancements scale as $1/N$ if the Rabi splitting is fixed. Therefore, the practical route to realizing the cavity-induced coherence is not in the collective strong coupling regime with large number of systems but rather in single systems with large couplings to the cavity.

II. SEMICLASSICAL APPROXIMATION TO TUNNELING

Consider a metastable system described by a potential

$$V(q) = \begin{cases} \frac{1}{2}\omega_0^2 q^2, & q \leq a, \\ -\infty, & q > a, \end{cases} \quad (1)$$

where a determines the energy of the potential barrier $E_b = \frac{1}{2}\omega_0^2 a^2$ as in Fig. 1(a). The quadrature q is defined here so that the conjugate momentum quadrature p is given simply by $p = \dot{q}$. Although this potential has been used before [18, 19], it lacks a name and, so, I call it the ski-jumping potential. I set $\hbar = 1$ everywhere.

Next, consider N identical metastable systems coupled to a single harmonic cavity mode whose position quadrature is x , normalized similarly to q . I assume that this coupling is directly between the quadratures x and q . The total Hamiltonian of this polaritonic system is given

* kalle.kansanen@gmail.com

by

$$H = \frac{1}{2}\dot{x}^2 + \sum_{i=1}^N \frac{1}{2}q_i^2 + V_{\text{tot}}, \quad (2)$$

where

$$V_{\text{tot}} = \sum_{i=1}^N V(q_i) + \frac{1}{2}\omega_c^2 x^2 + \sum_{i=1}^N \lambda_i^2 x q_i. \quad (3)$$

Here, the apparent eigenfrequency of the cavity mode is ω_c while the light-matter coupling is encoded within λ_i^2 . It can be related to the coupling constant g_i obtained from a quantum electrodynamics calculation [20] by $\lambda_i^2 = \sqrt{\omega_c \omega_0} g_i$. If one considers the ski-jumping potential to be a simplistic model of a potential energy surface of a molecule, the exact value of each coupling constant depends on the orientation and position of the molecule within the cavity [20].

There are several methods to calculate the tunneling decay rate of a metastable system. Here, I use the so-called *Im F* method [21] as it can straightforwardly be used for multidimensional systems and provides the possibility to extend the theory to include dissipation [1, 19]. Physically, the idea is simple: the metastability of the ski-jumping potential means that there are no stationary states. This may be represented by the eigenenergies obtaining a finite imaginary part which is associated to a tunneling decay rate. Likewise, the partition function \mathcal{Z} defined in terms of the states within the ski-jumping potential obtains an imaginary part. Then, the tunneling decay rate k at low temperature may be expressed as

$$k = \frac{2}{\beta} \text{Im} \ln \mathcal{Z}, \quad (4)$$

where $\beta = 1/k_B T$ is the inverse temperature [1, 22]. The partition function \mathcal{Z} can be represented by an Euclidean path integral

$$\mathcal{Z} = \int D(\phi) \exp\{-S_E[\phi(\tau)]\} \quad (5)$$

over β -periodic paths in imaginary time $\tau = it$. Here, $\phi = (x, q_1, \dots, q_N)^T$ represents a column vector of all the dynamical degrees of freedom and the Euclidean action is given by

$$S_E = \int_{-\beta/2}^{\beta/2} d\tau \left[\frac{1}{2} \dot{\phi}^T \dot{\phi} + V_{\text{tot}}(\phi) \right]. \quad (6)$$

One can associate this Euclidean action to the classical action of systems moving in the inverted potential $-V_{\text{tot}}$.

For independent systems, the total potential energy can be written as a sum of system's potential energies. Thus, the partition function factorizes as $\mathcal{Z} = \mathcal{Z}_1^N$ for identical systems. Whatever the single-system tunneling decay rate k_1 is, the total rate is then $k = Nk_1$.

In general, solving the path integral exactly to obtain the partition function is difficult. Thus, I resort to the

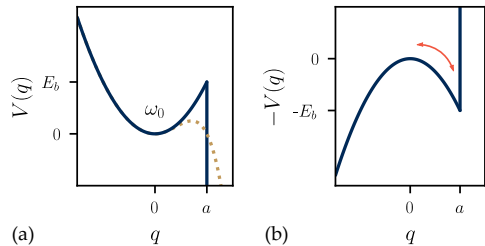


FIG. 1. (a) Ski-jumping potential of Eq. (1). It is obtained by a limiting process from a potential $E_b[(q/a)^2 - \theta(q)(q/a)^n]$ with θ being the Heaviside step function and $n \rightarrow \infty$. The dotted line represents $n = 4$. (b) Inverted potential $-V(q)$. The arrow indicates the instanton solution in which the system moves from $q = 0$ to $q = a$ and back.

semiclassical approximation which is valid when the barrier energy E_b is large compared to the real part of the ground state energy (which is of the order of ω_0) [22]. I expand the path integral around the classical solutions and take into account only the quadratic fluctuations

$$\mathcal{Z} \approx \sum_{\mu} I_{\mu} e^{-S_E(\phi_{\mu})}, \quad (7a)$$

$$I_{\mu} = \int D(r_{\mu}) \exp\left\{-\frac{1}{2} r_{\mu}^T [\partial_{\tau}^2 + \mathcal{V}(\phi_{\mu})] r_{\mu}\right\}. \quad (7b)$$

Here, ϕ_{μ} represents one possible classical β -periodic path and I_{μ} the contribution of quadratic fluctuations which may be expressed using a second derivative matrix $\mathcal{V}_{ij} = \partial^2 V_{\text{tot}} / \partial \phi_i \partial \phi_j$ evaluated at the corresponding classical solution ϕ_{μ} . The integration variable r_{μ} is the deviation from ϕ_{μ} with the boundary conditions $r_{\mu}(\pm\beta/2) = 0$. As the action S_E is a real variable, the imaginary part of the partition function must be in fluctuations I_{μ} .

The ski-jumping potential allows for the solution of classical paths in a general case but it complicates the evaluation of the fluctuations as the potential is discontinuous at $q_i = a$. These problems can mostly be avoided since the quadratic fluctuations can be expressed in terms of the classical solutions exactly in the case of a closed system [23, 24].

A. Solution of the Euclidean action

First, I solve the classical periodic paths in imaginary time. The problem is the same as solving classical motion in real time but in the inverted potential. Note that $q_i = a$ represents a wall in the inverted potential as in Fig. 1(b). Thus, at this point, the velocity \dot{q}_i is discontinuous. Rather than trying to piece together solutions before and after hitting the wall, I expand the mathematical trick presented in Ref. 18 for a polaritonic system and take this discontinuity into account at the level of the equations of motion. If a single quadrature q_1 hits

the wall at time τ_1 , that is, $q_1(\tau = \tau_1) = a$, the dynamics in the inverted potential is determined by

$$-\ddot{x} + \omega_c^2 x + \sum_{i=1}^N \lambda_i^2 q_i = 0, \quad (8a)$$

$$-\ddot{q}_1 + \omega_0^2 q_1 + \lambda_1^2 x = A\delta(\tau - \tau_1), \quad (8b)$$

$$-\ddot{q}_i + \omega_0^2 q_i + \lambda_i^2 x = 0, \quad i = 2, 3, \dots, N. \quad (8c)$$

The unknown constant A is determined from the condition $q_1(\tau = \tau_1) = a$.

Since I am searching for periodic solutions, the way to proceed is to write all dynamical quantities as Fourier series. Here, I choose the convention $f(\tau) = \sum_m f_m e^{i\omega_m \tau}$ with $\omega_m = 2\pi m/\beta$ being the bosonic Matsubara frequency. The inverse transformation is then $f_m = \frac{1}{\beta} \int d\tau f(\tau) e^{-i\omega_m \tau}$. By applying the latter definition to Eqs. (8), I find

$$(\omega_c^2 + \omega_m^2)x_m + \sum_{i=1}^N \lambda_i^2 q_{i,m} = 0, \quad (9a)$$

$$(\omega_0^2 + \omega_m^2)q_{1,m} + \lambda_1^2 x_m = \frac{A}{\beta} e^{-i\omega_m \tau_1}, \quad (9b)$$

$$(\omega_0^2 + \omega_m^2)q_{i,m} + \lambda_i^2 x_m = 0. \quad (9c)$$

This set of linear equations can be solved. The idea is first to find the dynamics of the cavity mode x which then gives the solutions of the individual quadratures q_i . This is achieved by defining a collective variable $Q_m = \sum_{i=1}^N \frac{\lambda_i^2}{\langle \lambda^2 \rangle} q_{i,m}$ with $\langle \lambda^2 \rangle = \sum_i \lambda_i^2 / N$ representing the average over the couplings. The dynamics of Q can be determined from Eqs. (9b)–(9c), which allows for solving the dynamics of x . After a short calculation I find the solutions in Fourier space to be

$$x_m = -\frac{A}{\beta} \lambda_1^2 \chi_P(\omega_m) e^{-i\omega_m \tau_1}, \quad (10a)$$

$$q_{i,m} = \frac{A}{\beta} \frac{\lambda_i^2 \lambda_1^2}{\omega_m^2 + \omega_0^2} \chi_P(\omega_m) e^{-i\omega_m \tau_1}, \quad (10b)$$

$$q_{1,m} = \frac{A}{\beta} \frac{1}{\omega_m^2 + \omega_0^2} [1 + \lambda_1^4 \chi_P(\omega_m)] e^{-i\omega_m \tau_1}, \quad (10c)$$

where I defined a short-hand notation describing the polaritonic response

$$\chi_P(\omega_m) = [(\omega_m^2 + \omega_0^2)(\omega_m^2 + \omega_c^2) - N \langle \lambda^4 \rangle]^{-1}. \quad (11)$$

The cavity-mediated interaction can be seen in the fact that the dynamics of all the quadratures q_i depend on the coupling λ_1^2 of the first quadrature.

The abstract Fourier space solutions become clearer in the zero-temperature limit $\beta \rightarrow \infty$. Then, the Fourier series can be transformed to an integral which I evaluate using the residue theorem. Setting $\tau_1 = 0$ for brevity,

this results in the imaginary-time paths

$$x(\tau) = A \frac{\lambda_1^2}{\sqrt{\langle \lambda^4 \rangle}} \sqrt{\frac{1 - \delta^2}{4N}} \left(\frac{e^{-\omega_+ |\tau|}}{\omega_+} - \frac{e^{-\omega_- |\tau|}}{\omega_-} \right), \quad (12a)$$

$$q_i(\tau) = A \frac{\lambda_1^2 \lambda_i^2}{\langle \lambda^4 \rangle} \frac{f(\tau)}{N}, \quad (12b)$$

$$q_1(\tau) = A \frac{e^{-\omega_0 |\tau|}}{2\omega_0} + A \frac{\lambda_1^4}{\langle \lambda^4 \rangle} \frac{f(\tau)}{N}, \quad (12c)$$

$$f(\tau) = \frac{1 + \delta}{2} \frac{e^{-\omega_+ |\tau|}}{2\omega_+} + \frac{1 - \delta}{2} \frac{e^{-\omega_- |\tau|}}{2\omega_-} - \frac{e^{-\omega_0 |\tau|}}{2\omega_0} \quad (12d)$$

with further definitions of the polariton eigenfrequencies ω_{\pm} without the rotating wave approximation and a detuning parameter $\delta \in [-1, 1]$ given by

$$\omega_{\pm} = \sqrt{\frac{\omega_0^2 + \omega_c^2}{2} \pm \frac{1}{2} \sqrt{4N \langle \lambda^4 \rangle + (\omega_0^2 - \omega_c^2)^2}}, \quad (13a)$$

$$\delta = \frac{\omega_0^2 - \omega_c^2}{\omega_+^2 - \omega_-^2}. \quad (13b)$$

The Rabi splitting is typically defined as $\omega_+ - \omega_-$ when the cavity is on resonance $\omega_c = \omega_0$. Finally, A resolves by demanding that $q_1(\tau = \tau_1) = a$. It gives rise to a weighted harmonic average

$$A = 2a \frac{N \langle \lambda^4 \rangle}{\frac{N \langle \lambda^4 \rangle - \lambda_1^4}{\omega_0} + \lambda_1^4 \left(\frac{1 + \delta}{2} \frac{1}{\omega_+} + \frac{1 - \delta}{2} \frac{1}{\omega_-} \right)} \equiv 2a\omega_{H,1}. \quad (14)$$

Here, the weights are the second-order coupling constants λ_i^4 and detuning factors $(1 \pm \delta)/2$. This expression already shows that, similarly to the discussion about dark states, the bare frequencies ω_0 are weighted with a factor proportional to $N - 1$ whereas the polariton frequencies ω_{\pm} have a weight close to unity, independently of N . Thus, in general, $\omega_{H,1} \approx \omega_0$ for $N \gg 1$. If $\lambda_1^2 = 0$, then $\omega_{H,1} = \omega_0$.

An example of the polaritonic instanton solution is shown in Fig. 2. Initially, $\tau \rightarrow -\infty$, all the quadratures are at zero. Very slowly, the first quadrature starts to evolve, pulling all the other systems with it. The exact direction the other systems are pulled towards depends on the relative signs of the coupling constants λ_i^2 . At time $\tau = 0$, the first quadrature is at the wall and bounces back. From this hitting time to $\tau \rightarrow \infty$, the inverse happens. The first quadrature starts to slow down and all the quadratures creep towards their initial position.

The Euclidean action follows directly from the instanton solutions at any temperature. I obtain

$$S_{E,1} = \frac{1}{2} a^2 \left[\frac{1}{\beta} \sum_m \frac{1 + \lambda_1^4 \chi_P(\omega_m)}{\omega_0^2 + \omega_m^2} \right]^{-1} \quad (15a)$$

$$\rightarrow 2 \frac{E_b}{\omega_0} \frac{\omega_{H,1}}{\omega_0} \equiv S_0 \frac{\omega_{H,1}}{\omega_0}, \quad \text{when } \beta \rightarrow \infty. \quad (15b)$$

In the low-temperature limit, the action is determined by two ratios: First, the barrier energy E_b is compared

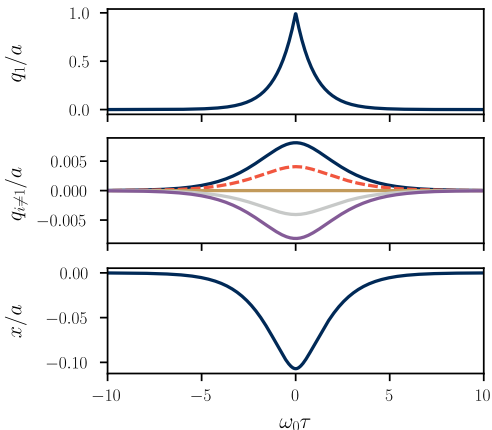


FIG. 2. Polaritonic instanton solution for $N = 6$ on resonance $\omega_c = \omega_0$. The coupling constants are chosen so that $\lambda_i^2/\omega_0^2 = 0.1$ and $\lambda_{i \neq 1}^2/\omega_0^2 \in \{0, \pm 0.1, \pm 0.2\}$. The dashed orange line in the middle graph also represents the second term in Eq. (12c) that describes the modification to the bounce due to the light-matter coupling.

to the pseudo-eigenenergy ω_0 . This is in contrast to the high-temperature result with $S_E = \beta E_b$. Second, the polaritonic effect is contained within the ratio of the harmonic mean frequency $\omega_{H,1}$ and the bare frequency ω_0 . This ratio is unity when there is no coupling, $\lambda_1^2 = 0$, and the action is just the bare action, $S_{E,1} = S_0$. A fully uncoupled system does not know about the polaritons, as expected.

There are also configurations in which multiple quadratures hit the wall. Finding such solutions is a well-defined classical problem which can be tackled similarly to the case of one-bounce instanton and is shortly discussed in Appendix A. However, these multi-bounce paths do not contribute to the tunneling rate. I argue this in simple terms: Consider only two systems coupled to a cavity with equal coupling strengths $\lambda_i^2 = \lambda^2$. Then, it is clear that the two systems obey the same imaginary-time equations of motion, except when they bounce off the wall. Consequently, one of the possible multi-bounce solutions is that the two quadratures are exactly the same, $q_1(\tau) = q_2(\tau)$ for all τ 's. However, this solution is not a saddle point of the Euclidean action. If you increase the temperature, the instanton path shrinks to a point that is near the maximum of the total potential V_{tot} , around $q_1 = q_2 \approx a$. This point is not a saddle point of the potential V_{tot} but the maximum — the Hessian matrix of the potential has two negative eigenvalues. In the limit of no coupling, $\lambda^2 \rightarrow 0$, we arrive at a contradiction with the case of independent systems; only the saddle points contribute to the imaginary part of \mathcal{Z} in the semiclassical approximation. It is thus hard to see how the “coherent transition state theory picture” of Ref. 25 can be mapped

to this low-temperature calculation.

B. Polaritonic tunneling rate modification

To get from the instanton solution (12) to the polaritonic tunneling decay rate, one needs to calculate the fluctuation factor I_μ . The program is somewhat cumbersome even in the one-dimensional case [22]. The first derivative of the instanton solution happens to be a zero eigenvalue mode for the fluctuations and I_μ formally diverges. The existence of the zero mode also implies that there exists a negative eigenvalue mode which makes I_μ imaginary. A further complication is that one should include multiple sequential bounces. Such paths are obtained by essentially glueing instanton solutions together: The imaginary-time axis can be separated into n partitions of length β/n . Since the instanton paths change appreciably only for the imaginary time $2/\omega_0$, using the instanton solution (12) for each partition of length β/n gives a path with n bounces. The error of this process is exponentially small in β when $2/\omega_0 \ll \beta$. In these steps, I follow closely the one-dimensional treatment of Ref. 24. I do this as the relatively recent literature [26, 27] cannot be applied since the instanton solution (12) is not differentiable at the hitting time.

The fluctuation factor of a single bounce can be obtained from a version of the Gelfand–Yaglom formula [22]

$$I_1^{n=1} \propto -i\beta\sqrt{S_{E,1}}\sqrt{\frac{\epsilon_1(\beta)}{D_1}}, \quad (16)$$

where $D_1 = \left| \det \left(\frac{\partial \phi_j(\beta/2)}{\partial \phi_i(-\beta/2)} \right) \right|$ is the fluctuation determinant evaluated in the $\beta \rightarrow \infty$ limit and $\epsilon_1(\beta)$ provides a finite temperature correction to it. In these and the following expressions, I denote the number of bounces as a superscript whereas the subscript refers to the quadrature that hits the wall. I also choose not to keep track of the powers of 2π ; in the end, they are fixed by comparing to the non-interacting result. By expanding the method in Ref. 28 to the multidimensional system at hand, I find

$$\epsilon_1(\beta) \approx 2 \frac{\dot{\phi}^T(-\beta/2)\ddot{\phi}(-\beta/2) - \dot{\phi}^T(\beta/2)\ddot{\phi}(\beta/2)}{\int_{-\infty}^{\infty} \dot{\phi}^T(\tau)\dot{\phi}(\tau) d\tau}, \quad (17)$$

where ϕ refers to the vectorized form of the instanton solution (12). The derivation of this result can be found in Appendix B. The factor $-i$ is the Maslov–Morse index, which takes into account the one negative eigenvalue mode. Mathematically, it follows from the singularity of the fluctuation determinant at the turning point of the classical solution (see e.g. Ref. 22). Lastly, $\beta\sqrt{S_{E,1}}$ follows from the Faddeev–Popov method as the hitting time τ_1 is in fact a free parameter. By a change of integration variables from the zero mode proportional to the first derivative of the instanton solution to τ_1 in I_μ , one integrates τ_1 over the whole range $[-\beta/2, \beta/2]$ while the Jacobian of the transformation is $\sqrt{S_{E,1}}$ [19, 22, 29].

To connect two bounces, in principle, one needs to calculate the action with variable ending points. This is not feasible in practice. However, since the instanton paths reside mostly near $\phi = 0$, it is justified to expand the action. Thus, from the initial $\phi(-\beta/2) = \phi_- = 0$ to an arbitrary point $\tilde{\phi}$, the action can be expressed in terms of the final point $\phi(\beta/2) = \phi_+ = 0$ as

$$S_E[\phi_-, \tilde{\phi}] \approx S_{E,1}[\phi_-, \phi_+] + \frac{1}{2}(\phi_+ - \tilde{\phi})^T \left[\frac{\partial^2 S_E}{\partial \phi_i \partial \phi_j} \right] (\phi_+ - \tilde{\phi}). \quad (18)$$

The Hessian matrix on the second row is calculated along the classical instanton path. The same structure is also obtained from a variable initial point and a fixed final point. Thus, the paths are connected by first dividing the path integral into two parts with a variable midpoint $\tilde{\phi}$ and then integrating over it. These two parts are assumed to obey the instanton solutions individually.

At this point, the multidimensional nature of the problem becomes relevant. To connect two bounces, I should take into account that the two bounces correspond to different quadratures. In the case of equal couplings, they are exactly the same. Thus, the integration over the midpoint $\tilde{\phi}$ is a Gaussian integral and the Hessian matrices in Eq. (18) are the same. In this case, the determinant rising from integration is equal to the inverse of the fluctuation determinant D_1 [23]. I assume here that this relation holds, at least to an approximation, also in the case of variable coupling constants.

The extension from two to n bounces does not require considerably more effort. One should note that there are now n hitting times, which are all free parameters and for which the Faddeev-Popov method gives an extraneous factor of $1/n!$. Otherwise, the fluctuation factor is similar to Eq. (16) for each bounce. Thus, the general n bounce contribution to the partition function is

$$I^n e^{S_E^n} \propto \sqrt{\frac{1}{D}} \sum_{\{k\}} \frac{(-i\beta)^n}{n!} \prod_{i=1}^n \sqrt{S_{E,k_i} \epsilon_{k_i}(\beta/n)} e^{-S_{E,k_i}}. \quad (19)$$

The vector k enumerates which quadrature hits the wall in each bounce and the sum is taken over all the possible n -bounce configurations ($k_i \in \{1, \dots, N\}$). There are n independent sums and, thus, in total N^n configurations. These sums can be alternatively written as

$$I^n e^{S_E^n} \propto \frac{(-i\beta)^n}{n!} N^n \left\langle \sqrt{S_E \epsilon(\beta/n)} e^{-S_E} \right\rangle^n. \quad (20)$$

Here, $\langle \cdot \rangle$ denotes the ensemble average over the coupling constants λ_i^2 .

The remaining problem is to calculate the finite temperature correction $\epsilon(\beta)$ and evaluate the sum over all bounces to arrive at the partition function \mathcal{Z} . The strategy I use is to approximate $\epsilon(\beta/n)^n \approx C(\beta)\epsilon(0)^n$ with a prefactor $C(\beta)$. This approximation renders the partition function \mathcal{Z} to an exponential form which gives the

leading order contribution in temperature to the tunneling rate. The function $C(\beta)$ plays no role in the rate as it becomes a real prefactor of the imaginary part in the partition function \mathcal{Z} . This approximation is further discussed in Appendix B. Effectively, it leads in Eq. (20) to

$$\epsilon_1(\beta/n) \rightarrow \epsilon_1(0) = 4\omega_{A,1}\omega_{H,1}. \quad (21)$$

where I need to define the weighted arithmetic average

$$\omega_{A,1} = \frac{(N \langle \lambda^4 \rangle - \lambda_1^4)\omega_0 + \lambda_1^4 \left(\frac{1+\delta}{2}\omega_+ + \frac{1-\delta}{2}\omega_- \right)}{N \langle \lambda^4 \rangle} \quad (22)$$

with the same weights as in the harmonic average $\omega_{H,1}$. Whenever the total coupling $N \langle \lambda^4 \rangle$ is small compared to $\omega_c^2 \omega_0^2$ (i.e., the rotating wave approximation is applicable), always $\omega_{A,1} \approx \omega_0$. In the limit $\lambda_1^2 \rightarrow 0$, one finds $\epsilon_1(\beta/n)^n = (2\omega_0)^{2n}$ without any approximations.

Finally, the sum over all classical solutions and their quadratic fluctuations can be evaluated to arrive at the partition function \mathcal{Z} . The important quantity here is the average modification r of the tunneling rate, defined as the ratio of the total tunneling rates with and without the coupling to the cavity, $r = k/k(\lambda = 0)$. I find

$$r = \left\langle \frac{\omega_H}{\omega_0} \sqrt{\frac{\omega_A}{\omega_0}} \exp \left[-S_0 \left(\frac{\omega_H}{\omega_0} - 1 \right) \right] \right\rangle. \quad (23)$$

This analytical result is for an arbitrary distribution of couplings. It directly shows that the most important polaritonic effects are contained in the harmonic frequency ω_H defined in Eq. (14) while the arithmetic mean frequency ω_A of Eq. (22) provides a small correction relevant only in the ultra-strong coupling regime.

The rate modification r describes the total tunneling rate modification of an N -body polaritonic system. The light-matter coupling modifies the tunneling for each system and, thus, there must be an ensemble average over the coupling constants. To be more precise, the average is over the second-order couplings λ_i^4 which are the weighing factors in the harmonic average ω_H . Using the expression $\lambda_i^2 = \sqrt{\omega_c \omega_0 g_i}$ it is instructive to write

$$\frac{\omega_H}{\omega_0} = \frac{1}{1 + \frac{g^2}{N \langle g^2 \rangle} \left(\frac{1+\delta}{2} \frac{\omega_0}{\omega_+} + \frac{1-\delta}{2} \frac{\omega_0}{\omega_-} - 1 \right)} \quad (24)$$

in terms of the true coupling constants g . Thus, the relevant distribution is that of g^2 . This is in contrast to our recent work focusing on bistable potentials in the thermal activation regime where we found that the distribution of g plays an important role [30].

III. ANALYSIS OF THE POLARITONIC RATE MODIFICATION

Let us consider the consequences of the rate modification (23). In the following, I assume that the rotating

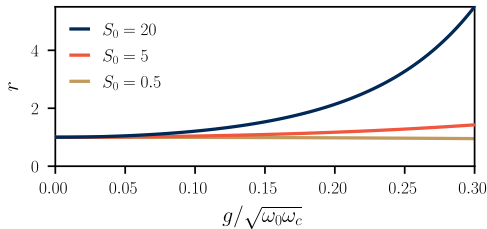


FIG. 3. Polaritonic tunneling rate modifications of a single system with different tunneling barriers $E_b/\omega_0 = S_0/2$.

wave approximation holds and that $\omega_c \approx \omega_0$. The polariton frequencies are effectively redefined as

$$\omega_{\pm} = \frac{\omega_c + \omega_0}{2} \pm \sqrt{N \langle g^2 \rangle + (\omega_c - \omega_0)^2/4} \quad (25)$$

and $\omega_A/\omega_0 = 1$. The harmonic average simplifies as the relation

$$\frac{1 + \delta}{2} \frac{1}{\omega_+} + \frac{1 - \delta}{2} \frac{1}{\omega_-} = \frac{\omega_c}{\omega_0 \omega_c - N \langle g^2 \rangle} \quad (26)$$

removes the need for the detuning parameter δ .

$N = 1$: For a single metastable system, the analysis is straightforward. The harmonic average is then over the polariton states which favors the lower polariton state. By employing the rotating wave approximation, I have $\omega_H/\omega_0 = 1 - g^2/\omega_0 \omega_c$. Inserting this relation to Eq. (23) gives

$$r = \left(1 - \frac{g^2}{\omega_c \omega_0}\right) \exp\left(S_0 \frac{g^2}{\omega_c \omega_0}\right). \quad (27)$$

Whether the tunneling rate is increased or decreased depends on the bare action $S_0 = 2E_b/\omega_0$. Expanding to the lowest order in the coupling gives $r \approx 1 + (S_0 - 1) \frac{g^2}{\omega_c \omega_0}$. A high tunneling barrier is represented by $S_0 > 1$ in which case the rate always increases due to the presence of the cavity. Higher the barrier, stronger the effect for a fixed coupling g . This is visualized in Fig. 3. It should be noted that $S_0 < 1$ is at odds with the semiclassical approximation and, thus, the result might not be accurate in such case.

The case of a single tunneling system coupled to a harmonic oscillator is relevant for experiments conducted in superconducting circuits [1]. The metastable quadrature could be, for instance, the superconducting phase difference of a Josephson junction in an electrical circuit. Then, Eq. (27) predicts the tunneling rate change if this circuit is connected to an external resonator.

$N \gg 1$ but $N \langle g^2 \rangle < \omega_0 \omega_c$: The case of macroscopically large N is the typical regime of polaritonic chemistry. The ensemble average in Eq. (23) could be calculated numerically for some model distribution of couplings but, rather, I calculate it with the cumulant ex-

pansion to the second order. This gives

$$r \approx \left[\left\langle \frac{\omega_H}{\omega_0} \right\rangle - S_0 \text{Var} \left(\frac{\omega_H}{\omega_0} \right) \right] \times \exp \left[S_0 - S_0 \left\langle \frac{\omega_H}{\omega_0} \right\rangle + \frac{1}{2} S_0^2 \text{Var} \left(\frac{\omega_H}{\omega_0} \right) \right], \quad (28)$$

where $\text{Var}(\cdot)$ refers to ensemble variance defined as $\text{Var}(x) = \langle x^2 \rangle - \langle x \rangle^2$. Thus, in principle, the variance of the coupling constants can modify the observed rate modification. However, for $N \gg 1$, the variance is well-approximated by

$$\text{Var} \left(\frac{\omega_H}{\omega_0} \right) = \left\langle \frac{\omega_H}{\omega_0} \right\rangle^4 \frac{\text{Var}(g^2)}{(\omega_0 \omega_c - N \langle g^2 \rangle)^2}, \quad (29)$$

because the fluctuation of couplings is also suppressed by the factor $1/N$ in the harmonic mean. Now, if $g_i^2/\omega_c \omega_0 \ll 1$ for all i , which is a typical assumption in the collective coupling regime, the variance can be neglected as $\text{Var}(g^2/\omega_c \omega_0) \ll 1$. Consequently, the expectation value of ω_H/ω_0 is given by

$$\left\langle \frac{\omega_H}{\omega_0} \right\rangle = \frac{\omega_0 \omega_c - N \langle g^2 \rangle}{\omega_0 \omega_c - (N-1) \langle g^2 \rangle} \approx 1 - \frac{1}{N} \frac{N \langle g^2 \rangle}{\omega_c \omega_0}. \quad (30)$$

Here, it appears that ω_H/ω_0 is determined as a ratio of polariton frequencies $(\omega_+ \omega_-)^2$ so that the polaritons in the denominator consist of $N-1$ systems and in the numerator of N systems. The latter equation is an expansion in the leading order of $\langle g^2 \rangle/\omega_0 \omega_c$. Using this expanded form I find

$$r \approx \left(1 - \frac{\langle g^2 \rangle}{\omega_c \omega_0}\right) \exp\left(S_0 \frac{\langle g^2 \rangle}{\omega_c \omega_0}\right), \quad (31)$$

which generalizes the single-system polaritonic rate modification of Eq. (27). In conclusion, there is no considerable collective tunneling effect, even if the collective coupling $\sqrt{N \langle g^2 \rangle}$ is a considerable fraction of $\sqrt{\omega_c \omega_0}$.

A. Comparison to high-temperature escape rate

Thermal activation is the main mechanism in the escape from a metastable potential whenever the temperature is above a threshold temperature proportional to ω_0 [8, 31]. The instanton path shrinks to a single point in the limit of high temperature, $\beta \rightarrow 0$. This follows from Matsubara frequency $\omega_{m \neq 0} \rightarrow \infty$. Thus, only $m = 0$ contributes in the Fourier series expressions. The action is in this case

$$S_{E,i} = \beta E_b \frac{\omega_0 \omega_c - N \langle g^2 \rangle}{\omega_0 \omega_c - (N \langle g^2 \rangle - g_i^2)}. \quad (32)$$

The similarity to the low-temperature action in Eq. (15) is evident: the bare action has changed from $S_0 =$

$2E_b/\omega_0$ to βE_b while the polaritonic modification is expressed in a form similar to Eq. (30) instead of $\omega_{H,i}/\omega_0$. However, I have not used the rotating wave approximation here as in Eq. (30).

In the high-temperature regime, one can also calculate the rate using the classical transition state theory. This approach gives the same exponent but it allows for a straightforward solution of the prefactor (also called the attempt frequency). The prefactor is proportional to

$$\omega_0 \sqrt{\frac{\omega_0 \omega_c - N \langle g^2 \rangle}{\omega_0 \omega_c - (N \langle g^2 \rangle - g_i^2)}}. \quad (33)$$

The structure of the classical escape rate is therefore different from the low-temperature one. Besides the change of the harmonic frequency ω_H to the ratio of polariton frequencies (which coincide in the rotating wave approximation), the modification of the action and prefactor are in different powers.

With both the low- and high-temperature limits of the rate modification at hand, one can imagine the following set of experiments (see e.g. Ref. 6): One varies the temperature of the polaritonic system and measures the escape rate. Starting from a high temperature and lowering it, the rate drops and eventually saturates to the quantum tunneling rate. By repeating this measurement without the cavity, the polaritonic coherence effect should become visible. The results I obtained imply, however, that this is likely only in single systems with sizable light-matter coupling because there is no collective enhancement of the rates.

IV. CONCLUSION

The work presented here is rather technical and, in many ways, cumbersome. Next, I try to clarify what I think are the main ideas and results of the work.

I show a simple, analytically solvable, toy model for polaritonic tunneling. In principle, there are numerous calculation techniques in the literature but the multidimensionality of the polaritonic system and the ski-jumping potential require some adaptation. These techniques might prove useful, for instance, in the investigations of macroscopic tunneling in superconducting circuit arrays or other interacting ensembles of metastable systems.

Even if the main result, the polaritonic tunneling rate modification (23), is obtained in a ski-jumping potential that does not directly correspond to any potential seen in nature, it has value. As a first guess, the structure of the solution is likely similar for a different potential: the modification is determined by the bare action and the harmonic frequency ω_H . The formation of polaritons affects the coherence properties in such a way that the tunneling rate may be increased. At the same time, if $N \gg 1$, the dark states spoil the effect of the polaritons to the tunneling decay rate out of any metastable potential. Of course, I would prefer to be proven wrong.

My work in the low-temperature regime coupled with the transition state results in Refs. 14 and 15 indicate that there is no collective polaritonic effect in the escape rate in the case of a large number N of molecules. Thus, it seems that one should take into account the possibility of systems returning back to the metastable state, or that there is no effect to be found in the first place.

This article considers only a truly metastable potential. An alternative system would be a bistable potential which we considered in the thermal activation limit [30]. For the low-temperature limit, the approach would have to be different than what I present here because there are no similar instantons. This is because these imaginary-time paths are at zero energy while the cavity changes the energies of the stationary states. Tunneling in bistable systems therefore requires another approach.

I did not take into account the friction or dissipation the systems realistically have. On the level of the action this would be, in principle, a straightforward extension [1, 19, 32, 33]. I expect dissipation to modify the tunneling rate modification: the modification should be larger for a nearly dissipationless cavity than for a bad cavity with a large dissipation rate. However, it cannot change, for instance, the N -scaling of the action.

ACKNOWLEDGMENTS

I thank Tero Heikkilä for useful discussions and for coining the term “ski-jumping potential”. This work has been supported by the Magnus Ehrnrooth foundation and the Academy of Finland (project numbers 317118 and 321982).

Appendix A: An approach to classical multi-bounce solutions

For completeness, I show how the method presented in the main text can be expanded to instanton configurations where multiple quadratures visit the point $q_i = a$. It requires modification.

One has to introduce a matrix-like structure to the delta functions in the equations of motion. From the viewpoint of Lagrangian mechanics, the delta function can be seen as a constraint force following from the condition $q_1(\tau_1) = a$. If there is another constraint, say, $q_2(\tau_2) = a$, the constraint on quadrature 1 affects also quadrature 2 due to the coupling via the cavity. The equations of motion to be solved are in general

$$-\ddot{q}_i + \omega_0^2 q_i + \lambda_i^2 x = \sum_j A_{ij} \delta(\tau - \tau_j) \quad (A1)$$

for all quadratures that hit the wall, $q_i(\tau_i) = a$.

If one assumes that all the off-diagonal elements of A_{ij} are zero, the delta functions do not conserve energy $E(\tau) = \frac{1}{2} \dot{\phi}^T \dot{\phi} - V_{\text{tot}}(\phi)$. (The energy is zero for

instanton solutions in the limit $\beta \rightarrow \infty$.) That is, the solution is only correct in a piecewise manner with abrupt changes in energy at hitting times τ_i . The energy is conserved for a single bounce.

One can fix the unknown parameters A_{ij} not only from the conditions $q_i(\tau_i) = a$ but also from the energy conservation and symmetry considerations. This seems clear for two bouncing quadratures, because the constraint forces between the two systems should be similar and, consequently, $A_{12} = A_{21}$. Whether or not it works in the solution of the general many-bounce dynamics, I do not know.

If there is a solution of the action in terms of the many hitting times, it is not evident what it means. Presumably, in the spirit of the least action, the classical path should be that of minimal action. I conjecture that this path is always for a polaritonic system such that the difference between hitting times is zero.

Appendix B: Finite temperature correction

For large but finite β , an exponentially small correction to the zero eigenvalue mode should be included. This section generalizes the discussion in Ref. 28 to multidimensional systems. Since the eigenvalues of the fluctuation determinant can be mapped to the eigenvalues in the time-independent Schrödinger equation, the question is, how do the energies change when a system is put into an infinite potential well. That is, there are two equations

$$(\partial_\tau^2 + \mathcal{V})f(\tau) = 0, \quad (\text{B1a})$$

$$(\partial_\tau^2 + \mathcal{V})g(\tau) = -\epsilon g(\tau) \quad (\text{B1b})$$

with boundary conditions $f(\tau \rightarrow \pm\infty) \rightarrow 0$ and $g(\tau = \pm\beta/2) = 0$. It can be shown that the solution of the former equation is related to the classical instanton path $\phi(\tau)$ by $f(\tau) = \dot{\phi}(\tau)$. By multiplying Eq. (B1a) by g^T from the right and similarly Eq. (B1b) by f^T , integrating over $[-\beta/2, \beta/2]$, and then subtracting the equations, I find

$$\begin{aligned} f^T(-\beta/2)\dot{g}(-\beta/2) - f^T(\beta/2)\dot{g}(\beta/2) \\ = \epsilon \int_{-\beta/2}^{\beta/2} f^T(\tau)g(\tau) d\tau. \end{aligned} \quad (\text{B2})$$

Since the correction must be small for large β , the integral on the right hand side can be approximated by replacing g by f and extending the integration limits to $\pm\infty$. Consequently, ϵ can be solved in terms of f and g . The question is then about the relation between the derivative of g and f at the boundaries $\pm\beta/2$.

For real-valued functions, the WKB approximation gives $\dot{g}(\pm\beta/2) \approx 2\dot{f}(\pm\beta/2)$. Alternatively, one can set $g(\tau) = c(\tau)f(\tau)$ and find c to first order in ϵ which results in $\dot{g}(\pm\beta/2) \approx 2\sqrt{3}\dot{f}(\pm\beta/2)$ for the ski-jumping potential. However, in this article, the exact proportionality constant is not of great importance as such factors cancel

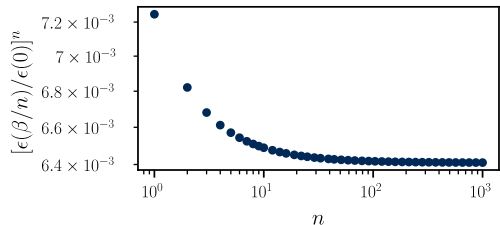


FIG. 4. The values of $[\epsilon(\beta/n)/\epsilon(0)]^n$ for $N = 1$, $\beta\omega = 5$ and $(1 \pm \delta)\omega_{\pm}/\omega_0 = 1 \pm 0.1$.

out when determining the cavity-induced modifications to the tunneling rate.

For vector-valued f and g , the argument is similar but less rigorous. It is possible that putting the system into a box changes both the magnitude of the derivative and its direction. However, the change of direction can be neglected in the ski-jumping potential: The potential matrix \mathcal{V} is close to a constant near the boundaries so one can diagonalize it by an orthogonal matrix. For the ski-jumping potential especially, \mathcal{V} is constant for all values of τ except the hitting time $\tau = \tau_1$. The argument for real-valued functions holds then for each component of the transformed vectors. Since the transformation is the same for both f and g , the result is also the same. Inserting the relations $\dot{g}(\pm\beta/2) \approx 2\dot{f}(\pm\beta/2)$ and $f = \dot{\phi}$ into Eq. (B2), I get Eq. (17). It should be noted, however, that this result will likely not hold for more complicated potentials but, in general, $\dot{g}(\pm\beta/2) = C\dot{f}(\pm\beta/2)$ where C is a matrix.

1. Correction for ski-jumping potential

The finite temperature correction (17) is readily obtained by using the instanton solutions (12). It should be noted that the denominator in the correction $\epsilon_1(\beta)$ is the action $S_{E,1}$ and that the instanton solutions are symmetric with respect to the hitting time $\tau_1 = 0$. I find

$$\begin{aligned} \epsilon_1(\beta) = 4\omega_{H,1} \frac{1}{N \langle \lambda^4 \rangle} \left[(N \langle \lambda^4 \rangle - \lambda_1^4) \omega_0 e^{-\beta\omega_0} \right. \\ \left. + \lambda_1^4 \left(\frac{1+\delta}{2} \omega_+ e^{-\beta\omega_+} + \frac{1-\delta}{2} \omega_- e^{-\beta\omega_-} \right) \right]. \end{aligned} \quad (\text{B3})$$

As implied in the main text, this expression is not particularly helpful because the partition function \mathcal{Z} depends on $\epsilon(\beta/n)$ so that n is summed over. A reasonable approximation is to replace $\epsilon(\beta/n)$ by $\epsilon(0)$ because it represents the $n \rightarrow \infty$ limit. Furthermore, it can be shown that, for a constant β , the value of $\epsilon(\beta/n)$ can be limited by $\epsilon(0)$ in the sense that $A \leq [\epsilon(\beta/n)/\epsilon(0)]^n \leq B$ for all n with suitable constants A and B . This is exemplified in Fig. 4. The prefactor in the approximation $\epsilon(\beta/n) \propto \epsilon(0)$

does not contribute to the imaginary part of the partition

function \mathcal{Z} and is thus unimportant.

-
- [1] J. Ankerhold, *Quantum Tunneling in Complex Systems*, 1st ed., Springer Tracts in Modern Physics (Springer, 2007).
- [2] A. B. Balantekin and N. Takigawa, Quantum tunneling in nuclear fusion, *Rev. Mod. Phys.* **70**, 77 (1998).
- [3] J. Tersoff and D. R. Hamann, Theory and application for the scanning tunneling microscope, *Phys. Rev. Lett.* **50**, 1998 (1983).
- [4] C. W. J. Beenakker, Colloquium: Andreev reflection and Klein tunneling in graphene, *Rev. Mod. Phys.* **80**, 1337 (2008).
- [5] C. Sangregorio, T. Ohm, C. Paulsen, R. Sessoli, and D. Gatteschi, Quantum tunneling of the magnetization in an iron cluster nanomagnet, *Phys. Rev. Lett.* **78**, 4645 (1997).
- [6] R. F. Voss and R. A. Webb, Macroscopic quantum tunneling in 1- μm Nb Josephson junctions, *Phys. Rev. Lett.* **47**, 265 (1981).
- [7] W. H. Miller, Semiclassical limit of quantum mechanical transition state theory for nonseparable systems, *J. Chem. Phys.* **62**, 1899 (1975).
- [8] P. Hänggi, P. Talkner, and M. Borkovec, Reaction-rate theory: fifty years after Kramers, *Rev. Mod. Phys.* **62**, 251 (1990).
- [9] J. Cao and G. A. Voth, A unified framework for quantum activated rate processes. I. General theory, *J. Chem. Phys.* **105**, 6856 (1996).
- [10] F. J. Garcia-Vidal, C. Ciuti, and T. W. Ebbesen, Manipulating matter by strong coupling to vacuum fields, *Science* **373**, eabd0336 (2021).
- [11] D. S. Wang and S. F. Yelin, A roadmap toward the theory of vibrational polariton chemistry, *ACS Photon.* **8**, 2818 (2021).
- [12] M. Hertzog, M. Wang, J. Mony, and K. Börjesson, Strong light-matter interactions: a new direction within chemistry, *Chem. Soc. Rev.* **48**, 937 (2019).
- [13] R. F. Ribeiro, L. A. Martínez-Martínez, M. Du, J. Campos-Gonzalez-Angulo, and J. Yuen-Zhou, Polariton chemistry: controlling molecular dynamics with optical cavities, *Chem. Sci.* **9**, 6325 (2018).
- [14] V. P. Zhdanov, Vacuum field in a cavity, light-mediated vibrational coupling, and chemical reactivity, *Chem. Phys.* **535**, 110767 (2020).
- [15] J. A. Campos-Gonzalez-Angulo and J. Yuen-Zhou, Polaritonic normal modes in transition state theory, *J. Chem. Phys.* **152**, 161101 (2020).
- [16] T. E. Li, A. Nitzan, and J. E. Subotnik, On the origin of ground-state vacuum-field catalysis: Equilibrium consideration, *J. Chem. Phys.* **152**, 234107 (2020).
- [17] M. Rontani, Tunneling theory of two interacting atoms in a trap, *Phys. Rev. Lett.* **108**, 115302 (2012).
- [18] H. Grabert, U. Weiss, and P. Hänggi, Quantum tunneling in dissipative systems at finite temperatures, *Phys. Rev. Lett.* **52**, 2193 (1984).
- [19] A. Altland and B. D. Simons, *Condensed Matter Field Theory*, 2nd ed. (Cambridge University Press, 2010).
- [20] D. F. Walls and G. J. Milburn, *Quantum Optics* (Springer, 2008).
- [21] J. S. Langer, Theory of the condensation point, *Ann. Phys.* **41**, 108 (1967).
- [22] H. Kleinert, *Path integrals in quantum mechanics, statistics, polymer physics, and financial markets*, 5th ed. (World Scientific, 2009).
- [23] R. F. Dashen, B. Hasslacher, and A. Neveu, Nonperturbative methods and extended-hadron models in field theory. I. Semiclassical functional methods, *Phys. Rev. D* **10**, 4114 (1974).
- [24] J.-Q. Liang and H. Müller-Kirsten, Bounces and the calculation of quantum tunneling effects, *Phys. Rev. D* **45**, 2963 (1992).
- [25] P.-Y. Yang and J. Cao, Quantum effects in chemical reactions under polaritonic vibrational strong coupling, *J. Phys. Chem. Lett.* **12**, 9531 (2021).
- [26] G. V. Mil'nikov and H. Nakamura, Practical implementation of the instanton theory. II. Decay of metastable state through tunneling, *J. Chem. Phys.* **117**, 10081 (2002).
- [27] M. Eraković, C. L. Vaillant, and M. T. Cvitaš, Instanton theory of ground-state tunneling splittings with general paths, *J. Chem. Phys.* **152**, 084111 (2020).
- [28] E. Gildener and A. Patrascioiu, Pseudoparticle contributions to the energy spectrum of a one-dimensional system, *Phys. Rev. D* **16**, 423 (1977).
- [29] J. Zinn-Justin, *Path Integrals in Quantum Mechanics* (Oxford University Press, 2005).
- [30] K. S. U. Kansanen and T. T. Heikkilä, Cavity-induced bifurcation in classical rate theory (2022), arXiv:2202.12182 [cond-mat.stat-mech].
- [31] I. Affleck, Quantum-statistical metastability, *Phys. Rev. Lett.* **46**, 388 (1981).
- [32] A. O. Caldeira and A. J. Leggett, Influence of dissipation on quantum tunneling in macroscopic systems, *Phys. Rev. Lett.* **46**, 211 (1981).
- [33] U. Weiss, *Quantum Dissipative Systems*, 4th ed. (World Scientific, 2012).